FOG

Freiberg Online Geoscience

FOG is an electronic journal registered under **ISSN 1434-7512**

2016, VOL 48

Folke Meinardus

Chemical investigations of groundwater and submarine hydrothermal fluid exhalations at Panarea, Italy

95 pages, 45 figures, 37 tables, 86 references

Acknowledgments

Writing a master's thesis is never a project one does solemnly on his own, so I want to express my gratitude towards my supervisor Prof. Dr. Broder J. Merkel for he was always on par with me whether during the animated and motivating discussions in the field or during the writing process of this thesis. Further thanks goes to Dr. Thomas Pohl for his technical support regarding the diving during the training to become a scientific diver and especially during the field work in Panarea.

The analysis of the taken samples was made considerably easier by the former laboratory staff of the water laboratory of the department of hydrogeology at the Technische Universität Bergakademie Freiberg, Dr. Kummer, Ms. Schlothmann. Their friendly and open attitude helped my a great deal during the analysis.

My two biggest supporters are also the most important ones to me, so I want to thank my son Tammo for the daily joy he brings into my life and my wife Janna for supporting me all the way. Naturally my thanks expands to my whole family who was always there if I needed them.

Last but not least I want to thank Oliver Wiche for his "statistical support" and especially Carsten Kummerfeld and Sebastian Neumann for their proofreading.

Abstract

In 2015 samples of hydrothermal fluids of the submarine hydrothermal system Panarea at nine different investigation areas including the groundwater of the island Panarea were taken. The on-site parameters categorize the found hydrothermal fluids as acidic (pH <2.4-5.5), reducing (E_H: around -50 mV) and highly mineralized (up to 120 mS/cm). The investigation areas Black Point, Fumarolic Field, Hot Lake and La Calcara are singled out, showing the most distinguished characteristics, whereas the rest of the areas display characteristics closely to seawater. Chemical analysis of the fluid samples regarding their general chemical composition with IC (Ion Chromatography) and ICP-MS (Inductive coupled plasma-mass spectrometer) reveal an astonishing enrichment of the main constituents of seawater combined with a depletion of Mg^{2+} and SO_4^{2-} in descending order at Hot Lake, Fumarolic Field and Hot Lake. However, La Calcara shows signs of depletion of the main constituents compared to the local seawater, indicating a lowly mineralized water source at La Calcara. Trace elements are tremendously enriched at Black Point and Hot Lake, whereas REE are solemnly enriched at Black Point and partly at Area 26. Problematic with all samples is the surrounding seawater, overwriting typical hydrothermal signatures at areas like Bottaro Nord/West and Area 26.

The isotopic composition regarding Deuterium and Oxygen reveals δ^{18}O-shifted (enriched) seawater as dominant water source of the hydrothermal system, a connection between the groundwater of Panarea and the investigation area La Calcara can be excluded.

In the second part over 200 hydrothermal water samples of the submarine hydrothermal system Panarea collected between 2006 and 2015 by the Scientific Diving Center Freiberg (SDC) were statistically evaluated. Conducted factor analysis reveal two factors, the first representing mostly trace elements and REE and hence a magmatic input, the second represents the main constituents of seawater. Hot Lake and Fumarolic Field are mainly fed by the second factor, whereas Black Point is mostly represented by the first factor, indicating different fluid types or evolutions of the fluids at these investigation areas.

The Kruskall-Wallis-Test distinguishes as before Hot Lake and Fumarolic Field, Black Point and partly Area 26 as statistically significant different regarding their parameters from the rest of the investigation areas and from the local seawater, proving their hydrothermal status. Based on these findings a new model is proposed, explaining the ascent and evolution of the hydrothermal fluids as they are found at the various investigation areas. Phase separation seems to be the key to explain the tremendous differences between the found hydrothermal fluids, regarding their on-site parameters and especially their element concentrations. Still the submarine hydrothermal system Panarea is far to complex to be explained by one single model, further research is needed to fill all remaining gaps.

Zusammenfassung

Während der Feldkampagne 2015 wurden die hydrothermalen Fluide von neun verschiedenen Untersuchungsgebieten des submarinen hydrothermalen Systems Panarea beprobt (inklusive des Grundwassers der Insel Panarea). Die Vor-Ort-Parameter charakterisieren die gefundenen Fluide als sauer (pH $<$ 2,4 - 5,5), reduziert (E_H um die -50 mV) und hoch mineralisiert (bis zu 120 mS/cm). Die Untersuchungsgebiete Black Point, Fumarolic Field, Hot Lake und La Calcara unterscheiden sich durch ihre Vor-Ort Parameter und durch die Konzentrationen der gefundenen Elemente von allen anderen Punkten und dem lokalen Meerwasser. Durchgeführte Analysen mit IC und ICP-MS belegen eine extreme Anreicherung der Hauptionen des Meerwassers in Kombination mit einer Abreicherung von Mg^{2+} und SO_4^{2-} in den Untersuchungsgebieten Black Point, Fumarolic Field und Hot Lake. Im Gegensatz dazu sind in La Calcara Konzentrationsabreicherungen im Vergleich zum Meerwasser zu finden, welche Hinweise auf eine nur schwach mineralisierte Wasserquelle sind. Extreme Anreicherungen von Spurenelementen sind in Black Point und Hot Lake zu finden, wohingegen die seltenen Erden in extremer Anreicherung nur in Black Point zu finden sind. Problematisch während der Probennahme ist das umgebende Meerwasser, da es in vielen Fällen typische hydrothermale Merkmale überschreibt, z.B. in den Untersuchungsgebieten Bottaro Nord/West und Area 26.

Die Verhältnisse der stabilen Isotopen von Wasserstoff und Sauerstoff weisen auf $\delta^{18}O$ angereichertes Meerwasser als dominante Quelle des hydrothermalen Systems hin. Eine mögliche Verbindung des Grundwasser der Insel Panarea und den Proben von La Calcara kann somit ausgeschlossen werden.

Im zweiten Teil wurden über 200 Proben hydrothermalen Wassers, welche zwischen 2006 und 2015 vom Scientific Diving Center Freiberg (SDC) genommen wurden, statistisch ausgewertet. Durchgeführte Faktorenanalysen identifizieren zwei Faktoren: Der erste Faktor repräsentiert hauptsächlich Spurenelemente und seltene Erden und damit einen wahrscheinlichen magmatischen Einfluss, der zweite die Hauptbestandteile von Meerwasser. Hot Lake und Fumarolic Field werden vom zweiten, Black Point vom ersten Faktor repräsentiert, was auf unterschiedliche Fluidtypen, oder unterschiedliche Entstehungsvogänge an diesen Untersuchungsgebieten schließen lässt. Kruskall-Wallis-Tests differenzieren Hot Lake, Fumarolic Field, Black Point und teilweise auch Area 26 vom Rest der Untersuchungsgebiete und vom Meerwasser, welches den hydrothermalen Charakter dieser Gebiete bestätigt. Basierend auf diesen Grundlagen wird ein neuen Modell vorgestellt, welches den Aufstieg und die Bildung der an den jeweiligen Tauchpunkten gefundenen hydrothermalen Fluide erklärt. Phasentrennung scheint hierbei der Schlüssel zu sein, um die extremen Unterschiede in den Elementkonzentrationen erklären zu können. Trotzdem vermag dieses Modell nicht alle der hochkomplexen Vorgänge des submarinen hydrothermalen Systems Panarea zu erklären, sodass weitere Forschung diese verbleibenden Wissenslücken schließen muss.

Contents

List of Figures

List of Tables

List of abbreviations

BN	Bottaro Nord
BP	Black Point
BW	Bottaro West
E$_H$	Redox Potential [mV]
EC	Electrical Conductivity [mS/cm]
EMF	Electromotive Force [mV]
FA	Factor Analysis
FF	Fumarolic Field
HL	Hot Lake
IC	Ion Chromatography
ICP-MS	Inductive-coupled plasma - mass spectrometer
KWT	Kruskal-Wallis-Test
CAL	La Calcara (older abbreviation)
LC	La Calcara
LC BR	La Calcara Black Rock
LC C	La Calcara Chimney
LC NR	La Calcara New Rock
m.a.s.l.	meter above sea level
n.a.	not available
n.d.	not determined
P21	Point 21
PdP	Pozzo di Pina
REE	rare earth elements
T	temperature
WRI	Water-rock interactions
P	pressure

1. Introduction

1.1. Geology

The Panarea volcanic group consisting of the island Panarea and its associated islets Basiluzzo, Dattilo, Panarelli, Lisca Bianca, Bottaro, Lisca Nera (Lucchi et al. 2013) is located in the southwest of Stromboli and represents the eastern edge of the Aeolian Islands (cp. figure 1.1). Panarea and the islets are the remaining exposed parts of an eroded volcanic complex with a height of ca. 1700 m above the seafloor, 18 km diameter at the 1000 m isobath and its highest point at 421 m a.s.l. (Punta del Corvo, Panarea) (Chiodini et al. 2006; Lucchi et al. 2013). A shelf with an outer rim at depths between 100 and 130 m b.s.l. forms the ca. 60 km^2 flat summit from which Panarea and the other islets rise above sea level (Lucchi et al. 2013) (cp. figure 1.2). In the east of Panarea the islets Panarelli, Dattilo, Lisca Nera, Bottaro and Lisca Bianca trace a semicircular structure which encircles a shallow depression with depths between 25 and 30 m and a diameter of 1 km (Gabbianelli et al. 1990; Lucchi et al. 2013), as shown in fig. 1.2.

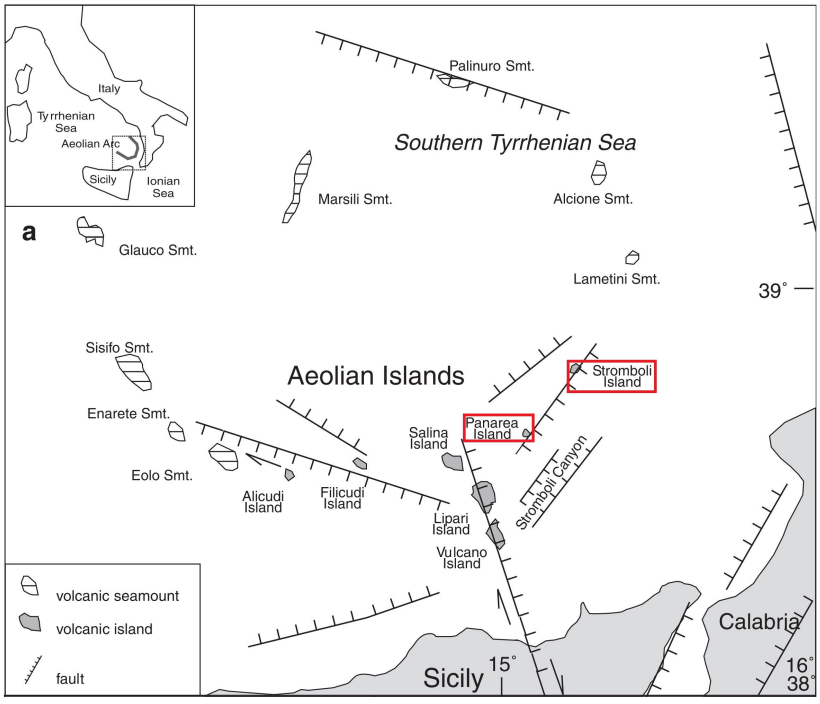

Fig. 1.1.: Geographical location of Panarea and the Aeolian Island Arc, modified after Chiodini et al. (2006).

The islets and the depression are home to a widespread active fumarolic field exhaling hydrothermal gases and fluids (Esposito et al. 2006; Gabbianelli et al. 1990, 1993; Italiano and Nuccio 1991). Besides this field additional fumarolic activity can be found on the northeast

coast of Panarea at the beach Calcara (cp. fig. 2.1) and the investigation area La Calcara (cp. fig 1.2) and in the vicinity of Basiluzzo (Lucchi et al. 2013).

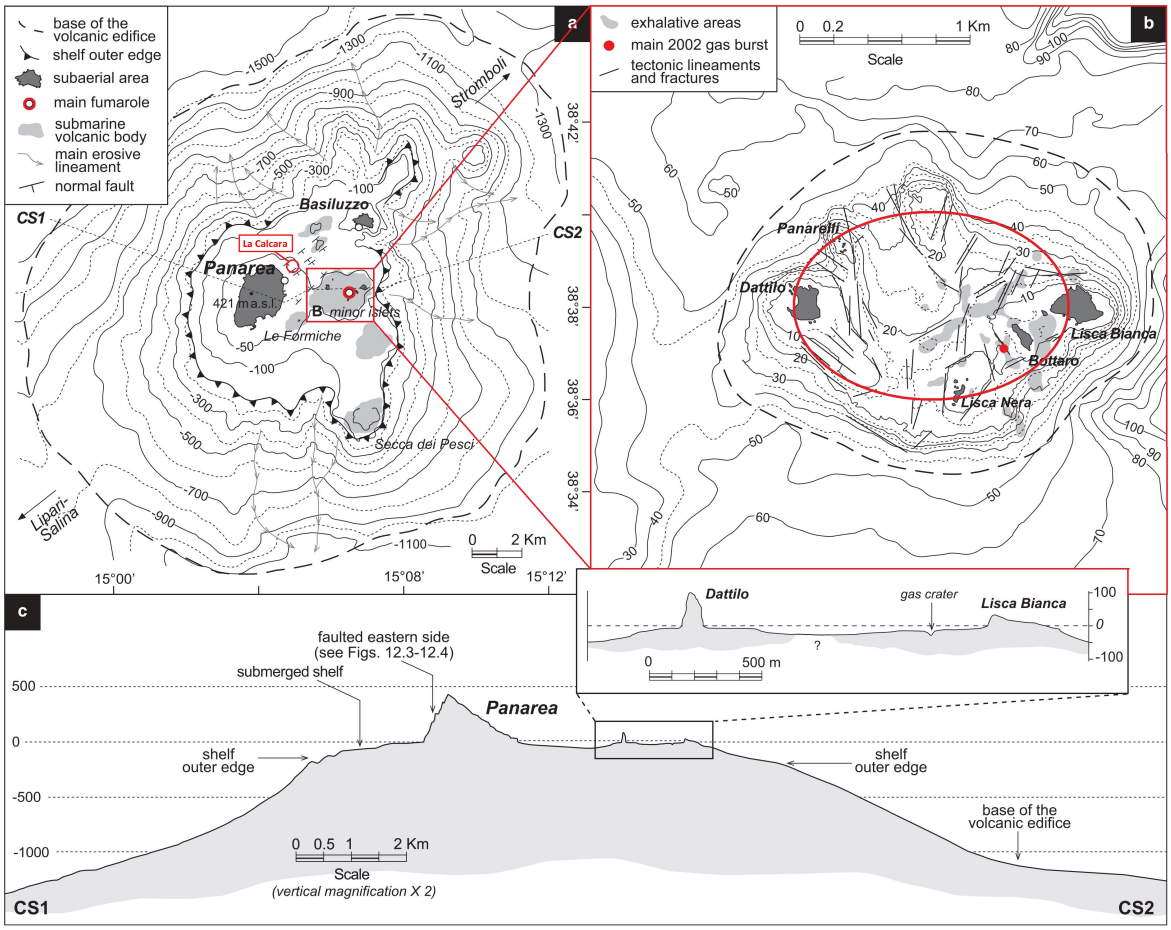

Fig. 1.2.: Location and geological setting of Panarea, encircled in red the main investigation area and the proposed caldera, modified after Lucchi et al. (2013).

A short note should be placed here, regarding the naming of the gas and fluid exhalations and the mentioning of fumaroles, mofettes and solfatares: Fumaroles (it. *fumare* = smoking) are defined as volcanic gas-steam exhalations with various temperatures and chemical compositions, able to either dissolve surrounding materials or to sublimate materials (Murawski and Meyer 2010). Mofettes (Neapolitan folk expression) however are cool volcanic CO_2 exhalations, while solfatares (Italian locality, near Solfatara (Naples)) are fumaroles with temperatures from 100 to 250°C, containing H_2S, often place of iron sulfide precipitations and elementary sulfur (Murawski and Meyer 2010). On and near Panarea different types of gas and fluid exhalations or combination of both are found, making the correct naming somehow difficult. Also the changing chemical composition, various ratios of CO_2 and H_2S and different temperatures are reason to argue about the correct naming. In this work mostly the term exhalation point of either gas, fluid or a combination of both will be used in addition to the term "fumarole" as it is done in the literature about the Panarea system.

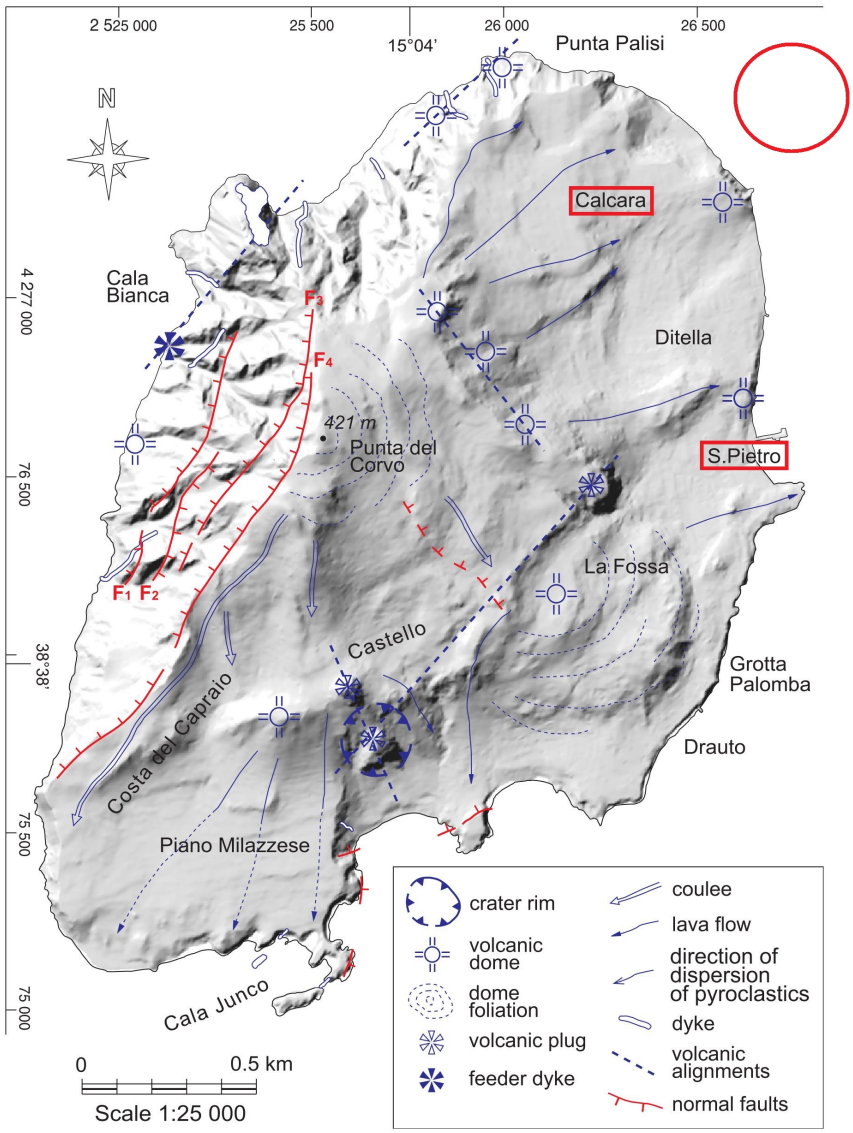

Fig. 1.3.: Morphological sketch of Panarea based on a DEM with volcanic features in the Gauss-Boaga-System (IGM). In red squares: Calcara as main investigation area (including red circle as location of fumaroles) and S. Pietro as starting point for the scuba dives, after Fabris et al. (2010) and Lucchi et al. (2013).

Both the Panarea volcanic group and Stromboli are the subaerial parts of a 45 km long volcanic belt situated along a major NE-SW regional fault system (Romagnoli et al. 2013), as shown in figure 1.1. The NE-SW oriented tectonic trend is found in both subaerial and submarine features of the Panarea volcanic group, e.g. directions of dykes, major faults and volcanic alignment and a submarine volcanic ridge in the NE of Basiluzzo (Lucchi et al. 2013). Furthermore a pattern of minor fractures and lineaments forming a NE-SW and NW-SW tectonic trend is clearly connected to submarine fumarolic activity in the depression between the islets in the east of Panarea (Esposito et al. 2006).

Investigations on fumarolic activity between Panarea and Stromboli strongly suggest a fluid-pressure related dependency based on a common reservoir between Panarea and Stromboli.

Hence the Panarea volcanic group and its fumarolic activity can be linked to the eruptive behavior of the Stromboli volcano (Heinicke et al. 2009).

Petrochemically Panarea consists mainly of andesitic and dacitic features like lava domes, pyroclastics and flows, showing a high-potassium calc-alkaline (HKCA) affinity (Calanchi et al. 2002). Besides shoshonitic basalts found at submarine centers, thin layers of mafic calc-alkaline (CA) rocks exist in late erupted strombolian scoriae (Calanchi et al. 2002). The latter show similar geochemical and radiogenic isotopic compositions as samples from the western part of the Aeolian Arc whereas the composition of HKCA and shoshonitic basalts place the island between the chemical composition of Vulcano and Stromboli as a mixture of western arc mantle and mantle of Stromboli, making Panarea a transition island between both systems (Calanchi et al. 2002).

1.2. Hydrothermal systems

Considering that over 80% of the active volcanoes in the world are found in the oceans and the majority of submarine superficial hydrothermal systems are situated at plate margins (Lowell 1991; Sigurdsson 2000), it is not surprising that the Panarea volcanic group, as part of an active back-arc system, is a location of subaerial and submarine hydrothermal activity (Hannington et al. 2005). 65% of the known submarine superficial hydrothermal systems are located at mid-ocean ridges, 22% at back-arc basins, 12% at volcanic arcs and 1% at intraplate volcanism (Baker and German 2004; Hannington et al. 2004).

All of the above mentioned hydrothermal systems have common features: (1) heat sources for the convective system, (2) recharge areas of the infiltrating fluids, (3) circulation cells of the convective moved fluids within the crust and (4) discharge areas marked by points of exhalations (vents, fractures) (Piranjo 2010). Most fundamental are the heat source and the fluid(s) of a hydrothermal system. The heat source provides the necessary energy for the hydrothermal system, whether it originates from magmatic sources, the geothermal gradient, radiogenic decay, metamorphism or a combination of these sources (Piranjo 2010). The ascent of hydrothermal fluids is steered by the heat source and small pathways in the bedrock (cracks, fissures etc.) generating a "plumbing" effect, which let the fluids ascent driven by high pressure and temperature (Piranjo 2010).

Fluids in hydrothermal systems generally can have their origin in a variety of sources like meteoric water, seawater, connate water, magmatic water, juvenile water and any thinkable combination (Pichler 2005; Piranjo 2010). Isotopic signatures, chemical compositions, temperature profiles and gas contents as geochemical indicators and tracers are strongly affected by the mixing of different water sources (Pichler 2005). The original chemical composition of hydrothermal fluids strongly depends on the composition of the host rock, the residence time (available time for chemical/physical reactions), the temperature and possible direct magmatic contributions. Often the chemical composition of the fluids are the result of equilibrium or rather steady-state conditions between the fluids and the host rock and its mineral

assemblage (German and Seyfried 2014; Pichler 2005). Still the chemical composition can vary strongly from vent to vent on a time scale from minutes to years, making comparisons between different systems over time rather difficult (German and Seyfried 2014; Von Damm 1995).

Generally submarine hydrothermal systems are fed mainly if not entirely by seawater, altered by 4 main processes: (1) WRI plus phase equlibria, (2) phase separation, (3) biological activity (4) and magmatic degassing (German and Seyfried 2014).

WRI lead to gain or loss of constituents of hydrothermal fluids, leading to alteration of the bedrock and of the original seawater and subsequently to either enrichment or depletion of certain elements in the bedrock and/or the seawater (German and Seyfried 2014). High reaction kinetics at high temperatures regarding mineral-fluid interaction (or WRI) for most involved reactions let several authors assume the majority of the WRI take place near the heat source in a hydrothermal system (German and Seyfried 2014; Pester et al. 2011; Seewald and Seyfried 1990; Seyfried and Shanks 2004). Low temperature hydrothermal fluids venting diffusely through the upper part of the seafloor (temperatures up to 100°C) in submarine hydrothermal systems may have a chemical composition close to seawater, but are often enriched in gases such as CO_2, H_2S, NH_3, N_2, H_2, CH_4 and $B(OH)_3$ (Nicholson 1993; Piranjo 2010; Von Damm 2001) and in trace elements as Fe and Mn (Von Damm 2001). High CO_2 concentrations and very high He/heat ratios are an indicator for magmatic degassing within the hydrothermal system (German and Seyfried 2014). Low temperature hydrothermal fluids are also the place for possible biological activity, altering the chemical composition of the fluids by consuming or generating chemical species, e.g. precipitation of iron sulfides. In which dimensions this biological alteration takes place needs still to be answered (German and Seyfried 2014).

Typical high temperature submarine hydrothermal fluids have a low pH (< 4) (German and Seyfried 2014; Herzig and Hannington 2000; Mason 2013; Von Damm 2001), are strongly reducing and are depleted in SO_4^{2-} and Mg^{2+} but are enriched in H_2, CH_4, H_2, He, Si, Li^+, Fe^{2+} and Mn^{2+} (German and Seyfried 2014; Von Damm 2001). Mg^{2+} can form Mg-OH silicates generating H^+-cations leading to the low pH, typical for submarine hydrothermal fluids (German and Seyfried 2014; Seyfried and Shanks 2004). Furthermore low pH values < 3 are an indicator for precipitation of massive sulfides (producing protons) and/or of magmatic degassing of SO_2 and HF, as observed in hydrothermal systems located in back-arc basins (German and Seyfried 2014; Mottl et al. 2011). The strongly reducing conditions mobilize certain elements during water-rock interactions, e.g. Li, K, Rb, Cs, Ca, Sr, Si, transitions metals in their reduced forms, especially Fe, Mn, Cu and Zn and lead to their enrichment which can be several magnitudes above the local seawater (German and Seyfried 2014; Von Damm 2001). Na^+ can be either depleted, due to Na-Ca replacement reactions in plagioclase-feldspars (albitization) in combination with an enrichment of Ca^{2+}, or enriched depending on the Cl^- concentrations and the electroneutrality of the hydrothermal fluids (German and Seyfried 2014; Von Damm 2001). Mg^{2+}-cations are removed from the seawater by WRI and

alteration of the bedrock, taking typically the places of Mn^{2+}, Ca^{2+}, Fe^{2+} and Cu^{2+}, leading to a depletion of Mg^{2+} and a typical enrichment of Mn^{2+}, Ca^{2+}, Fe^{2+} and Cu^{2+} in submarine hydrothermal fluids (German and Damm 2004). SO_4^{2-} is removed from the seawater due to precipitations in the subsurface of the recharge area when the temperature exceeds 130°C and $CaSO_4$ precipitates from seawater (Bischoff and Seyfried 1978) and reduction to sulfides (mainly H_2S) (German and Seyfried 2014; Ono et al. 2007; Shanks 2001). Cl^- remains as the almost only anion in the solution, while Br^- (in seawater usually proportionally to Cl^-) exists in neglectable concentrations in terms of the ion balance (German and Seyfried 2014; Von Damm 2001).

The Cl^- concentrations in absence of any major mineralogical sinks (except for halite (NaCl)) are mainly influenced by phase separation of the hydrothermal fluids (German and Seyfried 2014). Also magmatic HCl formed from NaCl, H_2O and Si (products are Na_2SiO_3 and HCl) under high T and P conditions (Truesdell et al. 1989) can dissolve and thus add more Cl^- to the hydrothermal fluids, explaining further Cl^- excess compared to the local seawater and the low pH of the systems. During the buoyancy-driven ascent of the hot hydrothermal fluids phase separation can occur e.g. if the pressure decreases: the phase separates into a low-density vapor phase and into a metal-rich, high saline, dense brine (Bischoff and Rosenbauer 1984). After phase separation the vapor phase can become extreme dense, while the liquid phase can expand until both phases reach the critical point of 374°C and 225 bar (fresh water) or 407°C and 298 bar (salt water) (Bischoff and Rosenbauer 1985; Driesner 2007; Von Damm 2001). Eventual mixing during the ascent makes them indistinguishable (Piranjo 2010; Williams-Jones and Heinrich 2005). Seawater as proposed main source of water in submarine hydrothermal systems undergoes phase separation after it is heated up in the subsurface and begins to ascent. The fluid will be "split" into a brine(higher concentrations than original seawater) and water vapour (less Cl^- than original seawater) (German and Seyfried 2014). Remixing of both the brine and the water vapour during the ascent with seawater result in a a high Cl^- phase (brine + seawater) and a low Cl^- phase (water vapour + seawater). The high Cl^- concentrations as a result of the phase separation determine in combination with the cation/Cl^- ratio of the local seawater whether a cation has been removed from the hydrothermal fluids or added (e.g. Na^+), to maintain electroneutrality (Von Damm 2001). Almost all cations form chlorocomplexes with Cl^-, hence the concentration of Cl^- (varying from <6% to 200% of seawater concentrations in known submarine hydrothermal systems) determines partly the maximum concentrations of cation species (German and Seyfried 2014), according to the neutral electrical balance of a water. Observations and experiments have proven most cations and Br^- (s. above) maintain their cation/Cl^- ratio even during/after phase separation (Berndt and Seyfried 1990; Damm et al. 2003; German and Seyfried 2014; Von Damm 2000). Exceptions are B, often found in the low Cl^- phase (Berndt and Seyfried 1990) and Br^-, affected by halite precipitation and exclusion from the mineral structure, leading to a changed Br^-/Cl^- ratio (Berndt and Seyfried 1990; German and Seyfried 2014; Von Damm 2000).

Sampling these fluids at the surface the chemical composition contains information about chemical and physical conditions of the subsurface imprinted in the fluids during their ascent, such as the P and T conditions during the reactions leading to the chemical composition of the fluids and enables to gain insights about the hydrothermal system (German and Seyfried 2014; Pichler 2005).

Depending on their location hydrothermal systems are categorized in two types: deep-sea or terrestrial systems (Pichler 2005). Additional to these two types in the last two decades a transitional system was classified, located in shallow marine near-shore environments or at the summits of seamounts (Pichler et al. 1999; Sedwick and Stuben 1996). Systems of this type like the system near Panarea have characteristics of terrestrial systems and are transient between terrestrial hot springs and deep-sea hydrothermal vents (Pichler 2005).

While the origin of the hydrothermal fluids in some systems is relatively easy to predict (e.g. for hydrothermal systems located at mid-ocean ridges seawater will be the most likely source with an possible magmatic fraction, on-land hydrothermal systems are mostly recharged by meteoric water and maybe a magmatic fraction) the sources for transitional systems are hard to determine (Giggenbach 1992; Pichler 2005), because marine and terrestrial sources are combined resulting in a complex system with a mixture of characteristic signatures.

1.3. Investigation areas

The Scientific Diving Center Freiberg (SDC) has investigated several areas over the last 10 years to cover different aspects of the submarine hydrothermal system Panarea. The main investigation areas are described in detail by Sieland (2009) and Stanulla (2012). Since 2012 several changes in the environment of the investigation areas occurred, e.g. Hot Lake is now a ”cold lake” with temperatures close to the seawater temperature. The fumarolic activity at the nearby Fumarolic Field and in Point 21 has declined since the first investigations in 2006. All other areas seem to be mostly unchanged, except for minor changes like sea grass coverage etc. As point of interest the investigation area La Calcara is described in more detail.

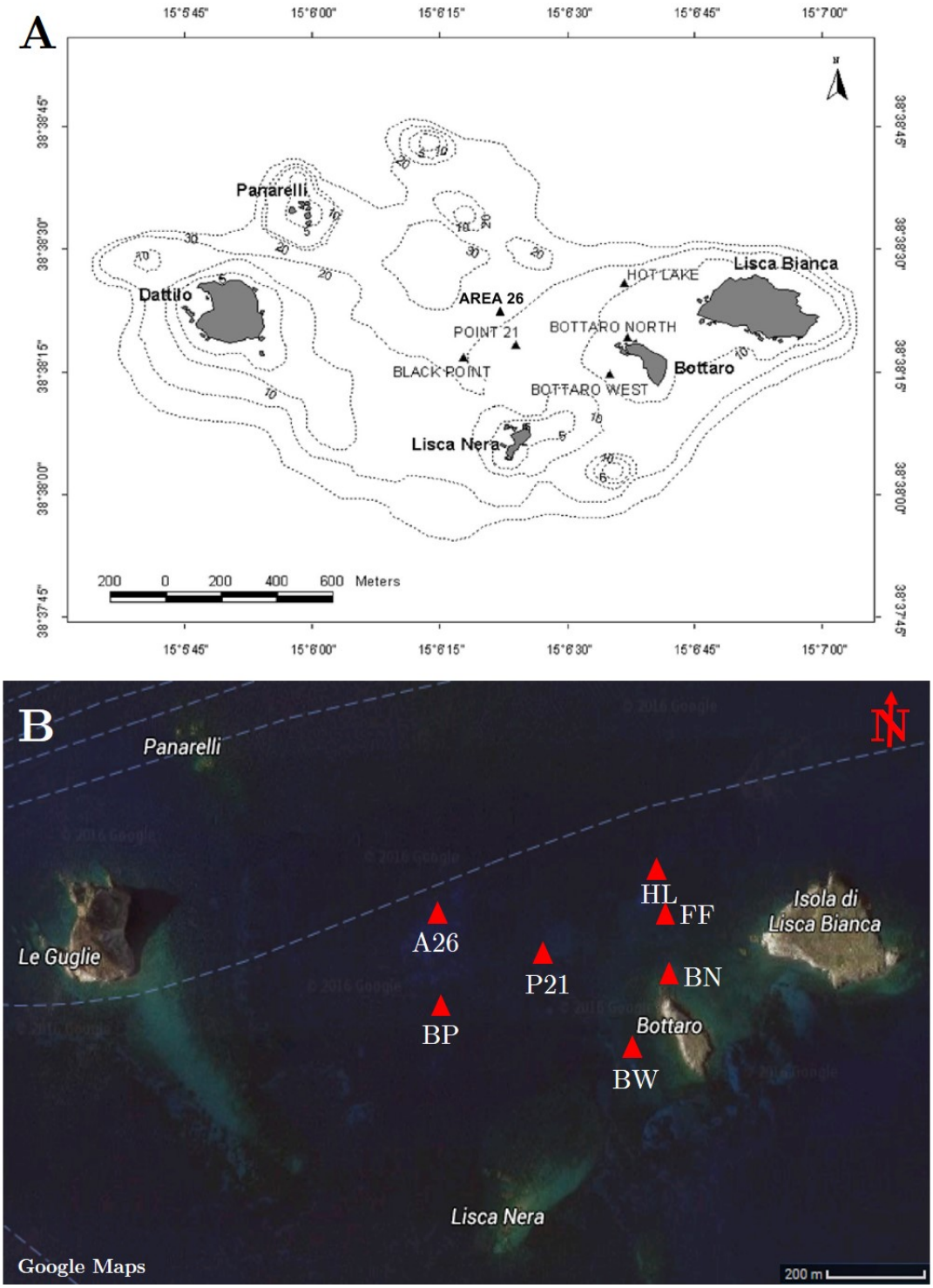

Fig. 1.4.: A: Location of the different investigation areas between the islets in the east of Panarea, after Sieland (2009) and Rohland (2007). B: Satellite picture of the areas, taken and modified from Google Maps (2016b).

1.3.1. La Calcara

La Calcara is closely located to the beach Calcara in the north-east of Panarea (cp. fig. 1.3). In an average depth of around 23m ample sand fields with ripples of around 30cm height alternate with meadows of see grass. The area is characterized by few, mostly moderate gas exhalation points, often in connection with sintered hydrothermal channels within the sediment (cp. fig 1.5. Temperatures up to 132°C and a weak acidic pH of around 5 characterize the submarine hydrothermal fluids of La Calcara.

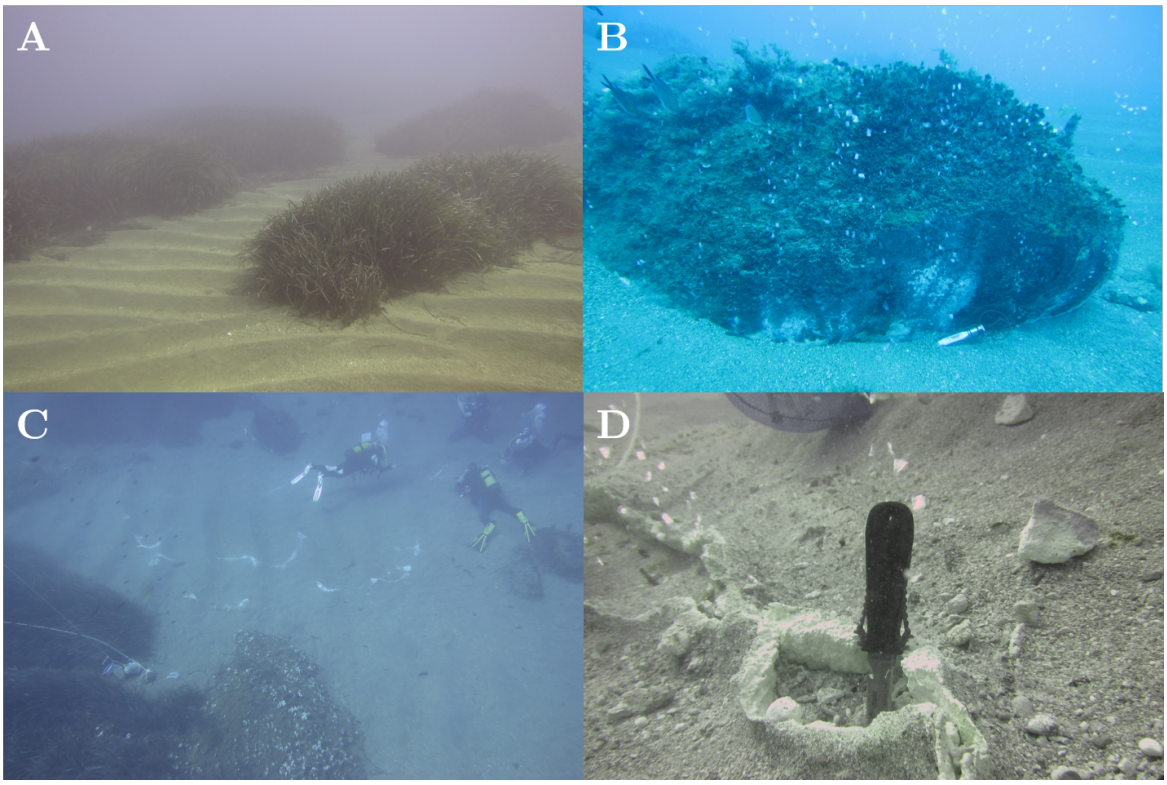

Fig. 1.5.: Investigation area La Calcara and its characteristics. A: ample sand fields, ripples and see grass meadows. B: Sampling point Black Rock with bacteria mats at the exhalation point of hot thermal water. C: precipitate channels in the sediment, marked by white bacteria. D: Close up of a precipitated channel with ascending gas bubbles, diving knife has a size of approximately 20cm. (SDC 2005-2015)

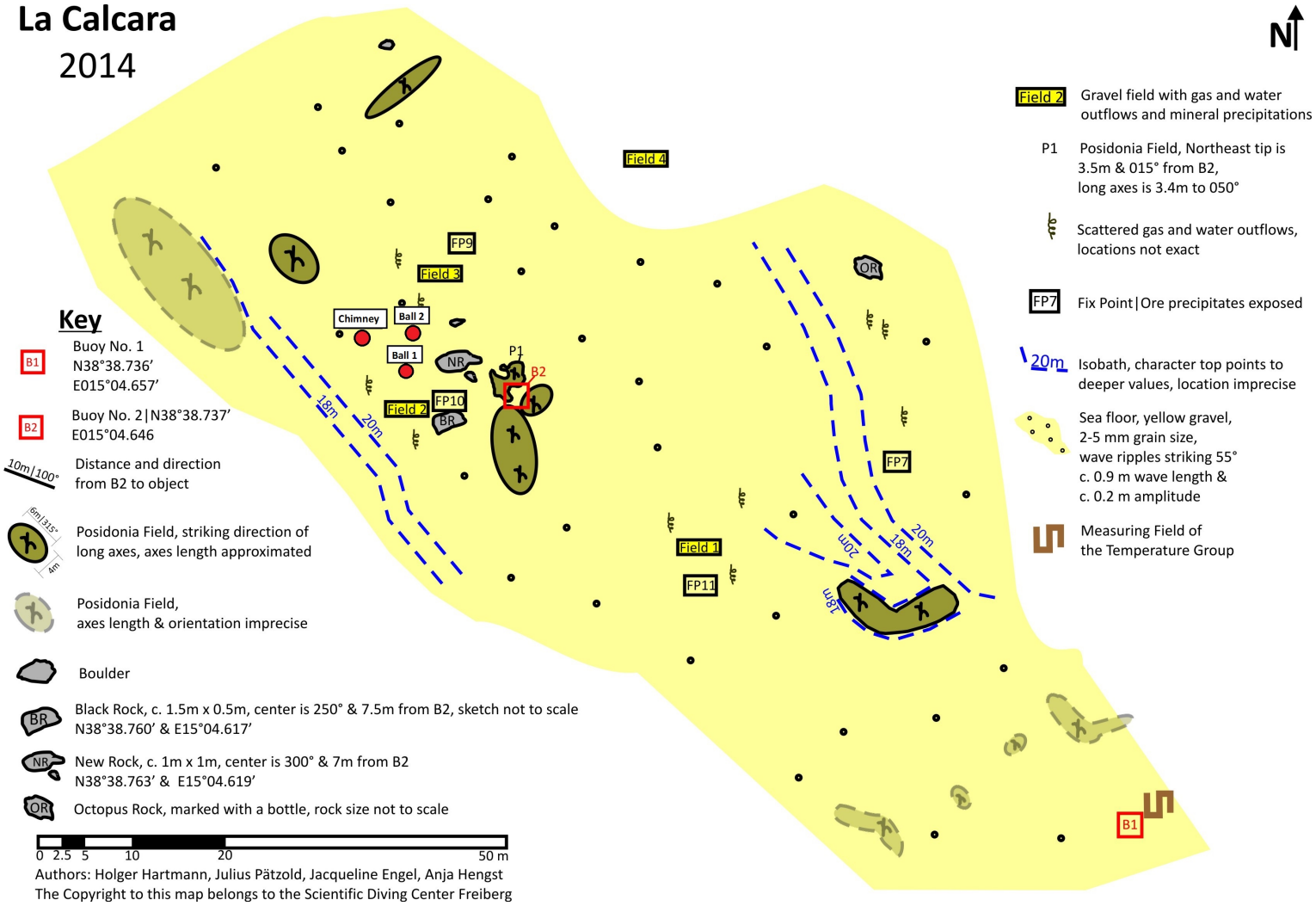

Fig. 1.6.: Investigation area La Calcara and its main features. Buoy 2 is used to descend and to take samples in the vicinity around it, e.g. from Black Rock. New sampling points are marked in red and described in white squares. (SDC 2005-2015)

1.4. Hydrothermal System Panarea

A probably oldest theory about the origin and evolution of the hydrothermal system Panarea is proposing a deep geothermal body with temperatures around 270°C, fed by mainly seawater and a magmatic component, which contributes thermically to the two different overlaying bodies with temperatures between 170-240°C (Italiano and Nuccio 1991). One of them is thought to be beneath Panarea, fed by meteoric waters, the other fed by sea water.

The interest in the hydrothermal system Panarea increased in November 2002 as a heavy gas outburst occurred between the islets of Panarea. Previous seismic activity in form of an earth quake on September 6th 2002 with a magnitude of 5.6 in the southern Tyrrhenian Sea, volcanic activity of Mt. Etna starting on October 27th, the eruption of the Stromboli on December 28th and the collapse of the north-western flank inducing two minor tsunamis formed an evident chain of events. This chain and the creation of a new submarine crater between the islets "Lisca Nera" and "Bottaro West" on November 3rd connected the system Panarea with the Stromboli and lead to further investigations (Esposito et al. 2006; Tassi et al. 2009). Several models were proposed to explain the processes which lead to the 2002 outburst, often with the notation to built a warning system for future outbursts.

Following the 2002 outburst a deep bi-phase reservoir is proposed (Caracausi et al. 2005), containing a high saline solution (Tassi et al. 2009) and vapor (containing 12mol% CO_2) in which CO, CH_4 and H_2 equilibrate at around 350°C and 16 MPa (confirmed by (Taran 2005)).

Two other models try to explain the origin of the submarine emissions (Chiodini et al. 2006): (1) Either a hydrothermal system with a-typical redox conditions (more oxidizing than expected) and estimated temperatures about 300°C and bulk fluid pressure around 100 bar, (2) or residual volcanic gases, depleted in acid gases due to condensation and reactions with seawater, with estimated temperatures about 350-450°C feed the emissions.

The system is furthermore described as a continuous gas producing hydrothermal system in which sudden heavy gas releases can occur such as the one in November 2002 if the gas pressure exceeds the tensile forces or sediment pressure of the overlaying bedrocks (Esposito et al. 2006).

Significantly changes in the isotopic and chemical signatures of the gases from typical hydrothermal to magmatic signatures and the occurrence of magmatic gases such as SO_2, HCl and HF after the 2002 outburst prove magmatic contributions to the system (Caliro et al. 2004; Capaccioni et al. 2005, 2007; Caracausi et al. 2005; Chiodini et al. 2006). One explanation could be based on these contributions with a convective heat pulse from a deep magmatic body, causing the 2002 outburst by forming a transient bi-phase liquid plus gas plume interfering with the hydrothermal aquifer based hydrothermal system (Capaccioni et al. 2007).

The assessment of data collected from 2002 to 2013 indicates that the 2002 outburst changed the chemistry of the exhaled hydrothermal fluids of the hydrothermal system Panarea significantly (Tassi et al. 2014). Although the plume of dry volcanic gas, replacing the signals

of the hydrothermal aquifer has already disappeared in 2003 (Capaccioni et al. 2007), the chemical composition of the gases determined in the 1990s has not been restored in 2012-2013 (Tassi et al. 2014). Furthermore the continuous report of new fumarolic vents in respect to the formerly reported small number of vents (Calanchi et al. 1995; Gabbianelli et al. 1990; Italiano and Nuccio 1991) and significantly decreasing H_2/CO ratios may imply an increasing CO_2 pressure over time and could indicate a new outburst similar to the one in 2002 (Tassi et al. 2014) and according to various models of a continuous gas producing system (Esposito et al. 2006; Tassi et al. 2009).

Contrary to the gases the chemical composition of the hydrothermal waters of the Panarea system seem to be restored after the 2002 outburst, but still show varying compositions (Tassi et al. 2009). In accordance with the explanation of the 2002 outburst three end members were determined based on the chemical composition of water samples between 2004 and 2007 (Tassi et al. 2009): (1) local unmodified Mediterranean seawater, mixed during the ascent through unconsolidated sediments or the sample procedure, (2) concentrated Mediterranean seawater, condensed by boiling and phase separation leading to an increased salinity and (3) chemically modified Mediterranean seawater, with low pH, strong Cl excess compared to seawater, impacted by hot, acidic, HCl bearing deep fluids. Changes in the permeability, due to seismic events and self-sealing induced overpressure induce changes in the chemical composition of the hydrothermal fluids. These changes could be used to forecast new outbursts (Tassi et al. 2009).

Still the origin and the sources of the hydrothermal waters exhaled at the submarine vents in the vicinity of Panarea are not conclusively determined. A classification of the hydrothermal fluids into three groups exists (Sieland 2009). All groups consist mainly of seawater with smaller magmatic and neglectable meteoric components, differing regarding their concentrations of main cations and anions, their reservoir temperature and their REE patterns.

A compilation of the existing theories about the origin of the water sources contributing to the hydrothermal system at Panarea is shown in table 3.2 based on ratios of the stable isotopes of Hydrogen and Oxygen (δ^2D and δ^{18}O or D/O) (Müller 2011). The isotopic composition of hydrogen and oxygen has been an useful tool since the 60ties to determine the origin of water. Due to fractionation processes during almost all of chemical and physical reactions water undergoes during it follows the hydrological cycle, the isotopic composition of water is changed characteristically. These characteristic changes enables to determine e.g. the origin of precipitation or the location of the recharge area of groundwaters. Five possible end members could theoretically influence the isotopic composition as shown in tab. 3.2 through mixing processes. Furthermore water-rock interactions (WRI), high temperature fractionation with temperature depending fractionation factors and phase separation during the ascend can influence the isotopic composition of the hydrothermal waters (Gat 2010).

One conclusion of the literature is that depending on the exhalation point the sources of water and their fractions vary (Müller 2011). For different exhalation points within the system different fractions of Mediterranean seawater, magmatic water and local meteoric water or

groundwater are determined (Müller 2011) using ternary plots. At the exhalation points in the north east of Panarea near Calcara heavy $\delta^{13}C$ and $\delta^{18}O$ values suggest a relatively high magmatic component, but the heavy $\delta^{13}C$ value is not unproblematic due to the assumed impact of evaporates of the Messinian Crisis (Müller 2011).

investigation areas like Area 26, Bottaro Nord, Black Point, Hot Lake and Fumarolic Field and Point 21 seem to contain higher fractions (around 30%) of meteoric water (Müller 2011) (see fig. 1.4).

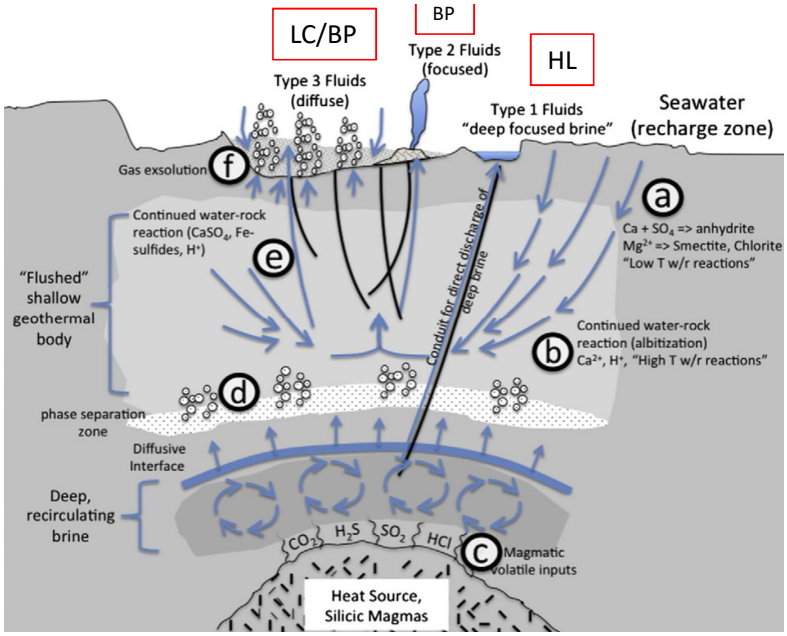

Fig. 1.7.: Latest theory about the evolution of the submarine hydrothermal fluids of the hydrothermal system Panarea, after Price et al. (2015). a) low temperature water-rock interactions, b) high temperature water-rock interactions, c) magmatic volatile input, d) phase separation, e) continued water-rock reactions, f) degassing of dissolved volatiles.

The latest hypothesis about the evolution of the hydrothermal fluids in the Panarea system (Price et al. 2015), is based on former findings (Italiano and Nuccio 1991; Tassi et al. 2009). Fig. 1.7 gives an overview over the basic principles of this theory. The authors define three distinct types of hydrothermal fluids, all of them marked by higher temperatures, lower pH and Mg^{2+} and SO_4^{2-} contents, compared to the local seawater. While type 1 fluid is marked by a high salinity, higher than type 2 and 3, the latter is close to seawater and shows a comparable chemical composition as seawater. Both type 1 and 2 originate from a layered hydrothermal system and type 1 originates from a deep, high salinity reservoir, while type 2 comes from a shallower, reservoir with a lower salinity. Both fluids develop in a system marked by a recirculation of brine fluids combined with a long-term loss of steam and volatiles, induced by phase separation, resulting in the highest Cl-end member concentrations to date. The authors speculate furthermore, type 3 could be influenced by degassing of volatiles and dissolution of CO_2, H_2S and various other gases into the fluid.

1.5. Aim of this thesis

This thesis aims to provide further understanding of the submarine hydrothermal system of Panarea including the groundwater of the island Panarea. The first part of the thesis includes the field work of 2015 in Panarea: Multiple water samples taken from the submarine exhalation points at the investigation area “La Calcara" are compared to samples taken from other areas and from the to our knowledge only accessible well “Pozzo di Pina" (PdP) (Italian for Pina’s Well) located at the hotel “Oasis di Pina". Analyzing the water samples for their general chemical composition with IC (Ion Chromatography), ICP-MS (Inductive coupled plasma-mass spectrometer) and the isotopic composition regarding Deuterium and Oxygen gives information about the origin of the submarine hydrothermal fluids. A special focus lays on the area La Calcara in the north east of Panarea (see fig. 1.2) and its possible connection the groundwater of the island Panarea.

In the second part over 200 hydrothermal water samples of the submarine hydrothermal system Panarea collected between 2006 and 2015 by the Scientific Diving Center Freiberg (SDC) are statistically evaluated. Factor analysis and Kruskall-Wallis-Test identify characteristics and trends of on-site parameters and/or element concentrations of the different investigation area, explaining the development of the hydrothermal fluids. The results of the evaluation are compared to the findings of the field campaign 2015 and partly to the latest hypothesis regarding the hydrothermal system Panarea of Price et al. (2015). In the end a model is developed, which explains the origin and evolution of the submarine hydrothermal fluids at the different investigation area in the light of the presented results of this thesis. Furthermore remarkable investigation area will be described in their main characteristics providing fundamentals for further work on the submarine hydrothermal system Panarea.

2. Methods

2.1. Sampling procedures

2.1.1. Groundwater

To put it mildly, the sampling conditions for groundwater on Panarea are adverse: Most former known wells are abandoned, filled or simply not accessible. In the north-east of Panarea directly at the beach "Calcara" natural fumaroles or solfatares can be found (compare with fig. 2.1 A - C). At these points, located within the beach ridge, close to the remains of an ancient settling of the roman area (compare with fig. 2.1 A) volcanic gases exit the underground. It is suspected that at these exit points also geothermaly impacted groundwater was found, used to fill thermal pools in former times. Unfortunately but unsurprisingly during the field campaign 2015 none of these exit points delivered any water, because of the lower groundwater recharge during the summer. Still sulfur precipitations and a strong smell of H_2S are indicators of the existence of the springs and of the thermal influence on these springs (compare with fig. 2.1 B - C).

Nevertheless three samples from a well have been taken. The well ”Pozzo di Pina” (pozzo = italian for well) is located on the perimeters of the hotel "Oasis da Pina". Within the well a submersible pump is installed and the pumped water is used - at least during the tourism season - on a daily basis to fill a thermal pool for the guests (compare fig. 2.2 B and a hose with a length of ca. 30 m connects the pump with the tap (verbally communicated by Franco Italiano, 09/04/2015). Still the use of a pump is doubted by the author, because a submerged pump in the later described conditions of the groundwater would face a considerable wearing. So one also has to consider a possible artesian aquifer or even an aquifer standing under considerable volcanic gas pressure, forcing the water upwards. The water exiting the tap was under considerable pressure and in the beginning of the sampling a considerable amount of foam built up, vanishing after 5-10 minutes of steady water flow. The on-site parameters EMF, Temperature, EC, pH and after cooling of the hot water the O_2 content were measured using a plastic container overflown by the water, in which the tap was submerged. An installation of a flow through cell was not possible, given the above described circumstances of the well. The first sample was taken after the water runs for over 5 minutes (PAN_09032015_PdP), the second sample right in the beginning of the sampling process (PAN_09042015_PdP) and the last sample was taken, after the on-site parameters stabilized (PAN_09042015_PdP_equ) after 30 minutes of letting the tap running and five prior measurements (cp. tab. B.1 and fig. B.1). Table B.1 contains the on-site parameters from Pozzo di Pina. Information about the depth to groundwater, the depth of the well, filtration, pump type etc. are not available, hence further interpretation of the water chemistry is biased.

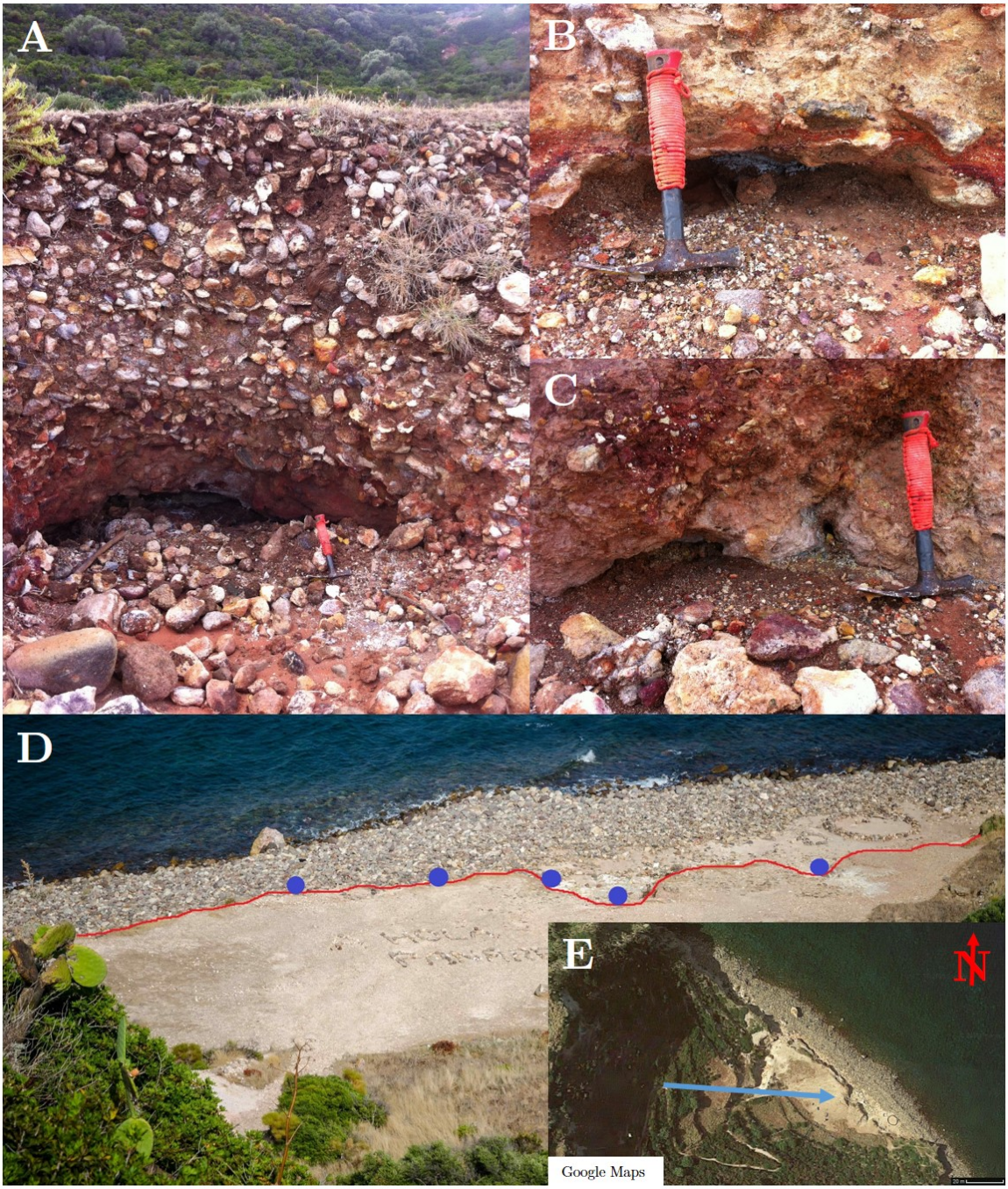

Fig. 2.1.: A-C: Various natural fumaroles/solfatares within the beach ridge of the beach Calcara with different precipitations e.g. of elemental sulfur and their location in the north-east of Panarea (compare to fig. 1.3). D: In red the beach ridge, in blue the locations of several exit points in various sizes. E: The viewpoint of D is marked as a blue arrow, modified from Google Maps (2016c) and SDC(2005-2015).

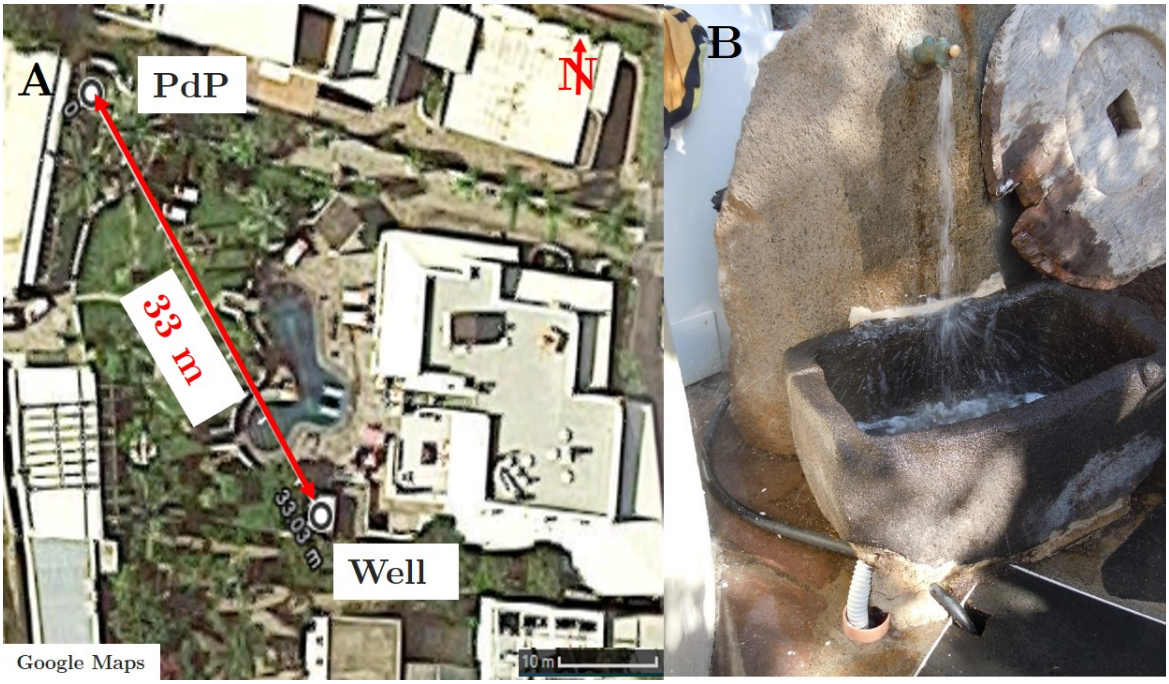

Fig. 2.2.: A: Location of the well and the tap (WGS 84: 38 38'16.0548"/15 04'30.1908"), modified after Google Maps (2016a) and SDC (2005-2015). B: Location of the well and the tap, modified after Google Maps (2016a) and SDC (2005-2015).The water at Pozzo di Pina exits the tap under high pressure.

2.1.2. Submarine hydrothermal waters

Sampling under adverse conditions like the submarine environment makes it necessary to use reliable and sometimes robust techniques to guarantee a successful sampling and to avoid any additional dives and hence more investment of time and money. The sampling procedure of hydrothermal waters is elementary: a syringe for medical or veterinary purposes (100 or 450 ml) is connected to a PTFE tube (or Teflon as brand name) via a three-way stopcock (see fig. 2.3). A hose (or tube) is suitable for discharge points from fractures occurring in hard ground or solid rock. A lance with a screen section at the bottom end is suitable in soft ground/ sediments. In the most simple case the screen is a zone of perforation by means of about 100 one-millimeter boreholes. The first syringe is filled two times: the first time to flush the tube and the syringe with hydrothermal fluids, the second time is the sampling itself. The 3-way stopcock enables the diver to flush the syringe without the necessity to flush the whole sampling tube by adjusting the stopcock accordingly. To avoid any infiltration of seawater into the sample, the syringe is filled slowly so that the estimated discharge rate of the exiting water equals the withdrawal rate. During this sampling campaign the sampling rate was 1-2 ml per second. Furthermore the syringes are not filled completely with fluid, because of the high pressure in the sampling environment (varying between 2-3.3 bars, depending on the sampling depth) gases are solved in the water sample which degas and expand during the ascent, and could push the piston out of the syringe. During the diving campaigns of the last years the handling of smaller syringes with a volume of 100 ml has been proven advantageous. After

the sampling, the syringes were closed with self-made rubber caps, to avoid any infiltration of seawater (cp. fig. 2.3). Even with these measures to avoid contamination by seawater, one has to consider the seawater surrounds the diver and its sample completely, hence the probability of a contamination with ambient seawater must always be considered regarding the interpretation.

After the ascend the syringes containing the samples were stored in the shadow on the zodiac and were brought to the field laboratory. The on-site parameters and the sample preparations were immediately conducted. Still between the sampling under water and the measurement of the on-site parameters and the sample preparation up to 45 minutes could elapse, increasing the risk of biasing the samples with e.g. oxygen from the atmosphere, changing e.g. the redox potential of the samples. Precipitations of constituents during this time are possible but due to the small time frame unlikely or of no greater concern. During his master thesis Seebauer took several water samples along transect lines leading away from hydrothermal fluids exhalations points at Area 26, La Calcara and Point 21 (Seebauer 2015). The total of eleven samples have been averaged to gain representative concentrations of constituents of the local seawater at the submarine hydrothermal system Panarea. This averaged seawater is later referred to as local seawater and is used to calculate the deviation of constituents in the submarine hydrothermal fluids compared to the local seawater. The water samples were prepared for their transport and later analysis in the laboratory at the Technische Universität Bergakademie Freiberg according to the analytical methods applied (s. tab. 2.1).

Tab. 2.1.: Sample preparation of taken water samples

Applied method	Preparation	Storage
On-Site parameters	none	none/immediate determination
Photometry	eventually filtration ($0.2\mu m$)	none/immediate determination
IC	filtration ($0.2\mu m$)	30/50 ml PE bottles
ICP-MS	acidification, filtration ($0.2\mu m$)	30/50 ml PE bottles
TIC and DOC	none	100 ml glass bottles, air free
Stable Isotopes	none	30 ml PE bottles, air free

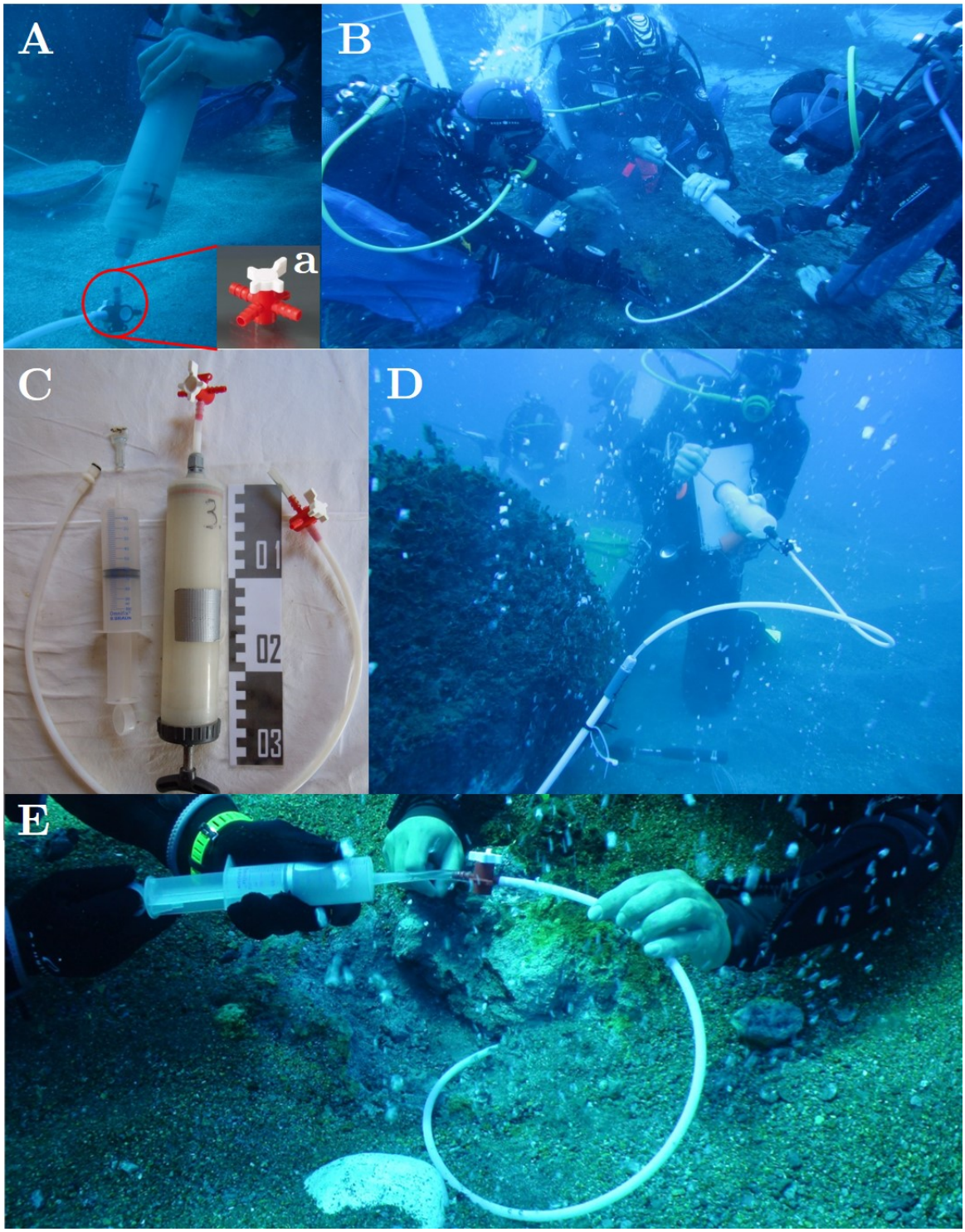

Fig. 2.3.: A: 450 ml veterinary syringe with 3-way-stopcock in close-up (a). B: team work during the sampling: diver on the left places the sampling tube, diver in the middle operates the syringe, diver on the right stabilizes and operates the 3-way stopcock and/or reaches for new syringes. C: 100 ml with rubber cap and 450 ml syringes, PTFE hose and 3-way stop-cocks. D: sampling with a PTFE lance. E: Diver on the right places the sampling PTFE tube, the other one operates the 100ml laboratory syringe. (SDC 2005-2015)

2.2. Analysis: Water chemistry

2.2.1. On-site parameters and Photometry

All samples were carefully decanted into standard glass laboratory beakers using the side of the beakers to let the samples trickle slowly into the beaker, avoiding an unnecessary turbulence and atmospheric contact. Afterward the measuring devices were placed and the beaker was sealed with Parafilm M® to avoid any further atmospheric contact of the sample. The temperatures of the samples were measured twice, in-situ (under water) with a temperature device GMH-3350 with 50 cm sensor length, and again in the lab to calibrate temperature-depending parameters e.g. the redox potential. Oxygen (O_2), Electromotive force (EMF, correction to E_H), Electrical Conductivity (EC) and pH were measured within 1-2 hours after the samples were taken. Furthermore photometry for Sulfide, Ferrous Iron and Nitrite were conducted. Sieland gives a detailed description how the on-site parameters are measured (Sieland 2009). However following devices are used to determine the on-site parameters: for pH and electrical conductivity (EC) measurements a *WTW pH340i*, for Oxygen and the Electromotive Force (EMF) a *Hach HQ40d multi/FDO Check*, for Photometry a *Hach DR/890 Colorimeter*. The electrodes to measure the pH and the EC are calibrated on a daily basis. Standard buffer calibrations with a pH of 4 and 7 are used to calculate a 2-point calibration for the pH, the EC device is calibrated using a standard with a given electrical conductivity of 1413 μS/cm. Eventual deviations from the latter standard are then calibrated by adjusting the cell constant χ accordingly in the menu of the WTWpH340i until the EC of the standard is measured. The measured EMF was first calibrated based on a standard with a redox potential of 220 mV (cp. first part of equ. 2.1) . The calibrated EMF_{cal} was temperature-corrected (cp. middle part of equ. 2.1) and later converted into the E_H referring to the standard hydrogen electrode (cp. last part of equ. 2.1).

$$E_H[mV] = \text{EMF} + (220 - EMF_{cal}) - (0.198 * T_{sample}(ex - situ)) + (-0.7443 * 25 + 225) \quad (2.1)$$

Furthermore to gain a pH-independent unit for the redox potential of the samples, the E_H values are transformed into rH values, using the measured pH values, according to equ. 2.2 with E_N = Nernst-voltage (59.16 mV) (Hölting and Coldewey 2013).

$$\text{rH} = 2 * (E_H/E_N) + 2pH \quad (2.2)$$

The oxygen FDO Check device and the colorimeters do not require any calibration, during the measurement process standards (LED for the FDO Check) are used to determine any deviations. The on-site parameters are used as first plausibility check of the taken samples. Implausible parameters or implausible parameter combinations lead to a double-check of the results and if the implausibility is not resolved it leads to the exclusion of the samples from further assessment and analysis.

2.2.2. Ion analysis

The analysis of the main anions (F^-, Cl^-, Br^-, NO_3^-, PO_4^-, and SO_4^{2-}) and cations (Li^+, Na^+, NH_4^+, K^+, Mn^+, Ca^{2+} and Mg^{2+}) are carried out in the water laboratory of the department of hydrogeology at the Technische Universität Bergakademie Freiberg. Due to the high salinity and hence high electrical conductivity of the samples, the already filtered anion samples are diluted with four different factors to avoid unnecessary strain for the used anion-IC "Metrohm Compact IC 881". All samples with an EC between 20 and 80 mS/cm are diluted 1:101 and 1:501. The samples from Hot Lake with an EC of around 120 mS/cm are diluted with factors of 1:201 and 1:1001. The analysis of the cations is carried out in the same fashion using a cation-IC "Metrohm Professional IC 850" with the difference that the samples are acidified with HNO_3 to establish a pH value around 3 to avoid any bias for the pH-dependent species of Ca^{2+} and Mg^{2+}. Standards measured between the samples during the analysis are used to calibrate the IC and to ensure an acceptable quality of the analysis. Sieland gives a more detailed description (Sieland 2009). The concentrations in mg/l for the anions are presented in the table C.1, the concentrations for the cations in table C.2 in the appendices. Table C.3 contains the ion balances for each sample taken, computed with the help of the geochemical software PHREEQC (Appelo and Postma 2005). Samples with unacceptable high percentage errors (>5%) (Appelo and Postma 2005) are sorted out and excluded from further analysis. Later on the concentrations of the major ions are used to compute their enrichment compared to the local seawater (Seebauer 2015).

2.2.3. TIC determination

The total inorganic carbon TIC content were analyzed using an "elementar liquid TOC" device at the water laboratory at the Technische Universität Bergakademie Freiberg. Its precision depends on the carbon concentrations of the samples: with >10 mg/l a precision of <2% is reached, for samples with <5 mg/l C a precision of <5% is reached. The samples were acidified with phosphoric acid towards a pH of <2, transforming all inorganic carbon species into CO_2, which is purged during the analysis by nitrogen. The amount of CO_2, equaling the amount of TIC, was then determined by means of non dispersive infrared. The measurements of several standards with C concentrations assumed to be in the range of the sample concentrations and CO_2-free blind values (deionized water purged with N_2) ensure an high quality of the analysis.

A simple titration to determine the TIC is not practical due to the high CO_2 contents in the submarine hydrothermal system Panarea and hence in the fluid samples. During the titration process the CO_2 would simply be lost into the atmosphere, biasing strongly the TIC concentration. Extreme concentrations of NaOH added to fix the CO_2 completely could be used, but are difficult to bring to the field lab on Panarea. The TIC was implemented into the geochemical modeling software PHRREQC (Appelo and Postma 2005), together with all major anion concentrations, the temperature and the pH. PHREEQC then automatically calculates the HCO_3^- concentrations, later needed for the electrical balance.

2.2.4. Multi-element analysis

The simultaneous determination of 60 elements was carried out in the water laboratory of the department of hydrogeology at the Technische Universität Bergakademie Freiberg using a "Thermo X-Series II ICP-MS". The already filtered and acidified samples were diluted 1:20 and 1:50 due to their their high electrical conductivity to avoid any masking effects and too high mass loads (and probably damage) on the mass detector of elements in high concentrations. Samples from the area Hot Lake and Fumarolic Field with high EC values ($>$ 100 mS/cm) were diluted 1:100. For internal calibration to each sample 100μl of a standard consisting of 65 % HNO_3 containing 5 mg/l ^{74}Germanium (Ge) and ^{103}Rhodium (Rh) and 1 ml/l ^{187}Rhenium (Re) were added. The results of all three dilutions were compared and the best results from each dilution were used to conduct further analysis. The measurement modi (normal or collision) for each element are presented in tab. D.1, the concentrations in mg/l for each element are presented in the tables D.2, D.3 and D.4 in the appendices. Similar to the major ion analysis the concentrations of the various elements were used to compute their enrichment compared to the local seawater (Seebauer 2015).

2.2.5. Stable Isotopes: Hydrogen and Oxygen

The determination of the isotopic composition of the stable isotopes of Hydrogen and Oxygen was conducted by the Hydroisotop PLC, Woelkestraße 9, 85301 Schweitenkirchen, Germany. For the measurements a Picarro L2130-i Isotope Analyzer, a A0211 vaporizer and an auto-sampler HTC-PAL-xt 225211 are used. The Picarro L2130-i Isotope Analyzer uses the Wavelength-Scanned Cavity Ring-Down spectroscopy (WS-CRDS) method to determine the concentrations of $\delta^2 H$ and $\delta^{18]} O$ within the water samples. The WS-CRDS is based on the absorption lines of each isotope at characteristic wavelengths, representing a certain molecule species. It enables to either determine the isotopic composition of the samples (the ratio) or the total concentrations of the isotopes in the samples (Picarro Inc. 2015). Between the samples standards from the IAEA with known isotope concentrations are measured to ensure a good calibration and the necessary quality of the measurements. Later on the isotopic composition was compared to the isotopic composition of a laboratory standard, resulting in the delta notation as shown in equations 2.3 and 2.4. The standard is the Vienna Standard Mean Ocean Water (VSMOW-Standard) produced by the International Atomic Energy Agency, resembling the isotopic composition of the mean ocean water ($^{18}O/^{16}O = 2005.2 * 10^{-6}$ and $^{2}H/^{1}H = 155.76 * 10^{-6}$). VSMOW was introduced by the IAEA after the original SMOW standard (Craig 1961) was depleted.

$$\delta^{18}O\ [‰] = \frac{R(^{18}O/^{16}O)_{sample} - R(^{18}O/^{16}O)_{Std}}{R(^{18}O/^{16}O)_{Std}} * 1000\% \tag{2.3}$$

$$\delta^{2}H\ [‰] = \frac{R(^{2}H/^{1}H)_{sample} - R(^{2}H/^{1}H)_{Std}}{R(^{2}H/^{1}H)_{Std}} * 1000\% \tag{2.4}$$

2.3. Statistical Analysis

Data acquired over the last 10 years of scientific diving at the Panarea hydrothermal system conducted by the Scientific Diving Center Freiberg (SDC) is the basis for further statistical analysis. These data sets comprise the on-site parameters pH, EC, E_H, O_2 [mg/l and %], IC-analysis of major cations and anions such as Li^+, Na^+, K^+, Ca^{2+} , Mg^{2+}, Mn^{2+}, F^-, Cl^-, Br^-, SO_4^{2-} and ICP-MS analysis of further 61 Elements. investigation areas with several sampling points, e.g. Black Point with the Black Point (vent) itself, Black Point Mini (BP_M) and Black Point Nord (BP_N)or some of the several sampling spots of La Calcara are combined to one sampling spot(e.g. BP_M and BP_N are merged into BP_MN and all data points from A26 are merged together)to ease the interpretation of the data.

Before even starting to conduct any statistical analysis the data sets need to be prepared accordingly. To avoid the loss of data and subsequent restraints regarding bi- and multivariate statistical test missing values have to be treated either by replacing them with the detection limit multiplied with a factor 0.33 as it is done in this thesis. More sophisticated but also more time consuming would be the use of linear/multiple linear regression (Merkel and Planer-Friedrich 2002).

Automatic outlier tests are not performed due to the extreme conditions under which the samples are taken and the overall fluctuating system, which makes it impossible to rely on an algorithm. Only the qualified individual check of the data sets lead eventually to the exclusion of single samples from the overall data and further statistical analysis.

The data and its distribution are the crucial factor on which the further statistical analysis bases. To decide which tests can be applied the data must be analyzed regarding its distribution. Parametric tests require the data to be normally distributed in addition to at least one interval scale level. Non parametric tests require merely ordinal or nominal scale levels and do not have any further requirements regarding the data distribution (Merkel and Planer-Friedrich 2002). Most tests have a so-called H_0-hypothesis which is tested with a probability of error α. The latter describe the probability the H_0-hypothesis is true but is falsely declined. The smaller the probability of error is chosen, the more secure is the validity of the results. The p-value (probability value) indicates the extremity of a statistical result. The smaller the p-value the more likely the H_0-hypothesis is not true. Often combined with the probability of error α the p-value indicates whether the H_0-hypothesis must be declined. E.g. α is set to 0.01 or 1% error probability and the p-value is below 0.01 or 1% the H_0-hypothesis must be declined.

After the exclusion of not clearly identifiable and implausible samples and the application of the above mentioned measures (missing value treatment) a data set of 184 samples (n = 184) and 80 parameters remains for further statistical analysis. During the statistical testing different variables will be excluded to gain as much complete cases as possible or to avoid doubled parameters (e.g. Li analyzed by the IC and the ICP-MS).

The statistical software Statgraphics XVII and the operating system Windows 10 is used

to conduct the below mentioned statistical tests.

2.3.1. Factor-Analysis

The main aim of a factor analysis is the reduction of the data set to a new minimized data set. During the application of this method the variance of all parameters is "loaded" on factors, using linear combinations (Merkel and Planer-Friedrich 2002). This way big become smaller and thus are easier to handle and to interpret. The factor loading is the Pearson correlation coefficient between the factor and the variables. A factor analysis consists of two parts: first the PCA, principal component analysis, which tries to put most of the variance on factor 1 and followed by a mathematical rotation, which tries to distribute the variance and factor loadings according to different concepts. Varimax was chosen to obtain as much variance and factor loading on the first factor, as possible and thus to ease the interpretation.

The quality of the factor loadings can be distinguished using the estimated communality, which represents the fractions of the variance of a parameter represented by all factors. If the estimated communality is close 1 (or 100%) the majority of the variance of a parameter is represented by the new factors. Contrary the specific variance represents the fraction of the variance of a parameter which is not represented by the new factors. The higher the specific variance of a parameter the harder and more questionable the interpretation of the new factors, because only small parts of the information (variance) of this parameter is represented by the factors.

An additional factorability test, here the Kaiser-Meyer-Olkin Measure of Sampling Adequacy (KMO) provides another measure to evaluate whether it makes sense to extract factors from the factor loadings or not. The test indicates the fraction of common variance of the whole factor analysis with a common threshold of 0.6. Results > 0.6 indicate a sufficient high common variability to have meaningful factors. The results of these tests are given in tab. 3.5.

The factor loadings are nothing else than the correlation coefficient r of a linear Pearson correlation between the new factor and the tested parameter. To ensure statistical significance the factor loading (R-score) and the number of samples are used to calculate the P-value with an α of 0.01 using an online P-value calculator for Pearson-correlations (Stangroom 2015). This tool enables to test whether the linear Pearson correlation between a new factor and a parameter is significant or not. For each factor analysis threshold factor loadings are calculated with a P-value only fractions below the chosen α (comp. tab. 3.5). If the factor loading for each parameter exceeds this threshold, the correlation with the new factor is statistically significant, both the correlation and the factor analysis yield meaningful results. Since all thresholds are below 0.3 a minimum extraction loading of <0.5 ensures highly significant values (comp. tab. 3.5). Furthermore, in all cases with a threshold <0.5 these parameters load also higher an other factors. In this case only the maximum loading was extracted to ease the interpretation.

The interpretation of the different factors is based on the corresponding factor loadings. If certain parameters have a high loading on only one factor, this factor combines all these

parameters and draws a connection between them. Negative loadings of parameters indicate an inverse connection of the concerned parameters with all other tested parameters. Which kind of relationship the parameters have among each other has to be interpreted by the user of the software in the context of his data and his work. Tab. 2.2 compiles the details of the conducted factor analysis.

Tab. 2.2.: Details of the conducted factor analysis

used parameters	number of parameters	complete cases	extraction method	factors	rotation
pH, EC, IC and ICP-MS	58	88	Eigenvalues > 1	8	Varimax
pH, EC, IC and ICP-MS	58	88	Factor number	4	Varimax
All elements	56	95	Factor number	4	Varimax
Major ions	9	122	Eigenvalues > 1	2	Varimax
REE	14	146	Eigenvalues > 1	2	Varimax
Trace elements	20	161	Eigenvalues > 1	3	Varimax

2.3.2. Kruskal-Wallis-Test

Lacking a normal distribution of the data, the Kruskal-Wallis-Test (KWT) is applied to distinguish significantly different element concentrations between the investigation areas. As an non-parametric test the KWT compares if the means of more than two samples regarding one parameter (e.g. pH) differ statistically significant or not. Basically the test tries to prove two or more samples have the same mean value regarding one parameter and if this null-hypothesis must be declined (p-value > significance level α), the samples differ statistically significant from each other. If the various areas differ significantly from each other in their element concentrations different histories of origin can be assumed and classifications based on these differences are possible. In total 35 parameters (pH, EC, E_H, main ions, trace elements and REE) are the basis for the conducted KWTs. The significance level α for the KWT is set to 0.01%, for the subsequent Bonferroni correction two significance levels of 5% and 0.1% are set. The stricter, more conservative Bonferroni correction with an α of 0.1% ensures highly statistical results, but also bears the danger of neglecting possibly true differences and will most likely distinguish only a few significant differences between the various areas, which could harden the interpretation. Therefore the second, less conservative α of 5% helps to distinguish more, but less significant differences between the areas, forming a bigger picture and hopefully eases the interpretation and comparison of the results. The KWT compares each investigation area with all remaining areas, forming lists of pairs and indicates significant differences between each pair. To interpret this mass of significant different pairs of investigation areas a simple matrix of all tested areas (including the groundwater of Panarea) is made and significant differences are simply ticked (cp. tables F.14 and following).

3. Results and Discussion

3.1. On-site parameters

Tab. B.3 contains all on-site parameters of the submarine samples, tab. B.1 of the groundwater samples from Pozzo di Pina measured in the field-lab on Panarea, already cleared of implausible samples. If the on-site parameters form a plausible picture of the samples and display consistent values for the various parameters, the taken samples are reliable and further analysis can be conducted.

3.1.1. pH

Sec. 1.2 depicts the common hydrothermal fluids of submarine hydrothermal systems as strongly acidic, thus strongly acidic samples are expected. The pH for all taken samples ranges from 2.84 to 6.63. The most acidic samples come from the investigation area Black Point (2.84 - 3.13), the most alkaline samples from La Calcara and from the groundwater Pozzo di Pina with values between 5.14 - 6.42 respectively 6.23 - 6.63. Most other samples like Area 26, Bottaro Nord, Fumarolic Field, Hot Lake and Point 21 have pH values between 5 and 5.5. However, all samples from the various investigation areas are far below the average pH of seawater of 8.2 (Brown 2001) and the pH of the local seawater in the bay of Panarea impacted by the manifold sea bottom fluid discharges of 7.89 (Sieland 2009). As described in sec. 1.2 the low pH can have its origin in either the formation of Mg-OH silicates, the dissolution of magmatic HCl and HF or in the precipitation massive sulfides. As later in sec.3.2.1 explained high F concentrations at Black Point indicate a magmatic HF contribution, resulting in the most acidic conditions (cp. sec. 1.2). Proposing all areas are fed by the same hydrothermal fluid with pH values < 3 a buffering of the pH by the surrounding bedrock of high-potassium calc-alkaline (HKCA) affinity (Calanchi et al. 2002) or a mixture with the local seawater could explain the pH around 5 ± 0.5 at Area 26, Bottaro Nord/West, Fumarolic Field, Hot Lake and Point 21. Buffering and mixture could consequently lead to precipitation/immobilization/removal of certain species and elements, thus altering the chemical composition of the hydrothermal fluids at all areas with a pH around 5. Distinguishing between the buffering by the bedrock and mixtures/contamination with local seawater is rather difficult, if not impossible. High pH values from La Calcara indicate either a contamination with seawater or eventually groundwater with elevated pH values. Still the sample quality from samples with an elevated pH value must be questioned. Fig. 3.1 gives an overview over both the pH and the redox potential E_H.

3.1.2. Redox Potential

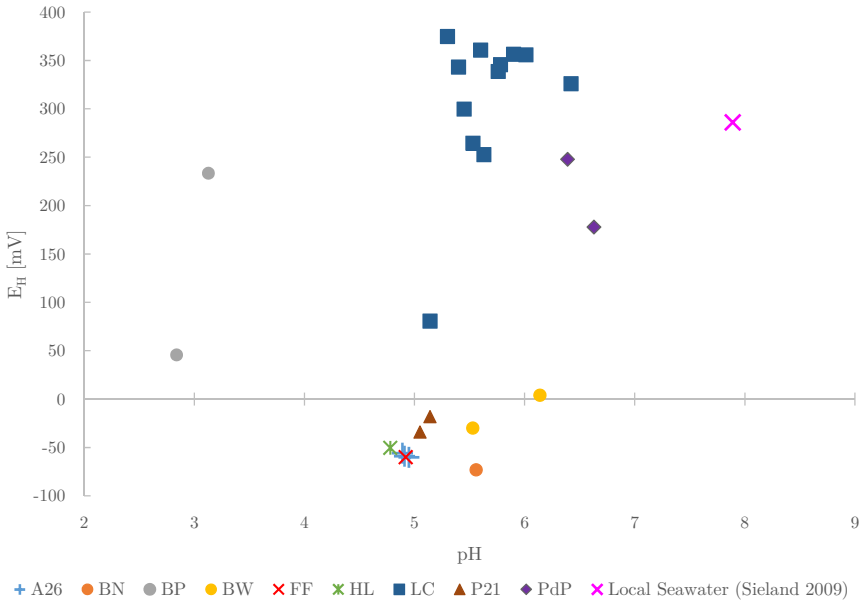

Fig. 3.1.: Comparison and classification of sampled waters from the 2015 diving campaign.

In combination with the pH, the redox potential can be used to classify waters and to determine whether we have oxidizing or reducing hydrochemical conditions. In fig. 3.1 the variety of the redox potential of the different samples is depicted, plotted with the pH. Expected are strongly reducing hydrothermal waters (cp. sec. 1.2). The samples from La Calcara, Hot Lake, Bottaro Nord and Pozzo di Pina are in the range between 180 and 400 mV, enclosing the local seawater with 286 mV (Sieland 2009). During the pumping at Pozzo di Pina the redox potential steadily decreased towards values around 180 mV, indicating a reduced and partly oxygen free environment for this water. The true redox potential may even be much lower, considering the fact, the water is pumped up and the redox measurements are taken in contact with ambient air. Most other samples are close to 0 mV or below, like Bottaro West (-12.9 to 4 mV), Point 21 (-33 to 18 mV), Area 26 (-60 to 56 mV), Fumarolic Field (-60 mV) and Hot Lake (-50 mV). Only Black Point has two samples with different values of 46 mV and Mini Black Point with 233 mV. The difference may be explained by the two different sampling locations within the same area or the sample with the redox potential of 233 mV is contaminated with seawater and/or ambient air, biasing the redox potential towards oxidizing conditions. Still these results correlate with former investigations, e.g. (Sieland 2009). Samples from the same sampling point cluster in this diagram, especially the samples from La Calcara, Black Point, Point 21 and Area 26. The clustering is an indicator for a reliable and reproducible sampling procedure and if in any case methodical errors. The plotting reveals three distinctive clusters: (1) Black Point has the lowest pH and forms the first cluster with contradicting redox readings, (2) Bottaro Nord and West, Fumarolic Field, Hot Lake and

Point 21 plot all around a pH of 5 (up to 6) and a redox potential of -50 mV comparable with typical values from the literature (cp. sec. 1.2), (3) samples from La Calcara and Pozzo di Pina form a cluster with an oxidizing redox potential higher than the average seawater in combination with the highest pH of all taken samples.

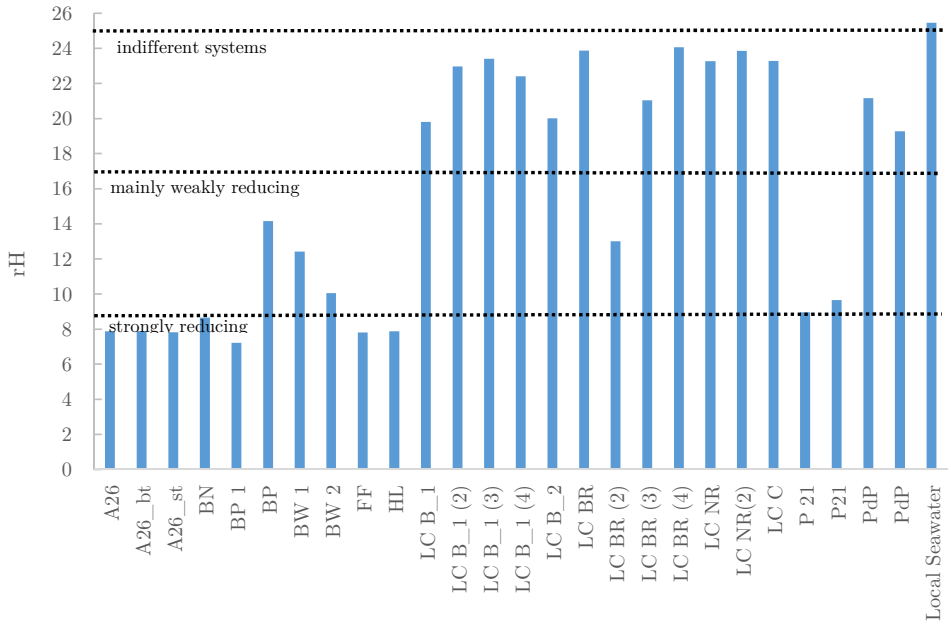

Fig. 3.2.: rH values for all 2015 taken samples. Note the E_H measurement has a great influence of the rH value, hence both units (E_H and rH) are prone to erroneous redox readings.

One should note that La Calcara has one single outlier with a comparably low redox potential of 80 mV and a pH around 5, close to the second cluster. An outlier and his exclusion from further evaluation could be suggested, or this outlier could connect both clusters the second and the third one based on following thoughts: In the submarine sampling environment seawater surrounds all sampling points and has the potential to bias all samples. In the extreme the samples could only contain traces of the hydrothermal fluids and mostly seawater. Having this in mind only extreme values differing strongly in their chemical and physical parameters from the local seawater are an reliable indicator for a sample containing fluids differently from seawater. A reducing redox potential cannot be explained by a contamination with seawater, the source must be in this case a hydrothermal fluid. Hence samples showing reducing conditions have to weighted differently, more strongly than samples close to the local seawater. In the case of the outlier of the La Calcara samples it seems as if this single sample displays partly the original redox conditions of the hydrothermal fluids at La Calcara. It is one of four taken samples from the same sampling point La Calcara Black Rock. The three other samples of the same sampling point reveal a highly oxidizing redox potential from 299 mV up to 356 mV, indicating a contamination with either seawater and or later in the field lab with the atmosphere, or even a mixture of both. This comment on the contamination potential of seawater on the taken samples is of course also true for all other evaluated on-site parameters

and for the element concentrations. Still for each parameter expectations need to be made, whether the parameter of the submarine hydrothermal fluids will be elevated (e.g. EC, trace metals, REE) or decreased (pH, E_H, Mg^{2+} and SO_4^{2-}) concentrations) compared the local seawater, to decide whether the minima or the maxima will partly depict the hydrothermal fluid. Again following assumption is valid: the more the parameters of the submarine hydrothermal fluids deviate from the local seawater, the lower is the contamination with local seawater.

Because the E_H is pH-dependent and Black Point and La Calcara differ between a pH of 2.5 and 6, it makes sense to calculate the pH-independent rH value to gain a parameter to compare the redox potential of all taken samples with each other, according to equ. 2.2. Fig. 3.2 displays the results and the difference of the rH for each taken sample. The combination of the E_H and the pH reveals Black Point as the point with the strongest reducing potential, close to Area 26, Fumarolic Field, Hot Lake and Point 21. Especially La Calcara but also Pozzo di Pina show mostly indifferent values, except for the before mentioned outlier with a low redox reading. Still the problematic readings of the E_H lead to biased rH values, hence these values need to be evaluated carefully and can only be used as indicators of trends, not as evidence.

3.1.3. Electrical conductivity

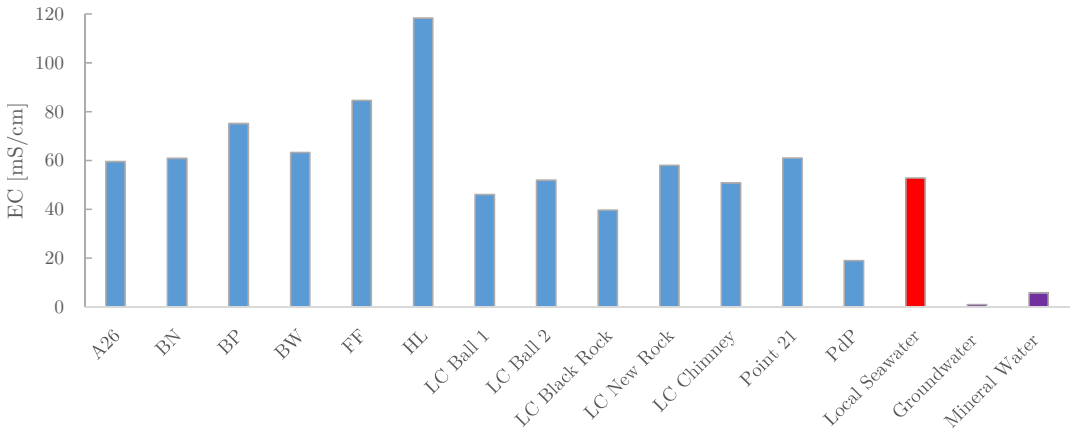

Fig. 3.3.: Comparison of the extreme values of the electrical conductivity, minima for La Calcara and Pozzo di Pina, maxima values for the rest of the areas, compared to values from local seawater (Seebauer 2015) and from fresh groundwater and mineral water (Hölting and Coldewey 2013).

High electrical conductivities are expected from the hydrothermal fluids because of found high concentrations of chemical constituents (Sieland 2009) for the hydrothermal system Panarea. Given the special submarine sampling setup only the extreme values (minima and maxima) of all taken samples are displayed in fig. 3.3 due to following reasons: If several samples of an investigation area show an elevated electrical conductivity compared to local

seawater the maximal value found is most likely the sample with the lowest contamination of seawater. Other way round: if values below the average electrical conductivity of seawater are found, they could only be biased by seawater towards its average value. Hence all values close to seawater are likely seawater or hydrothermal fluids diluted with seawater.

Plotting the electrical conductivity shows a partly indifferent picture of the different sampling points. While Area 26, Bottaro Nord, Bottaro West and Point 21 are slightly above the average of the local seawater of 52.82 mS/cm (Seebauer 2015), Black Point, Fumarolic Field and Hot Lake are significantly higher. Black Point has a maximum of 75.10 mS/cm, clearly higher are Fumarolic Field with 84.60 mS/cm and especially Hot Lake with 118.30 mS/cm. La Calcara shows an opposite trend, the minima of most sampling points are below the local seawater, e.g. Ball 1 (46.10 mS/cm), Ball 2 (51.90 mS/cm) and Chimney with (50.80 mS/cm). Especially Black Rock shows the lowest value with 39.70 mS/cm, which cannot be explained with a contamination of local seawater. Pozzo di Pina shows values between 18.00 and 22.20 mS/cm, which is already above the range of mineral waters (1.5 - 10 mS/cm), but below the average of seawater (45-55 mS/cm) (Hölting and Coldewey 2013). Either this water is a mixture of fresh water and seawater, or it is geothermaly influenced, explaining the high temperature and based on the latter higher WRI potential and thus more dissolved constituents.

The high values of Black Point, Fumarolic Field and Hot Lake could be indicators for hydrothermal fluids originating from a high Cl-content phase (cp. sec. 1.2), while La Calcara Black Rock seems to be fed by a low Cl-content hydrothermal phase, reducing the total amount of the main anion Cl^- and correlating cations (cp. sec. 1.2) in comparison with local seawater. Another possibility could be a connection between the groundwater of Panarea and the submarine hydrothermal system Panarea, in which the groundwater with its low EC dilutes the samples from e.g. La Calcara Black Rock, the sampling site of the outlier with a low EC.

3.1.4. Oxygen

The saturation of water samples with oxygen can give insight about the redox potential of the system and can be used to verify oxidizing or reducing trends, as done in fig. 3.4. Most of the samples show only a partly saturation with oxygen. Especially water from Area 26, Bottaro Nord, Fumarolic Field and Hot Lake seem to be nearly oxygen free ($<$ 10 %), followed by Point 21 ($<$ 30%). Black Point has only a small range of oxygen saturation between 64 and 66 %. Contrary Bottaro West displays values between 60 and almost 90 %. The samples from La Calcara do not follow a general trend, while Ball 2 and Chimney lay around 40 %, Black Rock and New Rock are almost fully saturated with almost 90%. The samples from Black Rock show a great range between 50 and 100 %. It can be assumed that samples with highly different saturation values are biased, due to their reading in the field lab under a normal air atmosphere or the contamination with atmospheric oxygen could occur during boat trip back to Panarea and the following transport to the lab. Surprisingly the groundwater from

Pozzo di Pina is only partly saturated with 43 %, if one remembers, the water is pumped up by a pump and finally released by a tap under high pressure, resulting in a spray of water (cp. sec. 2.1.1). Still it is consistent with the measured low redox potential, indicating a groundwater environment mostly deprived from oxygen.

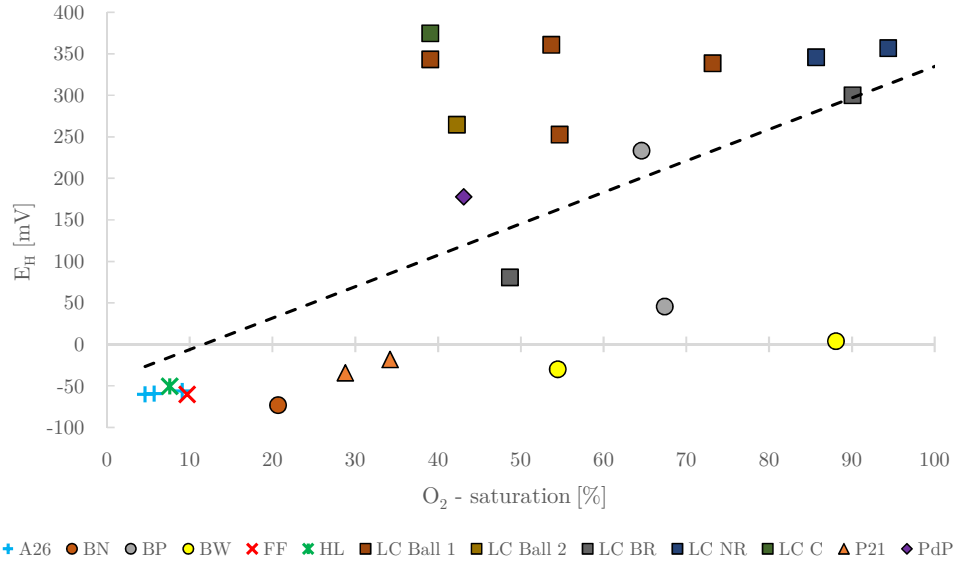

Fig. 3.4.: Comparison of the average oxygen saturation and the redox potential of the different water samples.

Fig 3.4 also compares the oxygen saturation and the redox potential to verify the plausibility of the measurements. Both parameters correlate only partly with each other. While Area 26, Fumarolic Field, Hot Lake, La Calcara Black Rock and Pozzo di Pina plot near the trend line, other samples from e.g. Bottaro Nord and West, Point 21 show a lower redox potential than their oxygen saturation suggests. The kinetic of redox reactions could explain this discrepancy: The sample is biased with atmospheric oxygen, still the redox partners are not fully oxidized during the measurement in the field lab, resulting in a low redox potential. Contrary samples from mostly La Calcara display redox potentials far higher than their oxygen saturation suggests, leaving a question mark behind these samples and the overall value of redox readings under these circumstances.

3.1.5. Reduced species

The presence of oxygen should exclude the presence of reduced species and should cause oxidizing conditions in terms of the redox potential. Or vice versa the presence of reduced species indicates reducing conditions and the lack of oxygen. Fig. 3.5 compares the average concentrations and range of values of reduced species to the oxygen saturation. The overall trend verifies the oxygen measurement and the measurement of the reduced species. Most water samples are undersaturated and hence we find reduced species in the water. If single samples are close to saturation the corresponding concentrations for reduced species are ex-

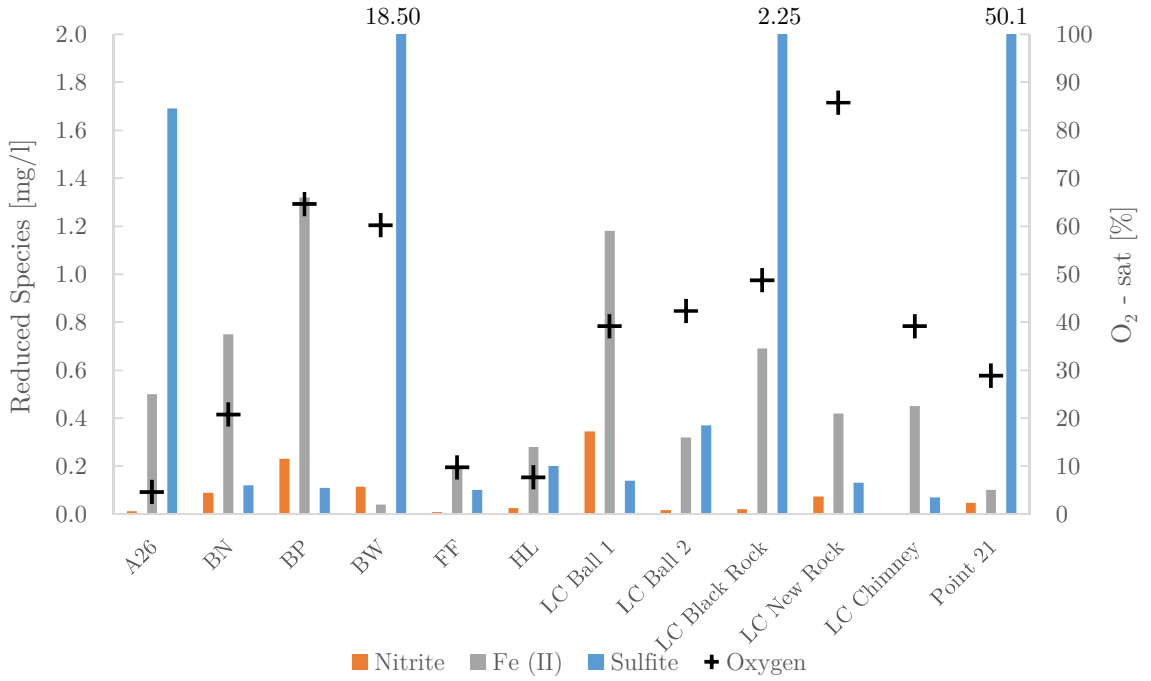

Fig. 3.5.: Average concentrations and range of values of reduced species compared to the oxygen saturation and its range of values of the water samples.

tremely low or close to zero. The nitrite concentrations are fairly low (<0.35 mg/l) and are more or less inconclusively distributed. Fe (II) concentrations tend to follow the oxygen saturation e.g. at Bottaro Nord, Black Point and LC Ball 1 which is curious, because the exact opposite trend would be expected. Still the concentrations of Fe (II) iron are so small, that the different concentrations are rather a product of the differences between the investigation areas and not of the oxygen concentration. Two areas have high values of sulfite: Bottaro West (18.50 mg/l)and especially Point 21 with 50.1 mg/l, while the others are all below 3 mg/l. The presence of sulfite could be a hint to high concentrations H_2S in the submarine gas exhalations around the sampling points, dissolving the in the hydrothermal fluids during the ascent, because both areas feature the strongest gas exhalations.

3.1.6. Temperature

During the field work under water and on the island temperatures are measured in-situ. However, due to the division of labor the attribution of the temperatures to each investigation are and to the taken water samples is problematic and erroneous, resulting in duplicated and contradictory temperatures for different areas and missing temperatures for some of the areas. Tab. B.1 and tab. B.3 display the temperatures as documented in the field. Especially LC_Ball_1 and LC_Black_Rock have all the same temperatures, only written in another order. However, at least the measured temperatures prove at all areas fluids are exhaled with

elevated temperatures compared to the local seawater, which ranges depending on the depth and sometimes the bottom current from 25°C at the surface to 18° C at the bottom at the deepest areas (Area 26). The coldest areas is Bottaro West (40.0°C), the hottest seems to be La Calcara (Black_Rock, or Ball_1 with 132.5°C) and Black Point (112.0°C). Area 26, Fumarolic Field and Point 21 range all between 62.3 and 68.1°C. If one assumes the same high temperature for the ascending hydrothermal fluids at all investigation areas the temperature could be seen as another indicator for the "purity" or mixture between hot hydrothermal fluid and cold local seawater. Accordingly it seems that La Calcara and Black Point show the lowest degree of mixture, while Bottaro Nord should be closest to the local seawater. The water taken from Pozzo di Pina (cp. tab. B.1) is clearly geothermaly influenced, resulting in temperatures between 55.2 and 49.4°C.

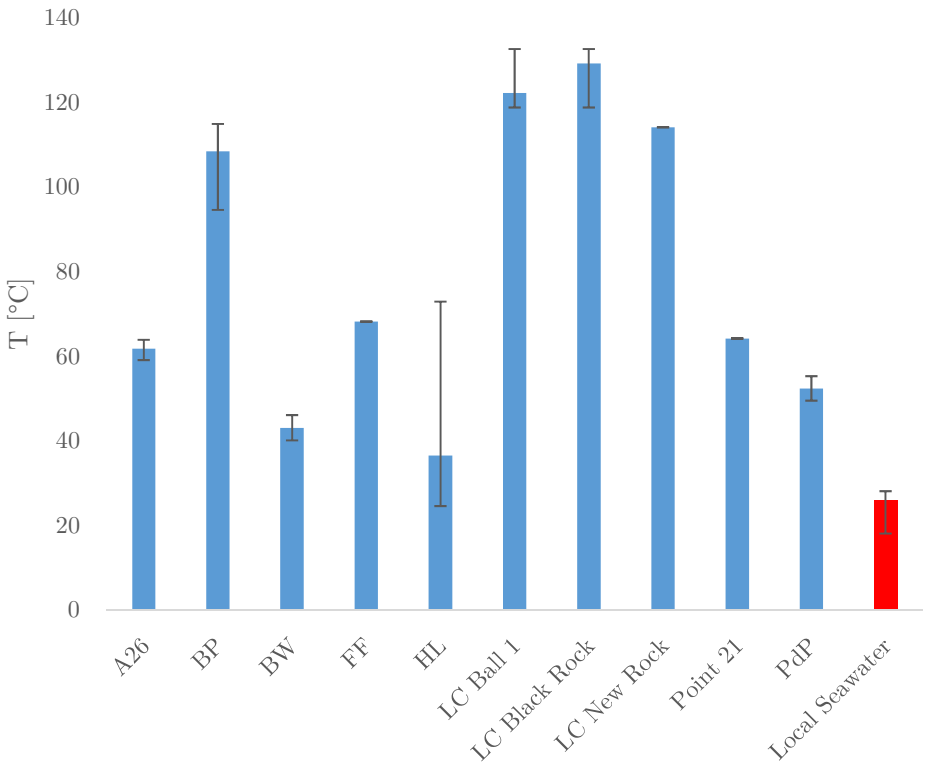

Fig. 3.6.: In-situ temperatures for the various investigation areas. Please note the temperature for Hot Lake is averaged from 19 measurements around the depression, marking Hot Lake.

3.2. Ion Analysis

Concentrations of the major anions are found in tab. C.1, concentrations of the cations in tab. C.2 of the appendix. Concentrations of major ions give the opportunity to apply the electrical balance (E.B.) or the percentage error on an analysis to grade its quality. The hydrochemical software PHREEQC (Appelo and Postma 2005) - using the phreeqc.dat database - was applied, modeling a simple solution containing all major ions and the pH of the samples to calculate the E.B. by forming the sums of positive and negative charges of the constituents of the water (see equation 3.1). Normally the positive charges of the cations should equal the negative ones of the anions, so the water should not be charged at all. Errors up to $\pm$ 2 % are inevitable and up to $\pm$ 5 % still acceptable (Appelo and Postma 2005).

$$\text{Electrical Balance [\%]} = \frac{(\text{sum cations} + \text{sum anions})}{(\text{sum cations} - \text{sum anions})} \cdot 100 \tag{3.1}$$

The results are shown in tab. C.3. Most samples are below 2% error except for sample PAN_094015_PdP (PdP(2)) (groundwater taken without equilibrium from Pozzo di Pina) with an error of 23.57%. A high error is anticipated because of the sampling conducted before the on-site parameters equilibrated themselves. All in all the analysis of the major ions give reliable results.

Please note the classical definitions of major and minor ions, but especially trace elements, cannot be applied here, because most elements occur in such high concentrations, that they exceed these classical definitions.

Various authors describe and demonstrate the removal of Mg^{2+} and to a lesser degree Na^{+}, K^{+} from heated seawater, in exchange for Ca, Fe, Mn and other metals, due to interactions with hydrothermal waters and hot bedrock (Bischoff and Seyfried 1978; Herzig and Hannington 2000; Mason 2013; Scott 1997; Seyfried and Mottl 1982; Thornton and Seyfried 1987). The generation of Mg-OH silicates in the subsurface would additionally explain low Mg^{2+} concentrations and could be partially responsible for the pH value < 4 (German and Seyfried 2014; Seyfried and Shanks 2004). Additionally SO_4^{2-} can be removed by mineral precipitation and/or reduction to SO_2^{2-} and eventually subsequent precipitation as e.g. iron-sulfide phases (Herzig and Hannington 2000; Mason 2013). The author expect these trends to be visible in the taken samples (cp. 1.2).

3.2.1. Anions

Fig. 3.7 depicts various trends of the anions: $\mathbf{Br^{-}}$ is in almost all samples depleted by 25 - 50%, except for Fumarolic Field and Hot Lake in which it is enriched by up to 140%. Normally in seawater, Br^{-} is enriched compared to freshwater. This could be an indicator for a different water source with lower Br^{-} concentrations. $\mathbf{SO_4^{2-}}$ shows weak depletion in most samples by 5 -15%, except for La Calcara New and Black Rock and Point 21 with enrichment up to 17% and does not follow the over all trend of high enrichment at Hot Lake, Fumarolic Field

and Black Point. $\mathbf{F^-}$ is extremely enriched at Black Point, up to 673% and also Area 26 (90%), Hot Lake (80%) and La Calcara New Rock (104%) show significant high values. $\mathbf{Cl^-}$ is highly enriched at Hot Lake (170%), Fumarolic Field (76%) and Black Point (45%). Other samples like Area 26, Bottaro Nord and West and Point 21 are slightly enriched by 10-25%, while the samples from La Calcara are slightly depleted, except for Black Rock and New Rock. $\mathbf{HCO_3^-}$ shows depletion at all investigation areas, especially at Black Point (-99%), La Calcara Chimney (-62%) and La Calcara Ball 1 (-52%). Enrichments are found at Bottaro Nord (enrichment up to 106%), Bottaro West (20%) and Pozzo di Pina (448%). Depending on the pH, the concentrations of HCO_3^- do not surprise: Black Point with a pH below 3 contains almost no HCO_3^-, while Pozzo di Pina with a relatively high pH of around 6.5 contains the most HCO_3^-.

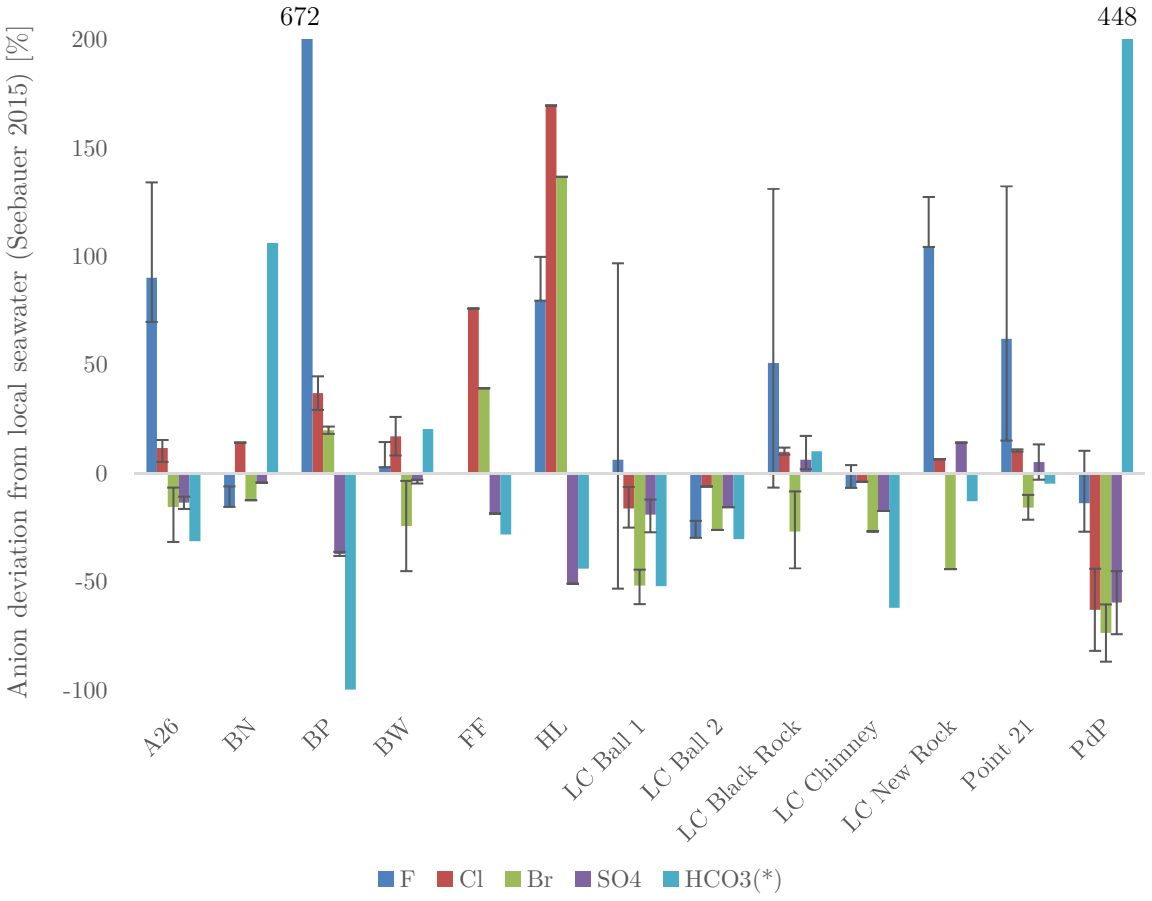

Fig. 3.7.: Deviations of the anion concentration of the water samples from the local seawater. $*$ HCO_3^- compared to the average seawater composition (Brown 2001). Please note the applied dilution factors to single anion concentrations.

The expected depletion of SO_4^{2-} could be explained by mineral precipitation of e.g. alunite (Dekov et al. 2013; Krahe unpublished). Especially at La Calcara (s. fig. 1.5) SO_4^{2-} mineral

phases such as alunite are located beneath or on the sand and gravel layers covering parts of the ground at La Calcara (Krahe unpublished) (cp. fig. 1.5). These found precipitates could explain the low SO_4^{2-} concentrations in the fluid samples in addition to the precipitation of anhydrite and gypsum as stated in the literature (Herzig and Hannington 2000; Mason 2013; Von Damm 2001). The SO_4^{2-} enrichment at La Calcara New Rock, Black Rock and Point 21 are rather small and may be explained by uncertainties in the sampling and analysis procedure.

As described in sec. 1.4 a chemically modified Mediterranean seawater is already proposed as main source for the submarine hydrothermal fluids of Panarea, with low pH and a strong Cl^- excess compared to seawater (Tassi et al. 2009). Proposed water is impacted by hot, acidic, HCl bearing deep fluids as part of the hydrothermal system which could partly explain the Cl^- excess at Hot Lake, Fumarolic Field and Black Point and the considerably low pH at e.g. Black Point. The Cl^- excess in the samples is in accordance to the literature describing phase separation in submarine hydrothermal systems, resulting in a low and a high Cl-content phase (cp. sec. 1.2). This Cl^- excess determines the overall concentrations of the cations and hence the EC, because of its dominant anion status, as depicted in fig. 3.8 and described in sec. 1.2: The EC follows closely the trend of the Cl^- concentrations of each sample, while exemplary for other cations the Ca^{2+} concentrations also follow the Cl^- concentrations and the EC pattern.

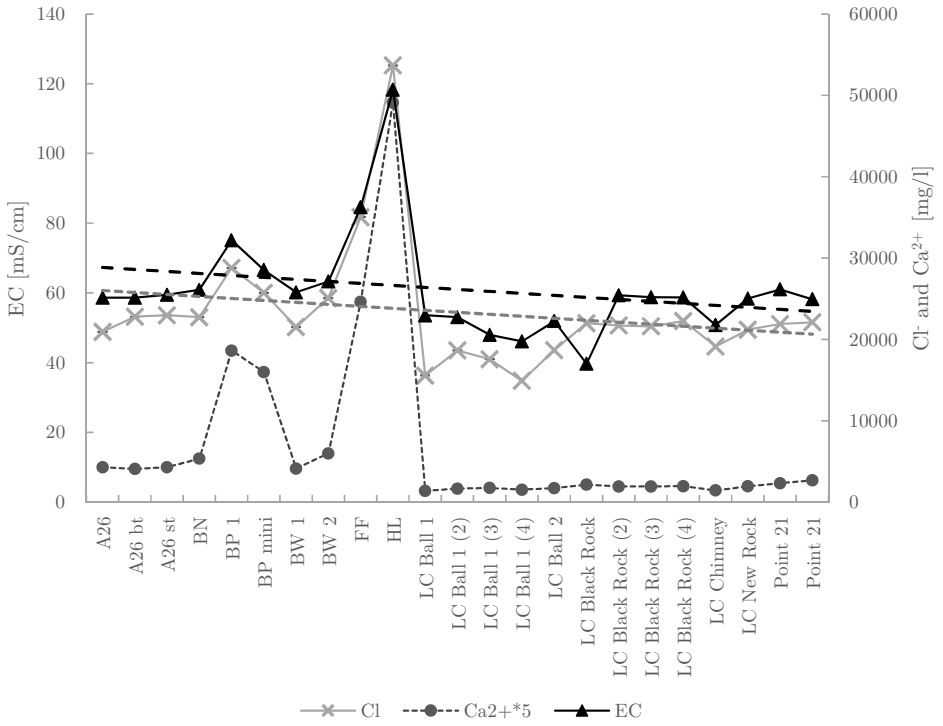

Fig. 3.8.: EC and the Cl^- and Ca^{2+} concentrations plotted, proving the dominant anion status of Cl^-, determining the cation concentration and hence the EC. Please note the applied factor for the Ca^{2+} concentration.

The high F^- concentration at Black Point could be an indicator for magmatic HF, con-

tributing to the low pH of Black Point. The overall enrichment pattern could indicate a hydrothermal water/component with low Cl-content (cp. sec. 1.2) and/or a smaller seawater fraction at La Calcara combined with groundwater from Pozzo di Pina with lower ion concentrations. The groundwater from Pozzo di Pina shows of course depletion of all anions in comparison to the local seawater, especially Cl^- is depleted. Still the depletion of the anions is rather small and similar to the other samples for F^-, Br^- and SO_4^{2-}.

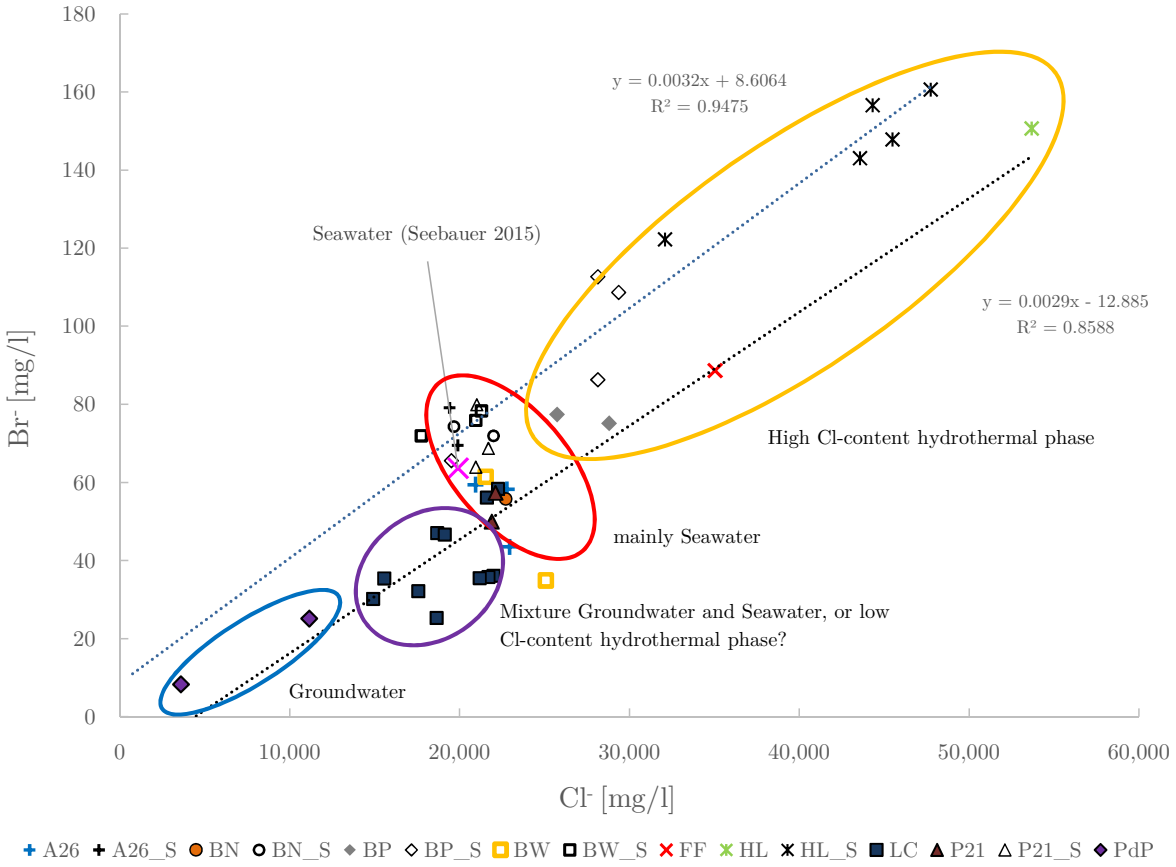

Fig. 3.9.: Br^-/Cl^- diagram to display the enrichment or depletion of both elements in comparison to the local seawater. Additional older fluid water samples (Sieland 2009) are displayed as black data points with higher Br^-/Cl^- ratios.

The determination of the main anions within the samples gives the possibility to compare the Br and Cl concentrations with each other. Br^- is naturally enriched in seawater samples in comparison to fresh- and groundwater. Comparing the local seawater Cl^-/Br^- with the taken water samples, seemingly four distinctive groups can be distinguished: fresh- and groundwater, seawater, an intermediate mixture between fresh and groundwater and hydrothermally influenced waters (cp. fig. 3.9). All samples, except for Black Point, Fumarolic Field and Hot Lake plot at low bromide concentrations compared to the local seawater. All areas with multiple samples taken tend to cluster, another indicator for reliable and reproducible samples. This classification is only relative, but displays the trend of the different water samples. However, most sampling points plot around the local seawater, while Black

Point, Fumarolic Field and Hot Lake show by far the highest concentrations of both elements consistently with their high electrical conductivities (s. fig 3.3) and are labeled as "High Cl-content hydrothermal phase" (cp. sec. 1.2). A precipitation of halite, excluding bromide from its lattice to explain the high bromide values of Black Point, Fumarolic Field and Hot Lake (Price et al. 2015) is rather speculating because their is no evidence that at any point of the geothermal system halite saturation is reached in the geothermal brine. The samples from La Calcara plot all near to the groundwater from Pozzo di Pina, exhibiting the lowest Br^- and Cl^- concentrations with a Cl^--excess compared to Br^-, except for one sample from Bottaro West. They could either be a mixture between the seawater and a water with low Br^- and Cl^- concentrations (e.g. groundwater) or a result of a low Cl^--content hydrothermal phase and the dissolution of halite, adding additional Cl^-. The differences between the investigation areas, regarding their concentrations could occur during phase separation in the subsurface, resulting in a low and a high-Cl content hydrothermal phase (cp. sec. 1.2). La Calcara seems to result from a low Cl-content phase, while Black Point, Fumarolic Field and Hot Lake seem to be fed by a high Cl-content phase in accordance to the correlating cation concentrations of La Calcara (low cation concentrations, compared to the local seawater) and high cation concentrations at Black Point, Fumarolic Field and Hot Lake (cp. sec. 1.2 and sec. 3.2.2).

The samples from 2015 show an interesting shift towards higher Cl^- concentrations and often lower Br^- concentrations compared to older samples (Sieland 2009). Curiously both trend lines for all samples from 2009 and 2015 have almost the same slope, which only underlines the evident shift towards higher chlorine concentrations. The reasons for that shift are hard to determine but either the system changed between these years, indicator for a highly variable system (cp. sec. 1.2) or simply the sampling and analyzing techniques differ, resulting in shifted results.

However, the mass ratio and the molar ratio between Br^- and Cl^- of the samples (cp. tab. C.4 and fig. 3.10) draw a another picture. The mass ratio of Cl/Br locates both the average and the local seawater between 291 and 313, the molar ratio is between 655 - 705. Interestingly the investigation areas with the highest concentrations of Cl^- and Br^- (Hot Lake, Fumarolic Field and Black Point) have elevated ratios, but are exceeded by areas with relatively low concentrations, especially samples from La Calcara have extreme high ratios, up to 739 (mass) and 1665 (molar) at Ball 1. These ratios indicate different conditions regarding the enrichment of Cl^- and Br^- between e.g Hot Lake, Fumarolic Field, Black Point and especially La Calcara Ball 1. It seems as if the fluids at investigation areas with high concentrations and low ratios result from a linearly enriched local seawater. At other areas however considerably more Cl^- or considerably less Br^- is dissolved in the fluids, increasing the ratios. Halite dissolution (e.g. from the Messinian Crisis) by a low-Cl hydrothermal phase during the ascent at La Calcara could explain high Cl/Br ratios in combination with comparable low Cl^- and Br^- concentrations. A withdrawal of Br^- ions, e.g. by precipitation under these circumstances is implausible.

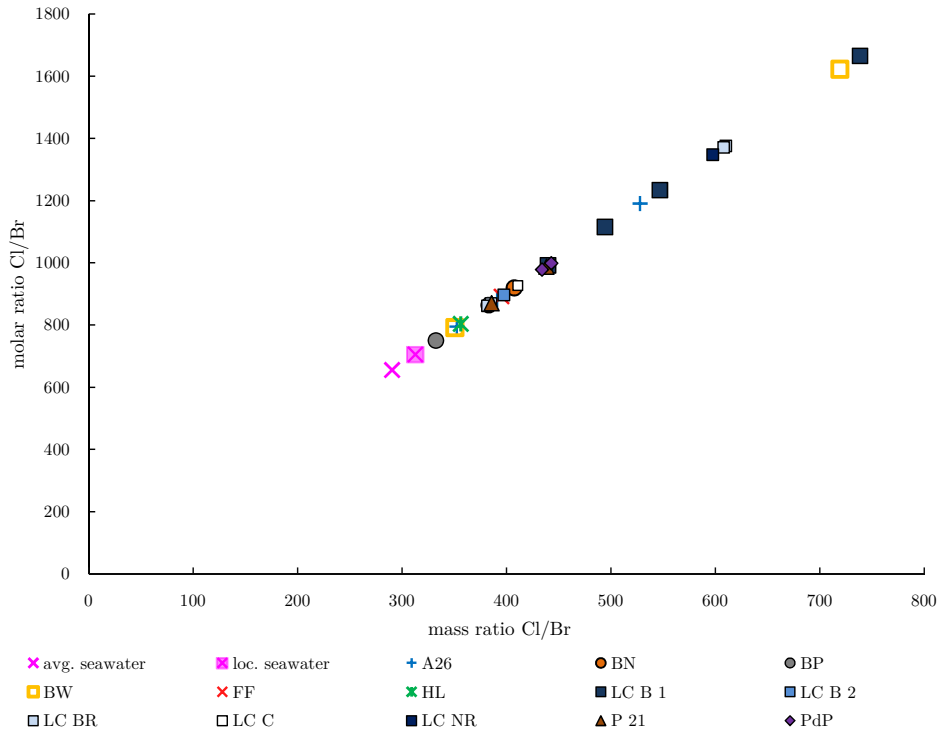

Fig. 3.10.: Cl^-/Br^- mass and molar ratios of the samples compared to average seawater (Brown 2001) and local seawater (Seebauer 2015).

3.2.2. Cations

Comparing the major cation concentrations with the concentrations of the local seawater provides another tool to group the water samples, which reveals remarkable deviations as presented in fig. 3.11. Due to the extraordinary dominant role of Cl^-, which determines the cation concentrations, a similar pattern/trend of cation concentrations tracing the Cl^- concentrations and EC is expected. The samples from Hot Lake, Fumarolic Field and Black Point show the highest deviations from the local seawater in accordance with their high Cl^- concentrations and high EC (cp. fig. 3.3 and fig. 3.8). Enrichment of up to almost 19500% for e.g. Mn^{2+}, over 2,500% for Li^+, over 2250% for Ca^{2+} and 750% for K^+ are impressive examples. As expected (cp. sec. 3.2), but still remarkable $\mathbf{Mg}^{2+}$ occurs in all samples in lower concentrations than in the local seawater, the highest depletion found in samples from Pozzo di Pina with -65%, followed by Black Point with 42%. Most of the other sampling points are enriched in Na^+, Li^+, K^+, Ca^{2+} and Mn^{2+} except for La Calcara and Pozzo di Pina. The samples of La Calcara are depleted in Na^+ (up to 29% at Ball 1), Mg^{2+} (up to 39% at Ball 1), Ca^{2+} (up to 34% at Chimney) and are depleted in K^+ (up to 14%), except for Black Rock. Still all of them are enriched in Mn^{2+}, Black Rock showing the smallest enrichment of only 7%. Samples from La Calcara have all the same trend towards low enrichment or depletion in common.

Of all cations Mg^{2+} and Na^+ in combination with extremely increased Ca^{2+}-concentrations

are most intriguing, because their depletion (Na^+ is removed by Na^+-Ca^{2+} replacement reactions) at most investigation areas suggests a hydrothermal origin of these fluids (Bischoff and Seyfried 1978; German and Seyfried 2014; Herzig and Hannington 2000; Mason 2013; Scott 1997; Seyfried and Mottl 1982; Thornton and Seyfried 1987). Often in hydrothermal systems K^+ and Ca^{2+} are also depleted, depending on the bedrock (German and Seyfried 2014; Herzig and Hannington 2000; Mason 2013). The enrichment of K^+ and Ca^{2+} in the samples is explained by the given geological background of Panarea of high potassium calc-alkaline affine magmas, base of the andesitic and dacitic rocks, forming the island and islets (Calanchi et al. 2002) (s. section 1.1). Furthermore subsurface dissolution of Ca-plagioclase and calcite could explain the high Ca^{2+} concentrations (Tassi et al. 2009).

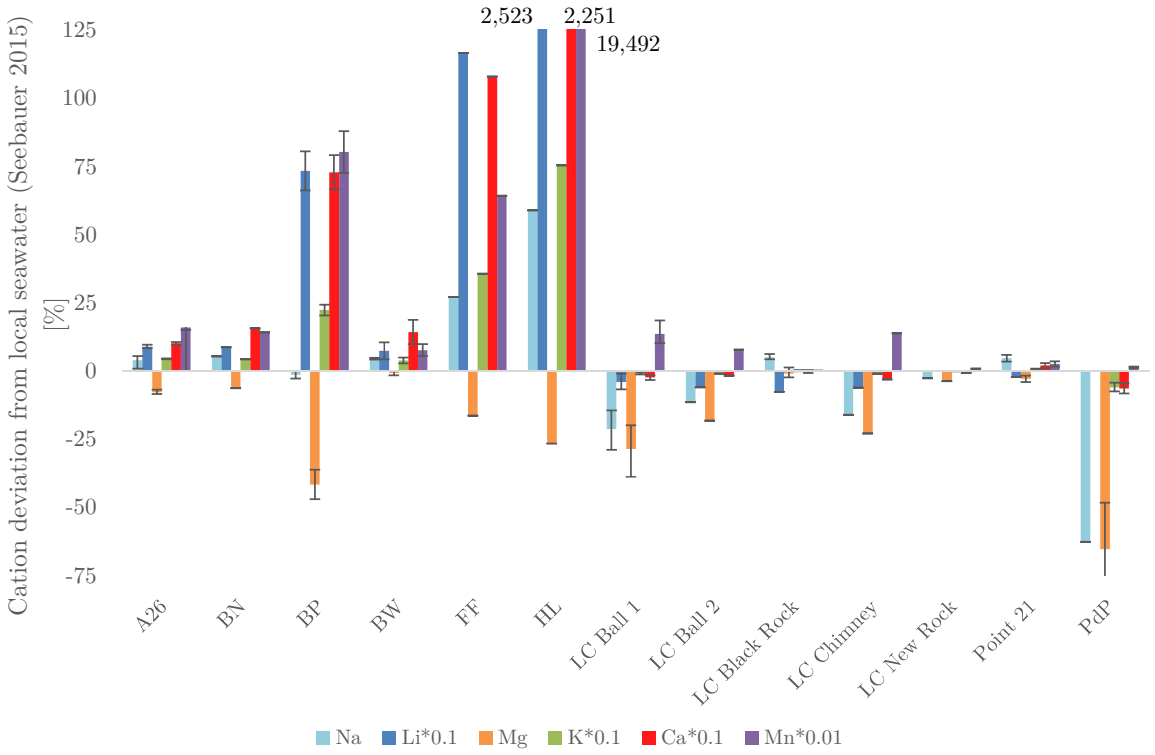

Fig. 3.11.: Deviations of the cation concentration of the water samples from the local seawater. Please note the applied dilution factors to single cation concentrations.

3.2.3. Chloride-Plots

It is commonly known that the Cl^- concentration determines the overall concentration of the cations in submarine hydrothermal fluids (cp. with sec. 1.2 and fig. 3.8), so the Cl^- to cation ratio is important to determine, whether a cation has been removed or added to the fluids and to distinguish between low and high Cl-content hydrothermal fluids. Fig. 3.12 plots the Cl^--concentrations against the concentrations of the major anions and cations of

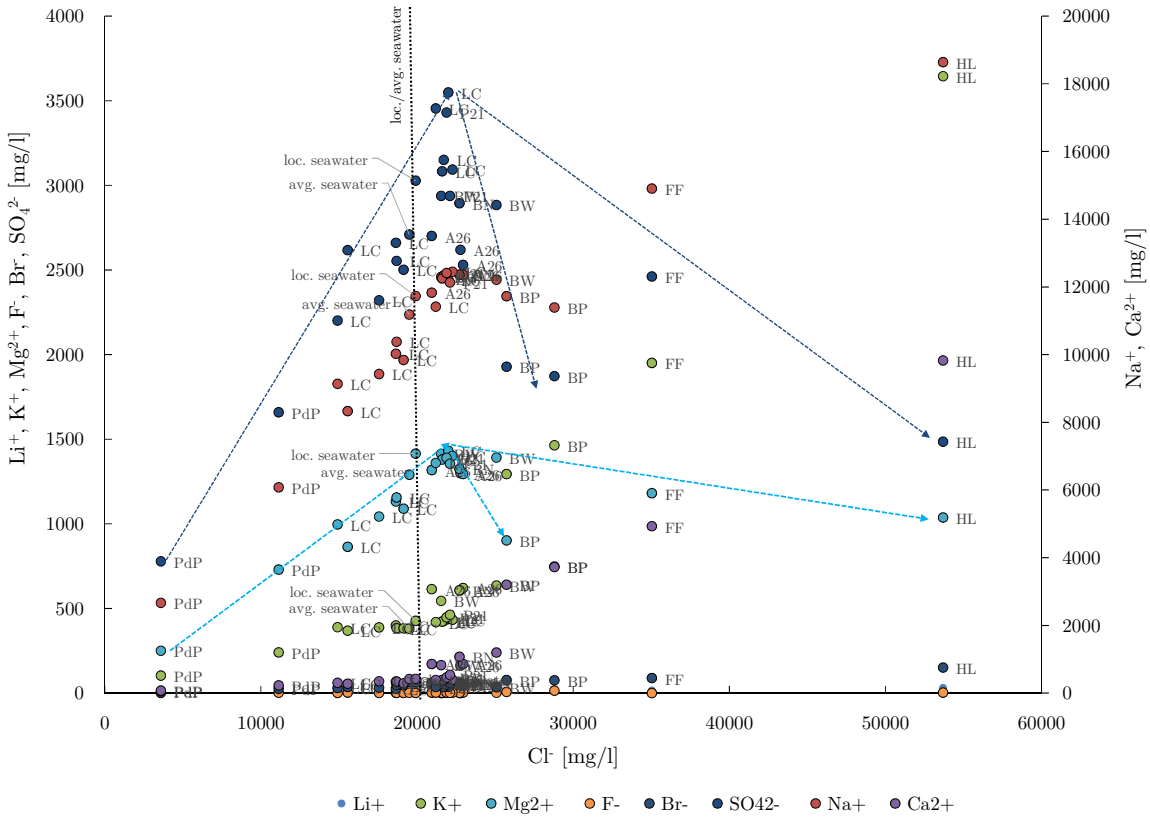

Fig. 3.12.: Li^+, Na^+, K^+, Mg^{2+}, Ca^{2+}, F^-, Br^- and SO_4^{2-} plotted with Cl^- in comparison with local seawater (Seebauer 2015) and average seawater (Brown 2001). The vertical black dotted line shows the Cl^- of both seawater values and the dotted arrows emphasize the trends of Mg^{2+} and SO_4^{2-}.

the samples from 2015 and reveals two trends: The ratios of Li^+, K^+, Ca^{2+} and Br^- with Cl^- increase from Pozzo di Pina over La Calcara towards the seawater ratios and increase furthermore from Black Point over Fumarolic Field to find their maximum at Hot Lake as expected by their EC, forming linear trend lines. Interestingly Na^+ increases also linearly from Pozzo di Pina towards the local seawater but then decreases at Black Point, contrary to its relatively high EC, to follow an slightly less steep increase over Fumarolic Field towards Hot Lake. Mg^{2+} and SO_4^{2-} ions have their maximum ratio near the seawater ratios, fall towards lower ratios at Black Point, increase slightly at Fumarolic Field and find their minimum (aside from the groundwater) at Hot Lake. These falling ratios at Black Point, Hot Lake and Fumarolic Field indicate hydrothermal influence on the local seawater and the removal of Mg^{2+}, SO_4^{2-} and partly Na^+ (at Black Point), an indication for seawater as major source of the submarine hydrothermal system Panarea (cp. sec. 1.2). At the same time the ratios of La Calcara with low Cl^- and ion concentrations are lower than seawater, distinguishing a hydrothermal fluid with lower Cl^- content and thus lower cation concentrations. As described in sec. 1.2 two phases can occur during phase separation. On the one hand, a phase with higher Cl-content than seawater can commence, on the other hand a lower Cl-content phase is possible.. The samples from La Calcara could be a hint or even a proof of such a low

Cl^- content hydrothermal fluid (lower than the surrounding seawater) with correlating low cation concentrations, while Black Point, Fumarolic Field and Hot Lake indicate a high Cl^- content fluid with correlating high cation concentrations (except of course for Mg^{2+} and partly at Black Point for Na^+). As for the other areas a high Cl^- content fluid is assumed, based on the partly enriched anion and cation concentrations, mixed with local seawater, thus overriding and buffering the typical elevated concentrations of cations and anions towards the seawater concentrations.

3.2.4. Magnesium plots

Plotting the main ions from samples taken in 2015 and from samples taken in 2009 (Sieland 2009) against the depleted Mg^{2+}-cation concentrations identifies three distinctive groups of water. Similar to other findings (Price et al. 2015) the ion ratios have their origin in the local seawater, at Hot Lake and Black Point all plotted ions have their maximum ion concentration together with the minimum Mg^{2+}-concentration. Hot Lake and Fumarolic Field display strongly increasing ion concentrations with weakly decreasing Mg^{2+} concentrations. Samples from Black Point show mostly trends towards moderate ion enrichment in combination with the strongest depletion of Mg^{2+}. Exceptions are the Na^+ concentrations with a neutral - depleting trend. Contrary samples from La Calcara and Pozzo di Pina describe mostly trends towards ion depletion or only slight enrichment compared to the local seawater in combination with depletion of Mg^{2+}. These trends of depletion for the main ions/Mg^{2+} ratios compared to local seawater at La Calcara indicate again a low Cl-content hydrothermal phase, in which Mg^{2+}-cations are still removed and replaced by e.g. Ca^{2+} and Mn^{2+}-cations, resulting in extreme high concentrations of both last mentioned cations. Furthermore subsurface dissolution of Ca-plagioclase and calcite could explain the high Ca^{2+} concentrations (Tassi et al. 2009).Exception is the plot for both mostly depleted ions Mg^{2+} and SO_4^{2-}. It results in two different trends of depletion: The first one is from the samples taken in 2015 and comes close to reach the zero point, indicating a complete removal of Mg^{2+} and SO_4^{2-} at the end of the trend line. Black Point is the investigation area with the highest removal of both ions, while the groundwater from Pozzo di Pina does not have high concentrations of both elements, hence is at the low concentration end of the trend line. The second trend line mostly formed from samples taken in 2009 intercept the x-axis at over 400 mg/l magnesium and places Hot Lake and Black Point at the highest removal rates, indicating only an incomplete removal of SO_4^{2-} from the hydrothermal fluids. This difference is hard to explain, either the sampling procedure was different, biasing the results, or the hydrothermal system changed and hence the results differ.

Still both sampling years reveal again the removal of both Mg^{2+} and SO_4^{2-}, typical for submarine hydrothermal systems (cp. with sec. 1.2). It should be noted that especially for samples from Hot Lake the results differ between 2009 and 2015 (cp. with fig. 3.13). In 2009 Hot Lake seems close to the samples from Black Point while the samples from Hot Lake and Fumarolic Field from the year 2015 differ strongly and display a far stronger enrichment trend

of the ions.

All samples have in common, that they depict the depletion of Mg^{2+} of the hydrothermal fluids compared to the local seawater in combination with ion enrichment as expected and in accordance to the EC of the corresponding investigation area. If one considers seawater as the main source of the submarine hydrothermal system Panarea, mostly Hot Lake, Fumarolic Field, Black Point and partly La Calcara are verifiably affected by Mg^{2+} -removal, typical for hydrothermal systems (cp. with sec. 1.2). All other areas are either only fed by hot unaltered seawater, or the hydrothermal fluids mixed in the subsurface with the local seawater and hydrothermal signatures such as the Mg^{2+}-removal are overwritten.

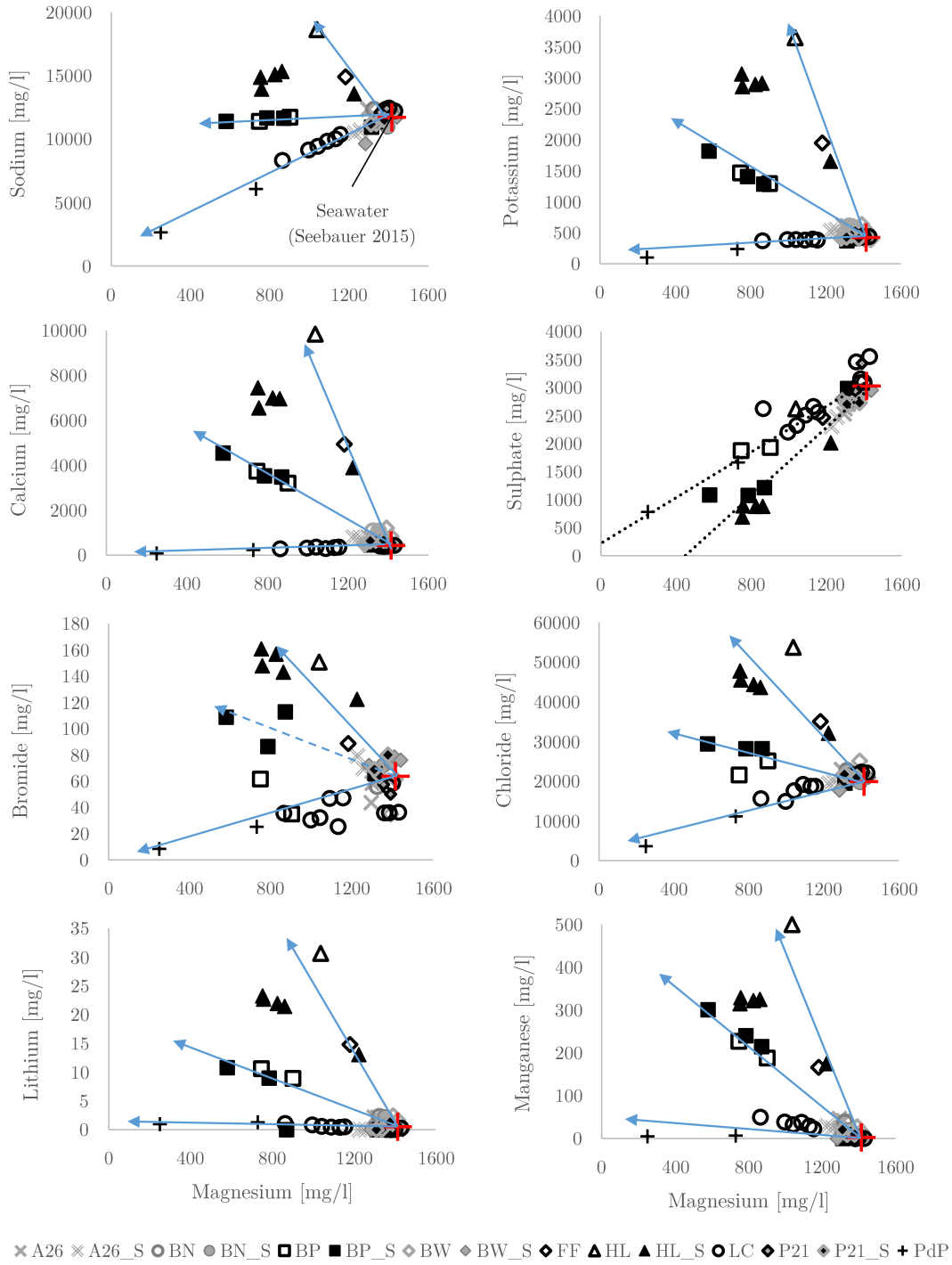

Fig. 3.13.: Mg^{2+} plots with Na^{+}, Li^{+}, K^{+}, Ca^{2+}, Mn^{2+}, Br^{-}, Cl^{-} and SO_4^{2-} forming three distinctive groups. Please note that older samples (Sieland 2009) are marked by an added _S in the legend.

Furthermore the samples from Pozzo di Pina seem to form end member points with the lowest concentrations of each element plotted together with Mg^{2+}. These plots give a strong hydrochemical indication that the groundwater from Panarea and the hydrothermal fluids from La Calcara are either connected with each other, evolve under similar conditions (mixtures?), or simply have similar ratios of ions and Mg^{2+}. La Calcara samples are either depleted in Mg^{2+} and the plotted ions, based on the local seawater or vice versa, La Calcara fluids start depleted/with low Mg^{2+} and ion concentrations and are then mixed and enriched by the local seawater, latter a strong indication of a low Cl-hydrothermal phase (cp. sec. 1.2).

3.3. Conservative elements

Conservative elements as Li, Br and Cl are not likely to be removed from the hydrothermal fluids once they are dissolved in them (cp. sec. 1.2). Of course Br can be excluded from halite precipitation, thus changing the Br-Cl ratio, by removing Cl and Br only to a minor share (cp. sec. 1.2). But the Na, Br and Cl concentrations are more or less linearly increasing, thus there is no indication of a NaCl precipitation and addition of Br to the hydrothermal fluids (cp. fig. 3.9 and cp. fig. 3.12). Hence these elements could partly mirror the hydrochemical composition of the hydrothermal fluids excluding the precipitations of primary and secondary minerals.

Fig. 3.14 reveals linear correlations between Li/Cl and Br/Cl: all three elements increase their concentrations in correlation to each other. Normed to the deviation of the normal seawater both Li/Cl and Br/Cl have similar slopes (cp. fig. 3.14). The three most distinguished sampling points are in ascending concentrations/deviations Black Point, Fumarolic Field and Hot Lake, while La Calcara displays scattered data points with low concentrations and/or depletion. The samples from Black Point, Fumarolic Field and Hot Lake seem to have the same origin or at least a similar evolution regarding their conservative element trends and seem to origin from a high Cl-content hydrothermal phase, as described in sec. 1.2. La Calcara has a tendency for lower Li, Br and Cl concentrations compared to seawater, indicating a low Cl-content hydrothermal fluid with corresponding low concentrations of Li as cation. Furthermore, the enrichment of the constituents seems to be linear: the more Li in the fluids, the more other elements are contained.

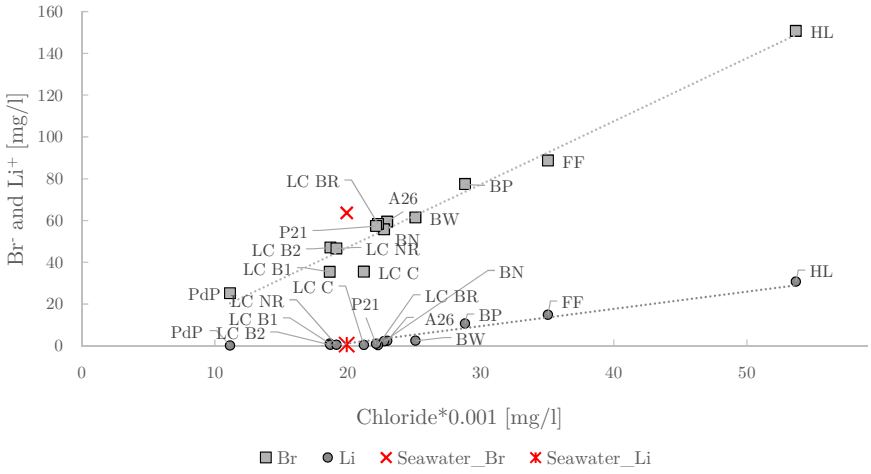

Fig. 3.14.: Lithium and Bromide concentrations/deviations plotted against chloride concentrations/deviations, revealing a correlating trend in all three element concentrations for at least the sampling points Black Point, Fumarolic Field and Hot Lake.

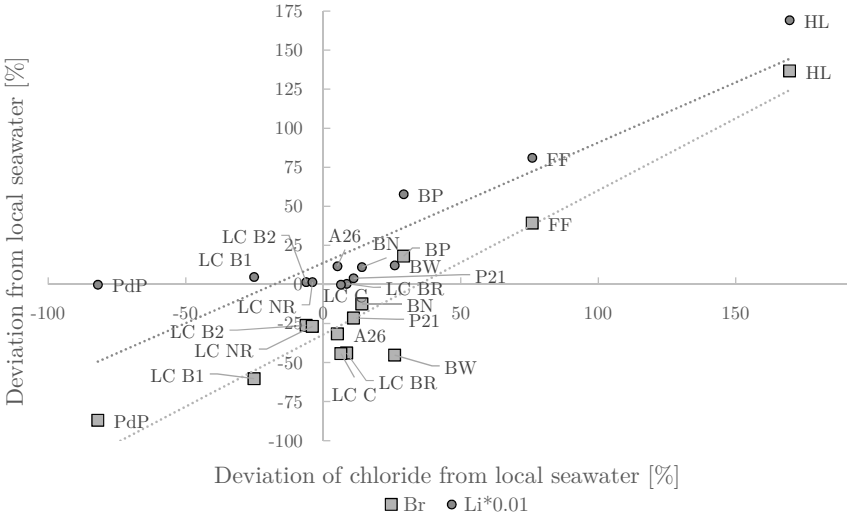

Fig. 3.15.: Deviation of lithium from local seawater plotted against bromide and chloride deviations, revealing a correlating trend in all three element concentrations for at least the sampling points Black Point, Fumarolic Field and Hot Lake.

3.4. Multi element analysis

The results of the multi-element analysis are displayed in the tables D.2, D.3 and D.4. Furthermore not all elements are included in the further assessment either because values for comparison of the local seawater are missing (e.g. all REE), or the elements are not detectable in sufficient sample points, making a comparison questionable. Both analytical measures, the ion chromatography analysis and the multi-element analysis result in a similar trend for the main ions and constituents of the taken water samples as described in the following. Fig. 3.16 and fig 3.17 compare the elements and their enrichment against the local seawater. Considering the electrical conductivity and the concentration of the main ions (cp. with figures 3.3, 3.7 and 3.11) in descending order Hot Lake, Fumarolic Field and Black Point show for most elements the highest enrichment compared to the local seawater. Samples from La Calcara and Pozzo di Pina show the lowest element enrichment and/or depletion compared to the rest of the samples.

Still besides this overall trend the different elements show various trends regarding their enrichment: **Beryllium** is strongly enriched in all samples (up to 12,840% at Hot Lake) except for La Calcara Ball 1, Ball 2, Black Rock, Chimney, New Rock and Pozzo di Pina with an enrichment between 100% and 243%. The values for La Calcara Ball 2, Chimney and Pozzo di Pina are below the detection limit. **Boron** shows a similar trend: While especially Black Point, Fumarolic Field and Hot Lake are highly enriched (up to 3,180% at Hot Lake), again the samples from La Calcara, Point 21 and Pozzo di Pina show weaker enrichment and/or depletion between -3.9 and 60%. **Aluminum** has only one clear peak at Black Point with an enrichment of 10,238%, probably due to the low pH of Black Point hindering a precipitation. Other samples are enriched between 52% at Bottaro West and 536% at Fumarolic Field and do not show a clear trend. **Vanadium** is highly enriched at Black Point (792%) and Pozzo di Pina (449%), all other samples show low enrichment from LC Ball 2 with 28% to highest depletion at -36% at Hot Lake, against the trend of all other elements. **Iron** has similar to Aluminum only one high peak at Black Point with a tremendous enrichment of 72,693%, followed by LC Black Rock (3,196%), LC New Rock (1,489%) and Fumarolic Field (1,164%). The peak at Black Rock can be easily explained with Black Point's low pH, hence the iron stays in solution and does not precipitate immediately. **Nickel** is equally distributed over all investigation areas, with only minor peaks at LC Chimney (680%), Hot Lake (623%) and Bottaro Nord (611%). All other areas lay in the range between 210% at Point 21 and 498% at Black Point, mostly around 300% enrichment. **Gallium** is also equally distributed: all samples except for Hot Lake (68%) are depleted in the range between -79% at LC Chimney and -12% and Black Point. LC Ball 2, Black Rock, New Rock and Pozzo di Pina have values below the detection limit. **Arsenic** is only found highly enriched in Black Point (8,701%), Bottaro Nord (1,041%), moderately enriched in La Calcara (51% - 248%) (except Black Rock with -64%) and lowly depleted in Point 21 (-24%). **Selenium** shows for all samples high enrichment up to 4,624% at Hot Lake, followed by Fumarolic Field (3,072%).

The lowest concentrations are found at Point 21 and Pozzo di Pina with "only" 850% and 530% enrichment. All other samples are in the range between these values. Showing strong enrichment at Hot Lake, Fumarolic Field and Black Point with values up to 11,330% (Hot Lake), and still high enrichment at Area 26, Bottaro Nord and Bottaro Nord **Rubidium** exhibits a clear trend: High enrichment at most sample points except for La Calcara (250% to -18%), Point 21 (150%) and Pozzo di Pina (-20%). **Strontium** follows again the general trend: Highest enrichment at Hot Lake (1,381%), followed by Fumarolic Field (897%) and Black Point (657%). Area 26, Bottaro Nord and West and Point 21 show slight enrichment between 10% at Point 21 and 146% at Bottaro West. La Calcara and Pozzo di Pina show depletion between -56% at Pozzo di Pina and -13% and LC New Rock. **Molybdenum** is depleted in all samples in the range between -90% at Bottaro Nord and -9% and LC New Rock. Only exceptions are LC Ball 2 (26%) and LC Chimney (223%). **Tellurium** shows considerable enrichment at especially Hot Lake (2,888%), Fumarolic Field (1,202%), Black Point (797%) and Bottaro Nord (401%). Values of minor enrichment are found at the rest of the investigation areas, with the minimum at Pozzo di Pina (-56%). **Barium** has three major peaks: Black Point (21,541%), Hot Lake (19,008%) and Fumarolic Field (12,773%). After these peaks no clear trend is recognizable, e.g. La Calcara ranges from 55% at Black Rock to 1,253% at Chimney, the other areas are between 467% at Point 21 and 1,401 at Pozzo di Pina. **Thallium** shows extreme enrichment at Fumarolic Field (91,133%), Hot Lake (90,927%) and Black Point (53,046%). Other investigation areas such as La Calcara show still high values of enrichment in the range between 402% - 3,500%. Area 26 (168%), Pozzo di Pina (170%) and Bottaro West (-55%) show the smallest enrichment. **Lead** is enriched at Black Point by 1,510%, but depleted in all other samples by around -100%, with Pozzo di Pina as minimum with 52%. **Bismuth** is equally depleted in the range between - 77% at LC New Rock and -23% at LC Black Rock. The only minor enrichment is to be found at Point 21 with 8%. **Uranium 235** is similar to Bismuth equally depleted in all samples in the range between -81% at Fumarolic Field and -8% at LC Chimney. Area 26, Bottaro Nord and Hot Lake are below the detection limit.

Silica does not have a distinctive trend. However, Pozzo di Pina exhibits high enrichment (6,448%), comparable to Hot Lake (6,053%) and Fumarolic Field (5,803%), only topped by Black Point (12,137%) and Area 26 (9,097%). Still the enrichment is lower for the samples of Bottaro West with 1,611%, La Calcara New Rock with 1,170% and La Calcara Black Rock with 488%. The high concentrations of Si can be both an indicator for the temperature and the residence time of the hydrothermal fluids, because the solubility of Si depends on the temperature and exposure time to the surrounding bedrock. The higher the temperature, the higher the solubility, indicating the geothermal influence on the taken water samples, especially for the groundwater of Pozzo di Pina. Hence high Si concentrations could indicate high temperatures and long contact times between the fluids and the surrounding bedrock, especially at Black Point, Area 26, Fumarolic Field, Hot Lake and Pozzo di Pina. At Black Point it seems as if both, high temperatures and a long contact time results in the highest Si

concentrations. However, mixing processes during the ascent with e.g. local, colder seawater can drastically reduce the solubility of Si leading to precipitation of Si and thus reduce the overall concentration of Si. So it is not possible to distinguish between long contact times and high temperatures as main reasons for high Si concentrations, e.g. at Black Point.

Curiously no elements are more depleted at Pozzo di Pina than at other sampling points, maybe except for strontium. Still Pozzo di Pina shows less enrichment in most elements or similar depletion in most elements as the other sampling points. Only exceptions are Si, V and Sr as described above. So the hope to find a strong tendency or a trend of enrichment and/or depletion for all elements, indicating the same source of water for La Calcara and Pozzo di Pina is not found.

However, the **main constituents** (Li, F, S, Cl, Na, Mg, K, Ca) and some trace elements, e.g. B, Be, Rb, Mn and Sr depict this trend as presented in fig 3.18. It shows mostly the same picture as the analysis of the major ions brought and aligns with the general trend: High enrichment at Hot Lake, Fumarolic Field and Black Point for all shown elements, except for magnesium and sulfur and low enrichment and/or depletion at the samples from La Calcara and Pozzo di Pina. **Sulfur** has two minor peaks at Point 21 (24%) and Bottaro Nord (18%). All other areas are depleted in the range from -76% at Black Point and -11% at Area 26 and **magnesium** is almost equally depleted in all samples, as shown before. **Potassium** is enriched at Black Point, Fumarolic Field and Hot Lake and depleted at all other areas, except for Area 26 and Bottaro West with almost no deviation from the local seawater. **Manganese** shows by far the most extreme enrichment of all elements with peaks up to 1,251,722% at Hot Lake, 633,682% at Black Point and 578,928% at Fumarolic Field. In contrast the rest of the samples range between 140,528% at Area 26 and 2,459% at LC Black Rock. Only LC Black and New Rock show "low" enrichment, the other samples are equal to the rest of taken water samples like Bottaro Nord and West etc. and seem to represent the normally enriched baseline of the hydrothermal fluids. **Strontium** follows again the general trend: Highest enrichment at Hot Lake (1,381%), followed by Fumarolic Field (897%) and Black Point (657%). Area 26, Bottaro Nord and West and Point 21 show slight enrichment between 10% at Point 21 and 146% at Bottaro West. La Calcara and Pozzo di Pina show depletion between -56% at Pozzo di Pina and -13% and LC New Rock.

Using the enrichment of the main constituents three groups of waters can be distinguished: 1. The extremely enriched (compared to local seawater) water from Hot Lake, Fumarolic Field and Black Point, 2. Partly enriched water samples such as Area 26, Bottaro Nord and West and Point 21 and 3. mostly depleted waters, which include all samples from La Calcara, having similar ranges of depletion of the elements as the groundwater from Pozzo di Pina. It seems as if Hot Lake, Fumarolic Field and Black Point are fed by waters passing their surrounding bedrock under extreme conditions, such as high temperature and high pressure, fostering the dissolution of elements and WRI (e.g. ion exchange), leading to the extreme enrichment of the elements as shown above. The dissolution processes at Hot Lake and Fumarolic Field could happen under similar conditions, due to the similarity regarding the

concentration and enrichment of the elements and the vicinity of the sampling points to each other (s. fig. A.1 and 1.4). Black Point however has some characteristics which separates it from Hot Lake and Fumarolic Field, e.g. the high concentrations of trace elements as (Si, Fe, As, V, Al, Ba and Pb) and furthermore it is spatially separated from both other sampling points (s. fig. 1.4). Hot Lake and Fumarolic Field show greater enrichment of of the main constituents (cp. fig. 3.18) and thus the assumption of two different sources/evolutions of the submarine hydrothermal fluids at Black Point and Hot Lake/Fumarolic Field is made. Seemingly Hot Lake and Fumarolic Field are fed by a condensed seawater or a high Cl-content hydrothermal phase (cp. 1.2), with greatly enriched main constituents and partly enriched in trace elements. Black Point however, already distinguished by its extremely low pH and higher temperature, also seems to be fed by high Cl-content hydrothermal phase source, presumably with a magmatic contribution (HF as indicator, explaining the extreme low pH and high F^- concentrations) and thus a higher leaching potential for trace elements.

The samples of La Calcara seem to mirror the samples of Pozzo di Pina regarding the trend of the elements, with only minor exceptions such as Black Rock showing enriched sodium and chlorine concentrations and New Rock with slight enrichment of chlorine. Still the depletion of sodium and chlorine in most samples from La Calcara could indicate a water source with lower concentrations of both elements in comparison to seawater, or more likely a low Cl-content hydrothermal phase as described in sec. 1.2 leading to low Na^+ concentrations as well as low concentrations for all other cations, referring to the electrical balance of the fluids. The samples with even higher concentrations of sulfur than seawater could indicate a low Cl-content hydrothermal fluids, undersaturated regarding SO_4^{2-} , which dissolves precipitated SO_4^{2-} mineral phases and has thus a higher concentration of sulfur than the surrounding seawater. Still one has to consider that the sulfur enrichment is maximally 24% at Point 21 and 18% at Bottaro West, both areas with a strong fumarolic degassing activity. So either the enrichment could be still in the range of error of the applied analytical measures, or H_2S contained in the ascending gases dissolves in the water column and increases the sulfur concentrations.

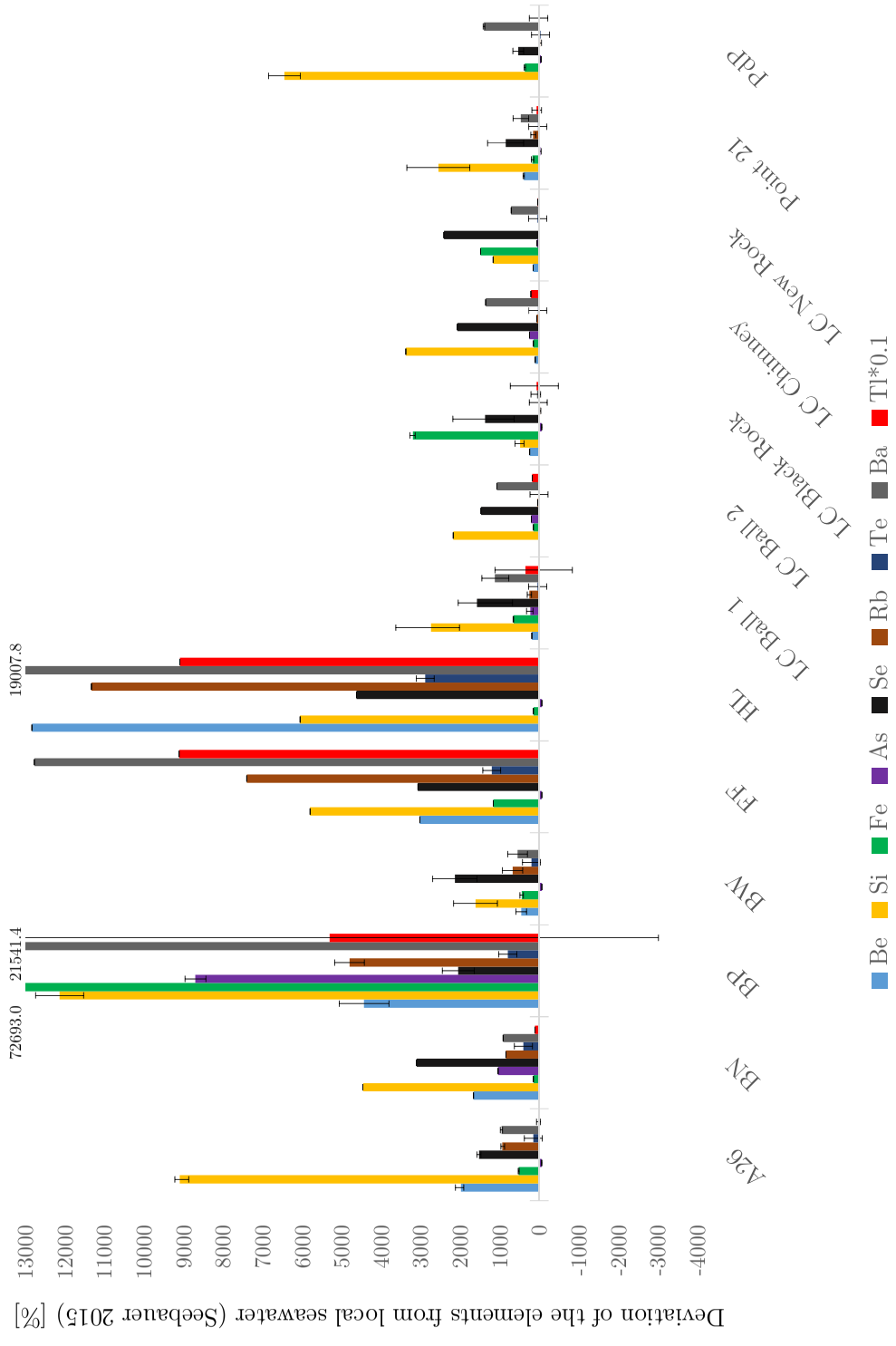

Fig. 3.16.: High deviations of trace elements compared to local seawater. Please note the applied dilution factors to single element concentrations.

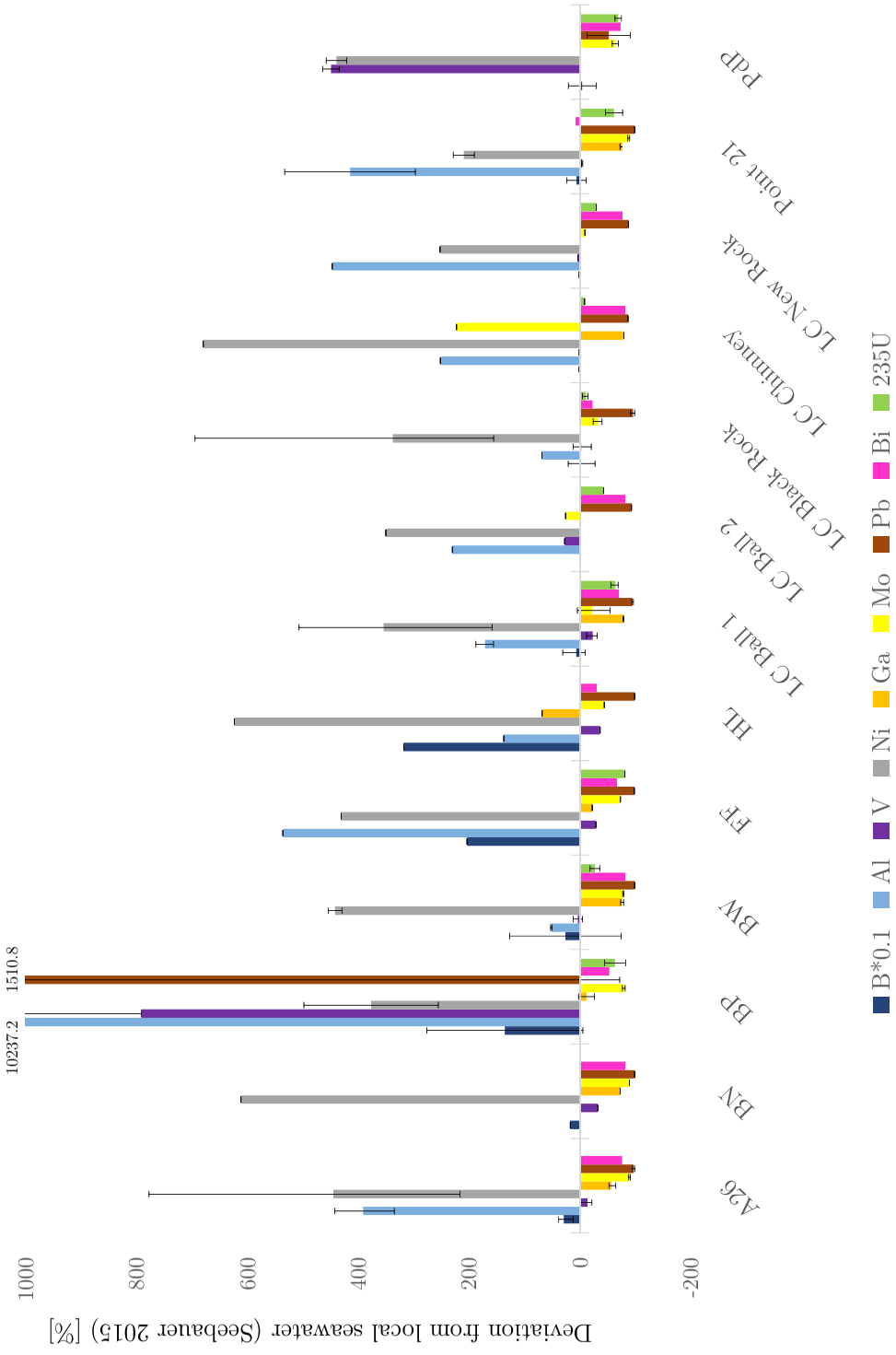

Fig. 3.17.: Low deviations of trace elements compared to local seawater. Please note the applied dilution factors to single element concentrations.

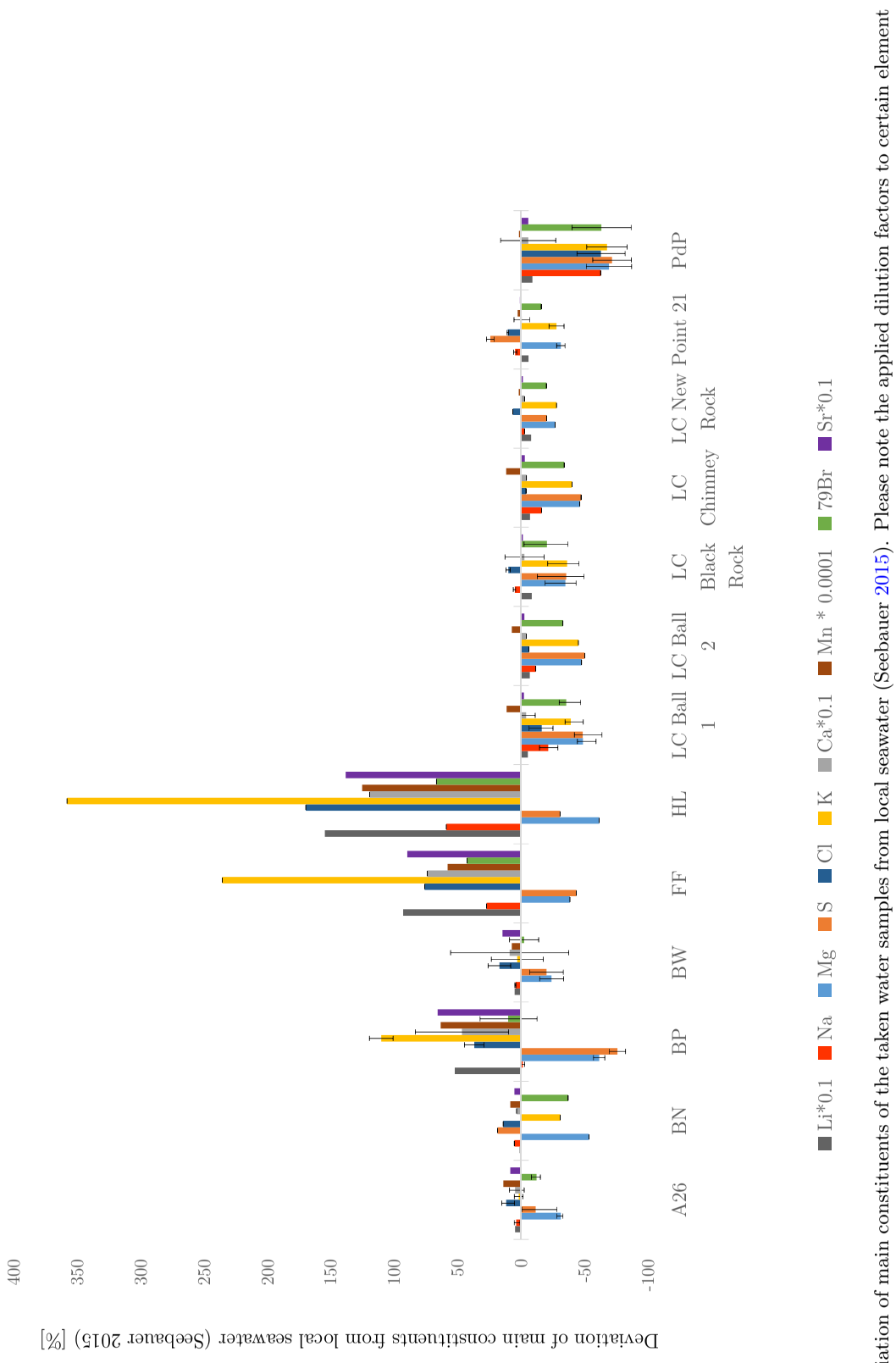

Fig. 3.18.: Deviation of main constituents of the taken water samples from local seawater (Seebauer 2015). Please note the applied dilution factors to certain element concentrations.

3.5. Stable Isotopes

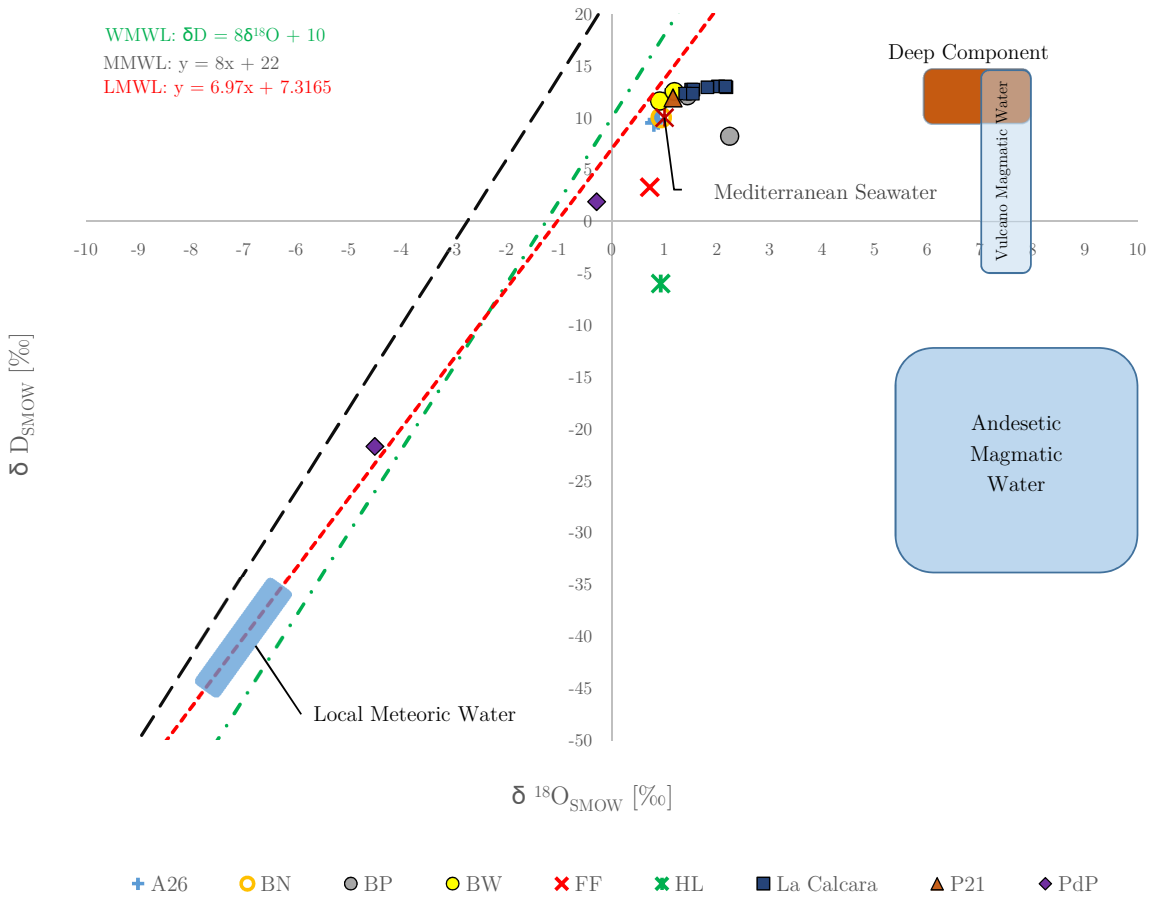

Fig. 3.19.: Isotopic composition of the taken water samples from 2015 in comparison to literature values of possible water sources contributing to the hydrothermal system Panarea (Bolognesi and D'Amore 1992; Capasso et al. 1997; Chiodini et al. 1995; Craig 1961, 1963; Gat and Carmi 1970; Gat 2010; Gerardo-Abaya et al. 2000; Giggenbach 1992; Italiano and Caruso 2011; Liotta et al. 2006a; Paonita et al. 2013; Tassi et al. 2009).

The isotopic compositions of the taken water samples from 2015 are displayed in tab. E.1 and are compared in fig. 3.19 to the VSMOW standard and literature values for possible sources contributing to the hydrothermal system Panarea as listed in tab 3.2. Furthermore the World Meteoric Water Line (WMWL) (Craig 1961), the Mediterranean Meteoric Water Line (MMWL) (Gat and Carmi 1970) and the average of both Local Meteoric Water Lines (LMWL) from Salina (Italiano and Caruso 2011) and Stromboli (Liotta et al. 2006a) describe the isotopic composition of the precipitation of the respective locations, as shown in tab 3.1.

Except for one sample from Pozzo di Pina, all samples plot on the right of the LMWL, displaying enriched $\delta^{18}O$ values, close to Mediterranean seawater. While for some samples the enrichment is noticeable, e.g. Hot Lake, Fumarolic Field and Black Point, for most other samples the enrichment is even below 1‰ (e.g. Area 26, Bottaro Nord and West, Point 21). The stable isotopes are in accordance with the results of the water chemistry insofar as the

Tab. 3.1.: Used Meteoric Water Lines

Source	Line	Equation
(Gat and Carmi 1970)	MMWL	$\delta^2D = 8\delta^{18}O + 22$
(Craig 1961)	WMWL	$\delta^2D = 8\delta^{18}O + 10$
(Italiano and Caruso 2011)	LMWL Salina	$\delta^2D = 6.97\ \delta^{18}O + 7.3165$
(Liotta et al. 2006a)	LMWL Stromboli	$\delta^2D = 6.5\ \delta^{18}O + 6.7$
	Average LMWL (Panarea)	$\delta^2D = 6.735\ \delta^{18}O + 7.00825$

isotopic compositions of Hot Lake, Fumarolic Field and partly Black Point are different from the rest of the submarine hydrothermal fluids sampled at other investigation areas. All in all Hot Lake displays the greatest deviation from the local seawater expressed the highest depletion of δ^2D (-6.0 ‰), followed by Fumarolic Field (3.3 ‰) and Black Point (8.2 ‰) compared to the LMWL. Exceptions are the groundwater samples with even lower values (s. below). Also noticeable are the two different trends of Hot Lake/Fumarolic Field (depleted δ^2D) and Black Point (slightly depleted δ^2D, but stronger enriched δ^{18}O).

As for other parameters before, the samples of La Calcara plot in a cluster, enriched in δ^2D and δ^{18}O compared to the seawater. Most importantly the samples form a short horizontal line to the right, to enriched δ^{18}O values, compared to the LMWL. These shifted δ^{18}O values could be a hint for water-rock interactions at La Calcara (Craig 1963). During the water-rock interactions, the isotopic composition of the water could be maximally shifted, until an equilibrium with the surrounding bedrock is established. Due to the location of the Panarea system between two distinguished formations (western and eastern aeolian arc) the hydrothermal fluids can react with both or only one of the bedrock lithologies (s. sec. 1.1) (Price et al. 2015).

The two groundwater samples taken in 2015 are most curious: both plot near the LMWL, but one sample (PAN_09042015_PdP_equ) plots at highly negative values for both δ^2D (-4.5 ‰) and δ^{18}O (-21.7 ‰), while the other sample (PAN_09032015_PdP) shows even slight enrichment for δ^2D (1.9 ‰) and only slight depletion for δ^{18}O (-0.3 ‰). So during the sampling process of these two samples at two different days the isotopic composition changes drastically from almost neutral and close to VSMOW to very light values, near to the isotopic composition of the local meteoric water. Maybe the pump withdraws water from two different sources, explaining different isotopic compositions. If we two have layered aquifers, on the top mostly meteoric water, beneath it geothermaly and maybe even seawater dominated impacted groundwater with an isotopic composition close to the local seawater both water sources could be pumped up, depending on the unknown frequency of the pumping and the unknown pumping rate (up-coning). Still the two taken water samples, with relatively heavy, enriched values, taken after short time of pumping could be distinguished as altered meteoric water, while the last taken sample, after the on-site parameters were stable, would represent the groundwater of Panarea. The vicinity of the δ^2D and δ^{18}O values to the range of the local meteoric water could validate the last option.

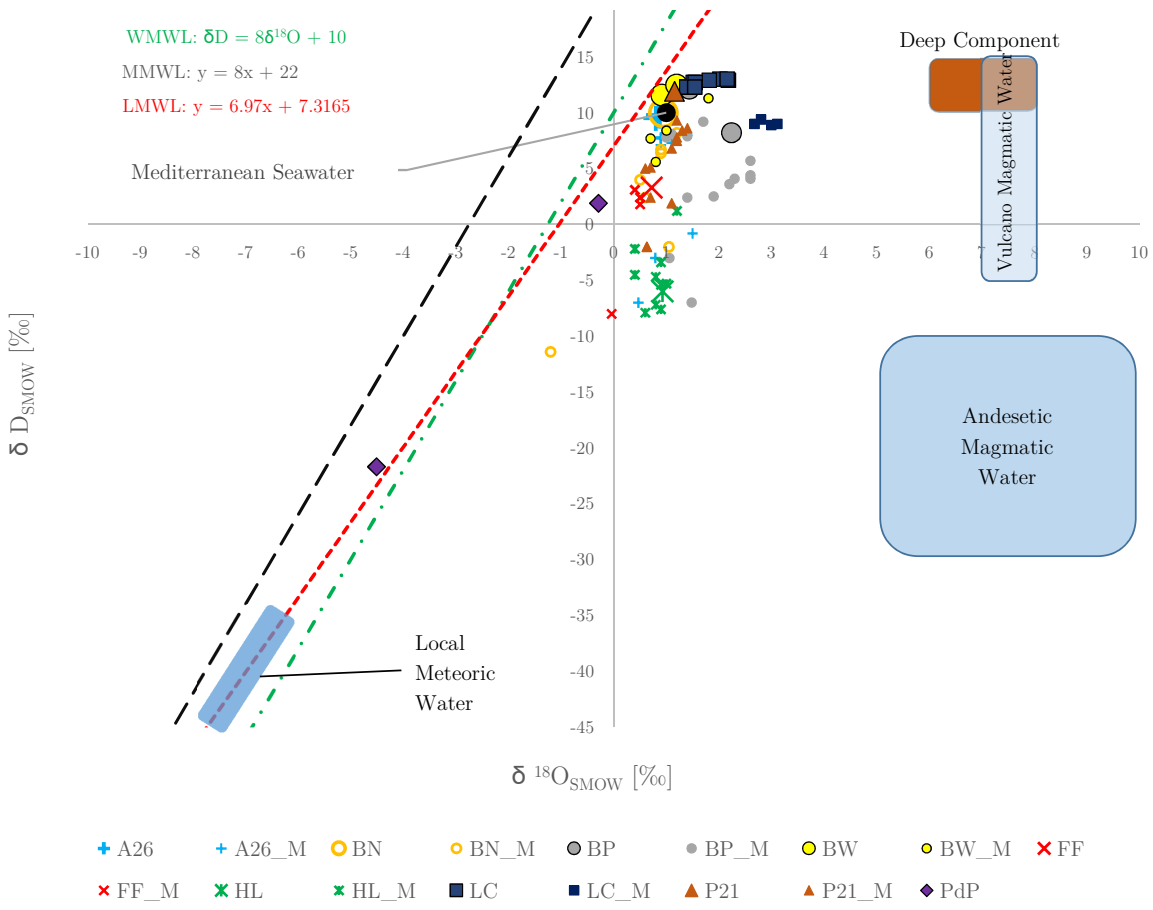

Fig. 3.20.: Isotopic composition of the taken water samples from 2015 and from 2007 to 2011 (Müller 2011) in comparison to literature values of possible water sources contributing to the hydrothermal system Panarea (Bolognesi and D'Amore 1992; Capasso et al. 1997; Chiodini et al. 1995; Craig 1961, 1963; Gat and Carmi 1970; Gat 2010; Gerardo-Abaya et al. 2000; Giggenbach 1992; Italiano and Caruso 2011; Liotta et al. 2006a; Paonita et al. 2013; Tassi et al. 2009). Please note that values from 2015 are depicted using bigger, framed symbols than older values compiled by Müller (2011).

Tab. 3.2 lists the possible influences and the following paragraph explains these influences, as presented in fig. 3.21 to explain the shifted (enriched) $\delta^{18}O$ isotope signatures of the water samples taken in 2007 to 2011 (Müller 2011) and 2015.

Comparing the isotopic composition from the samples taken 2015 with older samples from 2007 to 2011 ((Müller 2011)) the values are plausible (s. fig. 3.20 and fig. 3.21). Some sampling points like Hot Lake, Fumarolic Field and Bottaro West show clustering - including new and old data points - of their isotopic composition with only minor deviations. Other samples like Bottaro Nord, Black Point and Point 21 partly match but as well mismatch. The range of the deviations is greater for the $\delta^{2}H$ than for the $\delta^{18}O$ values. Both Black Point and Point 21 show the greatest range of values. Area 26 shows a cluster with three outliers towards depleted $\delta^{2}H$ values. Most curiously is the comparison for the values for La Calcara: Both new and old data form two horizontal lines, exhibiting enriched $\delta^{18}O$ values. While all of the new and old values of the various investigation areas are shifted towards enriched $\delta^{18}O$ the

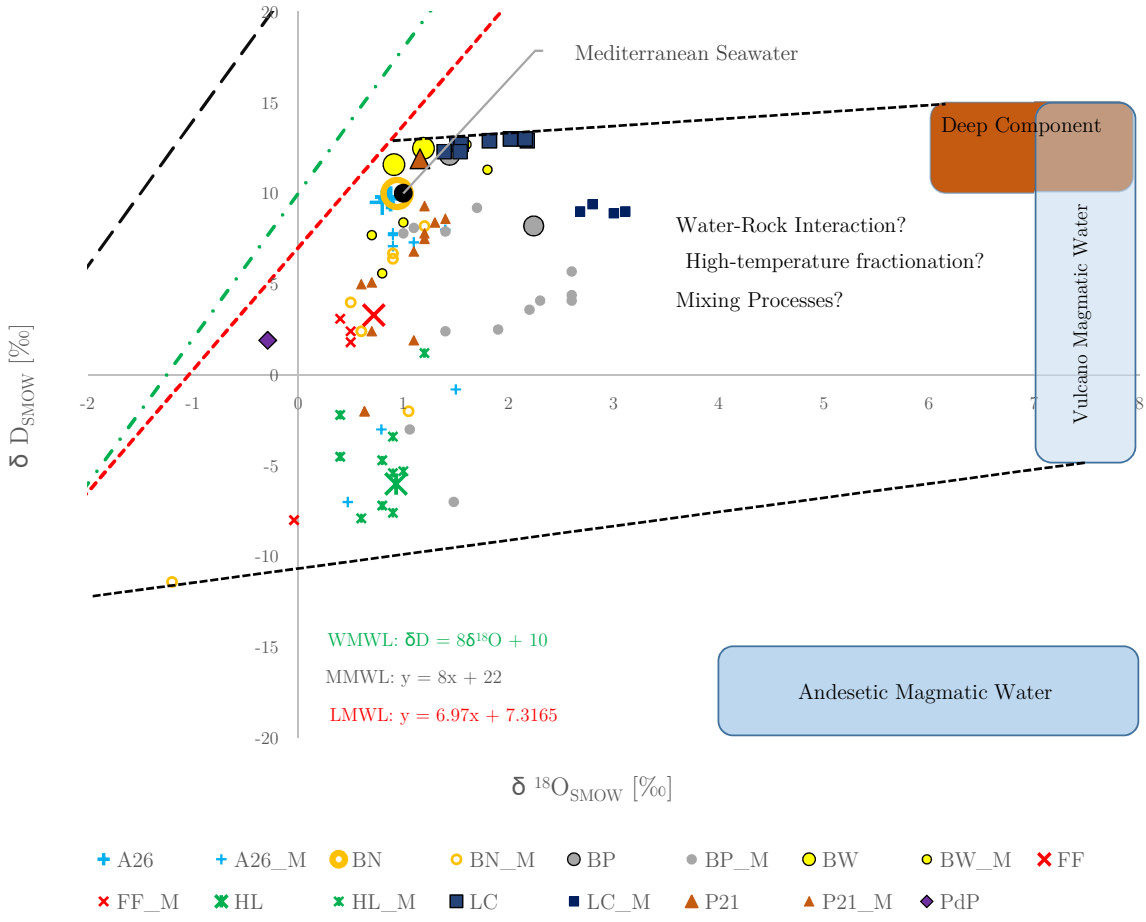

Fig. 3.21.: Possible processes explaining the shifted (enriched) $\delta^{18}O$ isotope signatures of the taken water samples from 2007 to 2011 (Müller 2011) and 2015 (Bolognesi and D'Amore 1992; Capasso et al. 1997; Chiodini et al. 1995; Craig 1963; Gat 2010; Gerardo-Abaya et al. 2000; Giggenbach 1992; Paonita et al. 2013; Tassi et al. 2009). Please note that values from 2015 are depicted using bigger symbols than older values compiled by Müller (2011).

La Calcara samples depict this trend (Craig 1963).

Tab. 3.2 lists the possible influences and the following paragraph explains these influences, as presented in fig. 3.21 to explain the enriched $\delta^{18}O$ isotope signatures and the depleted $\delta^{2}H$ signatures of the water samples taken between 2007 to 2011 (Müller 2011) and 2015.

In former investigations of geothermal systems the origin of geothermal spring water is explained with the major contribution of meteoric water (Craig 1963). Various thermal springs and their $\delta^{2}H$ plot on the local precipitation, but their corresponding $\delta^{18}O$ values are enriched to heavier values. This enrichment is the results of water-rock interactions (WRI) during which the oxygen of the water interacts with the oxygen of the surrounding bedrock (e.g. calcite and silica phases), resulting in heavier $\delta^{18}O$ values. During the WRI the hydrogen isotopes are almost unchanged, exceptions may occur during interactions with clay minerals or hydrated salt deposits (Gat 2010).

Tab. 3.2.: Potential water sources contributing to the hydrothermal system in Panarea and their isotopic compositions, (Müller 2011).

Potential water source	δ^2H_{VSMOW} [‰]	$\delta^{18}O_{VSMOW}$[‰]
Andesitic magmatic water (Global) (Chiodini et al. 1995; Giggenbach 1992)	-30 to -10	5.5 to 6.5
Deep component (Vulcano) (Capasso et al. 1997)	10 -to15	6 to 8
Local meteoric water (Stromboli) (Liotta et al. 2006a,b)	-35 to -45	-6.2 to -8.5
Magmatic water (Vulcano) (Bolognesi and D'Amore 1992; Paonita et al. 2013)	-5 to 15	7 to 8
Mediterranean seawater (Sicily) (Grassa et al. 2006)	1	10

However, the origin of hydrothermal water is far more complicated to explain than for geothermal springs. Often waters from hydrothermal systems plot in low slope lines at enriched oxygen isotope values to the right of the local meteoric water line (Gerardo-Abaya et al. 2000), as shown by the black dotted lines in fig. 3.21. The enrichment can result from a mixture of meteoric water and a hypothetical andesitic magmatic water with depleted δ^2H and enriched $\delta^{18}O$ values (Giggenbach 1992). Investigations of the isotopic composition of fumarole gases of the Vulcano system lead to the hypothesis of a "Vulcano magmatic water", enriched in both δ^2H and $\delta^{18}O$ values and a "deep component" with enriched δ^2H and $\delta^{18}O$ values (Capasso et al. 1997). "'Magmatic vapour" is found in the fumaroles on Vulcano Island and explains the high range of the δ^2H values with a deep and a connate (seawater)-contaminated magma source (Bolognesi and D'Amore 1992; Paonita et al. 2013). Lacking better sources and/or theories for the isotopic composition of the hydrothermal system Panarea, the findings of the Vulcano system are transferred to the Panarea system. Still all authors could not converge on one single magmatic source, making this source somehow questionable. To avoid the use of a hypothetical magmatic source high temperature fractionation was suggested (Truesdell et al. 1977). However, the disadvantage is, that the fractionation factors for the transition from liquid to vapour for hydrogen and oxygen are temperature dependent, hence each hydrothermal system behaves in a different way (Gat 2010). The discussion of possible water sources for hydrothermal systems and their isotopic compositions regarding hydrogen and oxygen isotopes is still an on-going one.

Three different types of Mediterranean seawater taking part in the submarine hydrothermal system Panarea are proposed (Tassi et al. 2009) as described in sec. 1.4, respectively three different types of hydrothermal fluids are distinguished (Price et al. 2015). The findings of the stable isotope analysis underline the Mediterranean seawater as major or even maybe only source of the submarine hydrothermal system Panarea. The original seawater now transformed into hydrothermal fluids at Black Point, Fumarolic Field and Hot Lake is strongly altered e.g. by WRI, indicating maybe a longer contact and reaction time with the underground, than

e.g. La Calcara had.

All areas with an isotopic composition close to the local seawater (Area 26, Point 21, Bottaro Nord and West and La Calcara) are either fed mainly by seawater slightly shifted towards higher/enriched δ^{18}O values (WRI or mixing with a deep component/magmatic water) or simply diluted again by local seawater, overriding any isotopic change from the original hydrothermal fluids. Hot Lake, Fumarolic Field and Black Point with their considerably altered isotopic compositions are also the areas with the greatest enrichment of the main constituents and trace elements. WRI would explain both, the shifted δ^{18}O values and the enrichment of several constituents of the hydrothermal fluids at these investigation areas.

However, the altered δ^{2}H values are problematic to explain. For instance the δ^{2}H values of vapors of fumaroles at Vulcano with an isotopic composition close to seawater (δ^{2}H = 10‰) mixed with magmatic fluids result in a depleted δ^{2}H between -15 to -25‰ (Paonita et al. 2002). Hence a mixing between magmatic fluids from the depth and vapour originating from local seawater could result in these depleted δ^{2}H values. Furthermore the two different trends of alteration of Hot Lake/Fumarolic Field (depletion of δ^{2}H, slight enrichment of δ^{18}O) and Black Point (slight depletion of δ^{2}H, enrichment of δ^{18}O) go along with the difference in the dominant enrichment of the main constituents at Hot Lake/Fumarolic Field and the dominant enrichment of trace elements at Black Point. However, the exact circumstances and processes influencing the isotopic composition of the found fluids are not determinable.

Concluding these results, a connection between the groundwater from Pozzo di Pina and La Calcara cannot be proven by means of stable hydrogen and oxygen isotopes, moreover seawater is proved to be the dominant or even the only mentionable source of the submarine hydrothermal system Panarea.

3.6. Evaluation of time series

The Scientific Diving Center Freiberg (SDC) works since 2006 on the submarine hydrothermal system Panarea and collected over the years more than 200 water samples of submarine hydrothermal fluids. In the following it is tried to describe and to explain trends and patterns of the hydrothermal fluids. Statistical methods are applied to gain further insight e.g. about patterns of concentrations of constituents and on-site parameters. At some points the findings of this thesis are compared to those of latest hypothesis regarding the hydrothermal system Panarea (Price et al. 2015) and commented on.

3.6.1. Constituent concentration extrema

To get a feeling and to be able to range the findings of the field campaign of 2015 tab. 3.3 displays extreme values of pH, EH, EC, major ions, trace elements and REE from samples of the last 10 years. Tab. 3.4 displays the deviation of the extreme values from preferably the local seawater (Seebauer 2015). If no values are available the average (Brown 2001) seawater is used (e.g. for all REE). To make these numbers more descriptive, fig. 3.22 displays the range of the various parameters and elements in form of Box- and Whisker-plots and the extreme values can be ranged in context with all other samples. The pH, E_H, Mg^{2+} and SO_4^{2-} of the submarine hydrothermal fluids are expected to show low values/concentrations (cp. sec. 1.2), hence the minima are displayed in tab. 3.3. Vice versa certain element concentrations (some main ions, trace metals, REE) are expected to be elevated, compared to local seawater, hence the maxima values are displayed to distinguish the fluids from the local seawater. Average values do not make sense, because the averages would mix all samples with their various grades of quality and would disguise extreme values, assuming to represent the "true" values/concentrations of the hydrothermal fluids for each parameter without any mixing and subsequent buffering with and towards local seawater (cp. sec. 1.2). For a complete overview over the minima and maxima and their corresponding deviations tab. F.1 and tab. F.3 show the maxima/minima of all parameters, while tab. F.2 and tab. F.4 show the corresponding deviations.

Compared to the findings of 2015 the general trend stays the same, beginning with the on-site parameters: The minimum values of the **pH** stay mostly between 5.4 (CAL_Ball 1) and 4.4 (Hot Lake). The single sampling point with a different pH is Black Point (vent) with a minimum pH of 2.4, which contradicts values published by Price et al. (2015). The latter publish pH values for Black Point vent fluids with an average of 4.23, based on only three samples, taken between 2008 and 2010 instead of the average of 2.79, based on 15 samples taken between 2007 and 2015, taken by the SDC Freiberg. Other samples from Black Point, taken from Black Point Mini and Black Point North have a minimum pH of 5.0, which separates the main Black Point vent from these two other sampling points. The minimum $\mathbf{E}_H$ is more curious: Contrary to all other areas, which have minima around -73 to - 27 mV, Black Point has a minimum of 42 mV, the mixed sampling point Black Point_MN 59 mV, La

Calcara Black Rock, 81mV and La Calcara Ball_1 265 mV. During further evaluation of the data set, a strong variation of the E_H is noted, e.g. Black Point has values up to 358 mV (cp. fig. 3.22). Calculating the **rH** shows most investigation areas have minima near the threshold between strongly reducing conditions (0-9) and weakly reducing conditions (9-17) with values between (7 and 9.5), with Black Point as absolute minimum (6.2). La Calcara Black Rock however and Ball_1 have minima in the weakly reducing field (13 and 20), the local seawater is at the threshold between indifferent systems and weakly oxidizing conditions (25.4). Still due to the broad and often inconsistent range of the E_H (oxidizing and reducing conditions at the same area) also the rH is affected and both parameters are thus excluded from further (statistical) analysis.

The **EC** maxima follow the trend of 2015: Hot Lake, Fumarolic Field and Black Point have in descending order the highest EC. Only one single sample of Bottaro North (82.4 mS/cm) lays in the range of Black Point (82.0 mS/cm) and Fumarolic Field (84.6 mS/cm). The EC of the remaining investigation areas (e.g Area 26, Bottaro West, Point 21) ranges mostly slightly above the local seawater ($\tilde{6}$0mS/cm). Because the EC follows the trend of 2015 (or vice versa) all other element concentrations are expected to be elevated at areas with elevated EC, which is proven in tab. 3.3 and 3.4. Typically depleted elements/ions in submarine hydrothermal systems like Mg^{2+} and SO_4^{2-} are also depleted at the Panarea submarine hydrothermal system. Both Mg^{2+} and SO_4^{2-} have their absolute minima over 10 years at Black Point, followed by Hot Lake and La Calcara. The enrichment/depletion is more clearly depicted in tab. 3.4. Fig. 3.22 shows the range of each parameter/element (except for the rH) as listed in tab. 3.3 and tab. 3.4.

Key parameters such as the pH, EC, Mg^{2+} and SO_4^{2-}, indicating hydrothermal influence (cp. sec. 1.2), follow the trend of 2015: Black Point shows by far the lowest pH within a small range, while La Calcara and the groundwater from Panarea mark the upper end with pH values up to 7.2. One reason for these differences could lay in the characteristics of the sampling points at Black Point and La Calcara. Whereas Black Point (vent) is a noticeable venting point with a well defined sampling point (drill hole), the samples from La Calcara are taken directly from the underground, mainly consisting of sand and gravel, probably resulting in varying sample qualities (contamination by surrounding seawater). The EC also follows the trend of 2015: Hot Lake, followed by Black Point and Fumarolic Field show the highest values, while the groundwater and La Calcara show the highest depletion compared to the local seawater. All other areas are mostly in the range of the local seawater or show slightly elevated values. Accordingly the concentrations of the main ions, the trace metals and the REE are also expected to be elevated at these areas (Hot Lake, Black Point, Fumarolic Field). The Cl^- concentrations more or less mirror the EC qualitatively, validating the importance of Cl^- as main anion and determinant of the overall ion concentration (cp. sec. 1.2). Both Mg^{2+} and SO_4^{2-} are depleted in all samples, only slight enrichments can be detected, which would fall within the error range of the analytical methods applied. Contradicting the EC both ions are mostly depleted at the investigation areas with the highest EC, namely Black Point and

Hot Lake, an exception is the groundwater). Additionally both ions are also strongly depleted at La Calcara, an area with a low EC but high temperatures, which leads to the precipitation of $CaSO_4$ and subsequent the depletion of SO_4^{2-}. Ubiquitous found precipitate structures at venting points prove the removal of SO_4^{2-} at La Calcara.

The extreme enrichment of the trace elements Mn, Rb, Cs and Ba emphasize again Hot Lake, Fumarolic Field and Black Point as extraordinary investigation areas and additionally the overall maximum Si concentration distinguishes Black Point from the other areas. Fe distinguishes only Black Point as remarkable different area with maximum concentration of 37,670 μg/l, resulting in a deviation of 186,000% compared to the local seawater. These findings contradict the statement of Price et al. (2015) referring to Black Point (vent) as an point with considerably low Fe concentrations and also referring to La Calcara as an area with remarkably high Fe concentrations, which cannot be seen in the data of the SDC Freiberg. In their paper Price et al. (2015) state their used analysis technique is not able to measure any iron concentration in the local seawater, thus they used literature values with an average of 0.63 μg/l for iron, instead of 20.3 μg/l found by the SDC Freiberg. Applying the literature values used by Price et al. (2015) one the maximum value found by the SDC, the maximum enrichment of Fe at Black Point increases by one order of magnitude to 5,990,000 μg/l.

The elevated concentrations of the REE emphasize the extraordinary positions of especially Black Point, Hot Lake and sometimes Fumarolic Field(cp. last part of fig. 3.22). Contrary the groundwater of Panarea and the investigation areas La Calcara and La Calcara Black Rock show often the lowest or even depleted concentrations compared to the average and the local seawater. Curiously also Area 26 exhibits elevated concentrations regarding the REE and displays the second highest concentrations after Black Point. But also Bottaro Nord and P21 show slightly elevated concentrations. Sec. 3.6.4 and sec. 3.6.5 validate the surprisingly high REE concentrations of A26 and comment on them.

Still one should note, the calculated enrichment of all REE is approximately 1-2 orders of magnitude too high. The local seawater from Seebauer (2015) lacks concentrations for REE but contains all in all higher element concentrations than the average seawater from Brown (2001) used for the calculation. This would indicate also higher REE concentration in the local seawater compared to the average seawater, hence smaller deviations of the REE concentrations from the local seawater would be expected.

Tab. 3.3.: Display of extreme values: Minima for pH, E_H, Mg, SO_4, maxima for rest of constituents. Local seawater concentrations are taken from Seebauer (2015), average seawater concentrations are taken from Brown (2001). Please note 5 digit number do not show 2 digits after the decimal point.

	Unit	BN	BW	P21	BP_MN	BP	HL	FF	A26	GW/PdP	CAL	CAL_BR	CAL_B1	local Seawater	average Seawater
pH	/	5.3	5.0	4.7	5.0	2.4	4.4	4.6	4.5	5.2	4.6	5.1	5.4	7.9	
E_H	mV	-73.10	-73.10	-48.90	-34.9	42.00	-75.10	-70.30	-60.04	-26.90	-32.00	80.66	264.7	286.00	
rH		8.4	7.6	7.9	9.4	6.2	7.0	7.3	7.7	9.5	9.0	13.0	20.0	25.4	
EC	mS/cm	82.40	63.30	61.00	59.4	82.00	118.30	84.60	68.70	24.03	64.80	59.30	53.6	57.10	
Li	mg/l	2.72	2.39	1.30	1.5	13.95	30.64	14.79	5.70	0.33	8.75	0.33	1.05	1.17	0.18
Na	mg/l	12,354	12,475	12,409	12,002	12,325	18,636	14,904	12,942	11,338	12,154	12,448	10,023	11,728	11,184
K	mg/l	706.00	634.93	549.00	772.00	1,890.73	3,644.21	1,950.23	958.86	447.00	1,020.54	437.07	399.71	427.05	380.00
Ca	mg/l	1,148.01	1,198.56	750.00	1,552.00	5,239.90	9,826.76	4,928.01	1,918.65	484.00	3,457.09	460.47	348.20	417.95	412.00
Mg	mg/l	1,226.1	1,295.7	1,073.7	1,084.6	579.2	752.6	1,116.4	1,226.2	249.7	692.7	978.9	864.1	1,414.16	1,290.00
F	mg/l	2.46	2.41	3.09	2.6	13.84	11.18	1.60	2.74	2.16	2.66	2.70	2.3	1.17	1.30
Cl	mg/l	23,630	25,081	22,898	23,535	31,447	53,684	35,042	27,176	17,744	25,392	22,534	18,642	19,909	19,500
Br	mg/l	84.49	112.00	93.66	108.00	131.93	222.00	118.00	87.43	75.00	90.19	63.71	35.36	63.65	67.10
S(6)	mg/l	1,342.0	2,619.6	1,116.0	2,032.6	178.1	564.0	1,703.4	1,109.0	778.2	1,328.0	2,190.6	2,200.6	3,027.44	2,710.00
Trace elements															
Si	μ g/l	81,930	32,800	51,180	99,360	183,800	109,400	60,200	106,000	98,700	94,773	25,840	38,040	1,020	2,000
Mn	μ g/l	39,500	29,840	24,970	75,850	366,700	479,900	169,200	153,200	8,736	204,700	27,430	40,090	29.22	0.030
Fe	μ g/l	1,640	5,000	5,740	8,610	37,670	6,100	3,690	2,050	5,040	6,035	2,433.00	416.60	20.28	0.055
Rb	μ g/l	2,723	1,497	784	2,956	14,000	22,640	10,380	5,258	247.80	6,904	530.90	559.00	138.38	120
Cs	μ g/l	739.00	480.20	210.90	803.60	3,868.00	7,985.00	3,936.00	1,277.00	13.06	2,236.33	152.30	204.70		0.40
Ba	μ g/l	760.00	690.00	6,966.00	1,381.70	7,617.00	5,654.70	1,786.00	992.40	262.50	6,337.00	154.00	215.40	13.87	2.00
Rare earth elements															
Sc	μ g/l	26.88	24.63	32.43	24.6	82.00	47.42	3.15	11.95	21.00	3.50	1.65	1.65		6.00E-04
Y	μ g/l	6.36	3.44	4.07	8.32	40.28	4.75	2.30	55.30	0.15	2.51	0.43	0.39		1.00E-03
La	μ g/l	0.66	2.87	1.39	1.927	4.24	1.34	1.85	1.46	0.11	0.82	0.21	0.098		3.00E-03
Ce	μ g/l	3.08	19.43	8.53	10.62	11.10	9.74	12.96	5.34	0.13	1.72	0.52	0.19		2.00E-03
Pr	μ g/l	0.12	0.70	0.37	0.53	1.15	0.37	0.49	1.01	0.02	0.22	0.06	0.03		6.00E-04
Nd	μ g/l	0.50	2.95	1.64	2.05	5.39	1.46	1.93	5.73	0.04	0.90	0.27	0.15		3.00E-03
Sm	μ g/l	0.16	0.66	0.40	0.66	2.26	0.49	0.49	2.73	0.02	0.29	0.08	0.06		6.00E-04
Eu	μ g/l	0.09	0.16	0.99	0.246	2.12	0.86	0.37	1.21	0.04	0.98	0.03	0.046		2.00E-04
Gd	μ g/l	0.30	0.66	0.70	1.03	4.64	0.76	0.45	6.11	0.02	0.43	0.07	0.08		7.00E-04
Tb	μ g/l	0.06	0.08	0.12	0.246	1.05	0.18	0.05	1.20	0.02	0.07	0.02	0.020		1.00E-04
Dy	μ g/l	0.44	0.49	0.63	1.230	6.46	0.87	0.33	8.09	0.02	0.44	0.08	0.066		9.00E-04
Ho	μ g/l	0.13	0.12	0.12	0.25	1.35	0.18	0.04	1.71	0.02	0.09	0.02	0.02		3.00E-04
Er	μ g/l	0.43	0.29	0.34	0.8	3.96	0.41	0.21	4.72	0.02	0.26	0.05	0.0		8.00E-04
Tm	μ g/l	0.06	0.03	0.04	0.082	0.55	0.06	0.02	0.60	0.02	0.03	0.02	0.020		2.00E-04
Yb	μ g/l	0.36	0.29	0.25	0.738	3.51	0.31	0.16	3.46	0.04	0.22	0.07	0.035		8.00E-04
Lu	μ g/l	0.08	0.08	0.04	0.123	0.53	0.06	0.02	0.51	0.02	0.03	0.02	0.020		2.00E-04

Tab. 3.4.: Deviations of parameters in % from the local seawater (Seebauer 2015) or (Brown 2001), respectively. Note the Fe∗ deviations are based on the value Price et. al (2015) used in their publication (average of 0.63 μ g/l for iron, instead of 20.3μ g/l).

	BN	BW	P21	BP_MN	BP	HL	FF	A26	GW	CAL	CAL_BR	CAL_B1
Li	132.9	105.0	11.3	29.0	1,094.4	2,522.7	1,166.2	387.6	-71.5	648.8	-71.5	-10.4
Na	5.3	6.4	5.8	2.3	5.1	58.9	27.1	10.3	-3.3	3.6	6.1	-14.5
K	65.3	48.7	28.6	80.8	342.7	753.3	356.7	124.5	4.7	139.0	2.3	-6.4
Ca	174.7	186.8	79.4	271.3	1,153.7	2,251.2	1,079.1	359.1	15.8	727.2	10.2	-16.7
Mg	-13.3	-8.4	-24.1	-23.3	-59.0	-46.8	-21.1	-13.3	-82.3	-51.0	-30.8	-38.9
F	110.6	106.3	164.5	122.9	1,084.6	857.0	37.2	134.1	84.9	127.4	131.1	96.9
Cl	18.7	26.0	15.0	18.2	58.0	169.7	76.0	36.5	-10.9	27.5	13.2	-6.4
Br	32.7	76.0	47.2	69.7	107.3	248.8	85.4	37.4	17.8	41.7	0.1	-44.4
S(6)	-55.7	-13.5	-63.1	-32.9	-94.1	-81.4	-43.7	-63.4	-74.3	-56.1	-27.6	-27.3
Trace Elements												
Si	7.93E+03	3.12E+03	4.92E+03	9.64E+03	1.79E+04	1.06E+04	5.80E+03	1.03E+04	9.58E+03	9.19E+03	2.43E+03	3.63E+03
Mn	1.35E+05	1.02E+05	8.54E+04	2.59E+05	1.25E+06	1.64E+06	5.79E+05	5.24E+05	2.98E+04	7.00E+05	9.38E+04	1.37E+05
Fe	7.99E+03	2.46E+04	2.82E+04	4.24E+04	1.86E+05	3.00E+04	1.81E+04	1.00E+04	2.48E+04	2.97E+04	1.19E+04	1.95E+03
Fe*	2.61E+05	7.95E+05	9.12E+05	1.37E+06	5.99E+06	9.69E+05	5.86E+05	3.26E+05	8.01E+05	9.59E+05	3.87E+05	6.61E+04
Rb	1.87E+03	9.81E+02	4.67E+02	2.04E+03	1.00E+04	1.63E+04	7.40E+03	3.70E+03	7.91E+01	4.89E+03	2.84E+02	3.04E+02
Cs	1.85E+05	1.20E+05	5.26E+04	2.01E+05	9.67E+05	2.00E+06	9.84E+05	3.19E+05	3.17E+03	5.59E+05	3.80E+04	5.11E+04
Ba	5.38E+03	4.87E+03	5.01E+04	9.86E+03	5.48E+04	4.07E+04	1.28E+04	7.05E+03	1.79E+03	4.56E+04	1.01E+03	1.45E+03
REE												
Sc	4.48E+06	4.11E+06	5.40E+06	4.10E+06	1.37E+07	7.90E+06	5.25E+05	1.99E+06	3.50E+06	5.83E+05	2.75E+05	2.75E+05
Y	6.36E+05	3.44E+05	4.06E+05	8.32E+05	4.03E+06	4.75E+05	2.30E+05	5.53E+06	1.46E+04	2.51E+05	4.32E+04	3.93E+04
La	2.18E+04	9.56E+04	4.64E+04	6.41E+04	1.41E+05	4.46E+04	6.17E+04	4.87E+04	3.40E+03	2.72E+04	6.93E+03	3.17E+03
Ce	1.54E+05	9.72E+05	4.26E+05	5.31E+05	5.55E+05	4.87E+05	6.48E+05	2.67E+05	6.20E+03	8.57E+04	2.59E+04	9.15E+03
Pr	2.04E+04	1.16E+05	6.14E+04	8.87E+04	1.92E+05	6.09E+04	8.19E+04	1.68E+05	3.40E+03	3.59E+04	9.40E+03	5.40E+03
Nd	1.66E+04	9.83E+04	5.46E+04	6.82E+04	1.79E+05	4.87E+04	6.41E+04	1.91E+05	1.30E+03	2.99E+04	8.90E+03	5.03E+03
Sm	2.72E+04	1.09E+05	6.66E+04	1.09E+05	3.77E+05	8.12E+04	8.19E+04	4.55E+05	3.40E+03	4.86E+04	1.24E+04	9.73E+03
Eu	4.34E+04	8.19E+04	4.92E+05	1.23E+05	1.06E+06	4.27E+05	1.86E+05	6.03E+05	2.04E+04	4.89E+05	1.24E+04	2.29E+04
Gd	4.28E+04	9.36E+04	9.99E+04	1.46E+05	6.63E+05	1.09E+05	6.43E+04	8.72E+05	2.88E+03	6.10E+04	9.19E+03	1.08E+04
Tb	6.09E+04	8.19E+04	1.23E+05	2.46E+05	1.05E+06	1.80E+05	5.39E+04	1.20E+06	2.02E+04	6.89E+04	1.99E+04	1.99E+04
Dy	4.88E+04	5.46E+04	6.96E+04	1.37E+05	7.18E+05	9.68E+04	3.63E+04	8.99E+05	2.12E+03	4.82E+04	9.12E+03	7.23E+03
Ho	4.26E+04	4.09E+04	4.09E+04	8.19E+04	4.49E+05	5.86E+04	1.36E+04	5.69E+05	6.57E+03	3.09E+04	6.57E+03	6.57E+03
Er	5.37E+04	3.58E+04	4.22E+04	1.02E+05	4.95E+05	5.12E+04	2.55E+04	5.90E+05	2.53E+03	3.23E+04	6.40E+03	5.53E+03
Tm	2.84E+04	1.64E+04	1.99E+04	4.09E+04	2.73E+05	2.80E+04	9.90E+03	2.97E+05	9.90E+03	1.69E+04	9.90E+03	9.90E+03
Yb	4.45E+04	3.58E+04	3.08E+04	9.22E+04	4.39E+05	3.80E+04	2.04E+04	4.33E+05	4.78E+03	2.77E+04	8.03E+03	4.28E+03
Lu	4.09E+04	4.09E+04	2.03E+04	6.14E+04	2.63E+05	3.01E+04	9.90E+03	2.52E+05	9.90E+03	1.64E+04	9.90E+03	9.90E+03

On-site parameters

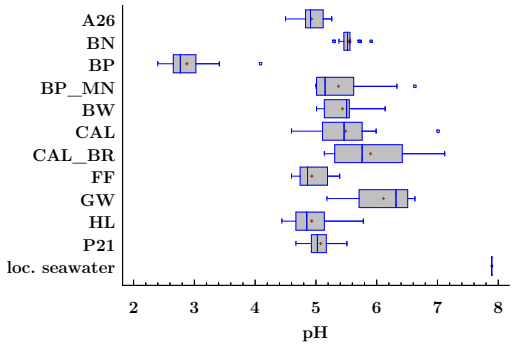

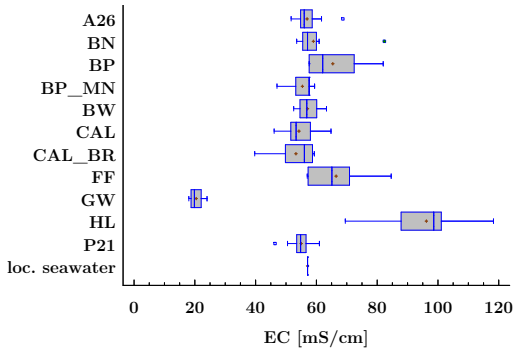

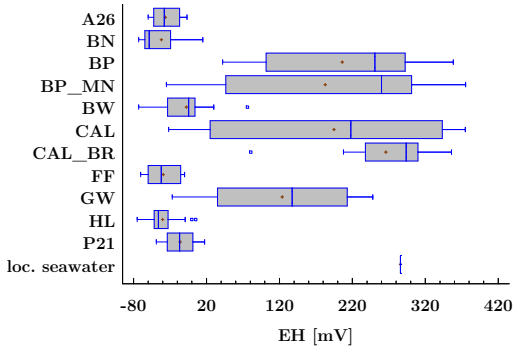

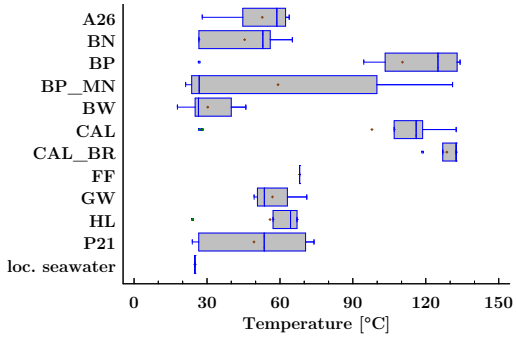

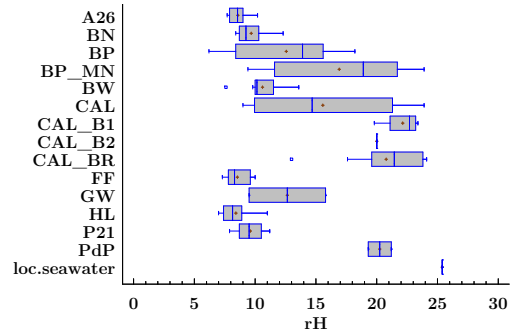

Major ions

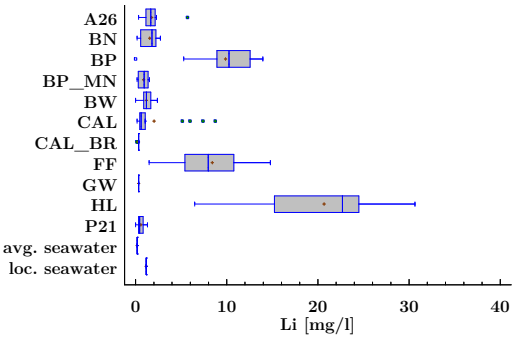

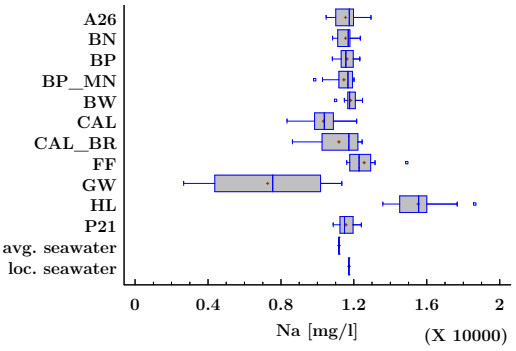

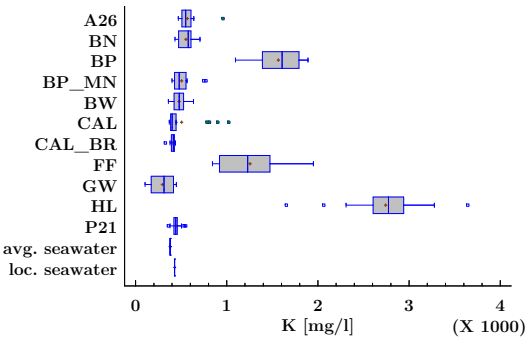
A26
BN
BP
BP_MN
BW
CAL
CAL_BR
FF
GW
HL
P21
avg. seawater
loc. seawater
0
1
2
3
4
K [mg/l]
(X 1000)

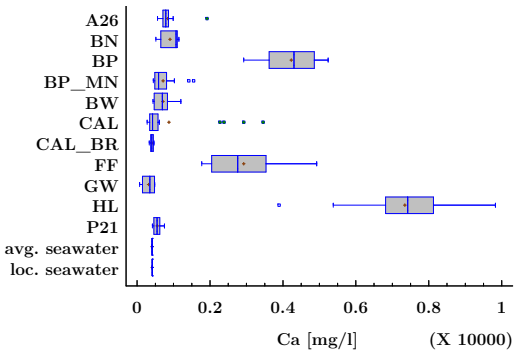
A26
BN
BP
BP_MN
BW
CAL
CAL_BR
FF
GW
HL
P21
avg. seawater
loc. seawater
0
0.2
0.4
0.6
0.8
1
Ca [mg/l]
(X 10000)

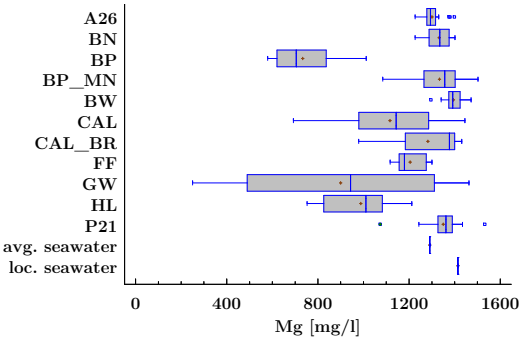
A26
BN
BP
BP_MN
BW
CAL
CAL_BR
FF
GW
HL
P21
avg. seawater
loc. seawater
0
400
800
1200
1600
Mg [mg/l]

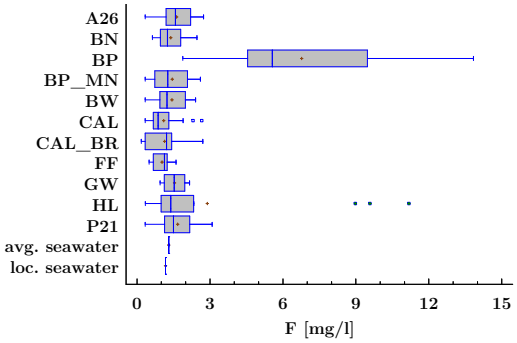
A26
BN
BP
BP_MN
BW
CAL
CAL_BR
FF
GW
HL
P21
avg. seawater
loc. seawater
0
3
6
9
12
15
F [mg/l]

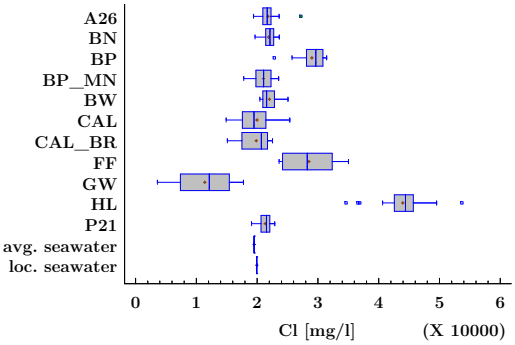
A26
BN
BP
BP_MN
BW
CAL
CAL_BR
FF
GW
HL
P21
avg. seawater
loc. seawater
0
1
2
3
4
5
6
Cl [mg/l]
(X 10000)

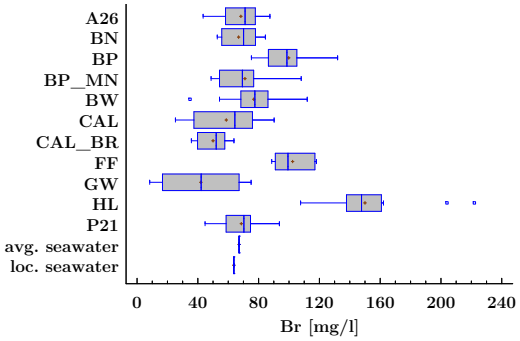
A26
BN
BP
BP_MN
BW
CAL
CAL_BR
FF
GW
HL
P21
avg. seawater
loc. seawater
0
40
80
120
160
200
240
Br [mg/l]

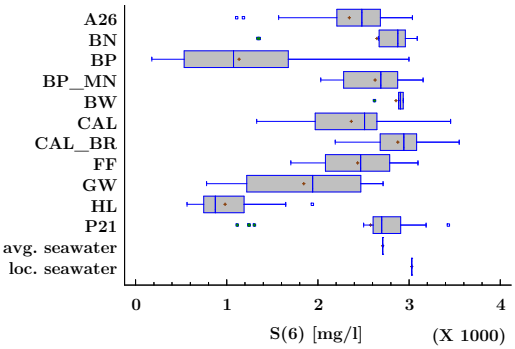
A26
BN
BP
BP_MN
BW
CAL
CAL_BR
FF
GW
HL
P21
avg. seawater
loc. seawater
0
1
2
3
4
S(6) [mg/l]
(X 1000)

Trace Elements

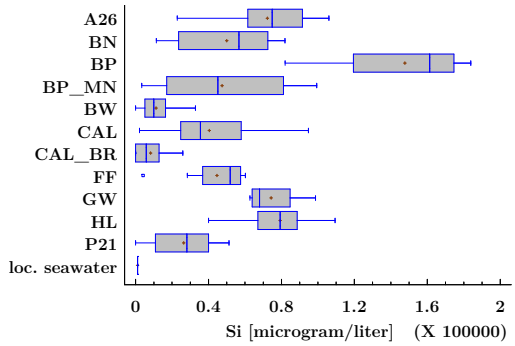

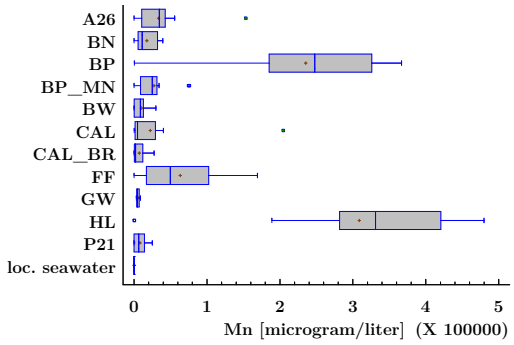

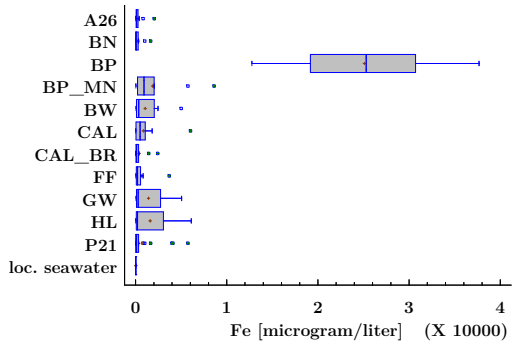

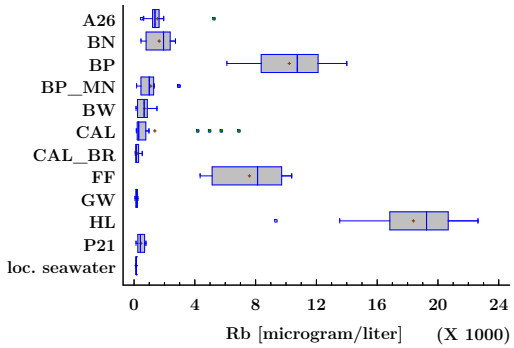

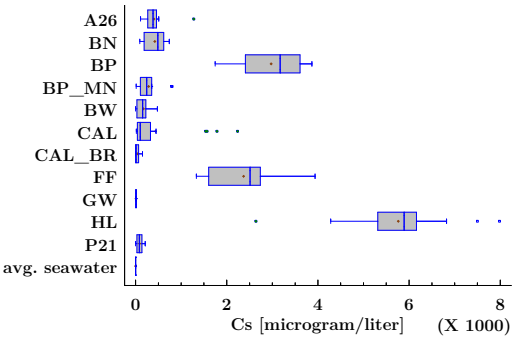

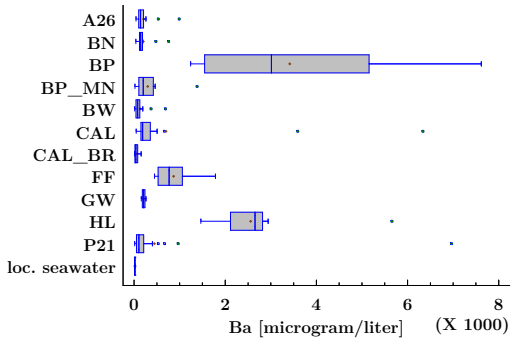

Rare earth elements

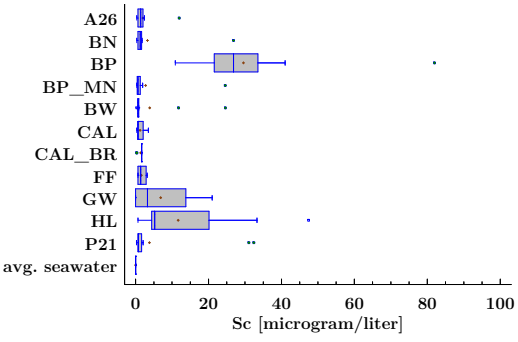

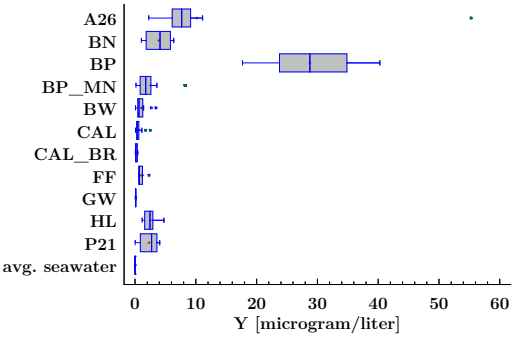

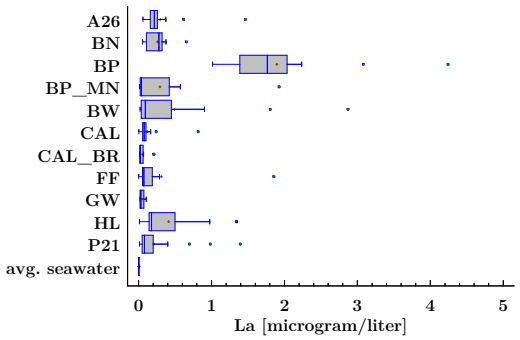
A26
BN
BP
BP_MN
BW
CAL
CAL_BR
FF
GW
HL
P21
avg. seawater
0 1 2 3 4 5
La [microgram/liter]

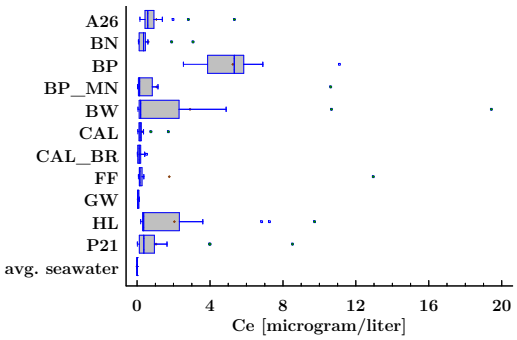
A26
BN
BP
BP_MN
BW
CAL
CAL_BR
FF
GW
HL
P21
avg. seawater
0 4 8 12 16 20
Ce [microgram/liter]

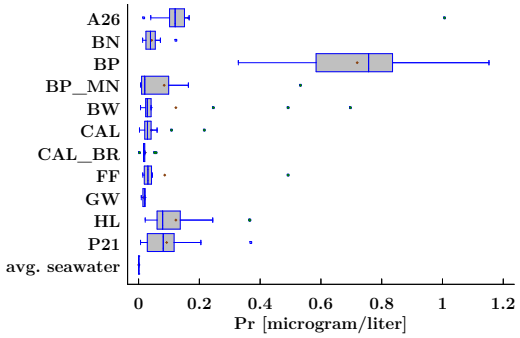
A26
BN
BP
BP_MN
BW
CAL
CAL_BR
FF
GW
HL
P21
avg. seawater
0 0.2 0.4 0.6 0.8 1 1.2
Pr [microgram/liter]

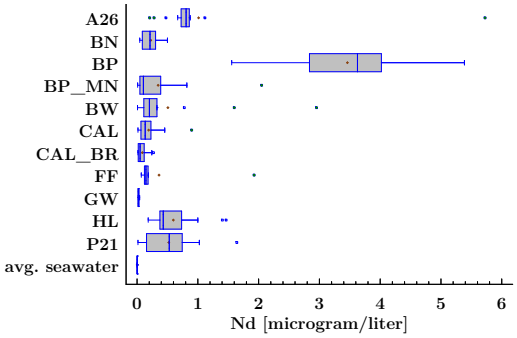
A26
BN
BP
BP_MN
BW
CAL
CAL_BR
FF
GW
HL
P21
avg. seawater
0 1 2 3 4 5 6
Nd [microgram/liter]

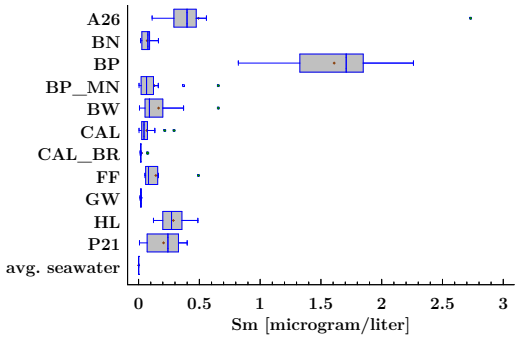
A26
BN
BP
BP_MN
BW
CAL
CAL_BR
FF
GW
HL
P21
avg. seawater
0 0.5 1 1.5 2 2.5 3
Sm [microgram/liter]

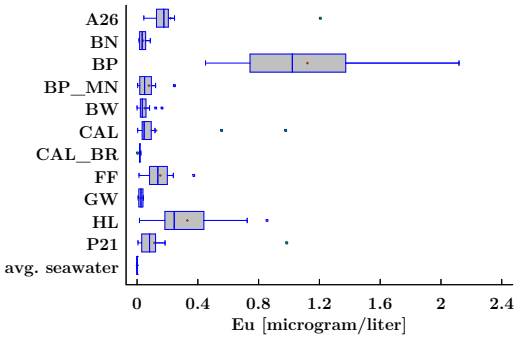
A26
BN
BP
BP_MN
BW
CAL
CAL_BR
FF
GW
HL
P21
avg. seawater
0 0.4 0.8 1.2 1.6 2 2.4
Eu [microgram/liter]

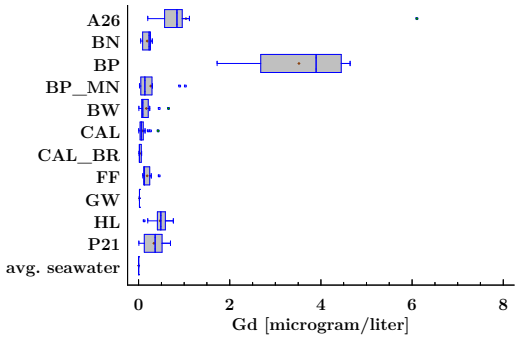
A26
BN
BP
BP_MN
BW
CAL
CAL_BR
FF
GW
HL
P21
avg. seawater
0 2 4 6 8
Gd [microgram/liter]

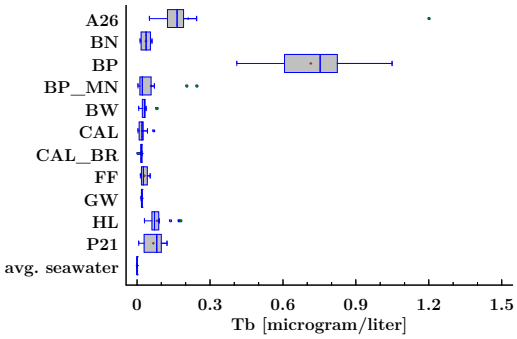
A26
BN
BP
BP_MN
BW
CAL
CAL_BR
FF
GW
HL
P21
avg. seawater
0 0.3 0.6 0.9 1.2 1.5
Tb [microgram/liter]

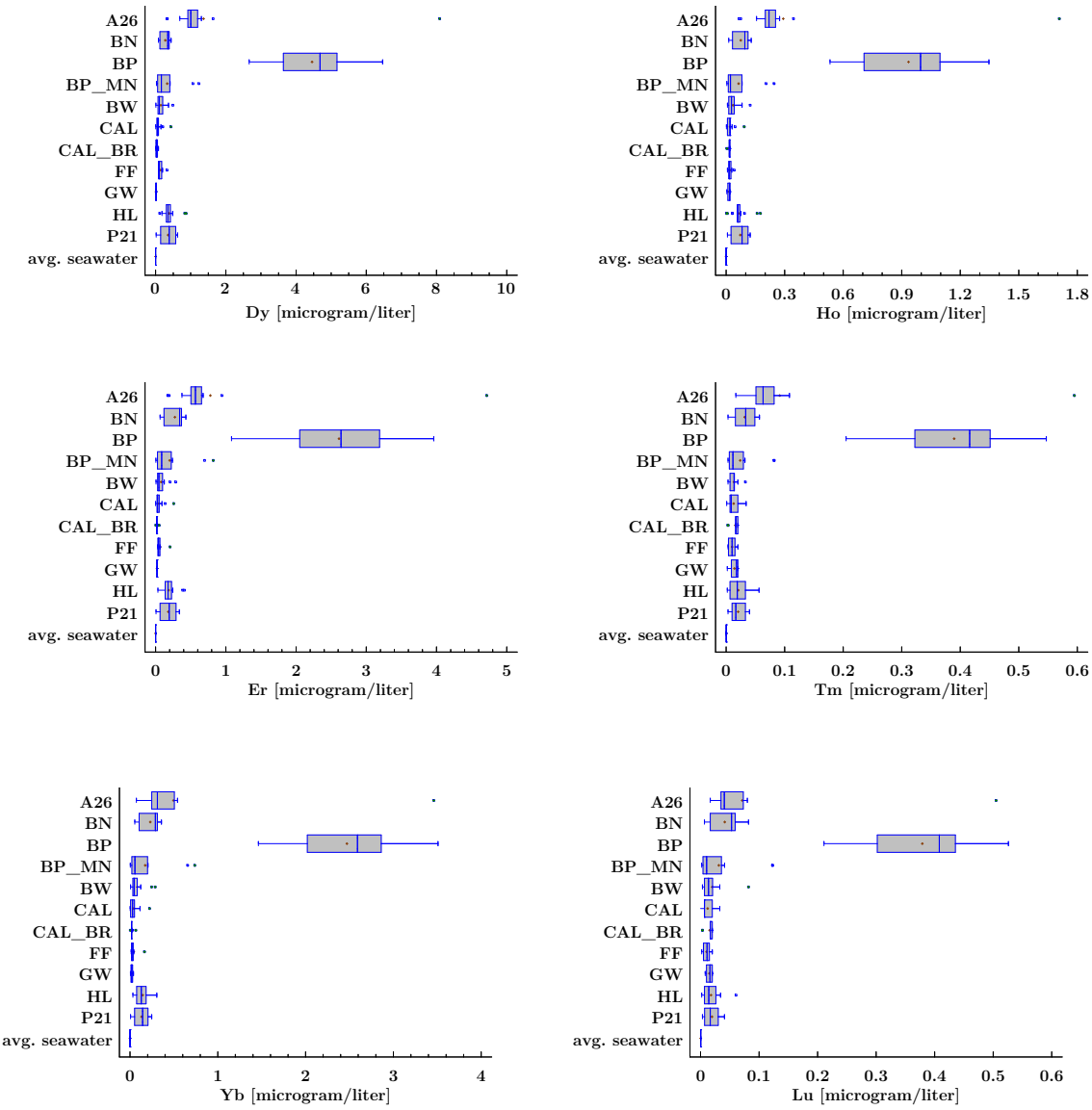

Fig. 3.22.: Ranges of in tab. 3.3 listed parameters. If available avg. seawater values from Brown (2001) and loc. seawater values from Seebauer (2015).

3.6.2. Time series Hot Lake

If data is collected over a time span of 10 years, time series would be most interesting to see any trends within the submarine hydrothermal system Panarea. The first step to create a meaningful time series is an evaluation of each data set with respect to outliers due to contamination with seawater, which is a general problem during the investigation of SDG (submarine groundwater discharge). Parameters such as the EC or the chlorinity only indicate, whether a sample is highly enriched or not, but e.g. low chloride phases, occurring during possible phase separation are hard to determine. Without any "true" hydrothermal fluid for comparison, the mixture ratio between hydrothermal fluid and local seawater is not distinguishable, hence the composition and thus the quality is unknown. At areas with a high EC (e.g. Hot Lake) samples with low EC are normally excluded as highly contaminated with local seawater. Possible natural changes in the EC cannot be proven. Only relative comparisons with the local seawater, considering mostly the extreme deviations (minima/maxima) are possible.

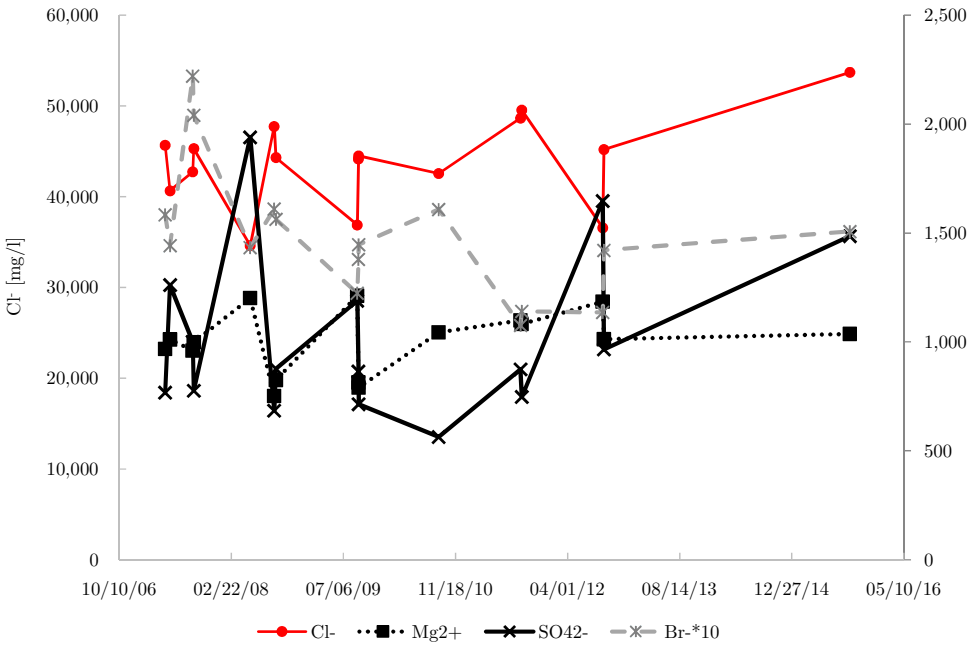

Fig. 3.23.: Time series (raw data) for Hot Lake of Cl^-, Br^-, Mg^{2+} and SO_4^{2-}. Please note the opposite trends of Cl^- and Br^- against Mg^{2+} and $SO4_4^{2-}$.

An attempt is made to create a time line for Hot Lake as one of the few sampling points yielding mostly meaningful and stable results over the years. At the same time the chosen parameters Cl^-, Br^-, SO_4^{2-} and Mg^{2+} serve the purpose to grade the quality of the samples by correlating them with each other. Fig. 3.23 shows the correlation between the concentrations of Cl^-, Br^-, SO_4^{2-} and Mg^{2+} with each other. Cl^- and Br^- have a similar pattern for most years, except for the years 2007 and 2011. Normally the Br^- and Cl^- concentrations are correlated with each other and their ratio stays more or less the same. In 2007 the

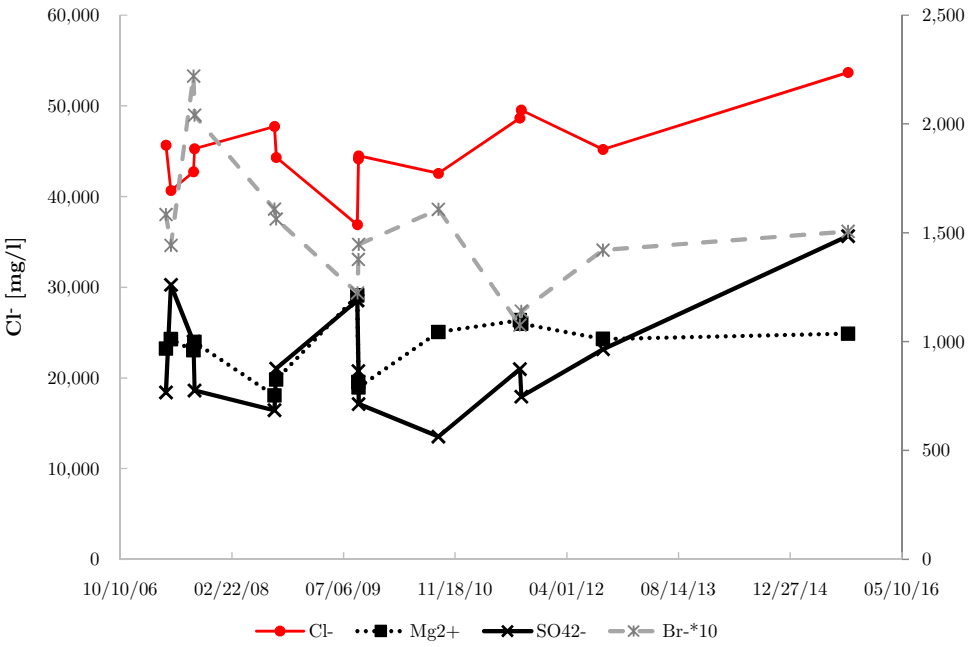

Fig. 3.24.: Corrected time series for Hot Lake of Cl^-, Br^-, Mg^{2+} and SO_4^{2-}.

Br^- concentrations increase drastically, while the Cl^- concentrations decrease, leading to a decreasing Cl/Br ratio, as shown in fig. 3.25. Vice versa, in 2011 the ratio increases drastically, as shown in fig. 3.25, meaning either the concentration of Br^- decreased, or the concentration of Cl^- increased. These changes cannot be explained by a simple contamination with the local seawater, because the original concentrations of Hot Lake would be changed by the local seawater, but the ratio would stay the same. Halite precipitation and halite dissolution could give an answer to the changing Cl/Br ratios: If halite is dissolved, "pure" NaCl is set free, the Cl^- concentration would increase, while the Br^- stays rather the same, thus the ratio would increase, as seen in 2011. Vice versa, if halite precipitated, again "pure" NaCl is withdrawn from the hydrothermal fluid, increasing relatively the Br^- concentration of the fluid. Still a halite precipitation is not likely, because the conditions are far away from a saturated solution regarding halite. Furthermore a Cl-withdrawal at the time as the high Br^- concentrations occur cannot be seen in the data. Phase separation and the influence of resulting low and high-Cl content hydrothermal phases are more likely to cause the changes in the Cl/Br ratio.

As discussed in sec. 3.2.2 and sec. 3.2.1 Mg^{2+} and SO_4^{2-} concentrations are mostly depleted in hydrothermal systems. Comparing them with the Cl^- concentration of Hot Lake over the years, results in a mirrored concentration pattern for all three ions: Both Mg^{2+} and SO_4^{2-} contradict the Cl^- concentration trend for most years. Whenever the Cl^- concentrations are high, both Mg^{2+} and SO_4^{2-} show low concentrations and vice versa. Especially in between the years 2007 and 2009 three distinct peaks depict clearly this contradicting pattern. Less clear is the pattern for the year 2010, both Cl^- and SO_4^{2-} concentrations decrease similarly,

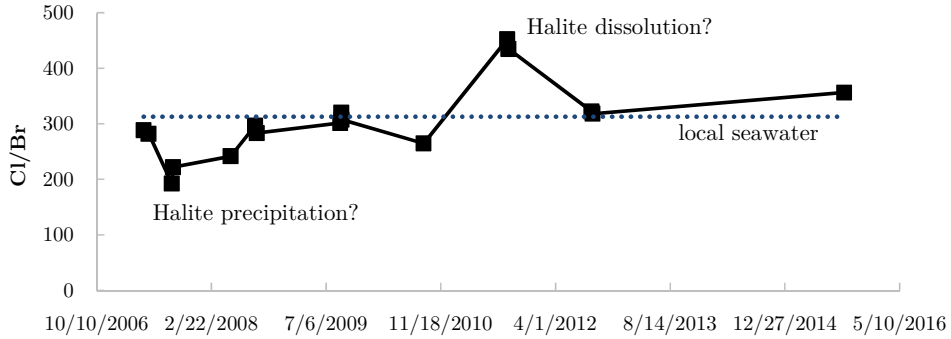

Fig. 3.25.: Time series for Hot Lake of the Br/Cl ratio.

while the Mg^{2+} concentration increases as before. Through an uncertain year 2011 the trend can be again clearly seen in the year 2012. These mirrored patterns prove the contamination with local seawater, decreasing the Cl^- concentrations on the one hand and increasing the normally depleted concentrations of Mg^{2+} and SO_4^{2-}. But even after these contaminated samples are excluded (cp. fig. 3.24) the mirror pattern remains, especially in the beginning (2009) and no clear trend can be seen, regarding falling or increasing overall concentrations. Erroneous sampling in the years 2013 and 2014 lead to missing values, hence the increasing trend towards 2015 is questionable.

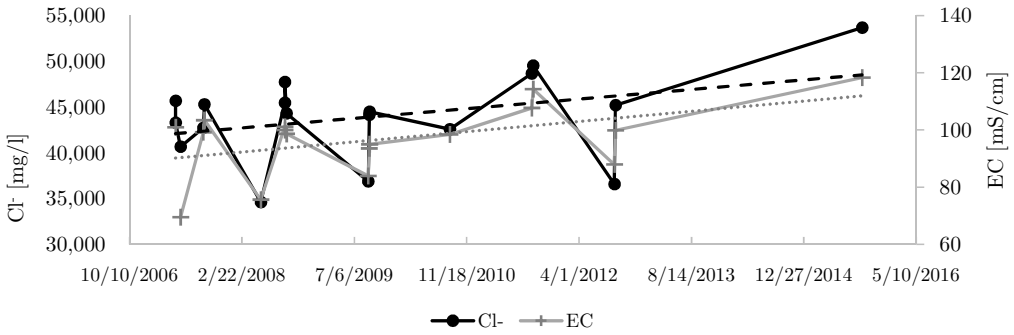

Fig. 3.26.: Time series for Hot Lake of the Cl^- concentration and the EC.

Having the adverse sampling conditions in mind, this contradicting pattern proves to be a good tool to distinguish the sampling quality over the years, because high Cl^- concentrations, expected as indicators of hydrothermal activity go along with corresponding low Mg^{2+} and SO_4^{2-} concentrations, expected in hydrothermal systems. Hence it is recommended to apply this apply this kind of logical comparisons to gain to gain a reliable indication of seawater contamination for the taken samples.

Besides proving the single anion status of Cl^- and its dominant role regarding the EC as done for the samples of 2015 (cp. sec. 3.2.2 and sec. 3.2.1) fig. 3.26 indicates an ongoing trend of an increasing EC for Hot Lake. The minor changes within the increasing trend over the years are either natural fluctuations, internal changes in the system, or more likely varying

sampling qualities with varying grades of seawater contamination.

Even with the presented tool to grade the sampling quality, unfortunately several circumstances create adverse conditions for a meaningful time series: (1) Varying sample quality, (2) varying sampling and measuring equipment and techniques, (3) insufficient resolution of time. In accordance to the relative quality, varying sampling and measurement techniques only amplify the quality problem and make a comparison questionable. Mostly the insufficient resolution of time speaks against time series of parameters. Only two weeks in the beginning of September and sometime samples from spring months are not sufficient to monitor changes in the hydrothermal system over a time span of several years. Monthly sampling or at least sampling every three months would drastically increase the informative value of any further time series.

3.6.3. Chloride-Plots

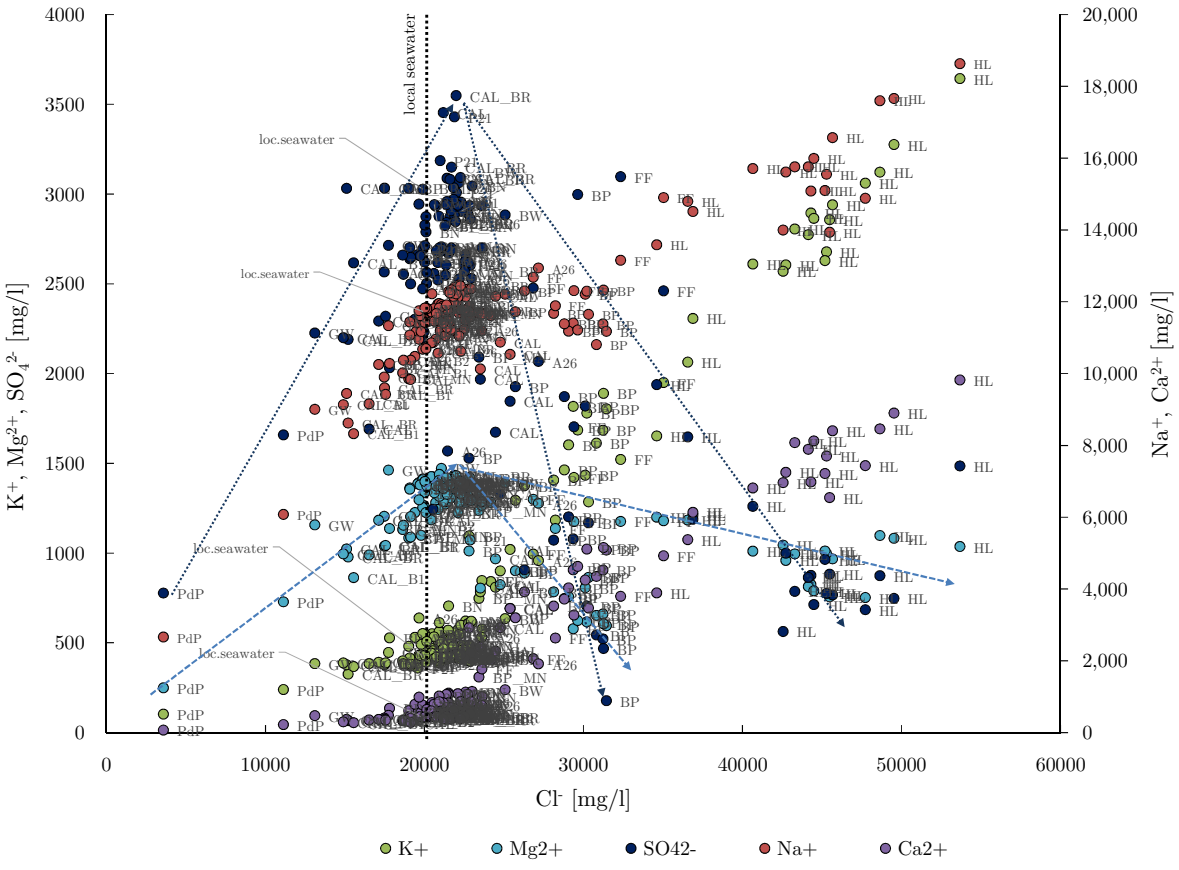

Fig. 3.27.: Na^+, K^+, Ca^{2+}, Mg^{2+} and SO_4^{2-} from samples taken between 2006 - 2015 in comparison with local seawater (Seebauer 2015) plotted against Cl^-. The black dotted line shows the Cl^- concentration of the local seawater, the dotted dark and light blue arrows clarify the trends of Mg^{2+} and SO_4^{2-}.

Similar to the samples of 2015 the concentrations of the major and minor ions from all samples from the last decade have been plotted against Cl^- (cp. fig. 3.27, 3.28 and 3.29),

resulting in similar trends as in 2015: Li^+, Na^+, K^+, Ca^{2+} and Br^- form linear trends with the local seawater in their middle and maintain their ion-Cl^- ratio in the majority of the cases. Pozzo di Pina marks in all cases the lowest Cl^- concentrations and mostly also the lowest ion concentrations. Hot Lake marks in all cases the maximum Cl^-concentration, except for Mg^{2+} and SO_4^{2-}. Mg^{2+} has its maximum near the seawater, indicating the seawater as main source for Mg^{2+} , while the maximum of SO_4^{2-} is also near the seawater but is topped by samples from La Calcara, La Calcara Black Rock, P21 and Fumarolic Field. Mg^{2+} only slightly depletes with increasing Cl^--concentrations with two minima at Black Point and Hot Lake. SO_4^{2-} depletes strongly and has also two minima at Black Point with moderate enriched Cl-concentrations and at Hot Lake with the maximum Cl^--concentrations. Again these plots reveal the correlation between the concentration of the dominant Cl^- and the cation concentrations of Li^+, Na^+, K^+, Ca^{2+} , distinguishing a low Cl-content hydrothermal fluid at La Calcara and high Cl-content hydrothermal fluids at Black Point, Fumarolic Field and Hot Lake.

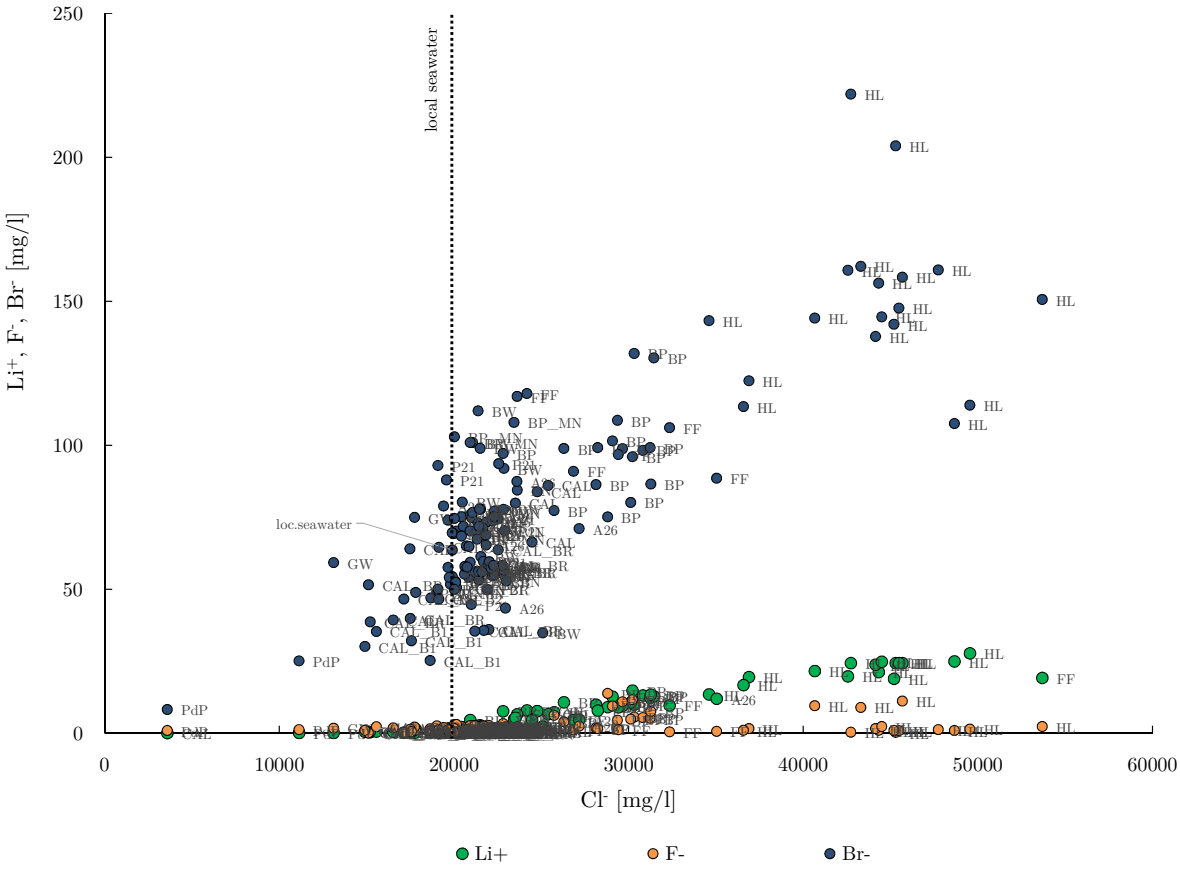

Fig. 3.28.: Li^+, F^- and Br^- from samples taken between 2006 - 2015 in comparison with local seawater (Seebauer 2015) plotted against the Cl^- concentrations. The black dotted line shows the Cl^- concentration of the local seawater.

To compare these results with 2015, again fig. 3.29 gives a more detailed overview over the

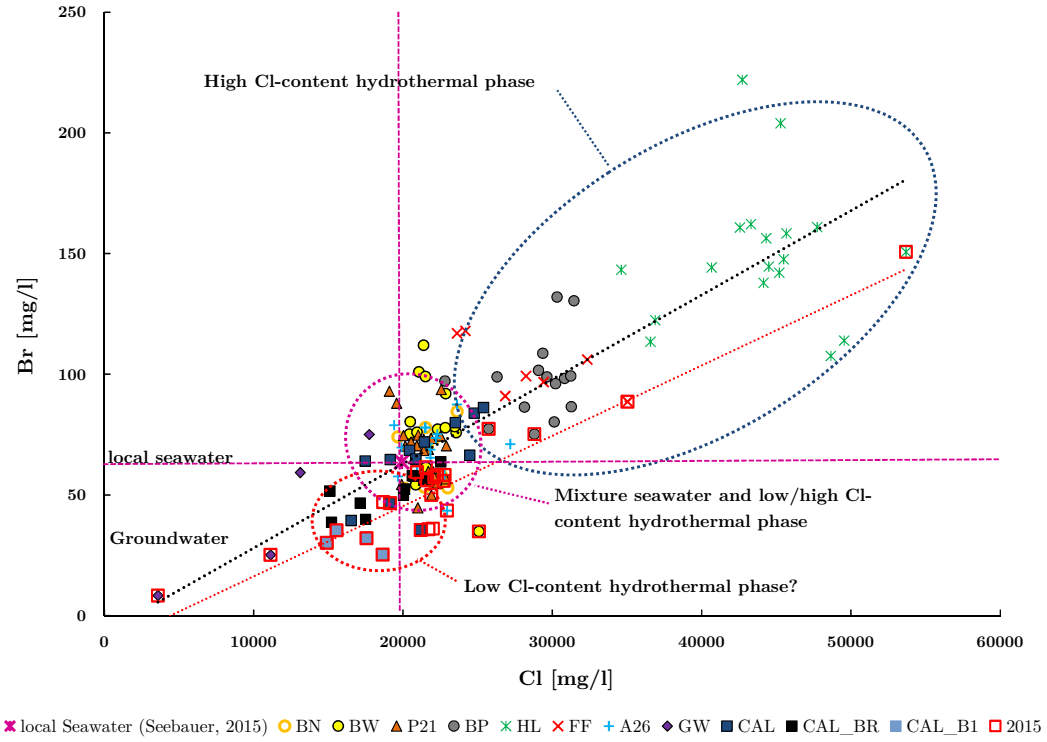

Fig. 3.29.: Br/Cl diagram to display the enrichment or depletion of both elements in comparison to the local seawater for data from the last decade. The shifted values from 2015 (framed in red) towards lower Br/Cl concentrations, as shown by the red trend line, indicating higher Cl^- or lower Br^- concentrations than before (black trend line).

Br/Cl ratio as it is done in fig. 3.28. The trend of 2015 is depicted also over the last decade and all values are shifted towards lower Br/Cl ratios (they have higher Cl-contents as in the years before). Whether the system as a whole changed and now generally higher Cl-contents can be found in the samples or the bromide concentrations are lowered is hard to determine. The Br/Cl ratios could be considerably lowered by the dissolution of halite, thus bringing more Cl into the fluids, lowering the ratios (cp. sec. 1.2 and especially sec. 3.6.2). Still the different groups (groundwater, low and high Cl-content hydrothermal phase and mixture between low Cl-content hydrothermal phase and local seawater at La Calcara) can be found again, hence the findings of 2015 fit into the data of the SDC Freiberg, collected over the past 10 years.

3.6.4. Factor Analysis (FA)

Fig. F.1 and tables F.5, F.6, F.8 give an overview over the first factor analysis (PCA + Varimax rotation) for a data set of 88 complete samples (note: The term complete samples refers to missing values for various parameters, which samples are then excluded from further analysis during the FA). The redox potential was excluded from further analysis due to concerns about the quality of the readings and the high likeliness of biases due to atmospheric contact of the samples. 8 factors were extracted by their eigenvalues > 1, which represent most factors with a high estimated communality (cp. tab. F.8). These extracted factors project most of

the variance of the used parameters. Specific variances >0.2 (20%) and up to 0.37 for the parameters pH, F, Co, Ni, As, Sn, Sb, Te, Ba, Th and U show the common factors are not able to represent all of the variance of these factors, but still the majority (cp. tab. F.8). The threshold R-Score (the factor loading) for a significant Pearson-correlation between the new factor and the compared parameter is 0.273 with P = 0.0098 and with $\alpha = 0.01$ (cp. sec. 2.3.1). Almost doubling the calculated threshold for statistical significant factor-parameter correlations ensures two things: 1. statistically highly significant values and 2. an simplification of the interpretation of each factor. In all cases where the factor loadings are <0.5 but above the threshold of 0.273 these parameters load also higher an other factors. In this case only the maximum loadings were extracted to ease the interpretation. Tab. F.6 gives the extracted factor loadings >0.5 of the new 8 factors.

Tab. 3.5.: Threshold calculation of factor loadings to gain a statistically significant Pearson-correlation between factor loadings of parameters and new factors.

Case	N	threshold (factor loadings)	α	P	KMO
All Data	88	0.273	0.01	0.0098	0.764
All elements	95	0.264	0.01	0.0097	0.759
Major Ions	122	0.233	0.01	0.0098	0.853
REE	146	0.213	0.01	0.0098	0.930
Trace Elements	161	0.203	0.01	0.0098	0.724

Curiously Mg is equally highly negatively loaded on the 1st and 2nd factor (-0.38) but has its maximum on the 8th factor with -0.57. Equally curious is Mo with its loading of >0.9 on the 7th factor together with relatively high loadings of In and Te (both >0.75). An explanation of the 7th factor representing a transition metal (Mo), a semi-metal (In) and a metalloid (Te) is not available, but it can be speculated that In, Te, and Mo are either contained in magmatic fluids or contained in elevated concentrations in volcanic rocks. Same problem occurs for the 3rd, 4th, 5th, 6th and 8th factor.

Given the great number of factors an interpretation for all of them would be difficult, hence the number of factors for the 2nd run was reduced to four factors. Table 3.6 gives the four factors and their factor loadings up to interpretation. The 1st factor representing 47.1% of the total variance of the data has high loadings (> 0.9) especially for almost all lanthanides, Y and Al. The pH, V, Fe, Zn, Cd, La, Ce, Eu and Pb have loadings > 0.75, while F, Sc and Si have loadings > 0.5. The pH is the only parameter which is negatively loaded. Given the representation of rare earth elements (REE) and mainly transition metals the first factor seems to represent a water which undergoes heavily leaching and water-rock-interactions with the bedrock, leading to an enrichment of these parameters. Especially F can be seen as an indicator for magmatic fluids, containing HF(cp. sec. 1.2). he low pH and the high concentrations of REE and trace metals are according to the literature for known submarine hydrothermal systems (German and Seyfried 2014; Herzig and Hannington 2000;

Mason 2013; Von Damm 2001).

The 2nd factor representing 18.8% of the total variance of the data contains besides the electrical conductivity the mostly the main constituents of seawater. Li^+, K^+, Ca^{2+}, Cl^-, B, Rb and Cs have loadings >0.9, Na^+, Mn(2), Br^-, Be and Mn have loadings >0.75 and S(6) (SO_4^{2+}) (negative loading), Ga, Sr, Ag, Ba and Tl have loadings >0.5. Because the main constituents of seawater (Na, Cl, K, Ca etc.) and the electrical conductivity are represented by the 2nd factor it seems highly likely these combined parameters and thus the 2nd factor represent the hydrothermally altered local seawater at Panarea. During the hydrothermal alteration and water-rock interactions leaching processes occur, increasing the concentrations of these elements, leading to an excess of element concentrations compared to the unaltered local seawater (cp. with the samples of 2015 in sections 3.2 and 3.4).

Tab. 3.6.: Extraction of the second factor analysis with loadings minimally >0.5. In bold factor loadings >0.9, in italic loadings >0.75 and in brackets negative factor loadings.

Factor	1	2	3	4
Variance [%]	47.1	18.8	7.9	4.9
Cumulative [%]	47.1	65.9	73.8	78.8
	[pH]	**EC**	Ni	[Mg]
	F	**Li**	Cu	As
	Al	*Na*	[Sr]	Sn
	Si	**K**	[Mo]	Sb
	Sc	**Ca**	Ag	Th
	V	*Mn(2)*	[In]	
	Fe	**Cl**	Sn	
	Zn	*Br*	Bi	
	Y	[S(6)]		
	Cd	*Be*		
	La	**B**		
	Ce	*Mn*		
	Pr	Ga		
	Nd	**Rb**		
	Sm	Sr		
	Eu	Ag		
	Gd	**Cs**		
	Tb	Ba		
	Dy	Tl		
	Ho			
	Er			
	Tm			
	Yb			
	Lu			
	Pb			

Ni, Cu, Ag, Sn, Bi as well as Sr, Mo and In with negative factor loadings are represented by the 3rd factor (7.9% of total variance) with factor loadings >0.5 or <-0.5, respectively.

Besides Sr as earth alkaline metal all other elements are either transition metals or semi-metals. Whereas this factor represents another water source, containing mostly the named constituents or simply groups these elements is hard to distinguish and an explanation does not come easily.

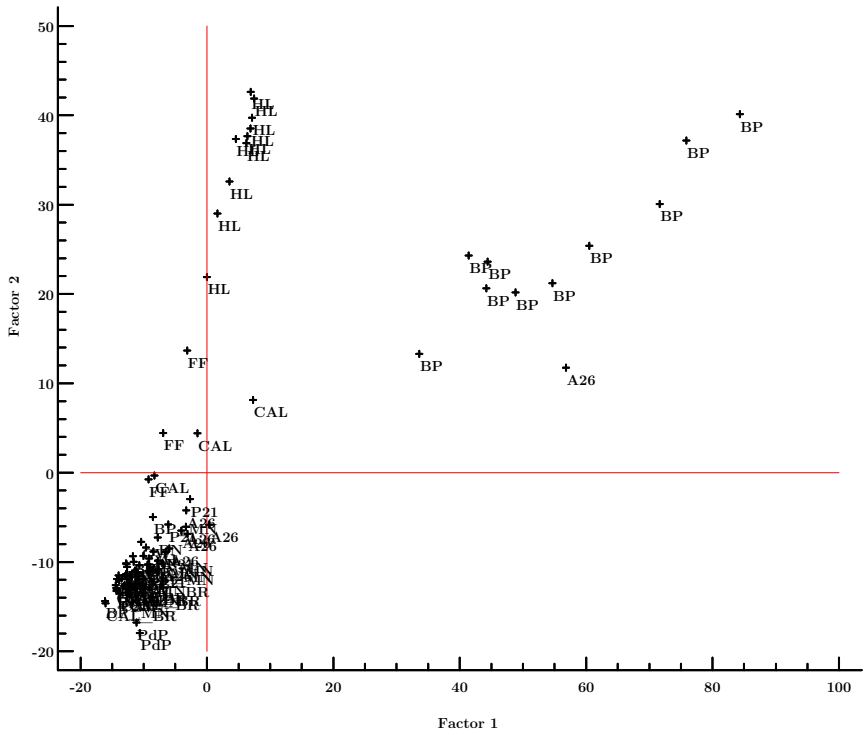

Fig. 3.30.: Scatter plot of the second factor analysis displaying the first two factors, representing a cumulative variance of 65.88 % of the data. Note Black Point is mainly represented by the 1st factor (up to 84%), but also has a high loading on the second factor (up to 40%), while Hot Lake and Fumarolic Field are more represented by the 2nd factor (43% and 14%).

As, Sn, Sb, Th and Mg (negatively loaded) have only factor loadings >0.5 or <-0.5, respectively on the 4th factor. Only common thing about these elements would be the vicinity of As, Sn and Sb in the periodic table and hence comparable chemical and physical characteristics. Otherwise the interpretation of this factor is difficult, except for the inverse relationship of Mg (depletion instead of enrichment) to all other elements as discussed before in section 3.2.2.

Fig. 3.30 plots the samples of the different areas according to their factor loadings on the first and second factor, representing 65.9 % of the total variance of all data. It is clearly visible samples from areas such as Hot Lake and Black Point form distinctive trends towards high factor loadings originating from a point cloud in the negative factor loading segment. Hot Lake is mainly represented by the 2nd factor and shows only minor factor loadings on the 1st factor. Fumarolic Field tends to follow the trend of Hot Lake, given the vicinity and similarities of the on-site parameters and measured concentrations it seems likely, they both are somewhat connected. Hence both areas seems to be fed mainly by altered local seawater, condensed and strongly enriched in the seawater's main constituents. Black Point also trends

towards high loadings of the 2nd factor but at the same time has high loadings (up to > 84%) of the 1st factor as well. Thus the high factor loadings of the 1st factor at Black Point, indicate a good representation of Black Point by the 1st factor, indicating an input of another source as Hot Lake and Fumarolic Field. The lanthanides, Y and Sc as rare earth elements on the first factor indicate a magmatic input not found at any other area, except from the single sample from A26. All other areas are indistinguishably lost in the data cloud thus are equally represented by both factors with low negative factor loadings, equal to the local seawater.

The second factor analysis has lost some of its representative power compared to the first one with more factors, because the overall variance represented by the factors has been reduced by 10.26% from 89.03% to 78.77% (cp. tab. F.5 and F.7). Some of the parameters are not represented as sufficiently as before the reduction to four parameters as compared in tab. F.8. Especially F, Sc, Cr, Co, Mo, Sb, Te shifted towards a higher specific variance and smaller estimated communality. Still the majority of the variance of the parameters except maybe for the one mentioned in the line before can be represented by the new four factors. In exchange for this loss of data the interpretation has been eased and the factor loadings of the new four factors for certain parameters has increased.

A third factor analysis with the same element concentrations but without the pH and the EC yield almost the exact same results as the second factor analysis as can be seen in tables F.9 and F.10. Only changes are As is now also represented by the first factor (0.50), Bi switches from the 3rd to the second factor (0.59), the specific variance of Co and Ni jumps to > 0.8 and Cu, Ag and Bi are all now inversely represented by the 3rd factor. Besides from these changes all other elements are represented by the same factors and with similar factor loadings. This would indicate the influence of the pH and the sum parameter EC are represented by the element concentrations, which are in turn represented mostly by the same factors as before.

3.6.4.1. Rare earth elements

In all three conducted factor analysis, the first factor contains all lanthanides. Together with Y and Sc these elements are also called rare-earth elements (REE) (Mason 2013; Nozaki 2010). Riverine input of REE into the marine environment represents the biggest fraction of overall input of REE, but during estuarine mixing 65-75% of the riverine influx of REE is removed (Mason 2013; Nozaki 2010). Near Panarea no rivers flow into the Mediterranean sea, hence higher concentrations of REE must origin from other processes, e.g. from the hydrothermal system of Panarea. Normally concentrations of REE in ocean waters are in the pM-scale (Mason 2013; Nozaki 2010). This low concentration and their similar chemical and physical behavior due to their similar electron configuration make these elements suitable tracers for e.g. hydrothermal processes in an submarine environment (Mason 2013; Nozaki 2010).

Tab. 3.7 gives an overview over the correlation between the REE and two new factors of a factor analysis, comprising 146 samples. These two factors represent almost 93% of the total variance of the REE. The KMO of 0.93 indicates a high amount of common variability

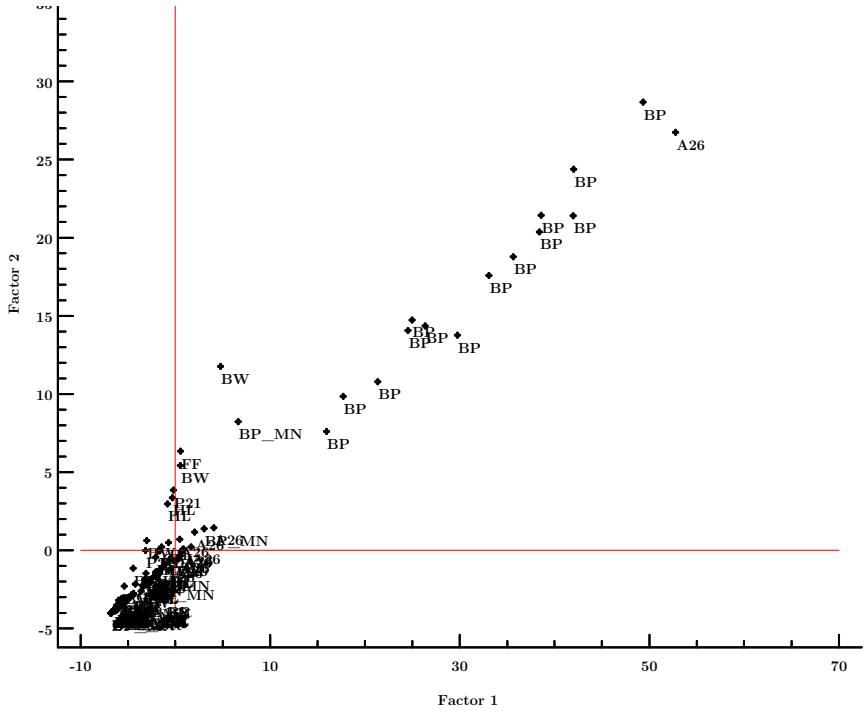

Fig. 3.31.: Scatter plot of the REE factor analysis displaying the first two factors, representing a cumulative variance of 92.87 % of the data. Black Point is mainly represented by the 1st factor (up to 49%), but also has a high loading on the second factor (up to almost 30%). All other areas remain in an indistinguishable data cloud in low negative values, exception is one sample from Area 26.

and tab. F.12 confirms the high common variability, making this analysis highly significant. Fig. 3.31 clarifies the singularity of Black Point regarding REE elements: the 1st factor (85% variance) representing Y, Nd, SM, Eu, Gd, Tb, Dy, Ho, Er, Tm, Yb and Lu with factor loadings >0.9 also represents samples from Black Point with the highest correlation coefficients (up to 49%). The 2nd factor (7% variance) represents mostly Ce and La, while Pr and Nd have medium to high loadings on both factors. Black Point is mainly represented by the 1st factor (up to 49%), but also has a high loading on the second factor (up to almost 30%). All other areas remain in an indistinguishable data cloud in low negative values, indicating a REE source contributing mainly to Black Point. Curios remains the single sample of Area 26 with high REE concentrations, yielding a higher loading on the 1st factor than samples from Black Point (almost 53%). Either the sample name is erroneous, making a Black Point sample an Area 26 sample, or also Area 26 is fed by the source, responsible for high REE concentrations. This sample would be the only proof after 10 years of sampling in this area. However, in sec. 3.6.1 Area 26 is identified among Black Point as a investigation area with elevated REE concentrations (cp. fig. 3.22).

3.6.4.2. Trace metals

As mentioned in sec. 1.2 certain elements display elevated concentration in submarine hydrothermal systems compared to seawater. Especially elevated concentrations of Rb, Cs, Si,

Tab. 3.7.: Extraction of the REE factor analysis with loadings minimally > 0.5. In bold factor loadings >0.9, in italic loadings >0.75 and in brackets negative factor loadings.

Factor	1	2
Variance	85.48	7.39
Cumulative	85.48	92.87
	Sc	*La*
	Y	**Ce**
	Pr	Pr
	Nd	Nd
	Sm	
	Eu	
	Gd	
	Tb	
	Dy	
	Ho	
	Er	
	Tm	
	Yb	
	Lu	

Fe, Mn, Cu, Co, Zn, Mn indicate submarine hydrothermal systems. A factor analysis based on these elements gives insight about the distribution of these elements between the various investigation areas and helps to distinguish differences. Three factors represent a total variance of 83.80 %, the KMO of 0.724 indicate meaningful factors and tab. F.13 displays specific variances for Si, Mn, Ba, Co, Cu between 0.17 and 0.30. The 1st factor represents Mn, Rb, Ba and Cs, the 2nd Si, Fe, Ba and Zn, the 3rd Co and Cu. Plotting the different areas reveals that similar to the results of the former factor analysis only Black Point and Hot Lake can be distinguished. Both areas are mainly represented by the first factor, while Black Point has higher loadings on the second factor. Firstly this analysis shows only hydrothermal fluids from Black Point and Hot Lake contain significant different trace element concentrations, distinguishing them from the rest of the areas and secondly also Black Point and Hot Lake differ from each other as indicated by the formerly conducted factor analysis. Still the low factor loadings indicate a limited representation of the areas by these factors, representing the named trace elements. All other areas, also La Calcara vanish in the data cloud and are not mainly represented by any factor.

3.6.5. Kruskall-Wallis-Test (KWT)

Lacking a normal distribution for the majority of the data, the Kruskal-Wallis-Test was applied to distinguish significantly different element concentrations between the investigation areas and thus to distinguish groups and trends within the investigation areas. The significance level α of the KWT was set to 0.01 and the subsequent conservative Bonferroni correction applied with significance levels α of 5% and 0.01%. KWTs were conducted for three on-

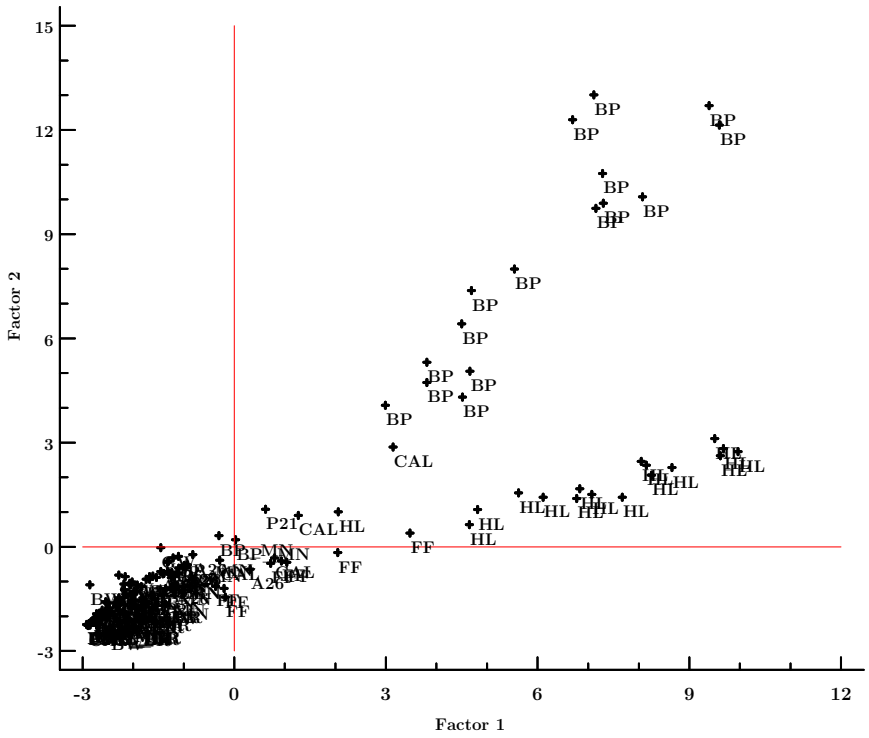

Fig. 3.32.: Scatter plot of the trace element factor analysis displaying the first two factors, representing a cumulative variance of 69.11 % of the data. Note both Black Point and Hot Lake are mainly represented by the 1st factor, but Black Point has higher loading on the second factor. Except for Fumarolic Field which follows the trend of Hot Lake all other areas remain in an indistinguishable data cloud in low negative values.

site parameters (pH, EC, E_H), nine main ions (Li^+, Na^+, K^+, Ca^{2+}, Mg^{2+}, F^-, Cl^-, Br^-, SO_4^{2-}), nine trace elements (Si, Fe, Mn, Rb, Cs, Ba, Zn, Co, Cu) and the REE (Y, Sc and the lanthanides). The investigation areas were paired with each other and tested for significant differences between the tested parameters. Tab. F.14 and following in the appendix display the matrices, showing the significant differences between the areas at both Bonferroni significance levels. Fig. 3.22 helps to determine the reasons for significant differences between different areas regarding each shown parameter (e.g. higher or lower concentrations than local seawater). In most cases the element concentrations mirror the EC, hence areas with a high EC will differ in their element concentrations from areas with a low EC, resulting probably in significant differences distinguished by the KWT. Exceptions are ions such as Mg^{2+} and SO_4^{2-}, typically depleted in hydrothermal fluids (cp. sec. 1.2).

3.6.5.1. On-site parameters

Using the more conservative Bonferroni correction the KWT based on the **pH** distinguishes only Black Point from most other investigation areas. A26, FF, HL and P21 are not significant different from Black Point (cp. tab. F.14 and fig. 3.22). The less conservative Bonferroni correction yields more significant differences, e.g. Area 26 differs from Bottaro Nord, La Calcara and La Calcara Black Rock, Bottaro Nord differs additionally from Hot Lake and

Tab. 3.8.: Extracted factors for the trace elements factor analysis with loadings minimally > 0.5. In bold factor loadings >0.9, in italic loadings >0.75 and in brackets negative factor loadings.

Factor	1	2	3
Variance [%]	52.05	17.06	14.69
Cumulative [%]	52.05	69.11	83.80
	Mn	Si	*Co*
	Rb	**Fe**	*Cu*
	Ba	Ba	
	Cs	**Zn**	

P21, La Calcara from the Groundwater, and La Calcara Black Rock from Hot Lake and P 21. Fig. 3.22 reveals the range of the pH for all areas and explains the background for the differences, e.g. Black Point has the lowest pH, while the groundwater and La Calcara Black Rock show the highest pH values. More conservatively Area 26, Black Point, Fumarolic Field, Hot Lake and Point 21 differ from the local seawater, less conservatively Black Point Mini/Nord (BP_MN) differs additionally. The rest of the areas cannot be distinguished from the local seawater, indicating either a massive contamination with seawater and the consequent buffering of the pH or other unknown buffer mechanisms, increasing the pH value of these areas towards the local seawater value.

The **EC** gives a similar picture: more conservatively only Black Point and Hot Lake differ from the local seawater and less conservatively Fumarolic Field differs additionally. Mostly Hot Lake differs from most other areas, because of its high EC. Black Point differs also, but only from La Calcara, the groundwater, Point 21. All other areas have a similar range as the local seawater and are hence not distinguishable.

As discussed previously problematic conditions to measure the $\mathbf{E}_H$ leave questions regarding the quality of these measurements. Hence the test results of the KWT show only differences for areas with a small range of their redox potential, making them distinguishable. Namely Area 26, Bottaro Nord and Hot Lake differ on the more conservatively level of the Bonferroni correction ($\alpha = 0.1$) from Black Point, Black Point Mini/Nord, La Calcara and La Calcara Black Rock, all with a wide range of their E_H (cp. fig. 3.22). Additionally on the less conservative level Fumarolic Field differs from the named areas with a wide range of their redox potential (from reducing towards oxidizing conditions). None of the areas differ from the seawater, clarifying the difficulty of the redox measurements.

Besides the EC the pH seems to be one of the most reliable indicators for the quality of a sample of submarine hydrothermal fluids. If one suggests the pH of Black Point as the original pH for the submarine hydrothermal fluids, all other areas seem to be contaminated with local seawater, buffering the pH towards more alkaline conditions. On the other hand the discrepancy between the extreme high EC of Hot Lake (up to 120 mS/cm) and the comparable average pH of around 5 and the extreme low pH of Black Point of around 2.5 but the comparable low EC of between 60 and 80 mS/cm has to be considered. Either the pH

is not the controlling/limiting parameter of the leaching the WRI in the subsurface or both waters undergo a different evolution and/or have a different origin such as varying bedrocks with an altering geochemical signature explaining the different overall solution of constituents in the fluids. As already in sec. 3.6.4 described, Black Point seems to be more influenced by an magmatic component compared to Hot Lake, which seems to originate more from altered local seawater.

3.6.5.2. Main ions

As stated in sec. 3.6.5, most elements follow the EC in their pattern of significant differences compared the local seawater and the other areas and $\mathbf{Li^+}$ does not make an exception. Area 26, Black Point, Fumarolic Field and Hot Lake differ from the local seawater on the more conservative level. Between each other again only Hot Lake differs on both levels of α from all other areas, except for Fumarolic Field, underlining again their similarity. Black Point differs only from areas with a low EC, such as Black Point Mini/Nord, and both, Hot Lake and Black Point, differ from La Calcara and the groundwater.

For $\mathbf{Na^+}$ the picture could not be clearer: Only Hot Lake differs from the local seawater and all other areas, except for Fumarolic Field, explainable again by the high EC and hence high Na^+ concentrations (cp. fig. 3.22) . Only La Calcara differs additionally from the seawater, Bottaro West and Fumarolic Field on the less conservative level, explainable by the low Na^+ concentrations, indicating a low Cl-hydrothermal phase at La Calcara which consequently limits the Na^+ concentration, depleted in comparison to the local seawater (cp. sec. 1.2).

$\mathbf{K^+}$ **and** $\mathbf{Ca^{2+}}$ behave geochemically similar and hence have the similar enrichment pattern within the areas and display similar significant differences (cp. fig. 3.22). Again only Hot Lake, Black Point and Fumarolic Field show differences from the local seawater. For Ca also A26 and Bottaro Nord differ from the local seawater on the less conservative level. Hot Lake differs from most other areas except for Black Point and Fumarolic Field for both elements. Black Point and Fumarolic Field (on the less conservative level) differs from areas with a low EC, such as Black Point Mini/Nord, La Calcara and La Calcara Black Rock, the groundwater, and Point 21.

Both $\mathbf{Mg^{2+}}$ **and** $\mathbf{SO_4^{2-}}$ are mostly depleted in the hydrothermal fluids, thus their concentrations contradict the EC as follows: Both Hot Lake and Black Points, areas with the highest EC differ significantly from the local seawater, because the concentrations of both Mg^{2+} and SO_4^{2-} are significantly below the concentrations of other areas and of the local seawater (cp. fig. 3.22). Hence samples from these two areas show on each level of α of the Bonferroni correction differences with most other areas. At La Calcara also both ions differ from the local seawater (depletion), at Area 26 only SO_4^{2-} differs from the seawater, indicating hydrothermal influence at these areas, leading to the removal of Mg^{2+} and SO_4^{2-}. Fluids from all other areas again seem to be either massively mixed with local seawater or do not undergo a hydrothermal alteration.

$\mathbf{F^-}$ gives an interesting picture of the hydrothermal system: All areas except for La Cal-

cara and La Calcara Black Rock, Fumarolic Field and the groundwater differ from the local seawater, Area 26, Black Point and Point 21 on the more conservative level. Among the investigation areas only Black Point differs from all areas except for Area 26, Bottaro Nord and the groundwater, distinguishing it as the exceptional area, regarding the F^- concentration. F^- is an indicator for magmatic input, via magmatic HF, giving the strong impression of Black Point as strongly influenced area (cp. sec. 1.2). The low pH at Black Point could validate a strong magmatic HF input. At area differing from the local seawater, this magmatic indicator seems to be diluted with e.g. local seawater to a certain degree, which makes a distinction between the areas impossible. La Calcara and La Calcara Black Rock, Fumarolic Field and the groundwater have such low F^- -concentrations, which are below the local seawater indicating a removal process or a hydrothermal fluid, without an magmatic input of F^- not contaminated with the local seawater, maintaining a low F^- concentration.

Cl^- mirrors more or less the EC, because as dominant anion and its enrichment due to hydrothermal induced phase separation in the subsurface (cp. sec. 1.2) the Cl^-concentration also determines the overall concentration of the cations. Hence the EC bases mostly on the Cl^- concentrations of each area. Again Hot Lake, Fumarolic Field and Black Point differ from the local seawater, due to their high EC. Hot Lake and Black Point differ from most other investigation areas (Black Point does not differ from Bottaro Nord, Bottaro West, Fumarolic Field and Hot Lake). Fumarolic Field differs additionally from areas with a low EC, such as La Calcara, La Calcara Black Rock and the groundwater. Even without a significant difference between La Calcara and the local seawater, still a low Cl-phase could explain the low Cl^--concentrations which are depleted compared to the local seawater.

The only difference between Cl^- and **Br^-** is the missing difference between the groundwater and Fumarolic Field. All other differences remain the same, sometimes they refer to another α.

The main ions follow mostly the pattern of the EC, which is determined by the Cl^- concentration of each area. A high EC indicates high element concentrations and is a proof among others of hydrothermal activity. Exceptions are Both Mg^{2+} and SO_4^{2-} which are normally depleted in hydrothermal systems. Both partly have their highest depletion at areas with the highest EC, such as Hot Lake and Black Point. This depletion is also considered as strong indicator of hydrothermal activity (cp. 1.2). Hot Lake, Black Point and Fumarolic Field show the most significant differences compared to the local seawater and between the investigation areas. Contrary areas with a low EC, such as La Calcara and La Calcara Black Rock show sometimes differences compared to the local seawater and between the areas, due to their low ion concentrations. All other areas hardly differ from the local seawater or from each other (e.g. Bottaro Nord, Bottaro West, Point 21) and massive contamination with local seawater, overwriting and buffering any typical hydrothermal signatures (elevated element concentrations for Li, K, Ca etc. and depletion of Mg and SO_4^{2-}) must be considered. In almost all cases Black Point differs from Black Point Mini/Nord, validating their difference and the exceptional position of Black Point among the investigation areas. The often missing

difference between Hot Lake and Fumarolic field underlines again their similarity, regarding their ion concentrations.

3.6.5.3. Trace Elements

Except for Bottaro West and La Calcara, the **Si** concentrations of all areas differ significantly from the local seawater, Area 26, Black Point and Hot Lake differ even on the more conservative α of 0.1. Si is an indicator for hydrothermal systems, due to its temperature dependent solubility, hence if its concentration is elevated, geothermal influence is likely at all areas except for Bottaro West and La Calcara Black Rock. Still the lastly named areas could also "suffer" from contamination with local seawater, diminishing the Si-signal. Among the areas, only Black Rock differs from most other area and Hot Lake shows differences with both Bottaro West and La Calcara Black Rock, most likely due their low Si-concentrations.

Black Point displays exceptional **Fe**-concentrations (cp. fig. 3.22), singling this area out from all the others. It is also the only area differing from the local seawater on the more conservative level of the Bonferroni correction. Among the investigation areas, again only Black Point differs from most other areas, except for the groundwater and Black Point Mini/Nord. Besides Black Point also Bottaro West, Black Point Mini/Nord, Hot Lake and La Calcara differ from the local seawater. While Hot Lake does not surprise, with its overall high element concentrations, the elevated concentrations of the other areas (cp. fig. 3.22) are not readily explained, but must be accepted. Regarding Black Point a high Fe-concentration could be expected, because of its exceptional low pH values, as discussed multiple times before.

As shown in tab. 3.4 Mn is the trace element with the greatest enrichment compared to the local seawater, over 1,000,000% enrichment at Black Point and Hot Lake are impressive examples for element enrichment at the submarine hydrothermal system Panarea. Most investigation areas differ significantly from the local seawater, exceptions are Bottaro West, La Calcara Black Rock, the groundwater and Point 21, all areas known for their moderately low element concentrations. Among the investigation areas, mainly Black Point and Hot Lake are distinguishable from most other areas, as indicated from their elevated Mn-concentrations (cp. fig. 3.22).

Rb depicts the overall trend, given by the EC: Hot Lake, Black Point and Fumarolic Field differ among the areas from most other areas, Fumarolic Field not in as many cases as the others, but mostly at areas with a low EC (La Calcara and La Calcara Black Rock, the groundwater, Point 21). Besides the typical three areas, also Area 26, Bottaro Nord and Black Point Mini/Nord differ from the local seawater, Area 26 and Bottaro Nord even on the more conservative level. Area 26 and Bottaro Nord differ also from La Calcara Black Rock, an area with low/depleted EC compared to the local seawater.

Cs mirrors almost perfectly the overall trend, as done by Rb: Again Hot Lake, Black Point and Fumarolic Field differ among the investigation areas and again Area 26 and Bottaro Nord differ also from La Calcara Black Rock, an investigation area with low/depleted EC compared to the local seawater. This time only the three "main" areas Hot Lake, Black Point

and Fumarolic Field differ form the local seawater, underlining again their exceptional position among the others.

Ba continues the clear pattern of Rb and Cs and marks Hot Lake, Black Point and Fumarolic Field as exceptional areas among all investigation areas (cp. fig. 3.22). Only surprise is the difference between La Calcara and La Calcara Black Rock, differentiating both from each other. All areas with elevated EC differ from the local seawater, areas with a low EC (La Calcara and La Calcara Black Rock, the groundwater, Point 21) cannot be distinguished from the local seawater, based on their Ba-concentration.

As additional trace element, not listed in tab. 3.4, **Zn** impressively underlines the exceptional status of Black Point, because except for the groundwater the enriched Zn concentrations differ from all other investigation areas and the local seawater.

Similar to the main ions, the trace elements mainly distinguish Hot Lake, Black Point and Fumarolic Field as hydrothermally influenced investigation areas. However, the Si-concentrations indicate a geothermal influence (elevated temperatures) for almost all areas, while the Mn-concentrations demonstrate the impressive enrichment gained in the submarine hydrothermal system Panarea mainly at Hot Lake and Black Point. Both Fe and Zn as pH-dependent soluble elements clearly distinguish Black Point from all other areas with its elevated concentrations as found out in the factor analysis in sec. 3.6.4 (both elements are on the first factor, by which Black Point is mostly represented). Contrary Rb, Cs and Ba depict the overall trend, of Hot Lake, Black Point and Fumarolic Field as the investigation areas with exceptional elevated element concentrations as proof for submarine hydrothermal activity, as found in sec. 3.6.4 (all three elements are on the second factor, by which Hot Lake is mostly represented). In almost all cases Black Point differs from Black Point Mini/Nord, validating their difference and the exceptional position of Black Point among the investigation areas. La Calcara Black Rock often differs from other areas, due to its low element concentrations, indicating a possible low Cl-hydrothermal phase, which determines a generally weakly enriched or even depleted hydrothermal fluid, compared to the local seawater.

3.6.5.4. Rare Earth Elements

Lacking the analysis for REE, Seebauer (2015) does not provide any concentrations for comparison, hence the average seawater from Brown (2001) is used for comparison. Both are similar (cp. fig. 3.22), only that most element concentrations are elevated in the local seawater, compared to the average seawater. However, as the average seawater contains only one concentration for each element, the KWT does not find any significant difference between multiple fluid samples from each investigation area and the average seawater. Since duplicating the average seawater would bias the results and the average seawater does not represent the local seawater, further comparisons with the seawater are omitted and the emphasis is laid on the differences among the investigation areas. Overall the REE mostly distinguish Black Point from other areas, but the heavier the REE become, the more Area 26 differs from other areas with low REE concentrations, also exhibiting elevated concentrations.

Sc clearly singles Black Point out, as the area differing from all other areas, except for the groundwater and Hot Lake, both with elevated Sc concentrations. Latter is the area differing additionally from Black Point Mini/Nord and Point 21. **Y** also singles Black Point out, but also underlines the depletion of La Calcara, La Calcara Black Rock and of the groundwater compared to e.g. Area 26 and Bottaro Nord, both considerably enriched in Y.

La, Ce, Pr, Nd and Sm all distinguish mainly Black Point from all other areas (except for Hot Lake) on the more conservative level, but also distinguish Area 26 mostly from La Calcara and La Calcara Black Rock, both with low REE concentrations. Sometimes Hot Lake differs also from La Calcara Black Rock and Point 21, but Black Rock remains in its exceptional role.

Eu, Gd, Tb, Dy, Ho, Er and Tm also distinguish mainly Black Point from all other areas, interestingly except for Area 26, which itself distinguishes itself from most other areas with low REE concentrations, as La Calcara and La Calcara Black Rock, but even from Fumarolic Field, which plays a major role, regarding the main ions and the trace elements. Again in a minor role Hot Lake differs from La Calcara and La Calcara Black Rock, but is far from major role it played regarding the main ions and trace elements.

Regarding their **Yb** concentrations besides Black Point, differing from other areas except for Area 26 and Bottaro Nord, both last named areas differ from La Calcara, La Calcara Black Rock and Fumarolic Field (Area 26 also from the groundwater), all areas with very low REE-concentration. **Lu** highlights again Black Point as exceptional area among the other investigation areas and underlines A26 as area with elevated concentrations differing from La Calcara, Fumarolic Field and even Hot Lake.

The KWT applied on the REE concentrations reveals differences between Black Point as mainly enriched in REE and Hot Lake as only partly enriched. Area 26 is also revealed as area considerably enriched in REE. The KWT validates the findings of the Factor Analysis (cp. sec:FA), which distinguishes Black Point from all other areas (The first factor, including mostly the REE, represents Black Point best). Various possibilities offer an explanation of the exceptional REE concentrations at Black Point: (1) The REE distinguish Black Point from all other investigation areas, (2) all areas are fed by the same source, but mixing with the local seawater dilutes and overwrites typical hydrothermal indicators, except for Black Point, (3) or all areas are fed by the same source, but the volcanic layers differ, resulting in various pathways and different leaching potentials, thus explaining the differences, as suggested by Price et al. (2015) (cp. sec. 1.2). The outlier of Area 26, found during the factor analysis (cp. sec:FA) is found to be part of the considerably enriched REE concentrations of Area 26.

4. Conclusion

Combining the findings of the samples from 2015 and the data from 10 years of scientific diving at the submarine hydrothermal system Panarea lead to following summarizing conclusions.

The **on-site parameters** describe the found hydrothermal fluids as acidic (pH <2.4-5.5), reducing (E_H: around -50 mV) and highly mineralized (up to 120 mS/cm). Black Point, Fumarolic Field and Hot Lake are singled out, comparing all investigation areas, showing the most distinguished characteristics, while the rest of the areas display characteristics closely to seawater. La Calcara and the groundwater from Pozzo di Pina instead display opposite values: oxidizing redox potential (250-350 mV), lower electrical conductivity than seawater (found minimum of 39 mS/cm) and a higher pH (6-6.5) in comparison to all other sites, but significant lower than common seawater (8.2).

IC and ICP-MS reveal an astonishing enrichment of several **main and trace elements** in the hydrothermal fluids, compared to the local seawater. The overall trend depicted by the major constituents (Li, F, S, Cl, Na, Mg, K, Ca) and some others, e.g. B, Be, Rb, Mn and Sr is in accordance to the EC: in ascending order Black Point, Fumarolic Field and Hot Lake show the highest enrichment, La Calcara shows mostly depletion or low enrichment, distinguishing these areas from the rest. All areas reveal a depletion of Mg^{2+} and SO_4^{2-}, with minimums at Black Point, Fumarolic Field and Hot Lake. Extremely elevated F^- concentrations at Black Point indicate a possible magmatic input by HF acid and explains the low pH at Black Point.

Br^-/Cl^--plots reveal again three groups, verifying the before described trends: (1) Pozzo di Pina and La Calcara have smaller concentrations than seawater, the latter a possible mixture between the groundwater and hydrothermal fluids or the result of a low Cl-content hydrothermal phase, (2) Black Point, Fumarolic Field and Hot Lake have the highest concentrations, probably resulting from a high Cl-hydrothermal phase, (3) all other investigation areas plot in the vicinity and are hence indistinguishable from the local seawater in accordance to their electrical conductivity. However, **Cl/Br mass and molar ratios** reveal higher ratios (than the average (Brown 2001) and the local seawater (Seebauer 2015)) at investigation areas with low Br^- and Cl^--concentrations, especially at La Calcara Ball 1. Halite dissolution e.g. at La Calcara could explain the low Br^- concentrations in comparison to the higher Cl^--concentrations. Areas with high concentrations of Br^- and Cl^- (e.g. Hot Lake and Fumarolic Field) show comparable low ratios close to the average and local seawater, indicating seawater enriched by phase separation as main source for these investigation areas.

Further x-y plots of the **main constituents** Li, F, S, Cl, Na, K, Ca, Mn against the depleted Mg-concentrations identify again three distinctive groups: (1) The main constituents are always enriched compared to the local seawater at Fumarolic Field and Hot Lake, (2) La Calcara is always depleted/lowly enriched and on a line with Pozzo di Pina showing the lowest concentrations, (3) and Black Point acts as an intermediate between both other groups. Other

investigation areas exhibit the same or similar concentrations of the compared elements as the local seawater with no distinct trend whatsoever.

The **conservative elements** Li, Br and Cl are related to each other: (1) Black Point, Fumarolic Field and Hot Lake are enriched in ascending order compared to the local seawater and (2) La Calcara is always depleted/lowly enriched and shows together with Pozzo di Pina the lowest concentrations.

Normalized to the deviations of these elements compared to local seawater Br^- and Li^+ show similar trends, hence similar slopes of enrichment in ascending order from Black Point, Fumarolic Field towards Hot Lake. The enrichment seems to be linear: the more Li in the fluids, the more other elements are contained.

The **stable isotopes** of hydrogen and oxygen reveal heavier isotopic compositions of the submarine hydrothermal fluids than the local meteoric water. The vast majority of the investigation areas plots close to Mediterranean seawater, only one single groundwater sample from Pozzo di Pina plots in the vicinity of the meteoric water. All samples are shifted towards heavier, enriched $\delta^{18}O$ values, La Calcara reveals the heaviest values, the lightest are shown by Hot Lake. With these results a connection between the groundwater of Panarea and the submarine hydrothermal fluids from La Calcara can be excluded. It seems more likely the hydrothermal fluids originate from local seawater, which is heavily altered by the hydrothermal system, regarding the shifted $\delta^{18}O$ values. Hot Lake and Fumarolic Field lay on one trend line starting at the local seawater and heading towards lighter δ^2H (mixing with magmatic fluids?) and heavier $\delta^{18}O$ values (WRI). Black Point is in an intermediate position between Hot Lake and La Calcara, mostly shifted towards heavier $\delta^{18}O$ values, indicating three different evolutions at Hot Lake/Fumarolic Field, Black Point and La Calcara.

Similarities regarding their on-site parameters and chemical composition indicate a connection or a mixture between the groundwater from Pozzo di Pina and La Calcara. The stable isotopes, however contradict this possibility, which leaves the author with the conclusion that in the light of the results presented in this thesis and the results of e.g. Italiano and Nucchio (1991), Tassi et al. (2009) and Price et al. (2015) the submarine hydrothermal system Panarea is mainly fed by Mediterranean seawater. As stated by Price et al. (2015) the different investigation areas "receive" different kinds of altered seawater, explaining the distinctions between the various areas. Furthermore, different ranges of mixtures between local unaltered seawater and the hydrothermally altered seawater exist. Black Point, Fumarolic Field and Hot Lake seem to be fed more or less directly by the hydrothermal system, without or with only minor mixtures with local seawater, resulting in distinctive peaks in their element concentrations, distinguished on-site parameters and the highest isotopic deviations from the local meteoric water line and the local seawater regarding the isotopic compositions of the stable isotopes. All in all it seems as if the samples from Black Point, Fumarolic Field and especially Hot Lake resemble the clearest picture of the submarine hydrothermal fluids we have so far:

1. low pH (<3 - 5),

2. negative redox potential (around -50mV),
3. high electrical conductivity (up to 120 mS/cm at Hot Lake),
4. partly tremendous enrichment of elements (esp. Li^{+}, Fe^{2+}, Mn^{2+}, Tl) compared to local seawater, but depletion in Mg^{2+} and SO_4^{2-},
5. altered isotopic compositions compared to Mediterranean seawater ($\delta^{18}O$ +2‰ and $\delta^{2}H$ -5‰) due to WRI with the bedrock.

The statistical analysis of the data of 10 years scientific diving conducted by the Scientific Dicing Center Freiberg validates most trends found in 2015 but also reveals new findings such as the differentiation between Black Point and Hot Lake, regarding their concentrations of main constituents and trace elements. The factor analysis distinguishes between Black Point, Hot Lake and the remaining investigation areas. Black Point is represented best by a factor containing mostly typical trace elements and REE. Hot Lake on the other hand is represented by another factor, mainly representing a condensed seawater, highly enriched in its main constituents (Na, K, Ca etc.).

The subsequently conducted Kruskall-Wallis Test validates the suggested differences from the factor analysis: Black Point differs statistical significantly from most other investigation areas and the local seawater regarding trace elements and REE. Hot Lake differs mostly regarding enriched main constituents of seawater but also differs due to tremendous enrichment of trace elements, whereas it does not differ significantly regarding its elevated REE concentrations. Surprisingly also Area 26 shows distinct and statistically significant elevated REE concentrations, differentiating this area from the rest and putting it closer to Black Point. Besides Hot Lake, Fumarolic Field, Black Point and Area 26 also La Calcara differs often from other investigation areas and the local seawater, but in most cases due to its low element concentrations, especially regarding the main constituents of the local seawater.

Furthermore a time series of Hot Lake data shows sampling must be conducted on a more regularly basis, not only every year in the beginning of September to gain informative time series. Comparing the time series of Mg^{2+}, SO_4^{2-}, Cl^{-} and Br^{-} at the investigation area Hot Lake proved to be a useful tool to grade the sample quality of the submarine hydrothermal fluids.

As described in the results before, Black Point, Hot Lake/Fumarolic Field and La Calcara are the investigation areas that stand out and their characteristics are thus summarized in the following:

Hence **Black Point (vent)** is characterized by following features:

1. clear differences between the vent of Black Point and the two other sampling points, Black Point Mini and Black Point Nord, both latter points do not show as distinct features as the vent.

2. lowest pH (average of 2.79) , contradicting E_H readings (42 - 358 mV), high temperatures (average of 129.98°C), intermediate EC between local seawater and Hot Lake (average of 71.85 mS/cm).

3. as only investigation area extremely enriched in F, indicator of magmatic input of HF, moderately elevated main ions, such as Li^+, K^+, Ca^{2+}, Cl^- and strongly depleted concentrations of Mg^{2+}, SO_4^{2-}, indicating that the low pH might be as well influenced by the formation of Mg-OH precipitates.

4. tremendously elevated concentrations of trace elements such as Si, Mn, Fe, Rb, Cs, Ba, including the all time maxima for Si, Fe and Barium.

5. heavily elevated concentrations of REE elements, singling Black Point out from all other investigation areas.

6. intermediate isotopic shift between Hot Lake and La Calcara with values around $\delta^{18}O$ +2‰ and δ^2H +7.5‰

Hot Lake and partly **Fumarolic Field** on the other hand are characterized by other features:

1. moderately low pH (average of 4.93), elevated temperatures between 67 and 45°C), low and stable E_H (average of -40.3 mV) and by far highest EC (average of 96.19 mS/cm with an maximum in 2015 of 118.3 mS/cm).

2. tremendously elevated concentrations of the main constituents, such as Li^+, Na^+, K^+, Ca^{2+}, Cl^- and strongly depleted concentrations of Mg^{2+}, SO_4^{2-}.

3. tremendously elevated concentrations of trace elements such as Si, Mn, Fe, Rb, Cs, Ba, including the all time maxima for Mn, Rb and Cs.

4. moderately towards neglectable concentrations of REE elements, close to the average of all other areas and considerably lower than Area 26.

5. strongest isotopic shift regarding δ^2H towards -7.5 to -2.5‰ and a $\delta^{18}O$ shift towards +1‰.

La Calcara is characterized by following features:

1. highest pH (average of 5.58) , oxidizing E_H readings (average of 306 mV), high temperatures at Black Rock (up to 132.50°C), lowest EC even below the local seawater (average of 52.90 mS/cm, minimum of 39.70 mS/cm at Black Rock).

2. as only investigation area mostly depleted in all major ions, especially Cl^-, on a trend line with the depleted groundwater from Pozzo di Pina regarding the Mg^{2+}-plots with other main ions, but weakly enriched in F^- and Mn and other trace elements.

3. no significant enrichment of further trace elements or REE.

4. strongest isotopic shift of $\delta^{18}O$ towards +2 to +3‰ and the highest $\delta^{2}H$ values of +13‰.

The remaining investigation areas, such as Area 26, Bottaro Nord and West seem to undergo a mixture between the ascending altered hydrothermal waters and the local seawater, buffering the found extremes from e.g. Hot Lake towards minor deviations from the local seawater. Fluids found at Point 21 with its strong gas exhalations (CO_2, originating from the mantle) are assumed to be the result of a mixture between ascending gases reducing the local seawater, creating hydrothermal fluids on its way upwards. La Calcara seems to be fed by a depleted water source or low Cl-content hydrothermal phase compared to the local seawater, still with some interesting features, such as high silicon concentrations but an isotopic composition close to seawater. Black Point, Fumarolic Field and Hot Lake as strongly altered investigation areas seem to have undergone an alteration e.g. by WRI, indicating maybe a longer contact and reaction time with the underground, than e.g. La Calcara had. Alternatively the hydrothermal fluids, as described by Price et al. (2015) undergo a different evolution regarding phase separation, which would also explain the depleted concentrations of the major constituents at La Calcara.

The data of 10 years scientific diving at the submarine hydrothermal system Panarea contradict partly the findings of Price et al. (2015) in following points:

1. questionable pH at Black Point: Price et al. (2015) publish pH values for Black Point vent fluids with an average of 4.23, based on three samples, taken between 2008 and 2010 instead of the average of 2.79, based on 15 samples taken between 2007 and 2015, taken by the SDC Freiberg.

2. contradicting iron concentrations at Black Point: Price et al. (2015) classify Black Point's iron concentrations as considerably low and emphasizes La Calcara's high iron concentrations. The SDC Freiberg found the maximum iron concentrations each year between 2007 and 2015 at Black Point with a concentration of 37,670μg/l and an enrichment of 1.86E+05%, one order of magnitude higher than the absolute maximum found at the investigation area La Calcara (cp. tab. 3.3). Especially if one would use the literature value for the iron concentration of the local seawater as used by Price et al. (2015) (average of 0.63μg/l for iron, instead of 20.3μg/l) the maximum enrichment increases drastically towards 5.99E+06% (cp. tab. 3.3), because the local seawater is clearly enriched in iron. It is assumed the maybe erroneous sampling of the Black Point vent fluids of Price et al. (2015) lead to a contamination with local seawater, thus biasing the pH and subsequently the pH-dependent iron concentrations.

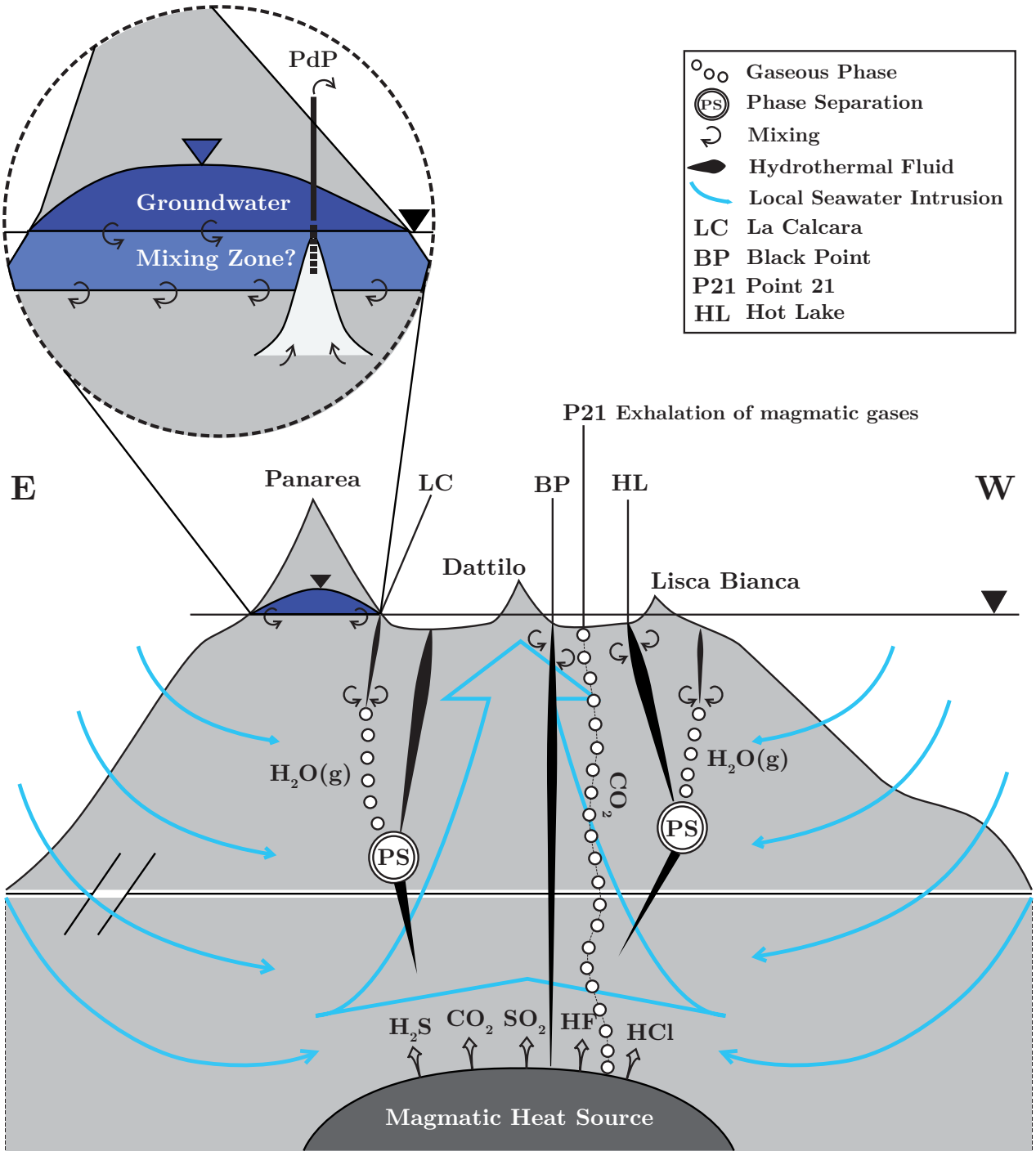

Fig. 4.1.: Model of the evolution of the various hydrothermal fluids found at La Calcara, Black Point, Point 21 and Hot Lake.

Due to these differences with Price et al. (2015) a new model for the origin of the submarine hydrothermal fluids found by the SDC in the last 10 years is proposed. The dominant source of the hydrothermal fluids at the different investigation areas is the same: The local seawater (s. sec. 3.5) infiltrating into the crust is heated by the magmatic heat source leaching under high pressure and temperature the surrounding bedrock, and ascends towards the surface. The ascent of the heated water creates a water vortex, sucking in seawater from the sides of the volcano dome into the system. Depending on the speed of the ascent, the fluid crosses the phase boundary of liquid water to water vapour (depending on temperature and pressure). Hence fast ascending water is more likely to reach an environment with a high temperature but a comparable low pressure, leading to a gaseous and a dense water phase, or a high Cl-content hydrothermal phase and a low Cl-content hydrothermal phase ascending.

La Calcara seems to be one exemplary investigation area fed by a gaseous low Cl-content hydrothermal phase (low element concentrations) which will transform into a liquid again according to T/P conditions and mixes with the local seawater, finally exhaled at La Calcara. Hot Lake on the other hand receives a high Cl-content hydrothermal phase (highest element concentrations), probably also mixed with local seawater during its ascent. Black Point is assumed to be fed by a slowly ascending fluid (high Si concentrations indicate either a high temperature or long contact times with the surrounding bedrock) without or only minor phase separations, still containing a magmatic input of HF given by the magmatic heat source and subsequent high concentrations of trace elements and REE. Point 21 with its strong gas exhalations, assumed to origin from within the mantle given high concentrations of mantle CO_2 is fed by a strong gas flow towards the surface, transporting and reducing surrounding seawater towards the surface, creating an own hydrothermal fluid, based on heated and reduced local seawater.

All investigation areas, regardless of the evolution of the hydrothermal fluid in the subsurface are facing not distinguishable mixing processes either between a gaseous and liquid phase and heated, altered (enriched regarding the chemical constituents) seawater and “fresh”, unaltered seawater near the surface. So no model as sophisticated as it may be, can fully describe the processes occurring in the subsurface, so further research has to close remaining gaps.

Bibliography

Appelo, C. A. J. and Postma, D. (2005). *Geochemistry, groundwater and pollution*. 2. ed. Leiden: Balkema.

Baker, E. T. and German, C. R. (2004). "On the global distribution of hydrothermal vent fields". In: *Mid-ocean ridges: hydrothermal interactions between the lithosphere and oceans* 148, pp. 245–266.

Berndt, M.E. and Seyfried, W.E Jr. (1990). "Boron, bromine, and other trace elements as clues to the fate of chlorine in mid-ocean ridge vent fluids". In: *Geochimica et Cosmochimica Acta* 54.8, pp. 2235 –2245.

Bischoff, J. L. and Rosenbauer, R. J. (1984). "The critical point and two-phase boundary of seawater, 200-500 °C". In: *Earth and Planetary Science Letters* 68.1, pp. 172 –180.

Bischoff, J. L. and Seyfried, W. E (1978). "Hydrothermal chemistry of seawater from 25 degrees to 350 degrees C". In: *American Journal of Science* 278.6, pp. 838–860.

Bischoff, James L. and Rosenbauer, Robert J. (1985). "An empirical equation of state for hydrothermal seawater (3.2 percent NaCl)". In: *American Journal of Science* 285.8, pp. 725–763.

Bolognesi, L. and D'Amore, F. (1992). "Isotopic variation of the hydrothermal system on Vulcano Island, Italy". In: *Geochimica et Cosmochimica Acta* 57, pp. 2069–2082.

Brown, Evelyn (2001). *Seawater: Its composition, properties and behaviour / prepared by an Open University Course Team*. 2nd ed. / authors, Evelyn Brown ... [et al.] Oxford: Butterworth Heinemann in association with the Open University.

Calanchi, N., Capaccioni, B., Martini, M., Tassi, F., and Valentini, L. (1995). "Submarine gas-emission from Panarea Island Aeolian Archipelago: Distribution of inorganic and organic compounds and inferences about source conditions". In: *Acta Vulcanologia* 7 (1), pp. 43–48.

Calanchi, N., Peccerillo, A., Tranne, C.A., Lucchini, F., Rossi, P.L., Kempton, P., Barbieri, M., and Wu, T.W. (2002). "Petrology and geochemistry of volcanic rocks from the island of Panarea: implications for mantle evolution beneath the Aeolian island arc (southern Tyrrhenian sea)". In: *Journal of Volcanology and Geothermal Research* 115.3-4, pp. 367 – 395.

Caliro, S., Caracausi, A., Chiodini, G., Ditta, M., Italiano, F., Longo, M., Minopoli, C., Nuccio, P.M., Paonita, A., and Rizzo, A. (2004). "Evidence of a recent input of magmatic gases into the quiescent volcanic edifice of Panarea, Aelian Islands, Italy". In: *Geophysical Research Letters* 31.7, pp. 1–5.

Capaccioni, B., Tassi, F., Vaselli, O., Tedesco, D., and Rossi, P.L. (2005). "The November 2002 degassing event at Panarea Island (Italy): Five months of geochemical monitoring". In: *Annals of Geophysics* 48.4-5, pp. 755–765.

Capaccioni, B., Tassi, F., Vaselli, O., Tedesco, D., and Poreda, R. (2007). "Submarine gas burst at Panarea Island (southern Italy) on 3 November 2002: A magmatic versus hydrothermal episode". In: *Journal of Geophysical Research: Solid Earth (1978–2012)* 112.B5.

Capasso, G., Favara, R., and Inguaggiato, S. (1997). "Chemical features and isotopic composition of gaseous manifestations on Vulcano Island, Aeolian Islands, Italy: An interpretative model of fluid circulation". In: *Geochimica et Cosmochimica Acta* 61.16, pp. 3425 –3440.

Caracausi, A., Ditta, M., Italiano, F., Longo, M., Nuccio, P. M., and Paonita, A. (2005). "Massive submarine gas output during the volcanic unrest off Panarea Island (Aeolian arc, Italy): Inferences for explosive conditions". In: *Geochemical Journal* 39.5, pp. 459–467.

Chiodini, G., Cioni, R., Marini, L., and Panichi, C. (1995). "Origin of the fumarolic fluids of Vulcano Island, Italy and implications for volcanic surveillance". In: *Bulletin of Volcanology* 57.2, pp. 99–110.

Chiodini, G., Caliro, S., Caramanna, G., Granieri, D., Minopoli, C., Moretti, R., Perotta, L., and Ventura, G. (2006). "Geochemistry of the Submarine Gaseous Emissions of Panarea (Aeolian Islands, Southern Italy): Magmatic vs. Hydrothermal Origin and Implications for Volcanic Surveillance". In: *Pure and Applied Geophysics* 163.4, pp. 759–780.

Craig, Harmon (1961). "Isotopic variations in meteoric waters". In: *Science* 133.3465, pp. 1702–1703.

– (1963). "The isotopic geochemistry of water and carbon in geothermal areas". In: *Nuclear Geology on Geothermal Areas*, pp. 17–53.

Damm, K.L. Von, Lilley, M.D., III, W.C. Shanks, Brockington, M., Bray, A.M., Grady, K.M., Olson, E., Graham, A., and Proskurowski, G. (2003). "Extraordinary phase separation and segregation in vent fluids from the southern East Pacific Rise". In: *Earth and Planetary Science Letters* 206.34, pp. 365 –378.

Dekov, V. M., Kamenov, G. D., Abrasheva, M. D., Capaccioni, B., and Munnik, F. (2013). "Mineralogical and geochemical investigation of seafloor massive sulfides from Panarea Platform (Aeolian Arc, Tyrrhenian Sea)". In: *Chemical Geology* 335, pp. 136–148.

Driesner, T. (2007). "The system H2O-NaCl. Part II: Correlations for molar volume, enthalpy, and isobaric heat capacity from 0 to 1000 °C, 1 to 5000 bar, and 0 to 1 {XNaCl}". In: *Geochimica et Cosmochimica Acta* 71.20, pp. 4902 –4919.

Esposito, A., Giordano, G., and Anzidei, M. (2006). "The 2002-2003 submarine gas eruption at Panarea volcano (Aeolian Islands, Italy): Volcanology of the seafloor and implications for the hazard scenario". In: *Marine Geology* 227.12, pp. 119 –134.

Fabris, M., Anzidei, M., Baldi, P., Bortoluzzi, G., and Aliani, S. (2010). "The high resolution combined topographic model of Panarea island (Aeolian islands, Italy)". In: *EGU General Assembly Conference Abstracts*. Vol. 12, p. 3046.

Gabbianelli, G., Gillot, P.Y., G., Lanzafame, Romagnoli, C., and Rossi, P.L. (1990). "Tectonic and volcanic evolution of Panarea (Aeolian Islands, Italy)". In: *Marine Geology* 92.34, pp. 313 –326.

Gabbianelli, G., Romagnoli, C., Rossi, P.L., and Calanchi, N. (1993). "Marine geology of the Panarea-Stromboli area (Aeolian Archipelago, Southeastern Tyrrhenian sea)". In: *Acta Vulcanol* 3, pp. 11–20.

Gat, J.R. and Carmi, I. (1970). "Evolution of the isotopic composition of atmospheric waters in the Mediterranean Sea area". In: *Journal of Geophysical Research* 75.15, pp. 3039–3048.

Gat, Joel (2010). *Isotope hydrology: A study of the water cycle / Joel R. Gat*. Vol. v. 6. Series on environmental science and management. London: Imperial College Press.

Gerardo-Abaya, J., D'Amore, F., and Arnorsson, St. (2000). "Isotopes for Geothermal investigations". In: *Isotopic and chemical techniques in geothermal exploration, development and use*. Ed. by St. Arnorsson. IAEA, pp. 49 –65.

German, C. R. and Damm, K.L. van (2004). "Hydrothermal Processes". In: *The Oceans and Marine Geochemistry*. Ed. by H.D. Holland and K.K. Turekian. Vol. 6. Treatise on Geochemistry. Elsevier, Amsterdam, pp. 181–222.

German, C. R. and Seyfried, W. E. (2014). "Hydrothermal Processes". In: *Treatise on Geochemistry*. Ed. by Holland, H. and Turekian, K. Vol. 8. Elsevier, pp. 191–233.

Giggenbach, W.F. (1992). "Isotopic shifts in waters from geothermal and volcanic systems along convergent plate boundaries and their origin". In: *Earth and planetary science letters* 113.4, pp. 495–510.

Google (2016a). *"Hotel Oasis da Pina, Panarea, Italy" Map*. Google Maps. URL: https://www.google.de/maps/@38.6376814,15.0753004,96m/data=!3m1!1e3.
– (2016b). *"Islets East of Panarea, Italy" Map*. Google Maps. URL: https://www.google.de/maps/@38.6384226,15.1059327,1420m/data=!3m1!1e3.
– (2016c). *"La Calcara, Panarea, Italy" Map*. Google Maps. URL: https://www.google.de/maps/@38.6456176,15.0744244,196m/data=!3m1!1e3.
Grassa, F., Capasso, G., Favara, R., and Inguaggiato, S. (2006). "Chemical and Isotopic Composition of Waters and Dissolved Gases in Some Thermal Springs of Sicily and Adjacent Volcanic Islands, Italy". In: *pure and applied geophysics* 163.4, pp. 781–807.
Hannington, M.D., Petersen, S., Herzig, P.M., and Jonasson, I.R. (2004). "A global database of seafloor hydrothermal systems, including a digital database of geochemical analyses of seafloor polymetallic sulfides". In: *Geol. Surv. of Can. Open File* 4598, p. 12.
Hannington, M.D., De Ronde, C. D. J., and Petersen, S. (2005). *Sea-floor tectonics and submarine hydrothermal systems*. Ed. by J. W. Hedenquist, J. F. H. Thompson, R. J. Goldfarb, and J. P. Richards. Littelton, Colorado, USA: Society of Economic Geologists, pp. 111–141.
Heinicke, J., Italiano, F., Maugeri, R., Merkel, B., Pohl, T., Schipek, M., and Braun, T. (2009). "Evidence of tectonic control on active arc volcanism: The Panarea-Stromboli tectonic link inferred by submarine hydrothermal vents monitoring (Aeolian arc, Italy)". In: *Geophysical Research Letters* 36.4.
Herzig, P.M. and Hannington, M.D. (2000). "Input from the deep: Hot vents and cold seeps". In: *Marine Geochemistry*. Springer, pp. 397–416.
Hölting, B. and Coldewey, W. G. (2013). *Hydrogeologie: Einführung in die allgemeine und angewandte Hydrogeologie*. 8. Aufl. Berlin and Heidelberg: Springer Spektrum.
Italiano, F. and Nuccio, P. M. (1991). "Geochemical investigations of submarine volcanic exhalations to the east of Panarea, Aeolian Islands, Italy". In: *Journal of Volcanology and Geothermal Research* 46.1-2, pp. 125–141.
Italiano, Francesco and Caruso, Cinzia (2011). "Detection of Fresh and Thermal Waters over an Island with Extinct Volcanism: The Island of Salina (Aeolian arc, Italy)". In: *Procedia Earth and Planetary Science* 4, pp. 39–49.
Krahe, L. (unpublished). "Mineralogical and economic geology evaluation of Fe-S-Precipitates from the location of La Calcara, Panarea, Aeolian Arc (Italy)."
Liotta, M., Brusca, L., Grassa, F., Inguaggiato, S., Longo, M., and Madonia, P. (2006a). "Geochemistry of rainfall at Stromboli volcano (Aeolian Islands): Isotopic composition and plume-rain interaction". In: *Geochemistry, Geophysics, Geosystems* 7.7.
Liotta, M., Favara, R., and Valenza, M. (2006b). "Isotopic composition of the precipitations in the central Mediterranean: Origin marks and orographic precipitation effects". In: *Journal of Geophysical Research* 111.D19.
Lowell, R. P. (1991). "Modeling continental and submarine hydrothermal systems". In: *Reviews of Geophysics* 29.3, pp. 457–476.
Lucchi, F., Tranne, C. A., Peccerillo, A., Keller, J., and Rossi, P. L. (2013). "Chapter 12 Geological history of the Panarea volcanic group (eastern Aeolian archipelago)". In: *The Aeolian islands volcanoes*. Vol. 37. GSL Memoirs. London: The Geological Society, pp. 351–395.
Mason, Robert P (2013). *Trace metals in aquatic systems*. John Wiley & Sons.
Merkel, J. B. and Planer-Friedrich, B. (2002). "Integrierte Datenauswertung Hydrogeologie". In: *Freiberg Online Geology* 7.
Mottl, M.J., Seewald, J.S., Wheat, C.G., Tivey, M.K., Michael, P.J., Proskurowski, G., McCollom, T.M., Reeves, E., Sharkey, J., You, C.-F., Chan, L.-H., and Pichler, T. (2011).

"Chemistry of hot springs along the Eastern Lau Spreading Center". In: *Geochimica et Cosmochimica Acta* 75.4, pp. 1013 –1038.

Müller, C. (2011). "Geothermal state of shallow submarine geothermal systems and isotopic signatures of Panarea, Aeolian Islands (Italy)". In: *Freiberg Online Geology* 30.

Murawski, Hans and Meyer, Wilhelm (2010). *Geologisches Wörterbuch*. 12. überarbeitete und erweiterte Auflage. SpringerLink : Bücher. Heidelberg: Spektrum Akademischer Verlag.

Nicholson, K. (1993). *Geothermal Fluids - Chemistry and Exploration Techniques*. Berlin Heidelberg New York, Springer Verlag.

Nozaki, Y. (2010). "Rare earth elements and their isotopes in the ocean". In: *Marine Chemistry and Geochemistry*. Ed. by J.H. Steele, S.A. Thorpe, and K.K. Turekian. Elsevier, Amsterdam, pp. 39–51.

Ono, S., Shanks, W. C. III, Rouxel, O. J., and Rumble, D. (2007). "S-33 constraints on the seawater sulfate contribution in modern seafloor hydrothermal vent sulfides". In: *Geochimica et Cosmochimica Acta* 71.5, pp. 1170 –1182.

Paonita, A., Favara, R., Nuccio, P.M., and Sortino, F. (2002). "Genesis of fumarolic emissions as inferred by isotope mass balances: {CO2} and water at Vulcano Island, Italy". In: *Geochimica et Cosmochimica Acta* 66.5, pp. 759 –772.

Paonita, A., Federico, C., Bonfanti, P., Capasso, G., Inguaggiato, S., Italiano, F., Madonia, P., Pecoraino, G., and Sortino, F. (2013). "The episodic and abrupt geochemical changes at La Fossa fumaroles (Vulcano Island, Italy) and related constraints on the dynamics, structure, and compositions of the magmatic system". In: *Geochimica et Cosmochimica Acta* 120, pp. 158–178.

Pester, Nicholas J., Rough, Mikaella, Ding, Kang, and Jr., William E. Seyfried (2011). "A new Fe/Mn geothermometer for hydrothermal systems: Implications for high-salinity fluids at 13 °N on the East Pacific Rise". In: *Geochimica et Cosmochimica Acta* 75.24, pp. 7881 –7892. ISSN: 0016-7037.

Picarro Inc. (2015). *Cavity Ring-Down Spectroscopy (CRDS)*. URL: http://www.picarro.com/technology/cavity_ring_down_spectroscopy.

Pichler, T. (2005). "Stable and radiogenic isotopes as tracers for the origin, mixing and subsurface history of fluids in submarine shallow-water hydrothermal systems". In: *Journal of Volcanology and Geothermal Research* 139.3-4, pp. 211 –226.

Pichler, T., Veizer, J., and Hall, G. E. M. (1999). "The chemical composition of shallow-water hydrothermal fluids in Tutum Bay, Ambitle Island, Papua New Guinea and their effect on ambient seawater". In: *Marine Chemistry* 64.3, pp. 229–252.

Piranjo, F. (2010). *Hydrothermal Processes and Mineral Systems*. 2010th ed. Springer Berlin Heidelberg.

Price, R. E., LaRowe, D. E., Italiano, F., Savov, I., Pichler, T., and Amend, J. P. (2015). "Subsurface hydrothermal processes and the bioenergetics of chemolithoautotrophy at the shallow-sea vents off Panarea Island (Italy)". In: *Chemical Geology* 407-408, pp. 21–45.

Rohland, K. (2007). "Investigation in submarine water and gas chemistry at Panarea, Aeolian Islands, Italy". In: *TU Bergakademie Freiberg, Department of Geology, Section for Hydrogeology*.

Romagnoli, C., Casalbore, D., Bortoluzzi, G., Bosman, A., Chiocci, F. L., DOriano, F., Gamberi, F., Ligi, M., and Marani, M. (2013). "Chapter 4 Bathy-morphological setting of the Aeolian Islands". In: *Geological Society, London, Memoirs* 37.1, pp. 27–36.

SDC (2005-2015). "CMAS Scientific Diving Center Freiberg; internal data".

Scott, SD (1997). "Submarine hydrothermal systems and deposits". In: *Geochemistry of hydrothermal ore deposits*, pp. 797–875.

Sedwick, P. and Stuben, D. (1996). "Chemistry of shallow submarine warm springs in an arc-volcanic setting: Vulcano Island, Aeolian Archipelago, Italy". In: *Marine Chemistry* 53.1, pp. 147–161.

Seebauer, L. (2015). "Seegraswiesen (Posidonia oceanica) bei Panarea (Äolische Inseln, Italien) - Vegetationsstruktur und der Einfluss von Gas- und Fluidaustritten." MA thesis. Technical University Mining Academy Freiberg.

Seewald, J.S. and Seyfried, W.E. Jr. (1990). "The effect of temperature on metal mobility in subseafloor hydrothermal systems: constraints from basalt alteration experiments". In: *Earth and Planetary Science Letters* 101.2-4, pp. 388 –403. ISSN: 0012-821X.

Seyfried, W. E. and Mottl, M. J. (1982). "Hydrothermal alteration of basalt by seawater under seawater-dominated conditions". In: *Geochimica et Cosmochimica Acta* 46.6, pp. 985–1002.

Seyfried, W. E. and Shanks, W. C. (2004). "Alteration and mass transport in mid-ocean ridge hydrothermal systems: Controls on the chemical and isotopic evolution of high-temperature crustal fluids". In: *Hydrogeology of the Oceanic Lithosphere*, pp. 451–495.

Shanks, WC (2001). "Stable isotopes in seafloor hydrothermal systems: vent fluids, hydrothermal deposits, hydrothermal alteration, and microbial processes". In: *Reviews in Mineralogy and Geochemistry* 43.1, pp. 469–525.

Sieland, R. (2009). "Chemical and isotopic investigations of submarine hydrothermal fluid discharges from Panarea, Aeolian Islands, Italy". In: *Freiberg Online Geology* 21.

Sigurdsson, H. (2000). "Volcanic episodes and rates of volcanism". In: *Encyclopedia of Volcanoes*, pp. 271–279.

Stangroom, J. (2015). *Social Science Statistics*. www.socscistatistics.com. URL: http://www.socscistatistics.com/pvalues/pearsondistribution.aspx.

Stanulla, R. (2012). "Geological record of submarine hydrothermal gas and water escape structures - morphology and geochemistry of the recent volcanic system of Panarea, Italy". Master. Freiberg: Technical University Mining Academy Freiberg.

Taran, Y. A. (2005). "A method for determination of the gas-water ratio in bubbling springs". In: *Geophysical Research Letters* 32.23.

Tassi, F., Capaccioni, B., Caramanna, G., Cinti, D., Montegrossi, G., Pizzino, L., Quattrocchi, F., and Vaselli, O. (2009). "Low-pH waters discharging from submarine vents at Panarea Island (Aeolian Islands, southern Italy) after the 2002 gas blast: Origin of hydrothermal fluids and implications for volcanic surveillance". In: *Applied Geochemistry* 24.2, pp. 246 –254.

Tassi, F., Capaccioni, B., and Vaselli, O. (2014). "Compositional spatial zonation and 2005-2013 temporal evolution of the hydrothermal-magmatic fluids from the submarine fumarolic field at Panarea Island (Aeolian Archipelago, southern Italy)". In: *Journal of Volcanology and Geothermal Research* 277, pp. 41–50.

Thornton, Edward C and Seyfried, WE (1987). "Reactivity of organic-rich sediment in seawater at 350 °C, 500 bars: experimental and theoretical constraints and implications for the Guaymas Basin hydrothermal system". In: *Geochimica et Cosmochimica Acta* 51.7, pp. 1997–2010.

Truesdell, A. H., Nathenson, M., and Rye, R. O. (1977). "The effects of subsurface boiling and dilution on the isotopic compositions of Yellowstone thermal waters". In: *Journal of Geophysical Research* 82.26, pp. 3694–3704.

Truesdell, A.H., Haizlip, J.R., Armannsson, H., and D'Amore, F. (1989). "Origin and transport of chloride in superheated geothermal steam". In: *Geothermics* 18.1, pp. 295–304.

Von Damm, K. L. (2000). “Chemistry of hydrothermal vent fluids from 9 ° 10 °N, East Pacific Rise: "Time zero", the immediate posteruptive period”. In: *Journal of Geophysical Research: Solid Earth* 105.B5, pp. 11203–11222.

Von Damm, KL (1995). “Controls on the chemistry and temporal variability of seafloor hydrothermal fluids”. In: *Seafloor Hydrothermal Systems: Physical, Chemical, Biological, and Geological Interactions*, pp. 222–247.

– (2001). “Chemistry of hydrothermal vent fluids”. In: *Marine Chemistry and Geochemistry*. Ed. by J. Steele, S. Thorpe, and K. Turekian. Elsevier, Amsterdam, pp. 81–89.

Williams-Jones, A. E. and Heinrich, C. A. (2005). “100th Anniversary Special Paper: Vapor Transport of Metals and the Formation of Magmatic-Hydrothermal Ore Deposits”. In: *Economic Geology* 100.7, pp. 1287–1312.

Appendices

A. Investigation areas

Tab. A.1.: Investigation areas and their GPS-coordinates (degree°, arc minute', arc second" according to WGS 84, (SDC 2005-2015)

Investigation area	Northing	Easting
Area 26	38°38'21.2"	15°06'18.5"
Black Point	38°38'16.7"	15°06'17.1"
Bottaro North	38°38'19.2"	15°06'36.4"
Bottaro West	38°38'17.4"	15°06'35.5"
Fumarolic Field	38°38'24.1"	15°06'35.8"
Hot Lake	38°38'24.5"	15°06'35.0"
La Calcara	38°38'48.2"	15°04'36.8"
Point 21	38°38'21.2"	15°06'18.5"
Pozzo di Pina	38°38'16.0548"	15°04'30.1908"

B. On-site parameters

Tab. B.1.: On-site parameters of the groundwater sampled at "Pozzo da Pina" well at the hotel "Oasis da Pina" taken during the 2015 diving campaign in Panarea (n.d = not determined).

Sample_ID	T [°C]	pH	EC [mS/cm]	EMF [mV]	E_H [mV]	O_2 [mg/l]	O_2 [%]
PAN_093015_PdP	55.2	6.4	18.0	54.0	247.9	n.d.	n.d.
PAN_094015_PdP	52.2	6.2	71.0	139.0	332.9	n.d.	n.d.
PAN_094015_PdP_equ	49.4	6.6	20.2	-16.0	177.9	2.61	43.1

Tab. B.2.: Stabilization of the on-site parameters at Pozzo di Pina after 6 measurements from the 4th of September 2015.

Measurement	T [°C]	pH	EC [mS/cm]	EMF [mV]	E_H [mV]	O_2 [mg/l (%)]
1	52.2	6.2	71	139	332.9	
2	51.7	6.4	54	117	310.9	
3	52.5	6.5	45	71	264.9	
4	52.5	6.5	39	31	224.9	
5	50.5	6.7	21	-12	181.9	
6	49.9	6.6	20	-16	177.9	2.61 (43.1)

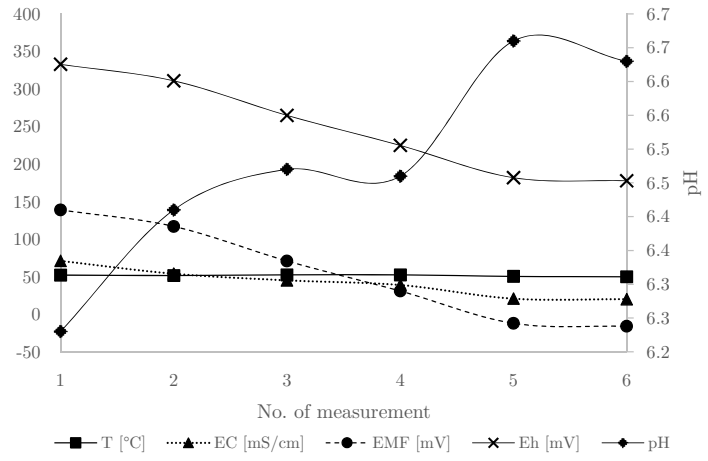

Fig. B.1.: Stabilization of the on-site parameters pH, T, EC, EMF, E_H. O_2 is measured once at the last measurement (no. 6) after 30 minutes of letting the tap water run.

The water was clear, colorless and without any visible particles and smelled very weakly like rotten eggs, an indicator for the presence of SO_2.

Tab. B.3.: On-site parameters of the 2015 diving campaign in Panarea. The temperature given is the in-situ temperature, measured directly in or at the submarine exhalations points of the hydrothermal fluids (n.d. = not determined; d.l. = detection limit). ∗ average value of 19 measurements around Hot Lake, in brackets the found maximum.

Sample ID	Depth [m]	T [°C]	pH /	EC [ms/cm]	E_H [mV]	O_2 [mg/L]	O_2 [%]	SO_2^- [mg/L]	NO_2^- [mg/L]	Fe^{2+} [mg/L]
PAN_09032015_A26	25.6	59.0	4.95	58.6	-60.0	0.37	4.6	0.04	0.013	0.02
PAN_09082015_A26_bt	25.6	62.3	4.89	58.6	-55.8	0.73	9.1	1.69	n.d.	0.5
PAN_09082015_A26_st	26.2	63.8	4.91	59.5	-59.0	0.46	5.7	0.8	n.d.	0.01
PAN_09012015_BN	7.9	n.d.	5.56	60.9	-73.1	1.61	20.7	0.12	0.089	0.75
PAN_08312015_BP(1)	23.5	112.0	2.84	75.1	45.6	5.12	67.4	0.11	0.23	n.d.
PAN_09072015_BP_mini	23.3	94.5	3.13	66.6	233.4	5.3	64.6	d.l.	n.d.	1.32
PAN_09022015_BW	12.1	40.0	6.14	60.2	4.1	6.99	88.1	0.7	0.113	0.04
PAN_09022015_BW(2)	12.1	46.0	5.53	63.3	-29.9	4.41	54.5	18.5	0.005	0.04
PAN_09042015_FF	16.5	68.1	4.92	84.6	-60.0	0.77	9.7	0.1	0.008	0.2
PAN_09012015_HL	18.7	34.4∗ (72.8)	4.78	118.3	-50.2	0.62	7.6	0.2	0.026	0.28
PAN_08312015_LC_Ball_1	20.7	132.5	5.63	53.6	252.7	4.23	54.7	0.03	0.133	0.7
PAN_09012015_LC_Ball_1(2)	20.7	118.7	5.76	53	338.7	5.61	73.2	n.d.	n.d.	n.d.
PAN_09022015_LC_Ball_1(3)	20.7	118.7	5.6	48	360.8	4.19	53.7	0.14	0.344	1.12
PAN_09032015_LC_Ball_1(4)	20.7	118.7	5.4	46.1	343.4	3.07	39.1	0.06	n.d.	1.18
PAN_09012015_LC_Ball_2	n.d.	n.d.	5.53	51.9	264.7	3.27	42.3	0.37	0.017	0.32
PAN_08312015_LC_BR	20.4	118.7	6.42	39.7	326.1	8.38	107.5	n.d.	n.d.	n.d.
PAN_09012015_LC_BR(2)	20.4	132.5	5.14	59.3	80.7	3.73	48.7	1.1	0.011	0.15
PAN_09022015_LC_BR(3)	20.4	n.d.	5.45	58.8	299.9	7.07	90.1	2.25	0.02	0.69
PAN_09032015_LC_BR(4)	20.4	n.d.	6.01	58.7	356.0	8.38	106.4	0.02	n.d.	0.16
PAN_08312015_LC_NR	20.4	114.0	5.78	58.4	345.9	6.58	85.7	0.13	0.073	0.42
PAN_09022015_LC_NR(2)	20.4	n.d.	5.9	58	356.7	7.34	94.4	n.d.	n.d.	n.d.
PAN_09022015_LC_C	n.d.	n.d.	5.3	50.8	374.8	3.05	39.1	0.07	d.l.	0.45
PAN_08302015_P21	n.d.	n.d.	5.05	61	-33.9	1.09	28.8	32.5	0.012	n.d.
PAN_09032015_P21(2)	21.6	64.1	5.14	58.2	-18.1	2.72	34.2	50.1	0.046	0.1

C. Major Ions

Tab. C.1.: Major anions of the waters samples in mg/l. Samples with the < symbol show values below the detection limit. Please note that PO_4^{3-} is not mentioned, because all measured values were below the detection limit of 1.01 mg/l .

Sample ID	F^-	Cl^-	Br^-	NO_3^-	SO_4^{2-}	HCO_3^-
PAN_09032015_A26	2.74	20938.73	59.40	<1.01	2700.71	108.37
PAN_09082015_A26_bt	<1.01	22782.82	58.26	<1.01	2618.55	93.12
PAN_09082015_A26_st	2.21	22949.33	43.47	<1.01	2530.32	90.49
PAN_09012015_BN	1.10	22720.80	55.75	238.90	2893.77	292.89
PAN_08312015_BP(1)	13.84	28801.07	75.17	236.51	1872.65	0.19
PAN_09072015_BP_mini	6.25	25732.00	77.38	<1.01	1927.92	0.51
PAN_09022015_BW	<1.01	21539.60	61.40	<1.01	2937.88	232.06
PAN_09022015_BW(2)	1.34	25081.47	34.86	248.65	2883.83	109.53
PAN_09042015_FF	<2.01	35041.57	88.62	<2.01	2461.46	101.78
PAN_09012015_HL	2.33	53684.28	150.66	<2.01	1485.49	79.45
PAN_08312015_LC_Ball_1	2.30	15557.68	35.36	245.27	2617.47	43.45
PAN_09012015_LC_Ball_1(2)	1.59	18641.58	25.24	252.07	2660.35	95.74
PAN_09022015_LC_Ball_1(3)	0.61	17568.10	32.11	<1.01	2320.13	63.64
PAN_09032015_LC_Ball_1(4)	1.03	14907.45	30.14	<1.01	2200.62	69.38
PAN_09012015_LC_Ball_2	0.91	18683.36	46.99	<1.01	2553.51	98.61
PAN_08312015_LC_BR	2.70	22002.44	36.06	247.59	3549.05	n.d.
PAN_09012015_LC_BR(2)	2.51	21711.14	35.71	248.24	3150.39	131.86
PAN_09022015_LC_BR(3)	1.21	21607.47	56.06	<1.01	3082.47	216.68
PAN_09032015_LC_BR(4)	1.42	22268.97	58.29	<1.01	3092.69	120.21
PAN_09022015_LC_C	1.21	19136.27	46.57	<1.01	2500.97	53.87
PAN_08312015_LC_NR	2.66	21196.93	35.47	246.44	3454.45	123.56
PAN_08302015_P21	2.71	21893.88	49.96	238.82	3430.17	120.02
PAN_09032015_P21(2)	1.50	22109.80	57.32	<1.01	2937.48	150.66
PAN_093015_PdP	1.29	11136.15	25.15	<1.01	1659.02	679.75
PAN_094015_PdP_equ	0.95	3592.86	8.28	<1.01	778.22	877.45

Tab. C.2.: Major cations of the waters samples in mg/l. Samples with the < symbol show values below the detection limit.

Sample ID	Li^+	Na^+	NH_4^+	K^+	Mn^{2+}	Ca^{2+}	Mg^{2+}
PAN_09032015_A26	2.15	11828.02	< 5.05	613.61	41.79	859.54	1316.67
PAN_09082015_A26_bt	2.14	12361.57	< 5.05	607.86	40.69	814.25	1298.57
PAN_09082015_A26_st	2.29	12362.95	< 5.05	620.75	46.94	859.56	1293.80
PAN_09012015_BN	2.17	12354.44	< 5.05	606.89	38.52	1068.61	1323.69
PAN_08312015_BP(1)	10.58	11390.58	< 5.05	1463.52	226.81	3723.95	747.66
PAN_09072015_BP_mini	8.89	11722.82	< 5.05	1294.37	187.76	3200.39	901.76
PAN_09022015_BW	1.66	12292.53	< 5.05	544.57	16.37	825.91	1413.86
PAN_09022015_BW(2)	2.39	12210.72	< 5.05	634.93	27.52	1198.56	1391.03
PAN_09042015_FF	14.79	14904.27	< 10.05	1950.23	166.43	4928.01	1180.95
PAN_09012015_HL	30.64	18635.77	< 10.05	3644.21	499.61	9826.76	1036.87
PAN_08312015_LC_Ball_1	1.05	8329.03	< 5.05	368.59	49.76	275.72	864.12
PAN_09012015_LC_Ball_1(2)	0.37	10022.86	< 5.05	399.71	28.38	330.71	1131.67
PAN_09022015_LC_Ball_1(3)	0.57	9424.95	< 5.05	388.40	32.19	348.20	1042.35
PAN_09032015_LC_Ball_1(4)	0.79	9135.22	< 5.05	388.94	38.46	303.77	996.08
PAN_09012015_LC_Ball_2	0.46	10373.86	< 5.05	383.47	22.36	344.09	1155.49
PAN_08312015_LC_BR	0.27	12221.30	< 5.05	437.07	< 5.05	427.64	1430.96
PAN_09012015_LC_BR(2)	< 1.01	12336.88	< 5.05	425.80	< 5.05	386.31	1383.49
PAN_09022015_LC_BR(3)	< 1.01	12250.32	< 5.05	422.22	< 5.05	382.85	1379.41
PAN_09032015_LC_BR(4)	< 1.01	12448.05	< 5.05	433.60	2.74	391.48	1401.07
PAN_09022015_LC_C	0.45	9839.04	< 5.05	381.91	37.73	287.27	1089.59
PAN_08312015_LC_NR	< 1.01	11412.35	< 5.05	418.71	4.47	386.96	1360.03
PAN_08302015_P21	< 1.01	12408.91	< 5.05	447.26	6.41	462.16	1389.51
PAN_09032015_P21(2)	0.89	12127.22	< 5.05	461.90	11.53	534.43	1355.08
PAN_093015_PdP	< 1.01	6079.35	< 5.05	240.27	6.65	227.08	729.41
PAN_094015_PdP	< 1.01	9424.04	< 5.05	358.82	7.51	371.00	1151.07
PAN_094015_PdP_equ	< 1.01	2663.51	1.16	103.30	5.19	70.09	249.67

Tab. C.3.: Percentage error of the Electrical Balance (E.B.) of the major ion analysis. Because of the high percentage error the sample PAN_094015_PdP (PdP(2)) is excluded from further assessment.

Sample ID	Sampling Point	E.B. [%]
PAN_09032015_A26	A26	2.59
PAN_09082015_A26_bt	A26 - big tub	0.19
PAN_09082015_A26_st	A26 - small tub	0.18
PAN_09012015_BN	BN	0.36
PAN_08312015_BP(1)	BP 1	-4.01
PAN_09072015_BP_mini	BP mini	1.25
PAN_09022015_BW	BW 1	2.45
PAN_09022015_BW(2)	BW 2	-3.56
PAN_09042015_FF	FF	0.29
PAN_09012015_HL	HL	-1.59
PAN_08312015_LC_Ball_1	LC Ball 1	-4.37
PAN_09012015_LC_Ball_1(2)	LC Ball 1 (2)	-2.79
PAN_09022015_LC_Ball_1(3)	LC Ball 1 (3)	-2.06
PAN_09032015_LC_Ball_1(4)	LC Ball 1 (4)	4.03
PAN_09012015_LC_Ball_2	LC Ball 2	-0.77
PAN_08312015_LC_BR	LC Black Rock	n.d.
PAN_09012015_LC_BR(2)	LC Black Rock (2)	-0.35
PAN_09022015_LC_BR(3)	LC Black Rock (3)	-0.20
PAN_09032015_LC_BR(4)	LC Black Rock (4)	-0.63
PAN_09022015_LC_C	LC Chimney	-4.59
PAN_08312015_LC_NR	LC New Rock	-3.05
PAN_08302015_P21	Point 21	-0.55
PAN_09032015_P21(2)	Point 21(2)	-0.81
PAN_093015_PdP	PdP	-2.92
PAN_094015_PdP	PdP(2)	23.57
PAN_094015_PdP_equ	PdP_equ	3.6

Tab. C.4.: Mass and molar Cl/Br ratios, compared to average seawater ratio (Brown 2001) and local seawater ratio (Seebauer 2015). Please note the high concentrations of Hot Lake, Fumarolic Field and Black Point, but their corresponding low ratios, similar to the local seawater. Masses taken from phreeqc.dat database: Cl: 35.453 mol/l, Br: 79.904 g/mol.

	mg/l		mmol/l		mass	molar
Sample ID	Cl^-	Br^-	Cl^-	Br^-	Cl/Br	Cl/Br
PAN_09032015_A26	20938.73	59.40	590.61	0.74	352	794
PAN_09082015_A26_bt	22782.82	58.26	642.62	0.73	391	881
PAN_09082015_A26_st	22949.33	43.47	647.32	0.54	528	1190
PAN_09012015_BN	22720.80	55.75	640.87	0.70	408	918
PAN_08312015_BP(1)	28801.07	75.17	812.37	0.94	383	864
PAN_09072015_BP_mini	25732.00	77.38	725.81	0.97	333	749
PAN_09022015_BW	21539.60	61.40	607.55	0.77	351	791
PAN_09022015_BW(2)	25081.47	34.86	707.46	0.44	719	1622
PAN_09042015_FF	35041.57	88.62	988.39	1.11	395	891
PAN_09012015_HL	53684.28	150.66	1514.24	1.89	356	803
PAN_08312015_LC_Ball_1	15557.68	35.36	438.83	0.44	440	992
PAN_09012015_LC_Ball_1(2)	18641.58	25.24	525.81	0.32	739	1665
PAN_09022015_LC_Ball_1(3)	17568.10	32.11	495.53	0.40	547	1233
PAN_09032015_LC_Ball_1(4)	14907.45	30.14	420.48	0.38	495	1115
PAN_09012015_LC_Ball_2	18683.36	46.99	526.99	0.59	398	896
PAN_08312015_LC_BR	22002.44	36.06	620.61	0.45	610	1375
PAN_09012015_LC_BR(2)	21711.14	35.71	612.39	0.45	608	1370
PAN_09022015_LC_BR(3)	21607.47	56.06	609.47	0.70	385	869
PAN_09032015_LC_BR(4)	22268.97	58.29	628.13	0.73	382	861
PAN_09022015_LC_C	19136.27	46.57	539.76	0.58	411	926
PAN_08312015_LC_NR	21196.93	35.47	597.89	0.44	598	1347
PAN_08302015_P21	21893.88	49.96	617.55	0.63	438	988
PAN_09032015_P21(2)	22109.80	57.32	623.64	0.72	386	869
PAN_093015_PdP	11136.15	25.15	314.11	0.31	443	998
PAN_094015_PdP_equ	3592.86	8.28	101.34	0.10	434	978
average Seawater	**19,500**	**67.1**	**550.02**	**0.84**	**291**	**655**
local Seawater	**19,909**	**63.7**	**561.55**	**0.80**	**313**	**705**

D. Multi-Element Analysis

Tab. D.1.: Measurement modi of the ICP-MS: elements with an additional 0V or 3V were measured in collision mode, the rest in normal mode.

7Li	95Mo
9Be	107Ag
10B	111Cd-3V
24Mg-3V	115In
27Al-0V	118Sn
28Si-3V	121Sb
31P-0V	125Te
34S-0V	133Cs
39K-3V	138Ba
43Ca	139La
45Sc-3V	140Ce
47Ti	141Pr
47Ti-3V	146Nd
51V-3V	147Sm
52Cr-3V	153Eu
55Mn-3V	157Gd
56Fe-3V	159Tb
59Co-3V	163Dy
60Ni-3V	165Ho
63Cu-3V	166Er
66Zn-3V	169Tm
71Ga	172Yb
75As-3V	175Lu
78Se-0V	182W
79Br	205Tl
81Br	208Pb
85Rb	209Bi
88Sr	232Th
89Y	235U
90Zr	238U
93Nb	

Tab. D.2.: Results of the element analysis using an ICP-MS in μg/l for the diving spots Area 26, Bottaro Nord, Black Point, Bottaro West and Fumarolic Field. The < symbol indicates values below the afterward given detection limit.

Elements	A26	A26bt	A26st	BN	BP(1)	BP mini	BW	BW(2)	FF
Li	1.77E+03	1.64E+03	1.77E+03	1.31E+03	9.10E+03	7.28E+03	1.17E+03	2.35E+03	1.20E+04
Be	2.92E+00	2.83E+00	2.83E+00	1.33E+00	5.99E+00	4.93E+00	5.09E-01	1.11E+00	3.97E+00
B	1.52E+04	1.43E+04	1.53E+04	1.04E+04	6.03E+04	4.96E+04	9.83E+03	1.74E+04	8.08E+04
Mg	1.18E+06	1.10E+06	1.10E+06	7.65E+05	5.58E+05	7.03E+05	1.09E+06	1.40E+06	1.01E+06
Al	1.04E+02	1.16E+02	9.30E+01	< 50	1.52E+03	1.41E+03	< 50	< 50	7.27E+01
Si	9.51E+04	9.48E+04	9.15E+04	4.65E+04	1.19E+05	1.31E+05	1.18E+04	2.31E+04	6.02E+04
P	< 500	< 500	< 500	< 500	< 500	< 500	< 500	< 500	< 500
S	1.32E+06	1.39E+06	1.00E+06	1.65E+06	2.46E+05	4.24E+05	9.33E+05	1.30E+06	7.87E+05
K	5.77E+05	5.40E+05	5.56E+05	3.78E+05	1.20E+06	1.10E+06	4.52E+05	6.76E+05	1.84E+06
Ca	8.50E+05	7.85E+05	8.40E+05	7.65E+05	3.40E+06	2.99E+06	8.09E+05	1.33E+06	4.73E+06
Sc	< 5	< 5	< 5	< 5	1.49E+01	9.14E+00	< 5	< 5	< 5
Ti	< 5	< 5	< 5	< 5	5.53E+00	< 5	< 5	< 5	< 5
V	< 5	< 5	5.03E+00	< 5	5.79E+01	3.70E+01	< 5	5.84E+00	< 5
Cr	6.91E+00	5.70E+00	< 5	< 5	< 5	< 5	< 5	< 5	< 5
Mn	4.18E+04	3.87E+04	4.28E+04	2.50E+04	2.01E+05	1.70E+05	1.27E+04	2.98E+04	1.69E+05
Fe	1.65E+02	1.48E+02	6.59E+01	< 50	1.68E+04	1.28E+04	< 50	1.71E+02	2.56E+02
Co	< 0.5	< 0.5	< 0.5	< 0.5	< 0.5	< 0.5	< 0.5	< 0.5	< 0.5
Ni	8.14E+00	8.26E+00	< 5	< 5	< 5	< 5	< 5	5.50E+00	7.95E+00
Cu	< 50	< 50	< 50	< 50	< 50	< 50	< 50	< 50	< 50
Zn	5.90E+01	< 50	< 50	< 50	4.14E+04	3.34E+04	< 50	< 50	< 50
Ga	< 0.5	< 0.5	< 0.5	< 0.5	8.19E-01	< 0.5	< 0.5	< 0.5	< 0.5
As	< 10	< 10	< 10	9.29E+01	1.01E+03	1.01E+03	< 10	< 10	< 10
Se	8.14E+01	7.93E+01	8.45E+01	1.61E+02	1.29E+02	8.79E+01	8.42E+01	1.41E+02	1.60E+02
79Br	8.64E+04	7.98E+04	8.15E+04	5.92E+04	1.03E+05	1.04E+05	8.10E+04	1.03E+05	1.34E+05
81Br	8.65E+04	7.98E+04	8.14E+04	5.85E+04	1.02E+05	1.04E+05	8.06E+04	1.02E+05	1.35E+05
Rb	1.46E+03	1.35E+03	1.48E+03	1.31E+03	7.31E+03	6.26E+03	7.19E+02	1.43E+03	1.04E+04
Sr	1.76E+04	1.66E+04	1.73E+04	1.41E+04	7.36E+04	6.60E+04	1.68E+04	2.86E+04	9.20E+04

Continued on next page

Tab. D.2 – continued from previous page

Elements	A26	A26bt	A26st	BN	BP(1)	BP mini	BW	BW(2)	FF
Y	9.52E+00	7.89E+00	8.96E+00	4.05E+00	2.11E+01	1.85E+01	6.02E-01	1.39E+00	1.20E+00
Zt	< 2.5	< 2.5	< 2.5	< 2.5	< 2.5	< 2.5	< 2.5	< 2.5	< 2.5
Nb	< 0.5	< 0.5	< 0.5	< 0.5	< 0.5	< 0.5	< 0.5	< 0.5	< 0.5
Mo	1.98E+00	1.50E+00	1.64E+00	1.73E+00	3.85E+00	3.04E+00	3.45E+00	3.78E+00	4.41E+00
Ag	< 0.25	< 0.25	< 0.25	< 0.25	< 0.25	6.01E-01	< 0.25	< 0.25	< 0.25
Cd	< 0.5	< 0.5	< 0.5	< 0.5	9.29E+01	1.28E+01	< 0.5	< 0.5	< 0.5
In	< 0.05	< 0.05	< 0.05	< 0.05	6.60E-02	< 0.05	< 0.05	< 0.05	< 0.05
Sn	< 2.5	< 2.5	< 2.5	< 2.5	< 2.5	< 2.5	< 2.5	< 2.5	< 2.5
Sb	< 0.5	< 0.5	< 0.5	< 0.5	< 0.5	< 0.5	< 0.5	< 0.5	< 0.5
Te	6.42E-01	< 0.5	5.22E-01	7.77E-01	3.07E+00	1.96E+00	6.69E-01	6.36E-01	2.74E+00
Cs	4.81E+02	4.58E+02	4.85E+02	4.29E+02	2.54E+03	2.16E+03	2.24E+02	4.80E+02	3.94E+03
Ba	1.51E+02	1.43E+02	1.45E+02	1.41E+02	3.04E+03	2.97E+03	5.56E+01	1.25E+02	1.79E+03
La	2.11E-01	2.01E-01	1.21E-01	2.33E-01	1.01E+00	1.31E+00	< 0.05	5.10E-02	8.00E-02
Ce	5.75E-01	5.13E-01	3.91E-01	2.64E-01	3.02E+00	3.43E+00	8.30E-02	1.77E-01	1.76E-01
Pr	1.21E-01	1.01E-01	1.01E-01	< 0.05	4.99E-01	5.20E-01	< 0.05	< 0.05	< 0.05
Nd	9.73E-01	7.57E-01	7.71E-01	1.69E-01	2.39E+00	2.49E+00	1.06E-01	2.62E-01	1.85E-01
Sm	5.02E-01	4.79E-01	4.09E-01	6.30E-02	1.14E+00	1.07E+00	5.20E-02	1.43E-01	1.44E-01
Eu	2.13E-01	1.71E-01	1.92E-01	< 0.05	1.04E+00	9.89E-01	< 0.05	6.60E-02	3.87E-01
Gd	1.02E+00	8.75E-01	9.30E-01	1.79E-01	2.52E+00	2.22E+00	9.20E-02	2.12E-01	2.53E-01
Tb	2.00E-01	1.80E-01	1.92E-01	< 0.05	5.30E-01	4.79E-01	< 0.05	< 0.05	< 0.05
Dy	1.38E+00	1.05E+00	1.23E+00	2.52E-01	3.28E+00	2.83E+00	8.20E-02	2.11E-01	1.83E-01
Ho	2.72E-01	2.24E-01	2.48E-01	7.90E-02	6.93E-01	5.93E-01	< 0.05	< 0.05	< 0.05
Er	7.03E-01	5.21E-01	6.10E-01	2.61E-01	2.02E+00	1.69E+00	< 0.05	1.07E-01	5.80E-02
Tm	7.50E-02	5.80E-02	6.30E-02	< 0.05	2.84E-01	2.43E-01	< 0.05	< 0.05	< 0.05
Yb	3.62E-01	2.71E-01	2.73E-01	2.25E-01	1.73E+00	1.46E+00	< 0.05	7.00E-02	< 0.05
Lu	5.10E-02	< 0.05	< 0.05	< 0.05	2.64E-01	2.32E-01	< 0.05	< 0.05	< 0.05
W	< 0.25	8.01E-01	1.91E+00	< 0.25	< 0.25	< 0.25	< 0.25	< 0.25	< 0.25
Tl	8.80E-01	1.10E+00	7.56E-01	4.04E+00	2.09E+02	1.53E+02	1.54E-01	1.51E-01	3.11E+02
Pb	6.68E-01	1.79E+00	< 0.5	< 0.5	6.00E+02	5.28E+00	< 0.5	< 0.5	< 0.5

Continued on next page

Tab. D.2 – continued from previous page

Elements	A26	A26bt	A26st	BN	BP(1)	BP mini	BW	BW(2)	FF
Bi	< 0.1	< 0.1	< 0.1	< 0.1	3.34E-01	< 0.1	< 0.1	< 0.1	< 0.1
Th	< 0.05	< 0.05	< 0.05	< 0.05	1.13E-01	1.01E-01	< 0.05	< 0.05	< 0.05
235U	< 2.5	< 2.5	< 2.5	< 2.5	< 2.5	4.74E+00	5.98E+00	6.52E+00	< 2.5
238U	7.21E-01	1.91E-01	2.47E-01	9.50E-02	6.41E-01	1.95E+00	2.52E+00	2.53E+00	7.18E-01

Tab. D.3.: Results of the element analysis using an ICP-MS in μg/l for the diving spots Hot Lake and La Calcara. Please note the further abbreviation of La Calcara Ball 1 to LC B1. The < symbol indicates values below the afterward given detection limit.

Elements	HL	LC B1	LC B1(2)	LC B1(3)	LC B1(4)	LC B2	LC BR	LC BR(2)	LC BR(3)
Li	1.92E+04	6.46E+02	4.75E+02	5.44E+02	5.32E+02	3.51E+02	1.53E+02	2.16E+02	1.78E+02
Be	1.14E+01	6.12E-01	< 0.5	< 0.5	< 0.5	< 0.5	< 0.5	< 0.5	< 0.5
B	1.24E+05	7.25E+03	5.85E+03	6.51E+03	5.74E+03	3.63E+03	2.89E+03	4.71E+03	4.10E+03
Mg	6.30E+05	8.71E+05	9.05E+05	9.12E+05	6.71E+05	8.58E+05	9.30E+05	1.33E+06	9.38E+05
Al	< 50	5.41E+01	< 50	< 50	< 50	< 50	< 50	5.59E+01	< 50
Si	6.28E+04	3.80E+04	2.16E+04	3.00E+04	2.63E+04	2.32E+04	< 5000	6.68E+03	< 5000
P	< 500	< 500	< 500	< 500	< 500	< 500	< 500	< 500	< 500
S	9.69E+05	8.10E+05	7.73E+05	7.83E+05	5.05E+05	6.96E+05	7.98E+05	1.22E+06	7.06E+05
K	2.51E+06	3.57E+05	3.40E+05	3.58E+05	2.79E+05	3.00E+05	2.98E+05	4.33E+05	3.13E+05
Ca	7.29E+06	3.44E+05	3.64E+05	3.62E+05	3.03E+05	3.29E+05	3.26E+05	5.01E+05	4.16E+05
Sc	< 5	< 5	< 5	< 5	< 5	< 5	< 5	< 5	< 5
Ti	< 5	< 5	< 5	< 5	< 5	< 5	< 5	< 5	< 5
V	< 5	< 5	< 5	< 5	< 5	5.72E+00	< 5	5.72E+00	< 5
Cr	< 5	< 5	< 5	< 5	< 5	< 5	1.41E+02	< 5	< 5
Mn	3.66E+05	4.01E+04	2.53E+04	3.35E+04	3.32E+04	2.15E+04	7.93E+01	6.62E+02	3.01E+02
Fe	< 50	4.17E+02	< 50	9.40E+01	< 50	< 50	2.43E+03	1.41E+02	< 50
Co	< 0.5	< 0.5	< 0.5	< 0.5	< 0.5	< 0.5	1.60E+00	< 0.5	< 0.5

Continued on next page

Tab. D.3 – continued from previous page

Elements	HL	LC B1	LC B1(2)	LC B1(3)	LC B1(4)	LC B2	LC BR	LC BR(2)	LC BR(3)
Ni	< 5	< 5	< 5	< 5	< 5	< 5	7.46E+01	5.84E+00	< 5
Cu	< 50	< 50	< 50	< 50	< 50	< 50	< 50	< 50	< 50
Zn	< 50	< 50	< 50	< 50	< 50	< 50	< 50	< 50	< 50
Ga	1.26E+00	< 0.5	< 0.5	< 0.5	< 0.5	< 0.5	< 0.5	< 0.5	< 0.5
As	< 10	5.01E+01	2.87E+01	3.67E+01	3.34E+01	2.90E+01	< 10	< 10	< 10
Se	2.38E+02	1.08E+02	8.33E+01	1.07E+02	3.89E+01	7.93E+01	3.71E+01	1.15E+02	8.16E+01
79Br	1.57E+05	6.15E+04	6.58E+04	6.51E+04	5.00E+04	6.30E+04	5.95E+04	9.19E+04	7.31E+04
81Br	1.55E+05	6.14E+04	6.54E+04	6.48E+04	4.99E+04	6.29E+04	5.92E+04	9.16E+04	7.32E+04
Rb	1.58E+04	5.59E+02	4.06E+02	4.88E+02	5.06E+02	2.00E+02	8.46E+01	1.33E+02	1.11E+02
Sr	1.37E+05	7.16E+03	7.42E+03	7.47E+03	6.43E+03	6.83E+03	6.22E+03	9.53E+03	7.92E+03
Y	2.42E+00	3.75E-01	3.92E-01	3.32E-01	3.94E-01	2.07E-01	5.30E-02	1.71E-01	6.80E-02
Zt	< 2.5	< 2.5	< 2.5	< 2.5	< 2.5	< 2.5	< 2.5	< 2.5	< 2.5
Nb	< 0.5	< 0.5	< 0.5	< 0.5	< 0.5	< 0.5	< 0.5	< 0.5	< 0.5
Mo	9.27E+00	1.60E+01	1.10E+01	1.73E+01	7.52E+00	2.08E+01	1.17E+01	9.93E+00	1.05E+01
Ag	< 0.25	< 0.25	< 0.25	< 0.25	< 0.25	< 0.25	< 0.25	< 0.25	< 0.25
Cd	< 0.5	< 0.5	< 0.5	< 0.5	< 0.5	< 0.5	< 0.5	< 0.5	< 0.5
In	6.50E-02	< 0.05	< 0.05	< 0.05	< 0.05	< 0.05	< 0.05	< 0.05	< 0.05
Sn	< 2.5	< 2.5	< 2.5	< 2.5	< 2.5	< 2.5	< 2.5	< 2.5	< 2.5
Sb	< 0.5	2.77E+01	2.98E+01	2.80E+01	2.67E+01	3.06E+01	7.12E-01	7.42E-01	< 0.5
Te	6.21E+00	5.24E-01	< 0.5	< 0.5	< 0.5	< 0.5	< 0.5	5.80E-01	< 0.5
Cs	5.77E+03	2.05E+02	1.36E+02	1.75E+02	1.82E+02	4.92E+01	7.27E-01	3.52E+00	2.27E+00
Ba	2.65E+03	2.15E+02	1.21E+02	1.83E+02	1.62E+02	1.63E+02	1.33E+01	4.33E+01	8.85E+00
La	9.70E-02	1.07E-01	7.10E-02	7.60E-02	7.80E-02	< 0.05	< 0.05	6.20E-02	< 0.05
Ce	2.40E-01	1.91E-01	1.35E-01	1.64E-01	1.81E-01	7.20E-02	< 0.05	1.38E-01	< 0.05
Pr	5.70E-02	< 0.05	< 0.05	< 0.05	< 0.05	< 0.05	< 0.05	< 0.05	< 0.05
Nd	4.28E-01	1.50E-01	1.08E-01	9.50E-02	1.26E-01	5.20E-02	< 0.05	6.50E-02	< 0.05
Sm	2.63E-01	< 0.05	5.10E-02	5.00E-02	5.50E-02	< 0.05	< 0.05	< 0.05	< 0.05
Eu	6.18E-01	5.40E-02	< 0.05	5.10E-02	< 0.05	< 0.05	< 0.05	< 0.05	< 0.05
Gd	4.47E-01	6.60E-02	6.80E-02	6.50E-02	9.40E-02	< 0.05	< 0.05	< 0.05	< 0.05

Continued on next page

Tab. D.3 – continued from previous page

Elements	HL	LC B1	LC B1(2)	LC B1(3)	LC B1(4)	LC B2	LC BR	LC BR(2)	LC BR(3)
Tb	5.80E-02	< 0.05	< 0.05	< 0.05	< 0.05	< 0.05	< 0.05	< 0.05	< 0.05
Dy	2.86E-01	6.50E-02	6.20E-02	< 0.05	6.00E-02	< 0.05	< 0.05	< 0.05	< 0.05
Ho	5.00E-02	< 0.05	< 0.05	< 0.05	< 0.05	< 0.05	< 0.05	< 0.05	< 0.05
Er	1.17E-01	< 0.05	< 0.05	< 0.05	< 0.05	< 0.05	< 0.05	< 0.05	< 0.05
Tm	< 0.05	< 0.05	< 0.05	< 0.05	< 0.05	< 0.05	< 0.05	< 0.05	< 0.05
Yb	8.30E-02	< 0.05	< 0.05	< 0.05	< 0.05	< 0.05	< 0.05	< 0.05	< 0.05
Lu	< 0.05	< 0.05	< 0.05	< 0.05	< 0.05	< 0.05	< 0.05	< 0.05	< 0.05
W	2.62E-01	< 0.25	< 0.25	< 0.25	< 0.25	< 0.25	< 0.25	< 0.25	< 0.25
Tl	3.10E+02	1.49E+01	8.22E+00	1.33E+01	1.27E+01	6.45E+00	7.36E-01	3.13E+00	1.65E+00
Pb	< 0.5	1.45E+00	1.07E+00	1.25E+00	8.66E-01	1.13E+00	1.21E+00	7.68E-01	< 0.5
Bi	2.39E-01	1.10E-01	< 0.1	< 0.1	< 0.1	< 0.1	3.91E-01	1.12E-01	< 0.1
Th	< 0.05	< 0.05	< 0.05	< 0.05	< 0.05	< 0.05	9.00E-02	< 0.05	< 0.05
235U	< 2.5	3.01E+00	4.27E+00	< 2.5	< 2.5	4.10E+00	5.39E+00	9.46E+00	6.74E+00
238U	1.12E-01	1.26E+00	1.73E+00	1.13E+00	1.00E+00	1.84E+00	2.29E+00	3.69E+00	2.69E+00

Tab. D.4.: Results of the element analysis using an ICP-MS in μg/l for the diving spots La Calcara, Point 21, Pozzo di Pina and the local seawater (Seebauer 2015). The < symbol indicates values below the afterward given detection limit.

Elements	LC BR(4)	LC C	LC NR	P21	P21(2)	PdP	PdP_equ	Local Seawater
Li	1.91E+02	3.37E+02	2.39E+02	4.10E+02	5.51E+02	1.69E+02	6.80E+01	1.17E+00
Be	< 0.5	< 0.5	5.15E-01	1.27E+00	6.50E-01	< 0.5	< 0.5	1.00E-04
B	4.00E+03	4.21E+03	4.28E+03	5.39E+03	6.72E+03	3.16E+03	1.26E+03	3.78E+00
Mg	1.08E+06	8.80E+05	1.20E+06	1.07E+06	1.18E+06	7.96E+05	2.12E+05	1.64E+03
Al	< 50	6.10E+01	1.32E+02	5.26E+01	1.12E+02	< 50	< 50	1.58E-02
Si	7.35E+03	3.54E+04	1.30E+04	5.62E+04	3.52E+04	7.09E+04	6.27E+04	1.02E+00
P	< 500	< 500	< 500	< 500	< 500	< 500	< 500	1.00E-01

Continued on next page

Tab. D.4 – continued from previous page

Elements	LC BR(4)	LC C	LC NR	P21	P21(2)	PdP	PdP_equ	Local Seawater
S	8.81E+05	7.36E+05	1.12E+06	1.70E+06	1.78E+06	6.07E+05	1.82E+05	1.40E+03
K	3.55E+05	3.28E+05	3.95E+05	3.62E+05	4.27E+05	2.64E+05	9.03E+04	5.48E+02
Ca	4.13E+05	3.18E+05	4.14E+05	4.95E+05	5.64E+05	3.71E+05	1.26E+05	5.64E+02
Sc	< 5	< 5	< 5	< 5	< 5	< 5	< 5	n.d.
Ti	< 5	< 5	< 5	< 5	< 5	< 5	< 5	n.d.
V	< 5	5.51E+00	5.18E+00	< 5	5.35E+00	2.23E+01	2.29E+01	4.38E-03
Cr	< 5	< 5	< 5	< 5	< 5	< 5	< 5	1.00E-03
Mn	1.95E+03	3.44E+04	5.05E+03	4.74E+03	1.13E+04	5.19E+03	4.09E+03	2.92E-02
Fe	< 50	< 50	3.22E+02	< 50	6.04E+01	< 50	1.39E+02	2.03E-02
Co	< 0.5	< 0.5	< 0.5	< 0.5	< 0.5	6.52E+00	4.50E+00	1.00E-04
Ni	< 5	< 5	5.20E+00	< 5	< 5	< 5	7.88E+00	1.00E-03
Cu	< 50	< 50	< 50	< 50	< 50	< 50	< 50	1.00E-02
Zn	< 50	< 50	9.12E+01	< 50	< 50	3.59E+02	3.05E+02	1.41E-02
Ga	< 0.5	< 0.5	< 0.5	< 0.5	< 0.5	< 0.5	< 0.5	1.00E-03
As	< 10	4.17E+01	2.04E+01	< 10	1.29E+01	< 10	< 10	1.19E-02
Se	6.26E+01	1.09E+02	1.26E+02	< 25	7.09E+01	3.87E+01	< 25	5.03E-03
79Br	7.48E+04	6.21E+04	7.53E+04	7.92E+04	7.88E+04	5.64E+04	1.25E+04	9.41E+01
81Br	7.46E+04	6.18E+04	7.51E+04	7.91E+04	7.88E+04	5.64E+04	1.25E+04	9.37E+01
Rb	1.27E+02	2.29E+02	1.55E+02	2.66E+02	4.36E+02	1.62E+02	5.96E+01	1.38E-01
Sr	8.02E+03	6.48E+03	7.99E+03	9.42E+03	1.08E+04	6.33E+03	1.83E+03	9.23E+00
Y	9.60E-02	3.14E-01	1.98E-01	1.63E+00	3.48E+00	8.60E-02	< 0.05	n.d.
Zt	< 2.5	< 2.5	< 2.5	< 2.5	< 2.5	< 2.5	< 2.5	n.d.
Nb	< 0.5	< 0.5	< 0.5	< 0.5	< 0.5	< 0.5	< 0.5	n.d.
Mo	1.26E+01	5.33E+01	1.50E+01	1.70E+00	2.22E+00	5.08E+00	6.90E+00	1.65E-02
Ag	< 0.25	< 0.25	< 0.25	< 0.25	< 0.25	< 0.25	< 0.25	9.24E-05
Cd	< 0.5	< 0.5	< 0.5	< 0.5	< 0.5	< 0.5	< 0.5	1.00E-04
In	< 0.05	< 0.05	< 0.05	< 0.05	< 0.05	< 0.05	< 0.05	n.d.
Sn	< 2.5	< 2.5	< 2.5	< 2.5	< 2.5	< 2.5	< 2.5	n.d.
Sb	3.59E+00	6.63E+01	1.30E+01	< 0.5	< 0.5	< 0.5	5.08E-01	n.d.

Continued on next page

Tab. D.4 – continued from previous page

Elements	LC BR(4)	LC C	LC NR	P21	P21(2)	PdP	PdP_equ	Local Seawater
Te	< 0.5	< 0.5	< 0.5	< 0.5	< 0.5	< 0.5	< 0.5	4.56E-04
Cs	9.85E+00	5.41E+01	2.06E+01	5.06E+01	1.06E+02	1.04E+01	3.63E+00	n.d.
Ba	2.06E+01	2.02E+02	1.13E+02	5.12E+01	1.06E+02	2.11E+02	2.05E+02	1.39E-02
La	< 0.05	< 0.05	8.30E-02	6.70E-02	1.22E-01	< 0.05	< 0.05	n.d.
Ce	5.30E-02	1.16E-01	1.67E-01	2.24E-01	5.16E-01	< 0.05	< 0.05	n.d.
Pr	< 0.05	< 0.05	< 0.05	5.80E-02	1.14E-01	< 0.05	< 0.05	n.d.
Nd	< 0.05	9.50E-02	8.80E-02	3.34E-01	6.72E-01	< 0.05	< 0.05	n.d.
Sm	< 0.05	< 0.05	< 0.05	1.45E-01	3.18E-01	< 0.05	< 0.05	n.d.
Eu	< 0.05	5.40E-02	< 0.05	5.90E-02	1.35E-01	< 0.05	< 0.05	n.d.
Gd	< 0.05	< 0.05	< 0.05	2.63E-01	5.58E-01	< 0.05	< 0.05	n.d.
Tb	< 0.05	< 0.05	< 0.05	< 0.05	1.06E-01	< 0.05	< 0.05	n.d.
Dy	< 0.05	6.40E-02	< 0.05	2.85E-01	6.04E-01	< 0.05	< 0.05	n.d.
Ho	< 0.05	< 0.05	< 0.05	5.50E-02	1.24E-01	< 0.05	< 0.05	n.d.
Er	< 0.05	< 0.05	< 0.05	1.49E-01	3.26E-01	< 0.05	< 0.05	n.d.
Tm	< 0.05	< 0.05	< 0.05	< 0.05	< 0.05	< 0.05	< 0.05	n.d.
Yb	< 0.05	< 0.05	< 0.05	9.70E-02	2.17E-01	< 0.05	< 0.05	n.d.
Lu	< 0.05	< 0.05	< 0.05	< 0.05	< 0.05	< 0.05	< 0.05	n.d.
W	< 0.25	< 0.25	< 0.25	< 0.25	< 0.25	2.61E+00	1.20E+00	n.d.
Tl	4.88E+00	7.57E+00	1.71E+00	2.14E+00	2.97E+00	1.72E+00	1.22E-01	3.41E-04
Pb	1.26E+00	2.46E+00	4.25E+00	< 0.5	< 0.5	1.59E+01	2.21E+00	1.80E-02
Bi	< 0.1	< 0.1	1.73E-01	1.05E+00	< 0.1	< 0.1	< 0.1	2.18E-04
Th	< 0.05	< 0.05	5.20E-02	8.50E-02	< 0.05	< 0.05	< 0.05	n.d.
235U	7.27E+00	7.52E+00	6.27E+00	4.21E+00	< 2.5	2.93E+00	< 2.5	8.32E-03
238U	2.91E+00	3.05E+00	3.06E+00	1.94E+00	7.84E-01	1.33E+00	8.46E-01	3.40E-03

E. Stable Isotopes

Tab. E.1.: Isotopic compositions and deuterium excess of the taken water samples (Hydroisotop PLC, Woelkestraße 9, 85301 Schweitenkirchen, Germany).

	δ^{18}O	δ^{2}H	Deuterium-Excess
	‰ VSMOW	‰ VSMOW	‰
PAN_09032015_A26	0.80	9.50	3.10
PAN_09082015_A26_bt	0.88	9.70	2.66
PAN_09082015_A26_st	0.85	9.80	3.00
PAN_09012015_BN	0.94	10.00	2.48
PAN_09072015_BP	1.44	12.10	0.58
PAN_09072015_BP_mini	2.24	8.20	-9.72
PAN_09022015_BW	0.91	11.60	4.32
PAN_09022015_BW(2)	1.19	12.50	2.98
PAN_09042015_FF	0.72	3.30	-2.46
PAN_09012015_HL	0.93	-6.00	-13.44
PAN_09012015_LC_Ball1(2)	2.18	12.90	-4.54
PAN_09022015_LC_Ball1(3)	2.02	13.00	-3.16
PAN_09032015_LC_Ball1(4)	2.16	13.00	-4.28
PAN_09012015_LC_Ball2	1.82	12.90	-1.66
PAN_09012015_LC_BR(2)	1.51	12.70	0.62
PAN_09032015_LC_BR(4)	1.55	12.70	0.30
PAN_09022015_LC_NR(2)	1.39	12.30	1.18
PAN_09022015_LC_C	1.54	12.30	-0.02
PAN_09032015_P21(2)	1.16	11.90	2.62
PAN_09032015_PdP	-0.29	1.90	4.22
PAN_09042015_PdP_equ	-4.51	-21.70	14.38

F. Evaluation of time series

Tab. F.1.: Maxima values for shown parameters, found in the last decade of scientific diving at the submarine hydrothermal system Panarea. Local seawater concentrations are taken from Seebauer (2015), average seawater concentrations are taken from Brown (2001).

	Unit	A26	BN	BW	P21	BP_MN	BP	HL	FF	GW/PdP	CAL	CAL_BR	CAL_B1	local Seawater	average Seawater
pH	/	5.26	5.91	6.14	5.51	6.63	4.09	5.78	5.39	6.63	5.99	7.12	5.76	7.9	
EC	mS/cm	68.7	82.4	63.3	61.0	59.4	82.0	118.3	84.6	24.0	64.8	59.3	53.6	52.8	
Eh	mV	-6.8	14.9	76.2	17.3	375.3	358.4	5.2	-10.0	247.9	374.8	356.0	360.8	286.0	
rH	/	10.2	12.3	13.6	11.2	23.9	18.2	11.0	10.0	21.2	23.9	24.1	23.4	25.4	
Main Ions															
Li	mg/l	5.7	2.7	2.4	1.3	1.5	14.0	30.6	14.8	0.3	8.7	0.3	1.0	1.2	0.18
Na	mg/l	12,941.7	12,354.4	12,475.3	12,408.9	12,002.2	12,325.2	18,635.8	14,904.3	11,338.0	12,154.3	12,448.1	10,022.9	11,728.4	11,184
K	mg/l	958.9	706.0	634.9	549.0	772.0	1,890.7	3,644.2	1,950.2	447.0	1,020.5	437.1	399.7	427.1	380.00
Ca	mg/l	1,918.7	1,148.0	1,198.6	750.0	1,552.0	5,239.9	9,826.8	4,928.0	484.0	3,457.1	460.5	348.2	418.0	412.00
Mg	mg/l	1,399.0	1,401.3	1,472.0	1,532.0	1,502.4	1,012.0	1,212.1	1,300.3	1,463.0	1,445.0	1,431.0	1,131.7	1,414.2	1,290.00
F	mg/l	2.7	2.5	2.4	3.1	2.6	13.8	11.2	1.6	2.2	2.7	2.7	2.3	1.2	1.30
Cl	mg/l	27,175.6	23,630.0	25,081.5	22,897.5	23,535.1	31,446.8	53,684.3	35,041.6	17,744.0	25,392.1	22,533.6	18,641.6	19,908.5	19,500
Br	mg/l	87.4	84.5	112.0	93.7	108.0	131.9	222.0	118.0	75.0	90.2	63.7	35.4	63.7	67.10
S(6)	mg/l	3,037.1	3,089.2	2,937.9	3,430.2	3,152.4	2,997.8	1,938.8	3,098.0	2,715.0	3,454.5	3,549.0	2,660.4	3,027.4	2,710.00
Trace Elements															
Si	μ g/l	106,000.0	81,930.0	32,800.0	51,180.0	99,360.0	183,800.0	109,400.0	60,200.0	98,700.0	94,773.3	25,840.0	38,040.0	1,019.8	2,000
Mn	μ g/l	153,200.0	39,500.0	29,840.0	24,970.0	75,850.0	366,700.0	479,900.0	169,200.0	8,736.0	204,700.0	27,430.0	40,090.0	29.2	0.030
Fe	μ g/l	2,050.0	1,640.0	5,000.0	5,740.0	8,610.0	37,670.0	6,100.0	3,690.0	5,040.0	6,035.0	2,433.0	416.6	20.3	0.055
Fe*	μ g/l	1,640.0	5,000.0	5,740.0	8,610.0	37,670.0	6,100.0	3,690.0	2,050.0	5,040.0	6,035.0	2,433.0	416.6	0.6	0.055
Rb	μ g/l	5,258.0	2,723.0	1,496.5	784.2	2,956.1	14,000.0	22,640.0	10,380.0	247.8	6,903.7	530.9	559.0	138.4	120
Cs	μ g/l	1,277.0	739.0	480.2	210.9	803.6	3,868.0	7,985.0	3,936.0	13.1	2,236.3	152.3	204.7		0.40
Ba	μ g/l	992.4	760.0	690.0	6,966.0	1,381.7	7,617.0	5,654.7	1,786.0	262.5	6,337.0	154.0	215.4	13.9	2.00
Rare Earth Elements															
Sc	μ g/l	2.69E+01	2.46E+01	3.24E+01	2.46E+01	8.20E+01	4.74E+01	3.15E+00	1.20E+01	2.10E+01	3.50E+00	1.65E+00	1.65E+00		6.00E-04
Y	μ g/l	6.36E+00	3.44E+00	4.07E+00	8.32E+00	4.03E+01	4.75E+00	2.30E+00	5.53E+01	1.47E-01	2.51E+00	4.33E-01	3.94E-01		1.00E-03
La	μg/l	6.56E-01	2.87E+00	1.39E+00	1.93E+00	4.24E+00	1.34E+00	1.85E+00	1.46E+00	1.05E-01	8.18E-01	2.11E-01	9.80E-02		3.00E-03
Ce	μ g/l	3.08E+00	1.94E+01	8.53E+00	1.06E+01	1.11E+01	9.74E+00	1.30E+01	5.34E+00	1.26E-01	1.72E+00	5.20E-01	1.85E-01		2.00E-03
Pr	μ g/l	1.23E-01	6.97E-01	3.69E-01	5.33E-01	1.15E+00	3.66E-01	4.92E-01	1.01E+00	2.10E-02	2.16E-01	5.70E-02	3.30E-02		6.00E-04
Nd	μg/l	5.00E-01	2.95E+00	1.64E+00	2.05E+00	5.39E+00	1.46E+00	1.93E+00	5.73E+00	4.20E-02	8.99E-01	2.70E-01	1.54E-01		3.00E-03
Sm	μ g/l	1.64E-01	6.56E-01	4.00E-01	6.56E-01	2.26E+00	4.88E-01	4.92E-01	2.73E+00	2.10E-02	2.92E-01	7.50E-02	5.90E-02		6.00E-04
Eu	μ g/l	8.70E-02	1.64E-01	9.85E-01	2.46E-01	2.12E+00	8.55E-01	3.73E-01	1.21E+00	4.10E-02	9.78E-01	2.50E-02	4.60E-02		2.00E-04
Gd	μ g/l	3.00E-01	6.56E-01	7.00E-01	1.03E+00	4.64E+00	7.63E-01	4.51E-01	6.11E+00	2.09E-02	4.28E-01	6.50E-02	7.60E-02		7.00E-04
Tb	μ g/l	6.10E-02	8.20E-02	1.23E-01	2.46E-01	1.05E+00	1.80E-01	5.40E-02	1.20E+00	2.03E-02	6.90E-02	2.00E-02	2.00E-02		1.00E-04
Dy	μ g/l	4.40E-01	4.92E-01	6.27E-01	1.23E+00	6.46E+00	8.72E-01	3.28E-01	8.09E+00	2.00E-02	4.35E-01	8.30E-02	6.60E-02		9.00E-04
Ho	μ g/l	1.28E-01	1.23E-01	1.23E-01	2.46E-01	1.35E+00	1.76E-01	4.10E-02	1.71E+00	2.00E-02	9.30E-02	2.00E-02	2.00E-02		3.00E-04
Er	μ g/l	4.30E-01	2.87E-01	3.38E-01	8.20E-01	3.96E+00	4.10E-01	2.05E-01	4.72E+00	2.10E-02	2.59E-01	5.20E-02	4.50E-02		8.00E-04
Tm	μ g/l	5.70E-02	3.30E-02	4.00E-02	8.20E-02	5.47E-01	5.62E-02	2.00E-02	5.95E-01	2.00E-02	3.40E-02	2.00E-02	2.00E-02		2.00E-04
Yb	μ g/l	3.57E-01	2.87E-01	2.47E-01	7.38E-01	3.51E+00	3.05E-01	1.64E-01	3.46E+00	3.90E-02	2.22E-01	6.50E-02	3.50E-02		8.00E-04
Lu	μ g/l	8.20E-02	8.20E-02	4.07E-02	1.23E-01	5.26E-01	6.05E-02	2.00E-02	5.05E-01	2.00E-02	3.30E-02	2.00E-02	2.00E-02		2.00E-04

Tab. F.2.: Maxima deviations of parameters in % compared to local seawater (Seebauer 2015) or average seawater (Brown 2001), respectively.

	A26	BN	BW	P21	BP_MN	BP	HL	FF	GW/PdP	CAL	CAL_BR	CAL_B1
pH	-33.33	-25.10	-22.18	-30.16	-15.97	-48.16	-26.74	-31.69	-15.97	-24.08	-9.76	-27.00
EC	30.06	56.00	19.84	15.49	12.46	55.24	123.97	60.17	-54.51	22.68	12.27	1.48
Eh	-102.38	-94.79	-73.36	-93.95	31.23	25.32	-98.18	-103.50	-13.34	31.05	24.46	26.17
rH	-59.80	-51.57	-46.65	-56.02	-6.05	-28.65	-56.71	-60.54	-16.86	-6.25	-5.48	-8.06
Main Ions												
Li	387.65	132.88	104.96	11.28	29.03	1094.42	2522.72	1166.21	-71.47	648.84	-71.47	-10.43
Na	10.35	5.34	6.37	5.80	2.33	5.09	58.89	27.08	-3.33	3.63	6.14	-14.54
K	124.53	65.32	48.68	28.55	80.77	342.74	753.34	356.67	4.67	138.97	2.35	-6.40
Ca	359.06	174.68	186.77	79.45	271.34	1153.71	2251.18	1079.09	15.80	727.15	10.17	-16.69
Mg	-1.07	-0.91	4.09	8.33	6.24	-28.44	-14.29	-8.05	3.45	2.18	1.19	-19.98
F	134.12	110.58	106.30	164.51	122.92	1084.59	857.01	37.21	84.90	127.40	131.14	96.88
Cl	36.50	18.69	25.98	15.01	18.22	57.96	169.65	76.01	-10.87	27.54	13.19	-6.36
Br	37.36	32.74	75.96	47.15	69.67	107.28	248.77	85.38	17.83	41.69	0.09	-44.44
S(6)	0.32	2.04	-2.96	13.30	4.13	-0.98	-35.96	2.33	-10.32	14.10	17.23	-12.13
Trace Elements												
Si	10293.86	7933.67	3116.21	4918.47	9642.77	17922.55	10627.24	5802.93	9578.05	9193.02	2433.75	3630.02
Mn	524173.51	135074.96	102016.98	85351.11	259470.14	1254802.71	1642190.18	578927.92	29795.91	700414.27	93769.60	137094.03
Fe	10010.14	7988.11	24558.89	28208.40	42362.60	185680.04	29983.84	18098.26	24756.16	29663.27	11899.01	1954.58
Fe	260529.28	794501.48	912102.50	1368203.74	5986427.53	969313.80	586315.89	325686.61	800858.29	958983.98	386553.08	66106.20
Rb	3699.74	1867.80	981.46	466.71	2036.25	10017.23	16261.01	7401.20	79.07	4889.00	283.66	303.97
Cs	319150.00	184650.00	119950.00	52625.00	200800.00	966900.00	1996150.00	983900.00	3165.50	558983.33	37975.00	51075.00
Ba	7053.01	5377.92	4873.37	50109.43	9859.00	54801.69	40657.86	12773.10	1792.04	45575.73	1010.00	1452.56
Rare Earth Elements												
Sc	4.5E+06	4.1E+06	5.4E+06	4.1E+06	1.4E+07	7.9E+06	5.2E+05	2.0E+06	3.5E+06	5.8E+05	2.7E+05	2.7E+05
Y	6.4E+05	3.4E+05	4.1E+05	8.3E+05	4.0E+06	4.7E+05	2.3E+05	5.5E+06	1.5E+04	2.5E+05	4.3E+04	3.9E+04
La	2.2E+04	9.6E+04	4.6E+04	6.4E+04	1.4E+05	4.5E+04	6.2E+04	4.9E+04	3.4E+03	2.7E+04	6.9E+03	3.2E+03
Ce	1.5E+05	9.7E+05	4.3E+05	5.3E+05	5.5E+05	4.9E+05	6.5E+05	2.7E+05	6.2E+03	8.6E+04	2.6E+04	9.2E+03
Pr	2.0E+04	1.2E+05	6.1E+04	8.9E+04	1.9E+05	6.1E+04	8.2E+04	1.7E+05	3.4E+03	3.6E+04	9.4E+03	5.4E+03
Nd	1.7E+04	9.8E+04	5.5E+04	6.8E+04	1.8E+05	4.9E+04	6.4E+04	1.9E+05	1.3E+03	3.0E+04	8.9E+03	5.0E+03
Sm	2.7E+04	1.1E+05	6.7E+04	1.1E+05	3.8E+05	8.1E+04	8.2E+04	4.6E+05	3.4E+03	4.9E+04	1.2E+04	9.7E+03
Eu	4.3E+04	8.2E+04	4.9E+05	1.2E+05	1.1E+06	4.3E+05	1.9E+05	6.0E+05	2.0E+04	4.9E+05	1.2E+04	2.3E+04
Gd	4.3E+04	9.4E+04	1.0E+05	1.5E+05	6.6E+05	1.1E+05	6.4E+04	8.7E+05	2.9E+03	6.1E+04	9.2E+03	1.1E+04
Tb	6.1E+04	8.2E+04	1.2E+05	2.5E+05	1.0E+06	1.8E+05	5.4E+04	1.2E+06	2.0E+04	6.9E+04	2.0E+04	2.0E+04
Dy	4.9E+04	5.5E+04	7.0E+04	1.4E+05	7.2E+05	9.7E+04	3.6E+04	9.0E+05	2.1E+03	4.8E+04	9.1E+03	7.2E+03
Ho	4.3E+04	4.1E+04	4.1E+04	8.2E+04	4.5E+05	5.9E+04	1.4E+04	5.7E+05	6.6E+03	3.1E+04	6.6E+03	6.6E+03
Er	5.4E+04	3.6E+04	4.2E+04	1.0E+05	5.0E+05	5.1E+04	2.6E+04	5.9E+05	2.5E+03	3.2E+04	6.4E+03	5.5E+03
Tm	2.8E+04	1.6E+04	2.0E+04	4.1E+04	2.7E+05	2.8E+04	9.9E+03	3.0E+05	9.9E+03	1.7E+04	9.9E+03	9.9E+03
Yb	4.5E+04	3.6E+04	3.1E+04	9.2E+04	4.4E+05	3.8E+04	2.0E+04	4.3E+05	4.8E+03	2.8E+04	8.0E+03	4.3E+03
Lu	4.1E+04	4.1E+04	2.0E+04	6.1E+04	2.6E+05	3.0E+04	9.9E+03	2.5E+05	9.9E+03	1.6E+04	9.9E+03	9.9E+03

Tab. F.3.: Minima values for shown parameters, found in the last decade of scientific diving at the submarine hydrothermal system Panarea. Local seawater concentrations are taken from Seebauer (2015), average seawater concentrations are taken from Brown (2001).

	Unit	A26	BN	BW	P21	BP_MN	BP	HL	FF	GW/PdP	CAL	CAL_BR	CAL_B1	local Seawater	average Seawater
pH	/	4.50	5.30	5.01	4.67	5.00	2.40	4.44	4.60	5.18	4.60	5.14	5.40	7.89	
EC	mS/cm	51.70	53.50	52.50	46.40	47.00	57.60	69.50	57.00	18.00	46.10	39.70	46.10	52.82	
Eh	mV	-60.04	-73.10	-73.10	-48.90	-34.90	42.00	-75.10	-70.30	-26.90	-32.00	80.66	264.74	286.00	
rH	/	7.66	8.42	7.61	7.92	9.36	6.22	6.99	7.28	9.45	9.02	13.01	20.01	25.45	
Main Ions															
Li	mg/l	0.33	0.17	0.00	0.00	0.17	0.00	6.48	1.48	0.33	0.33	0.17	0.37	1.17	0.18
Na	mg/l	10481.85	10832.52	10992.25	10861.86	9858.35	10812.35	13588.00	11614.00	2663.51	8329.03	8624.87	8329.03	11728.38	11183.72
K	mg/l	467.43	431.57	359.93	360.00	399.37	1096.00	1653.00	842.00	103.30	368.59	326.76	368.59	427.05	380.00
Ca	mg/l	560.57	517.39	437.00	423.37	444.64	2925.00	3893.00	1774.00	70.09	287.27	334.44	275.72	417.95	412.00
Mg	mg/l	1226.20	1226.08	1295.73	1073.67	1084.59	579.20	752.56	1116.38	249.67	692.71	978.89	864.12	1414.16	1290.00
F	mg/l	0.33	0.63	0.33	0.33	0.33	1.88	0.34	0.50	0.95	0.52	0.17	0.61	1.17	1.30
Cl	mg/l	19408.08	19660.80	20441.00	19085.00	17812.02	22811.00	34610.95	23616.00	3592.86	16531.02	15107.11	14907.45	19908.52	19500.00
Br	mg/l	43.47	52.73	34.86	44.70	48.76	75.17	107.60	88.62	8.28	35.47	35.71	25.24	63.65	67.10
S(6)	mg/l	1109.00	1342.00	2619.58	1116.00	2032.58	178.10	564.00	1703.36	778.22	1327.99	2190.60	2200.62	3027.44	2710.00
Trace Elements															
Si	μ g/l	22850.00	11420.00	0.66	0.66	3344.00	82000.00	40000.00	4100.00	62710.00	4596.00	0.33	21610.00	1019.83	2000.00
Mn	μ g/l	32.83	13.27	12.30	3.57	4.40	399.50	428.60	101.80	3192.00	240.93	79.29	25330.00	29.22	0.03
Fe	μ g/l	13.23	1.65	42.54	0.66	29.50	12760.00	16.30	37.50	50.00	26.87	0.33	50.00	20.28	0.06
Rb	μ g/l	508.00	457.20	132.50	131.70	166.90	6109.00	9330.00	4346.00	59.61	153.30	84.59	405.70	138.38	120.00
Cs	μ g/l	109.10	92.95	0.90	0.46	12.78	1746.60	2640.00	1332.50	3.63	14.40	0.73	136.30		0.40
Ba	μ g/l	41.08	37.58	12.30	11.40	17.39	1240.00	1465.00	446.90	157.50	110.60	8.85	120.70	13.87	2.00
Rare Earth Elements															
Sc	μ g/l	3.3E-01	3.3E-01	2.5E-01	3.3E-01	1.1E+01	6.6E-01	6.6E-01	3.3E-01	1.7E-03	6.6E-01	3.3E-01	1.7E+00		6.0E-04
Y	μ g/l	1.0E+00	7.5E-02	1.7E-02	1.6E-01	1.8E+01	1.2E+00	6.2E-01	2.2E+00	5.0E-02	1.9E-01	5.3E-02	3.3E-01		1.0E-03
La	μ g/l	5.4E-02	2.0E-02	1.3E-02	1.4E-02	1.0E+00	1.4E-02	3.0E-03	6.1E-02	2.0E-02	3.4E-03	1.7E-02	5.7E-02		3.0E-03
Ce	μ g/l	7.1E-02	5.5E-02	1.7E-02	2.2E-02	2.5E+00	2.0E-01	7.1E-02	1.6E-01	2.3E-02	5.6E-02	1.7E-02	1.4E-01		2.0E-03
Pr	μ g/l	1.3E-02	6.6E-03	6.6E-03	6.6E-03	3.3E-01	2.2E-02	1.4E-02	1.7E-02	9.0E-03	6.6E-03	3.3E-03	2.5E-02		6.0E-04
Nd	μ g/l	4.5E-02	6.6E-03	1.7E-02	1.0E-02	1.6E+00	1.8E-01	7.0E-02	2.1E-01	2.0E-02	3.8E-02	1.7E-02	1.1E-01		3.0E-03
Sm	μ g/l	1.6E-02	6.6E-03	6.6E-03	3.3E-03	8.2E-01	1.2E-01	5.2E-02	1.1E-01	1.1E-02	6.6E-03	1.2E-02	3.0E-02		6.0E-04
Eu	μ g/l	1.3E-02	7.0E-05	6.6E-03	3.3E-03	4.5E-01	1.6E-02	1.4E-02	4.5E-02	7.5E-03	6.6E-03	3.3E-03	3.1E-02		2.0E-04
Gd	μ g/l	4.6E-02	6.6E-03	6.6E-03	1.7E-02	1.7E+00	1.2E-01	9.5E-02	2.0E-01	1.6E-02	1.9E-02	1.0E-02	4.2E-02		7.0E-04
Tb	μ g/l	1.2E-02	6.6E-03	6.6E-03	3.3E-03	4.1E-01	3.0E-02	1.4E-02	5.1E-02	1.6E-02	6.6E-03	3.3E-03	2.0E-02		1.0E-04
Dy	μ g/l	7.9E-02	6.6E-03	1.7E-02	2.6E-02	2.7E+00	1.2E-01	8.2E-02	3.2E-01	4.1E-03	1.2E-02	3.3E-03	5.3E-02		9.0E-04
Ho	μ g/l	1.4E-02	6.6E-03	6.6E-03	3.3E-03	5.3E-01	2.0E-03	6.6E-03	6.6E-02	3.6E-03	1.7E-03	3.3E-03	2.0E-02		3.0E-04
Er	μ g/l	6.4E-02	6.6E-03	6.6E-03	3.3E-03	1.1E+00	3.3E-02	3.0E-02	1.7E-01	2.0E-02	6.7E-04	3.3E-03	2.7E-02		8.0E-04
Tm	μ g/l	3.3E-03	3.3E-03	3.3E-03	3.3E-03	2.1E-01	2.0E-03	3.0E-03	1.7E-02	2.1E-03	1.0E-03	3.3E-03	2.0E-02		2.0E-04
Yb	μ g/l	5.4E-02	6.6E-03	6.6E-03	3.3E-03	1.5E+00	3.3E-02	1.4E-02	7.3E-02	5.1E-03	1.7E-03	3.3E-03	2.0E-02		8.0E-04
Lu	μ g/l	6.6E-03	3.3E-03	3.3E-03	2.0E-03	2.1E-01	2.0E-03	2.0E-03	1.7E-02	7.9E-03	-3.3E-04	3.3E-03	2.0E-02		2.0E-04

Tab. F.4.: Minima deviations of parameters in % compared to local seawater (Seebauer 2015) or average seawater (Brown 2001), respectively.

	A26	BN	BW	P21	BP_MN	BP	HL	FF	GW/PdP	CAL	CAL_BR	CAL_B1
pH	-43.0	-32.8	-36.5	-40.8	-36.6	-69.6	-43.7	-41.7	-34.3	-41.7	-34.9	-31.6
EC	-2.1	1.3	-0.6	-12.2	-11.0	9.0	31.6	7.9	-65.9	-12.7	-24.8	-12.7
Eh	-121.0	-125.6	-125.6	-117.1	-112.2	-85.3	-126.3	-124.6	-109.4	-111.2	-71.8	-7.4
rH	103.2	110.2	106.3	82.3	84.7	126.3	173.1	124.0	-29.3	97.3	56.0	81.1
Main Ions												
Li	-71.5	-85.6	-100.0	-100.0	-85.6	-100.0	454.6	26.7	-71.5	-71.5	-85.6	-68.3
Na	-10.6	-7.6	-6.3	-7.4	-15.9	-7.8	15.9	-1.0	-77.3	-29.0	-26.5	-29.0
K	9.5	1.1	-15.7	-15.7	-6.5	156.6	287.1	97.2	-75.8	-13.7	-23.5	-13.7
Ca	34.1	23.8	4.6	1.3	6.4	599.8	831.4	324.5	-83.2	-31.3	-20.0	-34.0
Mg	-13.3	-13.3	-8.4	-24.1	-23.3	-59.0	-46.8	-21.1	-82.3	-51.0	-30.8	-38.9
F	-71.5	-46.0	-71.5	-71.5	-71.5	60.9	-70.9	-57.3	-18.7	-55.1	-85.6	-48.0
Cl	-2.5	-1.2	2.7	-4.1	-10.5	14.6	73.8	18.6	-82.0	-17.0	-24.1	-25.1
Br	-31.7	-17.2	-45.2	-29.8	-23.4	18.1	69.0	39.2	-87.0	-44.3	-43.9	-60.3
S(6)	-63.4	-55.7	-13.5	-63.1	-32.9	-94.1	-81.4	-43.7	-74.3	-56.1	-27.6	-27.3
Trace Elements												
Si	2140.6	1019.8	-99.9	-99.9	227.9	7940.5	3822.2	302.0	6049.0	350.7	-100.0	2019.0
Mn	12.3	-54.6	-57.9	-87.8	-84.9	1267.1	1366.7	248.4	10823.5	724.5	171.3	86583.1
Fe	-34.8	-91.9	109.8	-96.7	45.5	62829.5	-19.6	84.9	146.6	32.5	-98.4	146.6
Rb	267.1	230.4	-4.2	-4.8	20.6	4314.7	6642.4	3040.7	-56.9	10.8	-38.9	193.2
Cs	27175.0	23137.5	125.5	15.3	3095.0	436550.0	659900.0	333025.0	808.0	3500.0	81.8	33975.0
Ba	196.1	170.9	-11.3	-17.8	25.3	8837.7	10459.4	3121.2	1035.2	697.2	-36.2	770.0
Rare Earth Elements												
Sc	54900.0	54900.0	41400.0	54900.0	1814900.0	109900.0	109900.0	54900.0	175.0	109900.0	54900.0	274900.0
Y	101800.0	7400.0	1550.0	15900.0	1767000.0	115800.0	61400.0	224500.0	4900.0	19100.0	5200.0	33100.0
La	1700.0	566.7	333.3	366.7	33766.7	366.7	0.0	1933.3	566.7	12.6	450.0	1800.0
Ce	3450.0	2650.0	725.0	1000.0	127000.0	9800.0	3450.0	7700.0	1050.0	2700.0	725.0	7000.0
Pr	2066.7	1000.0	1000.0	1000.0	54566.7	3539.8	2233.3	2650.0	1402.5	1000.0	450.0	4066.7
Nd	1400.0	120.0	450.0	233.3	51833.3	6000.0	2233.3	6833.3	566.7	1166.7	450.0	3433.3
Sm	2566.7	1000.0	1000.0	450.0	136566.7	20233.3	8566.7	18400.0	1716.6	1000.0	1900.0	4900.0
Eu	6400.0	-65.2	3200.0	1550.0	225400.0	7983.8	6665.0	22400.0	3662.5	3200.0	1550.0	15400.0
Gd	6471.4	842.9	842.9	2328.6	245900.0	17328.6	13471.4	28757.1	2192.4	2566.7	1328.6	5900.0
Tb	11900.0	6500.0	6500.0	3200.0	409900.0	29704.3	13430.0	50900.0	16020.5	6500.0	3200.0	19900.0
Dy	8677.8	633.3	1733.3	2788.9	296011.1	13455.6	9011.1	35455.6	357.7	1196.3	266.7	5788.9
Ho	4410.0	2100.0	2100.0	1000.0	177566.7	571.0	2100.0	21900.0	1099.4	455.6	1000.0	6566.7
Er	7900.0	725.0	725.0	312.5	134900.0	4025.0	3650.0	21400.0	2400.0	-16.7	312.5	3275.0
Tm	1550.0	1550.0	1550.0	1550.0	102400.0	906.5	1400.0	8150.0	935.0	400.0	1550.0	9900.0
Yb	6650.0	725.0	725.0	312.5	182525.0	4025.0	1591.3	9025.0	535.7	108.3	312.5	2400.0
Lu	3200.0	1550.0	1550.0	900.0	105400.0	906.5	900.0	8150.0	3852.1	-266.7	1550.0	9900.0

Tab. F.5.: Factor loadings of the tested parameters of the first factor analysis using principal components as type of factoring, the Varimax rotation and the minimum eigenvalue extraction of STATGRAPHICS XVII centurion.

Factor	1	2	3	4	5	6	7	8
Percent of Variance	47.08	18.82	7.92	4.96	2.99	2.76	2.41	2.10
Cumulative Percentage	47.08	65.89	73.81	78.77	81.76	84.52	86.93	89.03
Eigenvalue	27.30	10.91	4.59	2.88	1.74	1.60	1.40	1.22
pH	-0.76	-0.34	-0.01	-0.25	-0.08	0.08	-0.06	0.02
EC	0.11	0.90	-0.07	0.01	-0.07	0.10	0.07	-0.28
Li	0.14	0.96	0.13	0.05	0.06	0.10	0.03	0.07
Na	0.00	0.80	0.10	-0.09	-0.22	0.02	0.02	-0.47
K	0.15	0.97	0.12	0.06	0.02	0.05	0.05	0.02
Ca	0.18	0.96	0.11	0.08	0.07	0.06	0.06	0.05
Mg	-0.38	-0.38	0.00	-0.27	-0.43	-0.01	0.02	-0.57
Mn(2)	0.31	0.89	0.09	0.11	0.21	-0.03	0.08	0.10
F	0.57	0.24	0.33	0.46	0.14	-0.23	-0.04	-0.03
Cl	0.10	0.96	0.08	-0.01	-0.05	0.07	0.06	-0.18
Br	0.09	0.81	0.27	0.00	-0.06	0.36	0.08	-0.07
S(6)	-0.28	-0.71	-0.13	-0.04	-0.19	-0.09	-0.08	-0.44
Be	0.26	0.86	0.12	0.05	-0.06	0.23	0.00	0.07
B	0.13	0.96	0.14	0.04	0.03	0.15	0.01	0.06
Al	0.86	0.16	0.00	0.32	0.25	-0.03	0.04	0.00
Si	0.64	0.42	0.01	0.27	0.12	-0.03	0.02	0.37
Sc	0.53	0.33	0.68	0.09	0.08	-0.17	0.00	0.08
V	0.78	0.14	-0.11	0.50	0.10	-0.05	0.08	0.12
Cr	-0.04	0.25	0.04	-0.02	-0.05	0.86	-0.07	0.00
Mn	0.37	0.86	0.09	0.11	-0.03	0.04	0.14	0.09
Fe	0.80	0.19	0.13	0.47	0.13	0.04	0.06	0.07
Co	0.00	-0.25	0.31	-0.02	0.06	0.12	0.06	0.69
Ni	0.00	0.30	0.58	-0.08	-0.07	0.58	-0.09	0.08
Cu	-0.04	0.32	0.39	-0.05	0.16	0.68	-0.22	0.15
Zn	0.78	0.14	-0.05	0.57	0.08	-0.03	0.08	0.02
Ga	0.20	0.74	0.41	0.05	0.00	0.10	-0.18	0.16
As	0.49	0.13	-0.04	0.27	0.54	-0.06	-0.06	-0.01
Rb	0.18	0.96	0.10	0.05	0.04	0.08	0.10	0.08
Sr	0.32	0.63	-0.39	0.17	0.10	-0.24	0.36	0.02
Y	0.99	0.12	0.02	-0.04	-0.04	-0.02	0.00	0.04
Mo	-0.10	0.05	-0.11	-0.04	0.01	-0.09	0.90	-0.03
Ag	-0.08	0.47	0.76	0.00	-0.04	0.22	-0.19	0.09
Cd	0.67	0.14	-0.07	0.63	-0.01	0.02	0.07	0.06
In	0.27	0.20	-0.13	0.28	-0.16	-0.05	0.79	0.07
Sn	-0.04	0.07	0.41	-0.06	0.66	0.18	-0.17	0.16
Sb	-0.12	-0.05	-0.15	-0.11	0.83	-0.01	0.03	0.00
Te	0.02	0.40	-0.08	-0.08	0.01	-0.07	0.77	0.01
Cs	0.15	0.97	0.09	0.06	0.06	0.05	0.11	0.07
Ba	0.35	0.66	0.04	0.25	0.38	0.09	0.05	0.12

Continued on next page

Tab. F.5 – continued from previous page

Factor	1	2	3	4	5	6	7	8
La	0.78	0.29	0.06	0.28	0.07	0.32	-0.01	0.08
Ce	0.71	0.27	0.10	0.09	0.08	0.58	-0.03	0.04
Pr	0.94	0.23	0.03	0.06	0.08	0.20	0.02	0.04
Nd	0.96	0.20	0.02	0.01	0.04	0.13	0.00	0.03
Sm	0.97	0.21	0.01	0.00	0.02	0.04	0.01	0.04
Eu	0.81	0.37	-0.18	0.23	0.20	-0.03	0.10	0.06
Gd	0.98	0.17	-0.01	0.02	-0.02	-0.01	0.02	0.04
Tb	0.98	0.14	0.02	-0.01	-0.01	-0.03	0.05	0.04
Dy	0.99	0.12	0.03	-0.03	-0.02	-0.02	0.00	0.03
Ho	0.99	0.11	0.01	-0.02	-0.02	-0.04	0.00	0.03
Er	0.96	0.10	0.05	-0.05	-0.04	-0.02	-0.02	0.03
Tm	0.98	0.10	0.07	0.05	0.03	-0.06	0.02	0.04
Yb	0.98	0.13	0.06	0.08	0.01	0.00	0.01	0.04
Lu	0.97	0.10	0.11	0.08	0.04	-0.07	0.02	0.04
Tl	0.46	0.73	-0.09	0.13	0.17	-0.14	0.21	0.06
Pb	0.65	0.11	-0.08	0.66	0.03	-0.02	0.05	0.01
Bi	0.04	0.39	0.85	-0.05	0.01	0.19	-0.15	0.09
Th	0.46	0.05	0.05	0.24	0.70	-0.11	0.00	-0.03
U	-0.22	-0.43	0.03	0.02	0.20	0.01	0.06	-0.50

Tab. F.6.: Extraction of the first factor analysis with loadings minimally > 0.5. In bold factor loadings >0.9, in italic loadings >0.75 and in brackets negative factor loadings.

Factor	1	2	3	4	5	6	7	8
Variance [%]	47.08	18.82	7.92	4.96	2.99	2.76	2.41	2.10
Cumulative [%]	47.08	65.89	73.81	78.77	81.76	84.52	86.93	89.03
	[pH]	**EC**	Sc	V	As	Cr	**Mo**	[Mg]
	F	**Li**	Ni	Zn	Sn	Ni	*In*	Co
	Al	*Na*	*Ag*	Cd	Sb	*Cu*	*Te*	
	Si	**K**	*Bi*	Pb	Th	Ce		
	Sc	**Ca**						
	V	*Mn(2)*						
	Fe	**Cl**						
	Zn	*Br*						
	Y	[S(6)]						
	Cd	*Be*						
	La	B						
	Ce	*Mn*						
	Pr	Ga						
	Nd	Rb						
	Sm	Sr						
	Eu	Cs						
	Gd	Ba						
	Tb	Tl						
	Dy							
	Ho							
	Er							
	Tm							
	Yb							
	Lu							
	Pb							

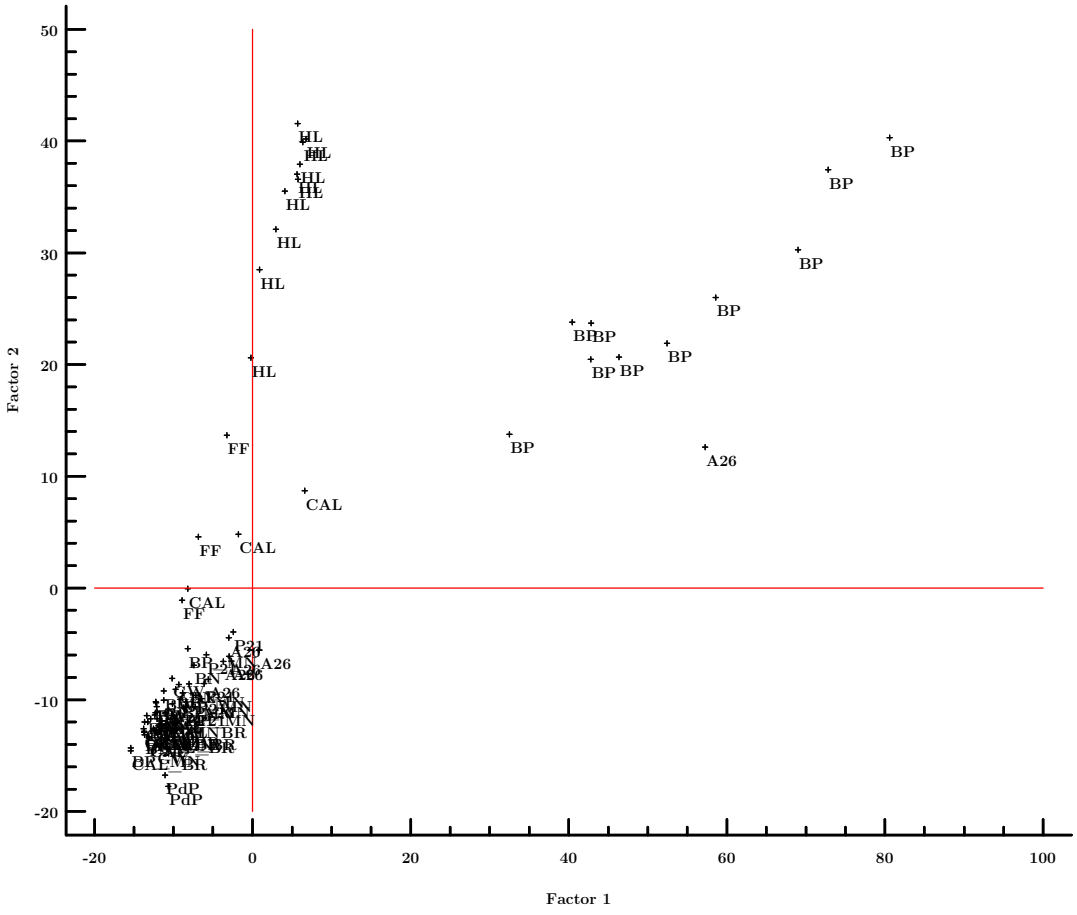

Fig. F.1.: Scatter plot of the first FA, displaying the first two factors, representing a cumulative variance of 65.88 % of the data. Note the distinct relations between both factors regarding the diving spots Hot Lake, Fumarolic Field and Black Point.

Tab. F.7.: Factor loadings of the tested parameters of the second factor analysis extracting four factors.

Factor	1	2	3	4
Variance [%]	47.077	18.818	7.919	4.959
Cumulative [%]	47.077	65.894	73.813	78.772
Eigenvalue	27.3045	10.9142	4.59303	2.87597
pH	-0.79	-0.33	0.11	-0.11
EC	0.11	0.90	-0.10	-0.16
Li	0.16	0.96	0.11	0.09
Na	-0.02	0.80	-0.03	-0.37
K	0.17	0.97	0.06	0.05
Ca	0.20	0.96	0.05	0.10
Mg	-0.45	-0.35	-0.08	-0.65
Mn(2)	0.34	0.88	0.00	0.25
F	0.64	0.24	0.06	0.28
Cl	0.10	0.96	0.01	-0.10
Br	0.10	0.86	0.28	-0.10
S(6)	-0.31	-0.72	-0.15	-0.32
Be	0.28	0.87	0.18	-0.03
B	0.15	0.96	0.15	0.05
Al	0.91	0.15	-0.07	0.27
Si	0.69	0.41	0.01	0.30
Sc	0.55	0.36	0.36	0.14
V	0.86	0.13	-0.19	0.26
Cr	-0.04	0.32	0.48	-0.15
Mn	0.40	0.87	-0.01	0.04
Fe	0.87	0.21	0.02	0.25
Co	0.02	-0.20	0.36	0.28
Ni	0.00	0.38	0.73	-0.11
Cu	-0.03	0.37	0.74	0.11
Zn	0.86	0.14	-0.17	0.23
Ga	0.22	0.74	0.42	0.08
As	0.53	0.09	-0.05	0.53
Rb	0.20	0.97	0.04	0.08
Sr	0.34	0.62	-0.59	0.16
Y	0.97	0.10	0.02	-0.10
Mo	-0.12	0.18	-0.59	-0.01
Ag	-0.05	0.52	0.71	0.01
Cd	0.77	0.15	-0.16	0.19
In	0.31	0.31	-0.56	-0.03
Sn	-0.04	0.08	0.51	0.59
Sb	-0.14	-0.07	-0.07	0.66
Te	0.01	0.50	-0.48	-0.01
Cs	0.18	0.97	0.02	0.10
Ba	0.39	0.66	0.03	0.43
La	0.82	0.31	0.18	0.10
Ce	0.72	0.32	0.36	0.00

Continued on next page

Tab. F.7 – continued from previous page

Factor	1	2	3	4
Pr	0.94	0.23	0.11	0.01
Nd	0.95	0.20	0.09	-0.04
Sm	0.96	0.20	0.04	-0.04
Eu	0.84	0.35	-0.20	0.22
Gd	0.97	0.16	-0.01	-0.07
Tb	0.97	0.13	-0.01	-0.06
Dy	0.97	0.11	0.02	-0.09
Ho	0.97	0.09	0.00	-0.08
Er	0.94	0.08	0.05	-0.11
Tm	0.98	0.09	0.01	0.00
Yb	0.98	0.12	0.03	-0.02
Lu	0.98	0.09	0.03	0.02
Tl	0.48	0.72	-0.25	0.21
Pb	0.75	0.11	-0.19	0.22
Bi	0.05	0.45	0.75	0.03
Th	0.49	0.03	-0.03	0.65
U	-0.23	-0.40	-0.08	0.00

Tab. F.8.: Comparison of both conducted factor analysis and their estimated communality and specific variance of each parameter. In bold parameters with specific variances > 0.2, in bold and italic specific variances > 0.5.

Variable	8 Factors Estimated Communality	Specific Variance	4 Factors Estimated Communality	Specific Variance	Difference Estimated Communality
pH	0.78	**0.22**	0.76	**0.24**	-0.01
EC	0.93	0.07	0.86	0.14	-0.08
Li	0.99	0.01	0.98	0.02	-0.01
Na	0.92	0.08	0.78	**0.22**	-0.14
K	0.98	0.02	0.97	0.03	-0.01
Ca	0.99	0.01	0.98	0.02	-0.01
Mg	0.87	0.13	0.75	**0.25**	-0.12
Mn(2)	0.97	0.03	0.95	0.05	-0.01
F	0.78	**0.22**	0.55	**0.45**	**-0.23**
Cl	0.98	0.02	0.94	0.06	-0.03
Br	0.87	0.13	0.84	0.16	-0.03
S(6)	0.85	0.15	0.74	**0.26**	-0.11
Be	0.89	0.11	0.87	0.13	-0.02
B	0.98	0.02	0.98	0.02	-0.01
Al	0.94	0.06	0.92	0.08	-0.02
Si	0.81	0.19	0.74	**0.26**	-0.07
Sc	0.89	0.11	0.58	**0.42**	-0.31
V	0.93	0.07	0.86	0.14	-0.07

Continued on next page

Tab. F.8 – continued from previous page

Variable	8 Factors Estimated Communality	Specific Variance	4 Factors Estimated Communality	Specific Variance	Difference Estimated Communality
Cr	0.81	0.19	0.35	***0.65***	**-0.46**
Mn	0.93	0.07	0.93	0.07	-0.01
Fe	0.94	0.06	0.87	0.13	-0.07
Co	0.65	**0.35**	0.25	***0.75***	**-0.41**
Ni	0.79	**0.21**	0.70	**0.30**	-0.09
Cu	0.82	0.18	0.69	**0.31**	-0.12
Zn	0.97	0.03	0.85	0.15	-0.12
Ga	0.83	0.17	0.78	**0.22**	-0.04
As	0.63	**0.37**	0.57	**0.43**	-0.07
Rb	0.99	0.01	0.98	0.02	0.00
Sr	0.88	0.12	0.87	0.13	-0.01
Y	0.99	0.01	0.96	0.04	-0.04
Mo	0.85	0.15	0.39	***0.61***	**-0.46**
Ag	0.90	0.10	0.78	**0.22**	-0.12
Cd	0.88	0.12	0.68	**0.32**	-0.20
In	0.86	0.14	0.50	**0.50**	-0.36
Sn	0.70	**0.30**	0.61	**0.39**	-0.08
Sb	0.74	**0.26**	0.47	***0.53***	**-0.26**
Te	0.78	**0.22**	0.48	***0.52***	**-0.29**
Cs	0.99	0.01	0.98	0.02	-0.01
Ba	0.80	**0.20**	0.78	**0.22**	-0.01
La	0.89	0.11	0.81	0.19	-0.08
Ce	0.94	0.06	0.75	**0.25**	-0.19
Pr	0.98	0.02	0.95	0.05	-0.04
Nd	0.99	0.01	0.96	0.04	-0.03
Sm	0.99	0.01	0.96	0.04	-0.03
Eu	0.93	0.07	0.91	0.09	-0.02
Gd	0.99	0.01	0.97	0.03	-0.02
Tb	0.99	0.01	0.96	0.04	-0.03
Dy	0.99	0.01	0.96	0.04	-0.04
Ho	0.99	0.01	0.96	0.04	-0.03
Er	0.94	0.06	0.91	0.09	-0.04
Tm	0.99	0.01	0.96	0.04	-0.02
Yb	0.99	0.01	0.98	0.02	-0.01
Lu	0.98	0.02	0.96	0.04	-0.02
Tl	0.86	0.14	0.85	0.15	-0.01
Pb	0.88	0.12	0.66	**0.34**	**-0.22**
Bi	0.94	0.06	0.76	**0.24**	-0.18
Th	**0.78**	**0.22**	0.67	**0.33**	-0.11
U	**0.52**	**0.48**	0.23	***0.77***	**-0.30**

Tab. F.9.: Factor loadings of the tested parameters of the third factor analysis based on element concentrations, without pH and EC.

Factor	1	2	3	4
Variance [%]	47.625	18.309	7.097	5.06
Cumulative [%]	47.63	65.93	73.03	78.09
Eigenvalue	26.67	10.25	3.97	2.83
Li	0.13	0.95	0.09	0.07
Na	-0.01	0.77	0.06	-0.41
K	0.17	0.97	0.05	0.02
Ca	0.21	0.96	0.06	0.08
Mg	-0.43	-0.38	0.00	-0.65
Mn(2)	0.34	0.87	0.13	0.24
F	0.65	0.26	-0.02	0.25
Cl	0.10	0.95	0.08	-0.14
Br	0.10	0.89	-0.14	-0.09
S(6)	-0.32	-0.73	0.03	-0.32
Be	0.29	0.88	-0.08	-0.05
B	0.16	0.98	-0.03	0.04
Al	0.91	0.15	0.11	0.26
Si	0.68	0.43	0.08	0.29
Sc	0.57	0.42	-0.31	0.15
V	0.86	0.12	0.21	0.24
Cr	-0.04	0.39	-0.36	-0.08
Mn	0.41	0.87	0.11	0.01
Fe	0.87	0.22	0.05	0.25
Co	0.02	-0.13	-0.29	0.32
Ni	-0.05	0.06	-0.27	-0.09
Cu	-0.01	0.53	-0.60	0.22
Zn	0.86	0.12	0.21	0.21
Ga	0.24	0.79	-0.36	0.09
As	0.50	0.10	0.10	0.54
Rb	0.20	0.97	0.07	0.06
Sr	0.33	0.54	0.68	0.09
Y	0.97	0.11	-0.01	-0.09
Mo	-0.12	0.09	0.64	-0.04
Ag	-0.04	0.65	-0.59	0.06
Cd	0.77	0.13	0.21	0.17
In	0.31	0.24	0.63	-0.06
Sn	-0.03	0.17	-0.43	0.65
Sb	-0.14	-0.08	0.10	0.67
Te	0.01	0.45	0.60	-0.04
Cs	0.18	0.97	0.10	0.08
Ba	0.40	0.67	0.10	0.41
La	0.84	0.35	-0.05	0.13
Ce	0.78	0.40	-0.21	0.07
Pr	0.94	0.26	-0.03	0.04

Continued on next page

Tab. F.9 – continued from previous page

Factor	1	2	3	4
Nd	0.95	0.22	-0.03	-0.02
Sm	0.96	0.21	0.00	-0.03
Eu	0.83	0.33	0.28	0.19
Gd	0.97	0.16	0.03	-0.06
Tb	0.97	0.14	0.02	-0.06
Dy	0.97	0.12	-0.01	-0.08
Ho	0.97	0.09	0.00	-0.08
Er	0.94	0.10	-0.05	-0.10
Tm	0.98	0.09	-0.01	-0.01
Yb	0.98	0.13	-0.01	-0.01
Lu	0.98	0.10	-0.03	0.02
Tl	0.47	0.69	0.36	0.18
Pb	0.75	0.09	0.23	0.20
Bi	0.07	0.59	-0.64	0.09
Th	0.50	0.03	0.06	0.63
U	-0.22	-0.43	-0.02	0.01

Tab. F.10.: Extraction of the only element factor analysis with loadings minimally > 0.5. In bold factor loadings >0.9, in italic loadings >0.75 and in brackets negative factor loadings.

Factor	1	2	3	4
Variance [%]	47.625	18.309	7.097	5.06
Cumulative [%]	47.63	65.93	73.03	78.09
	F	**Li**	[Cu]	[Mg]
	Al	*Na*	Sr	As
	Si	**K**	Mo	Sn
	Sc	**Ca**	[Ag]	Sb
	V	*Mn(2)*	In	Th
	Fe	**Cl**	Te	
	Zn	*Br*	[Bi]	
	As	[S(6)]		
	Y	*Be*		
	Cd	**B**		
	La	*Mn*		
	Ce	Cu		
	Pr	*Ga*		
	Nd	**Rb**		
	Sm	Sr		
	Eu	Ag		
	Gd	**Cs**		
	Tb	Ba		
	Dy	Tl		
	Ho	Bi		
	Er			
	Tm			
	Yb			
	Lu			
	Pb			
	Th			

Tab. F.11.: Factor loadings of the tested parameters of the third factor analysis based on REE.

Factor	1	2
Variance	85.48	7.39
Cumulative	85.48	92.87
Eigenvalue	13.68	1.18
Sc	0.63	0.11
Y	0.92	0.35
La	0.48	0.84
Ce	0.15	0.97
Pr	0.69	0.71
Nd	0.77	0.63
Sm	0.86	0.48
Eu	0.79	0.38
Gd	0.91	0.40
Tb	0.93	0.36
Dy	0.93	0.36
Ho	0.93	0.35
Er	0.91	0.35
Tm	0.94	0.33
Yb	0.91	0.39
Lu	0.92	0.36

Tab. F.12.: Estimated Communality and Specific Variance for the REE factor analysis. Only Eu has a specific variance worth mentioning of 0.23, all other elements are below 0.06.

Variable	Estimated Communality	Specific Variance
Sc	1.00	0.00
Y	0.99	0.01
La	0.94	0.06
Ce	0.98	0.02
Pr	0.99	0.01
Nd	0.98	0.02
Sm	0.98	0.02
Eu	0.77	0.23
Gd	0.99	0.01
Tb	0.99	0.01
Dy	0.99	0.01
Ho	0.99	0.01
Er	0.95	0.05
Tm	0.99	0.01
Yb	0.99	0.01
Lu	0.97	0.03

Tab. F.13.: Estimated Communality and Specific Variance for the trace element factor analysis. Si, Mn, Ba, Co, Cu have specific variances between 0.17 and 0.3, but still the majority of the variance of these elements is explained by the new parameters.

	Estimated	Specific
Variable	Communality	Variance
Si	0.79	0.21
Mn	0.83	0.17
Fe	0.95	0.05
Rb	0.96	0.04
Ba	0.70	0.30
Cs	0.97	0.03
Co	0.71	0.29
Cu	0.70	0.30
Zn	0.94	0.06

KWT

Tab. F.14.: Results of the KWTs with $\alpha = 0.01\%$: Matrices for significant differences concerning 35 parameters of the various diving spots at the submarine hydrothermal system Panarea. Bold, capital X = Bonferroni correction with $\alpha = 0.1\%$, small x = Bonferroni correction with $\alpha = 5\%$.

pH

P-value = 0	A26	BN	BW	BP	BP_MN	CAL	CAL_BR	FF	HL	GW	P21	loc. sw.
A26		x				x	x					**X**
BN	x			**X**					x		x	
BW				**X**								
BP		**X**	**X**		**X**	**X**	**X**			**X**	x	**X**
BP_MN				**X**								x
CAL	x			**X**					x			
CAL_BR	x			**X**					x		x	
FF												**X**
HL		x					x					**X**
GW				**X**		x						
P21		x		x			x					**X**
loc. sw.	**X**			**X**	x			**X**	**X**		**X**	

EC

P-value = 0	A26	BN	BW	BP	BP_MN	CAL	CAL_BR	FF	HL	GW	P21	loc. sw.
A26									**X**			
BN									**X**			
BW									**X**			
BP						**X**				x	**X**	**X**
BP_MN									**X**			
CAL				**X**					**X**			
CAL_BR												
FF										x		x
HL	**X**	**X**	**X**		**X**	**X**				**X**	**X**	**X**
GW				x				x	**X**			
P21				**X**					**X**			
loc. sw.				**X**				x	**X**			

E_H

P-Value = 0	A26	BN	BW	BP	BP_MN	CAL	CAL_BR	FF	HL	GW	P21	loc. sw.
A26				**X**	**X**	**X**	**X**					
BN				**X**		**X**	**X**					
BW												
BP	**X**	**X**						x	**X**		x	
BP_MN	**X**							x	**X**			
CAL	**X**	**X**						x	**X**		x	
CAL_BR	**X**	**X**						x	**X**		x	
FF				x	x	x	x					
HL				**X**	**X**	**X**	**X**					
GW												
P21				x		x	x					
loc. sw.												

Li

P-Value = 0	A26	BN	BW	BP	BP_MN	CAL	CAL_BR	FF	HL	GW	P21	loc. sw.
A26							x		x			**X**
BN									x			
BW									x			
BP					x	x	**X**			x	**X**	**X**
BP_MN				x					**X**			
CAL				x					**X**			
CAL_BR	x			**X**				**X**	**X**			
FF							**X**				x	**X**
HL	x	x	x		**X**	**X**	**X**			**X**	**X**	**X**
GW				x					**X**			
P21								x	**X**			
loc. sw.	**X**			**X**				**X**	**X**			

Na

P-Value = 0	A26	BN	BW	BP	BP_MN	CAL	CAL_BR	FF	HL	GW	P21	loc. sw.
A26									**X**			
BN									**X**			
BW						x			x			
BP									**X**			
BP_MN									**X**			
CAL			x					**X**	**X**			x
CAL_BR									**X**			
FF						**X**				x		
HL	**X**	**X**	x	**X**	**X**	**X**	**X**			**X**	**X**	x
GW								x	**X**			
P21									**X**			
loc. sw.						x			x			

K

P-Value = 0	A26	BN	BW	BP	BP_MN	CAL	CAL_BR	FF	HL	GW	P21	loc. sw.
A26							x		x			
BN							x		x			
BW				x					**X**			
BP			x		x	**X**	**X**			**X**	**X**	**X**
BP_MN				x					**X**			
CAL	x	x		**X**				x	**X**			
CAL_BR				**X**				**X**	**X**			
FF						x	**X**			x	x	x
HL			**X**		**X**	**X**	**X**			**X**	**X**	**X**
GW				**X**				x	**X**			
P21				**X**				x	**X**			
loc. sw.				**X**				x	**X**			

Ca

P-Value = 0	A26	BN	BW	BP	BP_MN	CAL	CAL_BR	FF	HL	GW	P21	loc. sw.
A26							**X**		x			x
BN							x		x			x
BW									**X**			
BP					x	**X**	**X**			**X**	**X**	
BP_MN				x					**X**			
CAL				**X**				x	**X**			
CAL_BR	**X**	x		**X**				x	**X**			
FF						x	x			x	x	**X**
HL	x	x	**X**		**X**	**X**	**X**			**X**	**X**	**X**
GW				**X**				x	**X**			
P21				**X**				x	**X**			
loc. sw.	x	x		**X**				**X**	**X**			

Mg

P-Value = 0	A26	BN	BW	BP	BP_MN	CAL	CAL_BR	FF	HL	GW	P21	loc. sw.
A26				**X**					x			
BN				**X**					x			
BW				**X**		**X**		x	**X**			
BP	**X**	**X**	**X**		**X**		**X**				**X**	**X**
BP_MN				**X**					**X**			
CAL			**X**								x	**X**
CAL_BR				**X**					x			
FF			x									x
HL	x	x	**X**		**X**		x				**X**	**X**
GW												
P21				**X**		x			**X**			
loc. sw.				**X**		**X**		x	**X**			

F

P-Value = 0	A26	BN	BW	BP	BP_MN	CAL	CAL_BR	FF	HL	GW	P21	loc. sw.
A26												**X**
BN				x								x
BW												x
BP			x		**X**	**X**	**X**	x	x		x	**X**
BP_MN				**X**								x
CAL				**X**								
CAL_BR				**X**								
FF				x								
HL				x								x
GW												
P21				x								**X**
loc. sw.	**X**	x	x	**X**	x				x		**X**	

Cl

P-Value = 0	A26	BN	BW	BP	BP_MN	CAL	CAL_BR	FF	HL	GW	P21	loc. sw.
A26				x					**X**			
BN									x			
BW									**X**			
BP	x				**X**	**X**	**X**			**X**	x	**X**
BP_MN				**X**					**X**			
CAL				**X**				x	**X**			
CAL_BR				**X**				x	**X**			
FF						x	x			x		**X**
HL	**X**	x	**X**		**X**	**X**	**X**			**X**	**X**	**X**
GW				**X**				x	**X**			
P21				x					**X**			
loc. sw.				**X**				**X**	**X**			

Br

P-Value = 0	A26	BN	BW	BP	BP_MN	CAL	CAL_BR	FF	HL	GW	P21	loc. sw.
A26				x					**X**			
BN				x					**X**			
BW							x		x			
BP	x	x			x	**X**	**X**			x	x	x
BP_MN				x					**X**			
CAL				**X**				x	**X**			
CAL_BR			x	**X**				**X**	**X**			
FF						x	**X**					x
HL	**X**	**X**	x		**X**	**X**	**X**			**X**	**X**	**X**
GW				x					**X**			
P21				x					**X**			
loc. sw.				x				x	**X**			

S(6)

P-Value = 0	A26	BN	BW	BP	BP_MN	CAL	CAL_BR	FF	HL	GW	P21	loc. sw.
A26									x			x
BN				**X**					**X**			
BW				x					x			
BP		**X**	x		**X**		**X**				**X**	**X**
BP_MN				**X**					**X**			
CAL									x			x
CAL_BR				**X**					**X**			
FF												
HL	x	**X**	x		**X**	x	**X**				**X**	**X**
GW												
P21				**X**					**X**			
loc. sw.	x			**X**		x			**X**			

Si

P-Value = 0	A26	BN	BW	BP	BP_MN	CAL	CAL_BR	FF	HL	GW	P21	loc. sw.
A26			**X**				**X**				x	**X**
BN				x			x					x
BW	**X**			**X**					**X**			
BP		x	**X**		**X**	**X**	x	x			**X**	**X**
BP_MN				**X**								x
CAL				**X**								x
CAL_BR	**X**	x		x					**X**	x		
FF				x								x
HL			**X**				**X**				**X**	**X**
GW							x					x
P21	x			**X**					**X**			
loc. sw.	**X**	x		**X**	x	x		x	**X**	x		

Fe

P-Value = 1.86E-8	A26	BN	BW	BP	BP_MN	CAL	CAL_BR	FF	HL	GW	P21	loc. sw.
A26				**X**								
BN				**X**								
BW				x								x
BP	**X**	**X**	x			**X**	**X**	x	x		**X**	**X**
BP_MN												x
CAL				**X**								x
CAL_BR				**X**								
FF				x								
HL				x								x
GW												
P21				**X**								
loc. sw.			x	**X**	x	x			**x**			

Mn

P-Value = 4.37E-10	A26	BN	BW	BP	BP_MN	CAL	CAL_BR	FF	HL	GW	P21	loc. sw.
A26												**X**
BN									x			x
BW				x					**X**			
BP			x			x	**X**				**X**	**X**
BP_MN												x
CAL				x					**X**			x
CAL_BR				**X**					**X**			
FF												**X**
HL		**x**	**X**			**X**	**X**				**X**	**X**
GW												
P21				**X**					**X**			
loc. sw.	**X**	x		**X**	x	x		**X**	**X**			

Rb

P-Value = 0	A26	BN	BW	BP	BP_MN	CAL	CAL_BR	FF	HL	GW	P21	loc. sw.
A26							**X**		x			**X**
BN							x		x			**X**
BW				**X**					**X**			
BP			**X**		x	**X**	**X**			**X**	**X**	**X**
BP_MN				x					**X**			x
CAL				**X**				x	**X**			
CAL_BR	**X**	x		**X**				**X**	**X**			
FF						x	**X**			x	x	**X**
HL	x	x	**X**		**X**	**X**	**X**			**X**	**X**	**X**
GW				**X**				x	**X**			
P21				**X**				x	**X**			
loc. sw.	**X**	**X**		**X**	x			**X**	**X**			

Cs

P-Value = 0	A26	BN	BW	BP	BP_MN	CAL	CAL_BR	FF	HL	GW	P21
A26							x		x		
BN							x		x		
BW				**X**				x	**X**		
BP			**X**		x	**X**	**X**			**X**	**X**
BP_MN				x					**X**		
CAL				**X**				x	**X**		
CAL_BR	x	x		**X**				**X**	**X**		
FF			x			x	**X**			x	**X**
HL	x	x	**X**		**X**	**X**	**X**			**X**	**X**
GW				**X**				x	**X**		
P21				**X**				**X**	**X**		

Ba

P-Value = 0	A26	BN	BW	BP	BP_MN	CAL	CAL_BR	FF	HL	GW	P21	loc. sw.
A26				**X**					**X**			x
BN				**X**					x			x
BW				**X**				x	**X**			
BP	**X**	**X**	**X**		x	x	**X**				**X**	**X**
BP_MN				x					x			x
CAL				x			x		x			**X**
CAL_BR				**X**		x		**X**	**X**			
FF			x				**X**					**X**
HL	**X**	x	**X**		x	x	**X**				**X**	**X**
GW												
P21				**X**					**X**			
l. sw.	x	x		**X**	x	**X**		**X**	**X**			

Sc

P-Value = 0	A26	BN	BW	BP	BP_MN	CAL	CAL_BR	FF	HL	GW	P21
A26				x							
BN				x							
BW				**X**							
BP	x	x	**X**		**X**	**X**	x	x			**X**
BP_MN				**X**					x		
CAL				**X**							
CAL_BR				x							
FF				x							
HL					x						x
GW											
P21				**X**					x		

Y

P-Value = 0	A26	BN	BW	BP	BP_MN	CAL	CAL_BR	FF	HL	GW	P21
A26			**X**			**X**	**X**			**X**	
BN						x	**X**			x	
BW				**X**							
BP	**X**		**X**		x	**X**	**X**	x		**X**	**X**
BP_MN				x							
CAL	**X**	x		**X**							
CAL_BR	**X**	**X**		**X**					x		x
FF				x							
HL							x				
GW	**X**	x		**X**							
P21				**X**			x				

La

P-Value = 0	A26	BN	BW	BP	BP_MN	CAL	CAL_BR	FF	HL	GW	P21
A26							x				
BN							x				
BW				x							
BP			x		**X**	**X**	**X**	x		**X**	**X**
BP_MN				**X**							
CAL				**X**							
CAL_BR	x	x		**X**					x		
FF				x							
HL							x				
GW				**X**							
P21				**X**							

Ce

P-Value = 1.99E-10	A26	BN	BW	BP	BP_MN	CAL	CAL_BR	FF	HL	GW	P21
A26						x	x			x	
BN				x							
BW				x							
BP		x	x		**X**	**X**	**X**	x		**X**	x
BP_MN				**X**							
CAL	x			**X**							
CAL_BR	x			**X**					x		
FF				x							
HL							x				
GW	x			**X**							
P21				x							

Pr

P-Value = 0	A26	BN	BW	BP	BP_MN	CAL	CAL_BR	FF	HL	GW	P21
A26						x	**X**				
BN				**X**							
BW				**X**							
BP		**X**	**X**		**X**	**X**	**X**	**X**		**X**	x
BP_MN				**X**							
CAL	x			**X**							
CAL_BR	**X**			**X**					x		x
FF				**X**							
HL							x				
GW				**X**							
P21				x			x				

Nd

P-Value = 0	A26	BN	BW	BP	BP_MN	CAL	CAL_BR	FF	HL	GW	P21
A26					x	**X**	**X**			x	
BN				**X**							
BW				**X**							
BP		**X**	**X**		**X**	**X**	**X**	**X**		**X**	x
BP_MN	x			**X**							
CAL	**X**			**X**							
CAL_BR	**X**			**X**					x		x
FF				**X**							
HL							x			x	
GW	x			**X**					x		
P21				x			x				

Sm

P-Value = 0	A26	BN	BW	BP	BP_MN	CAL	CAL_BR	FF	HL	GW	P21
A26		x			x	**X**	**X**			x	
BN	x			**X**							
BW				**X**							
BP		**X**	**X**		**X**	**X**	**X**	x		**X**	**X**
BP_MN	x			**X**							
CAL	**X**			**X**					x		
CAL_BR	**X**			**X**					**X**		x
FF				x							
HL						x	**X**				
GW	x			**X**							
P21				**X**			x				

Eu

P-Value = 0	A26	BN	BW	BP	BP_MN	CAL	CAL_BR	FF	HL	GW	P21
A26		x	x				**X**				
BN	x			**X**					x		
BW	x			**X**					x		
BP		**X**	**X**		**X**	**X**	**X**			**X**	**X**
BP_MN				**X**							
CAL				**X**							
CAL_BR	**X**			**X**				x	**X**		
FF							x				
HL		x	x				**X**				
GW				**X**							
P21				**X**							

Gd

P-Value = 0	A26	BN	BW	BP	BP_MN	CAL	CAL_BR	FF	HL	GW	P21
A26		x	x		x	**X**	**X**			**X**	
BN	x			**X**							
BW	x			**X**							
BP		**X**	**X**		**X**	**X**	**X**	**x**		**X**	**X**
BP_MN	x			**X**							
CAL	**X**			**X**					x		
CAL_BR	**X**			**X**					**X**		x
FF				**x**							
HL						x	**X**			x	
GW	**X**			**X**					x		
P21				**X**			x				

Tb

P-Value = 0	A26	BN	BW	BP	BP_MN	CAL	CAL_BR	FF	HL	GW	P21
A26		x	x		x	**X**	**X**	x		x	
BN	x			**X**							
BW	x			**X**							
BP		**X**	**X**		**X**	**X**	**X**	**X**		x	x
BP_MN	x			**X**							
CAL	**X**			**X**					x		x
CAL_BR	**X**			**X**					**X**		x
FF	x			**X**							
HL						x	**X**				
GW	x			x							
P21				x		x	x				

Dy

P-Value = 0	A26	BN	BW	BP	BP_MN	CAL	CAL_BR	FF	HL	GW	P21
A26			**X**			**X**	**X**	x		**X**	
BN				x			x				
BW	**X**			**X**							
BP		x	**X**		**X**	**X**	**X**	**X**	x	**X**	x
BP_MN				**X**							
CAL	**X**			**X**					x		x
CAL_BR	**X**	x		**X**					**X**		**X**
FF	x			**X**							
HL				x		x	**X**				
GW	**X**			**X**							
P21				x		x	**X**				

Ho

P-Value = 0	A26	BN	BW	BP	BP_MN	CAL	CAL_BR	FF	HL	GW	P21
A26			**X**		x	**X**	**X**	**X**		x	
BN				x							
BW	**X**			**X**							
BP		x	**X**		**X**	**X**	**X**	**X**	x	**X**	x
BP_MN	x			**X**							
CAL	**X**			**X**							x
CAL_BR	**X**			**X**							
FF	**X**			**X**							
HL				x							
GW	x			**X**							
P21				x		x					

Er

P-Value = 0	A26	BN	BW	BP	BP_MN	CAL	CAL_BR	FF	HL	GW	P21
A26			**X**		x	**X**	**X**	x		x	
BN						**X**	x				
BW	**X**			**X**							
BP			**X**		**X**	**X**	**X**	**X**	x	**X**	**X**
BP_MN	x			**X**							
CAL	**X**	x		**X**							
CAL_BR	**X**	**X**		**X**					x		x
FF	x			**X**							
HL				x			x				
GW	x			**X**							
P21				**X**			x				

Tm

P-Value = 0	A26	BN	BW	BP	BP_MN	CAL	CAL_BR	FF	HL	GW	P21
A26			**X**		x	**X**	x	x			x
BN											
BW	**X**			**X**							
BP			**X**		**X**	**X**	**X**	**X**	**X**	x	**X**
BP_MN	x			**X**							
CAL	**X**			**X**							
CAL_BR	x			**X**					x		x
FF	x			**X**							
HL				**X**			x				
GW				x							
P21	x			**X**			x				

Yb

P-Value = 0	A26	BN	BW	BP	BP_MN	CAL	CAL_BR	FF	HL	GW	P21
A26			x			**X**	**X**	x		x	
BN						**X**	x	x			
BW	x			**X**							
BP			**X**		**X**	**X**	**X**	**X**	**x**	**X**	**X**
BP_MN				**X**							
CAL	**X**	**X**		**X**							
CAL_BR	**X**	**x**		**X**					x		x
FF	x	x		**X**							
HL				**x**			x				
GW	x			**X**							
P21				**X**			x				

Lu

P-Value = 0	A26	BN	BW	BP	BP_MN	CAL	CAL_BR	FF	HL	GW	P21
A26						**X**		x	x		
BN											
BW				**X**							
BP			**X**		**X**	**X**	**X**	**X**	**X**		**X**
BP_MN				**X**							
CAL	**X**			**X**							
CAL_BR				**X**							
FF	x			**X**							
HL	x			**X**							
GW											
P21				**X**							